EFFECT of NANOPARTICLES ON THE PHOTOPHYSICOCHEMICAL BEHAVIOUR OF METALLOPHTHALOCYANINES

A thesis submitted in fulfilment of the requirements for the degree of

DOCTOR OF PHILOSOPHY

Of

RHODES UNIVERSITY

By

SHARON KEITUMETSE GAIL MPHELETSO MOENO

February 2011

DEDICATION

To

my mother Margaret Moeno

and

my late father Aldino Coppo

ACKNOWLEDGEMENTS

"When my disquieting thoughts became many inside of me, your own consolations began to fondle my soul" (Psalm 94:19).

Many were the days when I felt the load and burden were too much for me to carry, but see: He carried me through it all and so I thank Jehovah for holding my hand through the rest of my arduous journey and cradling me through the pains of it.

I hope to seize this chance to express appreciation to my supervisor Prof. Nyokong for letting me work under her supervision. It was an honor to work with someone with so much energy and with someone of your calibre Prof. Thank you, for your guidance through the PhD program, your insights and teaching methods were highly appreciated. May I also express gratitude for reading my thesis over and over again.!

I also hope to especially thank my mother and my friends: Terry, Vicki, Tsitsi, Tumi, Kedi, Val and all in the Grahamstown congregation for making my stay as warm as could be. Meshach and Philoh, I thank you for your loving kindness towards me and your friendship which sustained me in so many ways (the long chats were all I looked forward to on weekends). To my friends from Lesotho, Keke: Thank you for the constant string of sms's and calls which kept me sane, Itumeleng: Thank you for always being there, Kefue and uncle Manie, I also thank you for your interest in my welfare.

I would also like to express gratitude to Dr. Antunes, Dr. Idowu, Sam, Dr. Chidawanyika, Dr. Erdogmŭs and Dr. Litwinski for all their contributions during the course of this work. I hope to thank all the staff of the Chemistry department at Rhodes and the postgraduate students for all their help. Many thanks to the S22 group; you will all be sorely and dearly missed, but hey I know where to go to for a good laugh....

The financial support received from DAAD is gratefully acknowledged.

ABSTRACT

The synthesis, spectroscopic characterization, and studies of the photophysicochemical behaviour of selective anionic, cationic and neutral metallophthallocyanine (MPc) complexes were carried out and the results are presented herein. Studies on the effect of the central metal ion, the solvent used and the presence of nanoparticles on the photophysicochemical properties were conducted. The findings showed that the photophysicochemical parameters were mostly enhanced in the presence of central metal ions of high atomic numbers and also in the presence of nanoparticles. It was also observed that solvents that encouraged the monomericity of the MPc complexes also lead to improved photophysical and photochemical behaviour. CdTe quantum dots (QDs) stabilized with mercaptocarbonic acids were also observed to cause stimulated emission of the MPcs through Förster resonance energy transfer (FRET) thus acting as energy donors while the respective MPc acted as energy acceptors in all the FRET studies. FRET was observed following the photoexcitation of QDs for all monomeric anionic MPcs but it was also shown to occur for some cationic MPcs in organic media. Both the substituent and solvent used were found to exert a strong influence on the occurrence of FRET. Other cationic MPcs however showed different behaviour in the presence of the meraptocarbonic stabilized CdTe QDs; with the cationic porphyrazine giving clear indications of Pc ring reduction. The rest of the cationic MPcs did not give clear evidence of Pc ring reduction, instead they showed signs of aggregate formation possibly from the assembly of electrostatic ion pair complexes which could result in reduction of the quaternized pyridinium ring of the substituent. Both the QDs and the MPc complex emission spectra were significantly quenched for each in the presence of the other. Stern-Volmer quenching studies indicated that both static and dynamic quenching of the QDs in the presence of MPcs took place. The fluorescence lifetimes of the mercaptopropionic acid (MPA) capped CdTe QDs in the presence of various MPc complexes showed quenching of mostly

the longer lifetimes of the QDs in the presence of MPcs suggesting that the surface defects and states are involved in the interaction of the QDs and MPcs. An MPc complex terminating in thio tethers was employed in the conjugation to AuNPs. Spectroscopic and microscopic studies confirmed the formation of the MPc-AuNP conjugate which was also shown to exhibit improved photophysicochemical properties compared to the free MPc.

Contents

LIST OF ABBREVIATIONS

Abs	=	Absorbance
A	=	Acceptor
ADMA	=	Tetra sodium α,α-(anthracene-9,10-diyl)dimethylmalonate
AE	=	Acceptor excitation
AFM	=	Atomic force microscopy
ASE	=	Acceptor stimulated emission
BPAA	=	Bis-9,10-anthracene-(4-trimethylphenylammonium)dichloride
$CDCl_3$	=	Deuterated chloroform
CEL	=	Cremophore EL
D	=	Donor
DA	=	Donor absorption
DABCO	=	1,4-Diazabicyclo-octane
DBU	=	1,8-Diazabicyclo[5.4.0]undec-7-ene
DBN	=	1,5-Diazabicyclo[4.3.0]non-5-ene
DE	=	Donor emission
DMAE	=	Dimethylaminoethanol
DMF	=	Dimethylformamide
DMSO	=	Dimethylsulfoxide
DPBF	=	1,3-Diphenylisobenzofuran
DOS	=	Density of states
Eff	=	FRET efficiency
EM	=	Electron microscopy
EtOH	=	Ethanol

F	=	Fluorescence intensity
FRET	=	Förster resonance energy transfer
FT-IR	=	Fourier transform-infrared
FWHM	=	Full width at half-maximum
HOMO	=	Highest occupied molecular orbital
H_2Pc	=	Metal free phthalocyanine
HPLC	=	High performance liquid chromatography
IC	=	Internal conversion
IR	=	Infrared
ISC	=	Intersystem crossing
L-cys	=	L-cysteine
LED	=	Light emitting diodes
LUMO	=	Lowest unoccupied molecular orbital
ME	=	Mercaptoethanol
MPA	=	Mercaptopropionic acid
MPc	=	Metallophthalocyanine
NET	=	Non radiative energy transfer
NMR	=	Nuclear magnetic resonance
NPs	=	Nanoparticles
NR	=	Non-radiative
Pc	=	Phthalocyanine
PDT	=	Photodynamic therapy
PL	=	Photoluminescence
PMT	=	Photomultiplier tube
P	=	Phosphorescence

PT	=	Photothermal therapy
QDs	=	Quantum dots
STM	=	Scanning tunnelling microscopy
TEM	=	Transmission electron microscopy
TCSPC	=	Time correlated single photon counting
TFA	=	Trifluoroacetic acid
TGA	=	Thioglycolic acid
TCSPC	=	Time correlated single photon counting
TOP	=	Trioctylphosphine
TOPO	=	Trioctylphosphine oxide
TRES	=	Time resolved emission spectra
UV	=	Ultraviolet
UV-Vis	=	Ultraviolet-Visible
VR	=	Vibrational relaxation
XRPD	=	X-ray powder diffraction
XRD	=	X-ray diffraction

LIST OF SYMBOLS

α	=	Non peripheral position on phthalocyanine ring
Å	=	Angstrom
ΔA_T^{Sample}	=	Triplet state absorbance of phthalocyanine sample
ΔA_T^{Std}	=	Triplet state absorbance of the standard phthalocyanine sample
ΔA_S	=	Change in the absorbance of the ground singlet state
ΔA_T	=	Change in the absorbance of the triplet state
β	=	Peripheral position on phthalocyanine ring
e^-	=	Electron
ε_A	=	Acceptor molar extinction coefficient
ε_T^{Sample}	=	Triplet state extinction coefficients for the phthalocyanine sample
ε_T^{Std}	=	Triplet state extinction coefficients for standard phthalocyanine sample
E_i	=	Initial potential
E_f	=	Final potential
F	=	Faraday constant
F_0	=	Fluorescence intensity of a fluorophore in the absence of a quencher
F	=	Fluorescence intensity of a fluorophore in the presence of a quencher
F_∞	=	Fluorescence intensity of the fluorophore saturated with quencher
f_D	=	Normalized donor emission spectrum
I_{abs}	=	Rate of light absorption by the photosensitizer
I_{abs}^{Std}	=	Rate of light absorption by the standard
J	=	Förster overlap integral
κ^2	=	Dipole orientation factor

K_{SV} = Stern-Volmer quenching constant

k_Q = Bimolecular quenching constant

k_b = Binding constant

$^3MPc^*$ = Metallophthalocyanine in the excited triplet state

$^1MPc^*$ = Metallophthalocyanine in the excited singlet state

M = Concentration in molarity

n = Refractive indices of solvent

n = Number of binding sites

n_{Std} = Refractive indices of solvent with standard

Φ_F = Fluorescence quantum yield

$\Phi_{F(D)}$ = Fluorescence quantum yield of the donor

$\Phi_{F(DA)}$= Fluorescence quantum yield of the donor in the presence of the acceptor

Φ_T = Triplet state quantum yield for the phthalocyanine sample

Φ_T^{Std} = Triplet state quantum yield for the standard sample

Φ_Δ = Singlet oxygen quantum yield

Φ_Δ^{Std} = Singlet oxygen quantum yield for the standard

Q = Quencher

r = Centre to centre distance between the donor and acceptor chromophores

R_0 = Förster distance

S_0 = Ground singlet state

S_1 = First excited singlet state

Sub = Substrate

$^1O_2$ = Singlet oxygen

$^1\Delta_g$ = Singlet oxygen

$^3O_2$ = Ground state oxygen

$(^3\Sigma_g^-)$ = Ground state oxygen

τ_F = Fluorescence lifetimes

τ_T = Triplet state lifetimes

T = Temperature

T_1 = First excited triplet state

T_n = n^{th} Triplet state

λ = Wavelength of the acceptor

W_{DPBF} = Singlet oxygen scavenger photobleaching rate in the presence of the phthalocyanine sample

W_{DPBF}^{Std} = Singlet oxygen scavenger photobleaching rate in the presence of the standard sample

LIST OF FIGURES

LIST OF SCHEMES

LIST OF TABLES

Introduction

1

In this chapter a general preamble of quantum dots and the grounds for their unique properties and characteristic behaviour is given. A brief prelude of Au nanoparticles and their synthetic method is also included. A general introduction to the synthetic routes for quantum dots, their fluorescence lifetimes as well as their electrochemistry is considered. An overview on metallophthalocyanines (MPcs); their photophysicochemical properties and the properties they elicit in both the presence and absence of CdTe quantum dots or Au nanoparticles are also considered.

1.1 Quantum Dots

1.1.1 Basic properties of QDs

Quantum dots (QDs) are inorganic semiconductor nanocrystals composed of hundreds to hundreds of thousands of atoms and they have different electronic properties from their bulk material by virtue of their size [1,2]. A nanocrystal is referred to as a quantum dot if an electron-hole pair (exciton) is confined by a potential barrier in all the three directions, Figure 1.1. This inability of the bound exciton to move in all possible three directions is referred to as quantum confinement and for this reason QDs are considered to be zero dimensional structures [3-9]. QDs have diameters which are either close to or below the bulk material's Bohr-exciton radius. The Bohr-exciton radius that stipulates the size of QDs is the distance between the bound electron and hole pair in the excited state [8]

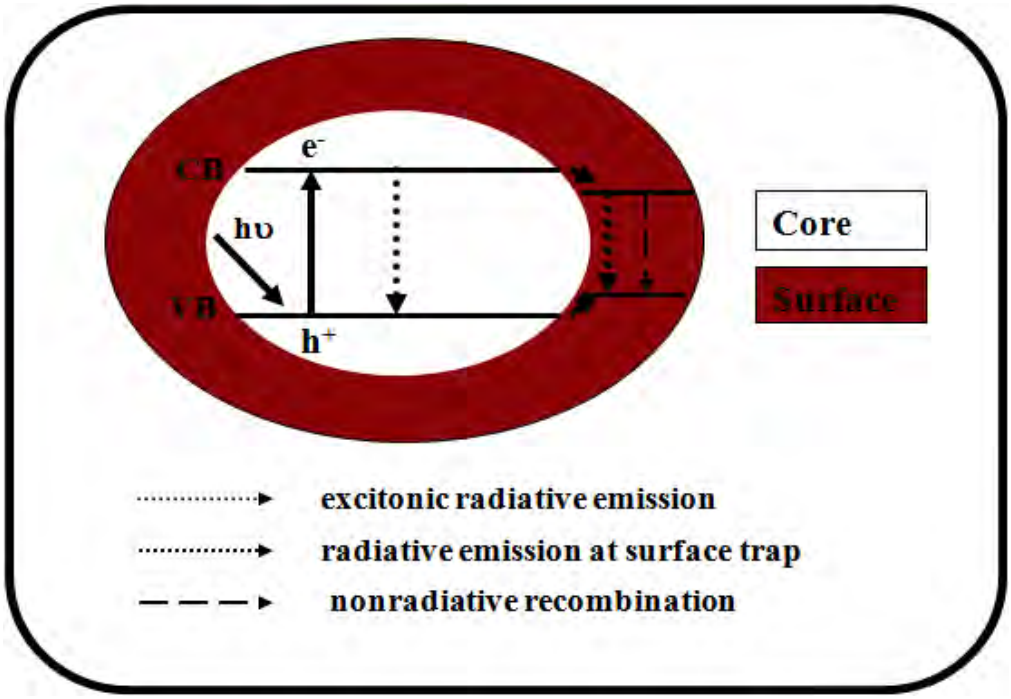

Figure 1.1: Representation of the confinement of the electron-hole pair in a quantum dot and the fate of the excited electron and hole pair within the zero dimensional structure [9].

Semiconductor nanoparticles (NPs) may be comprised of elements from groups 12-16 (II-VI), 13-15 (III-V) or 14-16 (IV-VI) of the periodic table. A few examples of QDs made from elements from these groups include ZnSe QDs, CdTe QDs (studied in this work), GaAs QDs and Si QDs. Gold (Au) NPs whose size is below the gold exciton Bohr radius may also be considered as QDs (also studied in this work). Over the past decade numerous studies have been carried out on semiconductor nanoparticles (CdTe QDs), including their conjugation to biomolecules and photosensitizers, however there have been very few conjugation studies with AuNPs. Due to this realisation, AuNPs are studied with the anticipation of attaching them to photosensitizers of choice in this work and thereafter to study the photophysicochemical properties of the conjugate. Since QDs may be constituted of a few hundred atoms they behave more like artificial atoms in that they have discrete energy levels [10-12]. As a result of the discrete energy levels in QDs, the nanoparticle band gap ($E_{g,QD}$) is larger than that for the bulk material ($E_{g,bulk}$) but smaller than for atoms ($E_{g,atom}$), Figure 1.2. [11-13].

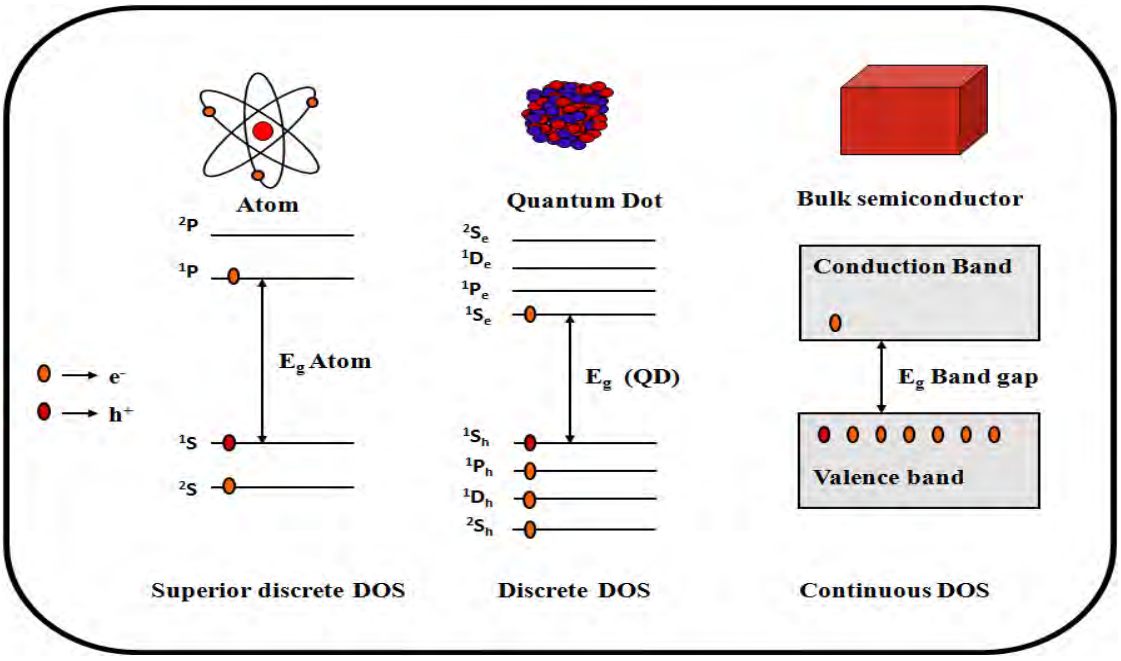

Figure 1.2: Representation of energy levels in atoms, quantum dots and bulk materials [13].

There is a significant deviation of the electronic, optical and physical properties of QDs from those of the bulk material [10,11]. The difference in properties of the QDs compared to bulk material is due to the quantum confinement of the exciton in the semiconductor nanoparticles. Quantum confinement is better described with the use of the distribution of the density of states (DOS), Figure 1.3 [14].

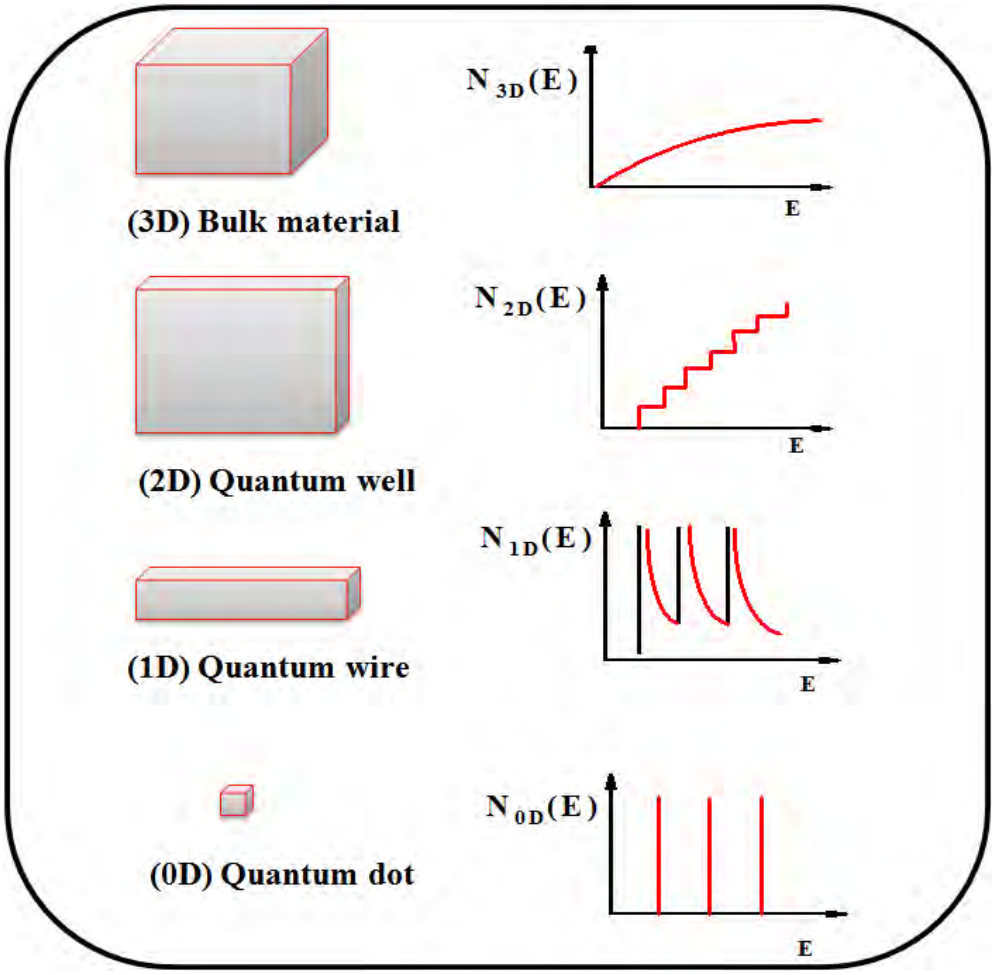

Figure 1.3: The progression of quantum confinement and the effects on the density of states [14].

Figure 1.3. shows QDs (0D) to have electronic confinement of the exciton in all three dimensions while quantum wires are one dimensional (1D) because the exciton is confined in two dimensions, while other materials such as quantum wells have their exciton confined in one dimension and are thus described as two dimensional (2D)

because the electron-hole pair can only move in two spatial dimensions and the bulk material is three dimensional (3D) since there is no confinement of the exciton [14,15], Figure 1.3.

1.1.2 General applications of quantum dots (QDs)

Quantum dots have unique properties conferred upon them by the quantum confinement of the exciton. These exceptional properties include size tuneable optical properties, photophysicochemical stability, and large surface area [16-19]. They are known to have a broad excitation range that spans the ultraviolet (UV) to the infrared (IR) region of the electromagnetic spectrum. In addition, they boast narrow emission spectra and exhibit excellent photoluminescence quantum yields. As a result of this distinct quality they are becoming more favourable than organic fluorophores in bioimaging applications [20]. They also find applications in for example; the manufacturing of light emitting diodes (LEDs), in quantum computing, in biomedicine and catalysis [2,4,19,21-23]. In the biomedical field, QDs are used for bio-labelling (e.g of tumour tissues), drug delivery and also in therapeutics such as photodynamic therapy (PDT) of cancer [3,22-24].

QDs have been reviewed for use in PDT because they can readily undergo intersystem crossing from the excited singlet state to the triplet state due to the heavy metal atoms which constitute them [24]. QDs in the triplet state then transfer energy to the ground state oxygen (($^3O_2$), which is also in the triplet state) thereby generating the cytotoxic singlet oxygen species ($^1O_2$) [24,25]. The results up until now however suggest that QDs result in very minimal cytotoxic specie this way [25]. As a result they are being used in combination with photosensitizers (e.g. phthalocyanines [26]) that have proved to be excellent PDT candidates, because it has been shown that they enhance the photosensitizer properties as well as allowing for imaging of tumour sites under treatment and thus making it possible to monitor necrosis of the tumour [25].

1.1.3 Methods of Synthesis of QDs

1.1.3.1 Semiconductor QDs

Varied methods for the synthesis of QDs are in use. They can however be split into three main categories; solid phase growth, gas phase growth and solution phase growth of QDs [27-30]. In this work the solution phase growth of QDs was employed and hence it is discussed. Solution phase growth of QDs is divided in two: the organic synthetic route and the aqueous route. The organic synthetic route involves the rapid injection of metal organic precursors into a very hot coordinating solvent under vigorous stirring [28]. In this synthetic pathway long chain alkylphosphines (e.g. trioctylphosphine (TOP)) and alkylphosphine oxides (e.g. trioctylphosphine oxide (TOPO)) may be used to anneal and passivate surface defects that form during the growth of QDs. The aqueous pathway for making QDs is an aqueous synthetic procedure which is favoured because it affords water soluble QDs [4]. Water soluble QDs are greatly desired especially for therapeutic applications since they would be more readily administered to patients [30].

The aqueous route has been employed to synthesise a considerable number of nanoparticles like HgTe, CdS, CdTe, CdSe, ZnO and ZnS QDs [4,31-35]. For the purpose of this work, water soluble QDs were focused on and special consideration was directed to CdTe QDs and to a lesser extent ZnS and AuNPs were also given attention. The common synthesis of water soluble QDs would require the dissolution of a particular metal salt (e.g. $CdCl_2$, as the source of Cd^{2+} ions for QD nucleation) in water. Water Solubilizing stabilizer (capping) reagents of choice are then added to the metal salt of interest in the aqueous media and to this mixture NaOH solution is added to adjust the pH so that it ranges from pH 9 to 12. The resulting mixture is then left under inert conditions for some time, after which H_2Te gas may be bubbled into the oxygen free mixture of the metal salt and stabilizer reagent or NaHTe solution may be introduced instead of the H_2Te gas, Figure 1.4 [4,32]. This causes nucleation of QDs which grow via the Ostwald ripening process upon heating, Figure 1.4 [4].

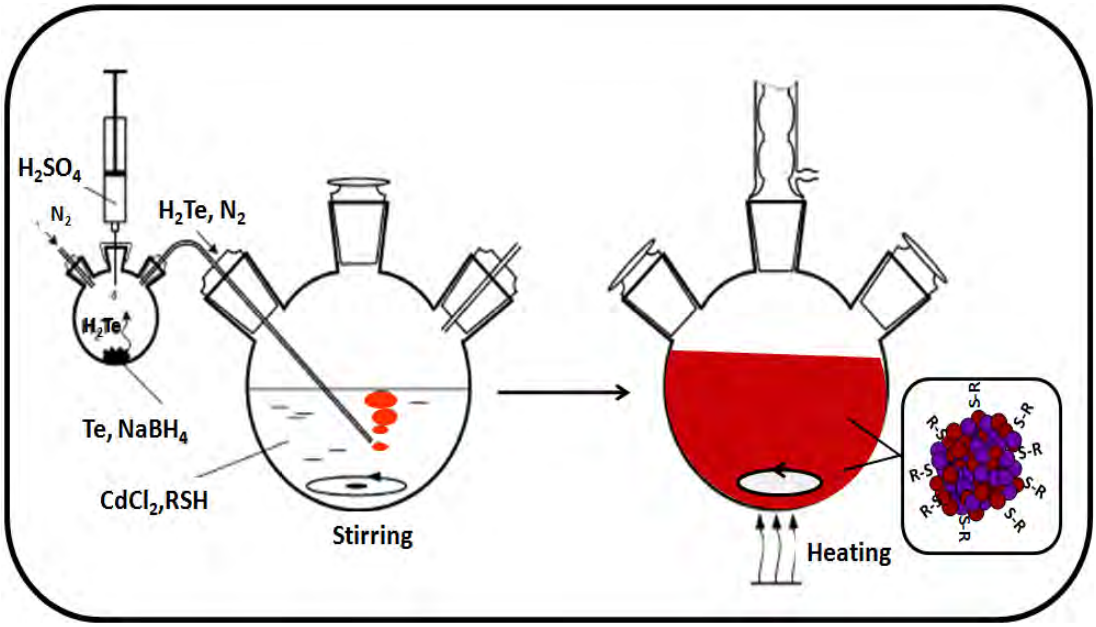

Figure 1.4: Schematic representation of the aqueous synthesis of quantum dots [4].

The growth of QDs to a desired size can thus be controlled and monitored since their growth involves a shift of the photoluminescence (PL) emission from the blue to the red of the visible spectrum [11,13,22]. Common stabilizer groups that were employed for this work include mercaptoethanol (ME), mercaptopropionic acid (MPA) and thioglycolic acid (TGA) and these bind to the surface of QDs via a coordinate covalent bond through the thiol group while terminating with hydroxyl and carboxyl moieties respectively, Figure 1.5. These stabilizers are responsible for the passivation of surface defects or dislocations that may be formed during growth of QDs and allow for the monodispersity of these nanoparticles [4,12,31].

The mercapto stabilizing groups play a huge role in controlling the QD structure as well as their stability thus affording good quality QDs which exhibit narrow PL emission and high PL quantum yields [19,31,32]. Success in making good quality nanoparticles is realized when QDs show excellent crystallinity, and a narrow size distribution which lies within 2% [36]

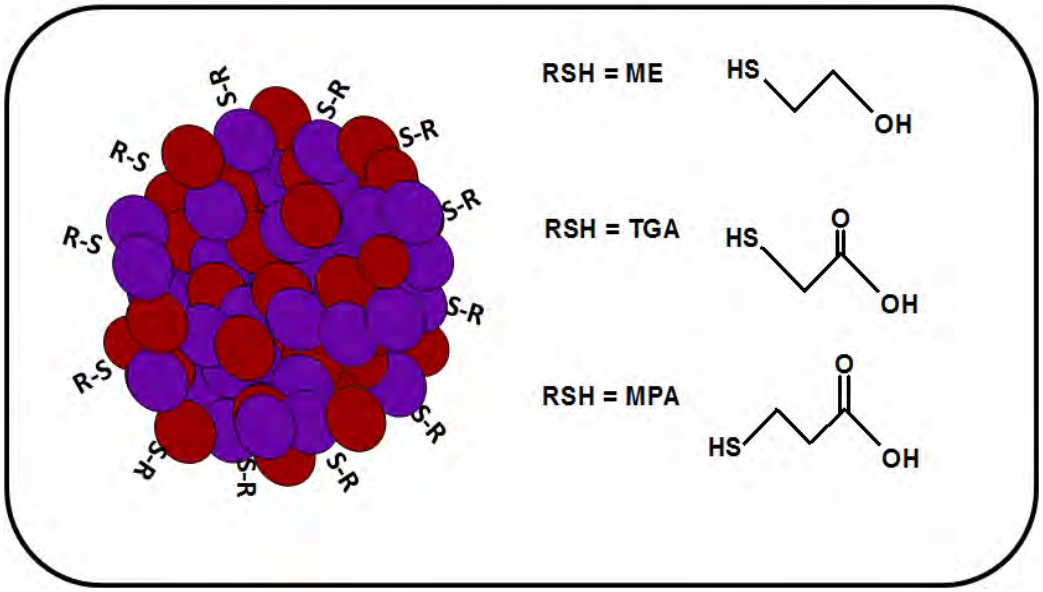

Figure 1.5: Schematic representation of a stabilized CdTe QD and the structures of water solubilizing groups used in this work.

An alternative method towards the preparation of water soluble QDs is that of employing hydrophobic QDs in a capping exchange strategy. This approach usually involves forming a ZnS or ZnSe shell around the core of the QDs under modification e.g. CdTe or CdSe QDs so as to enhance the photophysicochemical stability of the QDs upon removal of the organic stabilizing groups. It also eliminates surface defects or dangling bonds on the surface after removal of the original organic TOP or TOPO ligands [37,38]. When the ZnS or ZnSe shell has been successfully set over the core of the QD, stabilizer groups that facilitate hydrophilicity are introduced e.g. mercaptocarbonic acids or polyethylene glycol (PEG). The choice of the stabilizer to be used is very important because the stabilizer groups are the means by which QDs interact with their immediate environment. The different moieties available on the stabilizer molecule have the potential to allow for hydrogen bonding, electrostatic interactions, adsorption and they can in most cases enable linking of QDs to biomolecules (e.g. for bioimaging) or functionalized therapeutic drugs (e.g. for PDT) [39].

1.1.3.2 Gold Nanoparticles (AuNPs)

Gold nanoparticles are also used in this work and as such their synthesis is briefly described. AuNPs may be synthesized using various methods also [40-43]. The more common route towards their synthesis involves reduction of the gold salt by well known reducing agents e.g. potassium bitartrate, sodium borohydride and polyethyleneglycol (PEG) [42]. In most syntheses the reducing agent employed also serves the function of a phase transfer agent or protecting ligand as is the case with PEG. In the synthesis of the AuNPs, an aqueous or organic media and even a mixture of both solvents may be used depending on the reducing agent of choice. In this work tetraoctylammonium bromide (TOAB) was used as a phase transfer agent for the AuNPs, Figure 1.6 [40].

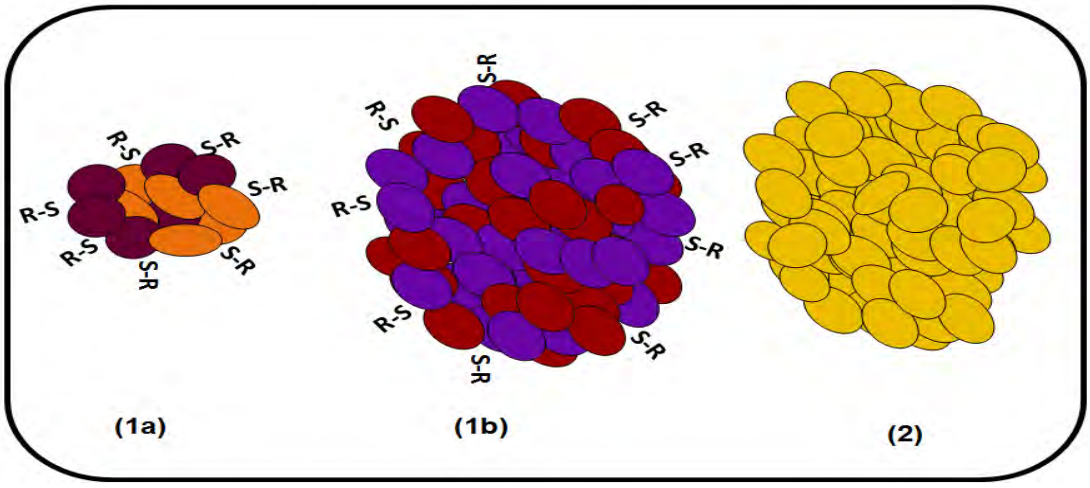

Figure 1.6: A representative schematic of mercapto ligand stabilized ZnS QDs (1a), CdTe QDs (1b) and tetraoctylammonium bromide (TOAB) stabilized AuNPs (2).

1.1.4 Characterization of QDs

There are varied methods of characterization of nanomaterials. One such method is that of electron microscopy (EM). Scanning electron microscopy (SEM) and transmission electron microscopy (TEM) are both forms of electron microscopy that image samples of very small sizes [44,45]. SEM is a powerful tool in the investigation

of surface topologies of samples. Figure 1.7 shows a representative SEM image of QDs [46].

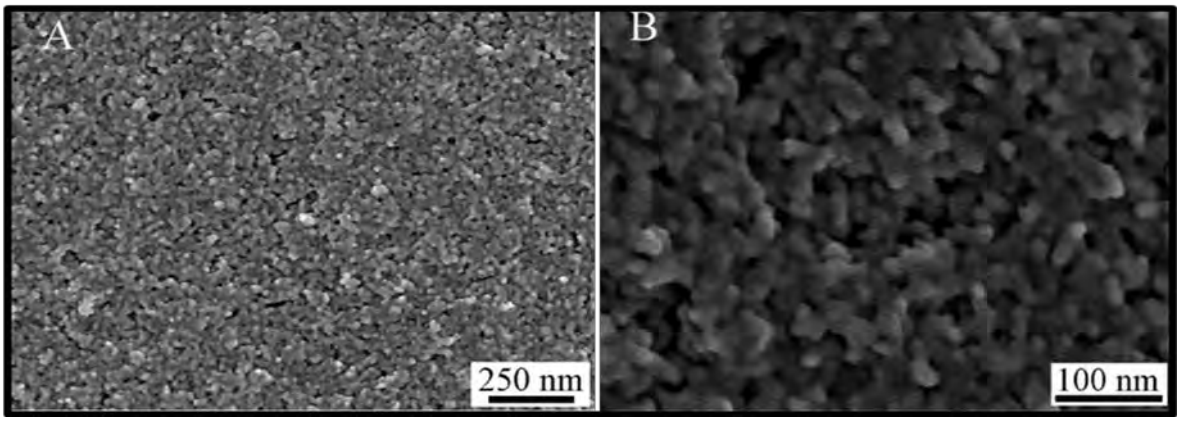

Figure 1.7: Typical SEM images of CdTe QDs at two different magnifications A and B [46].

TEM on the other hand can be used to obtain information on the surface arrangement of atoms in an augmented local microstructure [4,47]. The TEM specimens can be magnified up to 500, 000 times and this makes it possible to image individual atoms of a cluster in a given sample, Figure 1.8 [45,48].

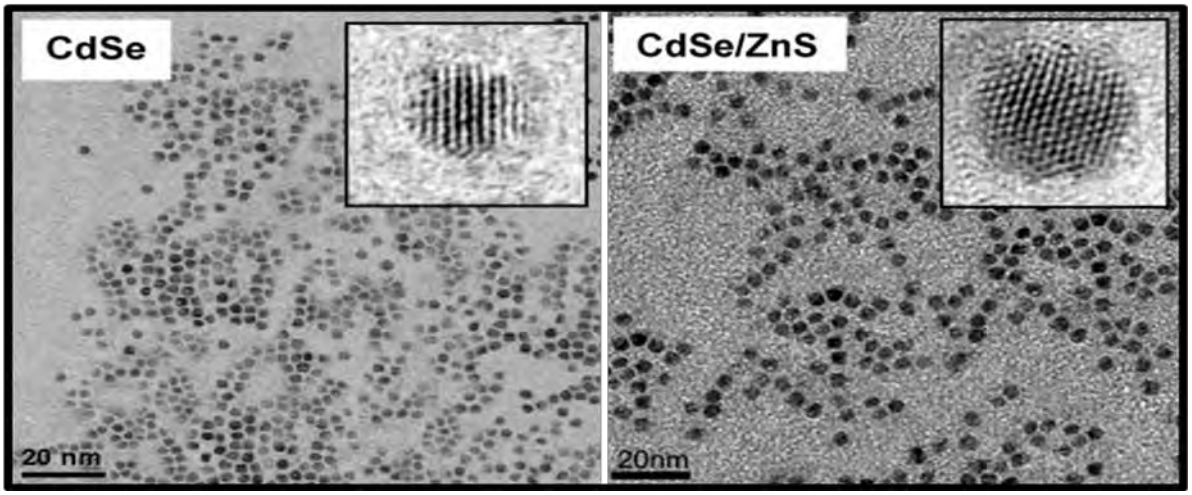

Figure 1.8: Typical TEM images of CdSe QDs in the absence and presence of a ZnS shell [48].

Scanning probe methods such as scanning tunnelling microscopy (STM) and atomic force microscopy (AFM) may also be used to determine details about the surface topography. AFM measurements of QDs are usually taken in the semi contact (tapping) mode at ambient conditions [49]. A representative AFM image of CdTe QDs is shown in Figure 1.9.

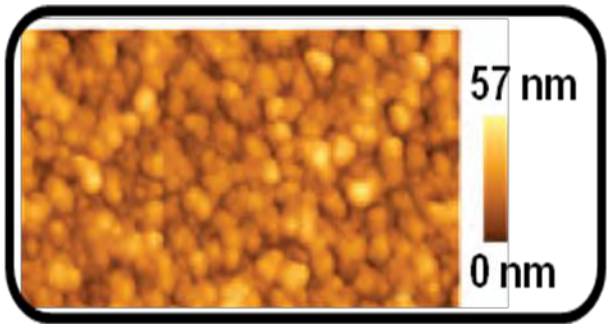

Figure 1.9: Typical CdTe QD AFM image [49].

Among other commonly used methods for QD characterization are FT-IR and x-ray photoelectron (XPS) spectroscopies. The latter is mainly used to analyze the structure of the surface and to carry out depth profiling of the specimen. XPS can also be employed to determine the elemental composition and hence the empirical formula of the elements within the given sample. UV-Vis and photoluminescence spectroscopies are used for optical characterization of the QDs as well as size estimation. The estimation of the size of QDs using UV-Vis spectroscopy measurements is carried out by applying the data to a polynomial fitting function [50]:

$$D = (9.8127 \times 10^{-7})\lambda^3 - (1.7147 \times 10^{-3})\lambda^2 + (1.0064)\lambda - (194.84) \quad (1.1)$$

This fitting function is only valid for CdTe and CdSe QDs with sizes within the size range of 1-9 nm [50].

X-ray powder diffraction (XRPD) is another spectroscopic technique used in the determination of the size of QDs as well as the crystalline structure of these

nanomaterials, Figure 1.10 [51-53]. The average size of QDs may be calculated from the Debye-Scherrer equation.

$$d(\mathring{A}) = \frac{k\lambda}{\beta Cos\theta} \qquad (1.2)$$

where k is an empirical constant equal to 0.9, λ is the wavelength of the X-ray source, (1.5405 Å, for Cu), β is the full width at half maximum of the diffraction peak, and θ is the angular position of the peak

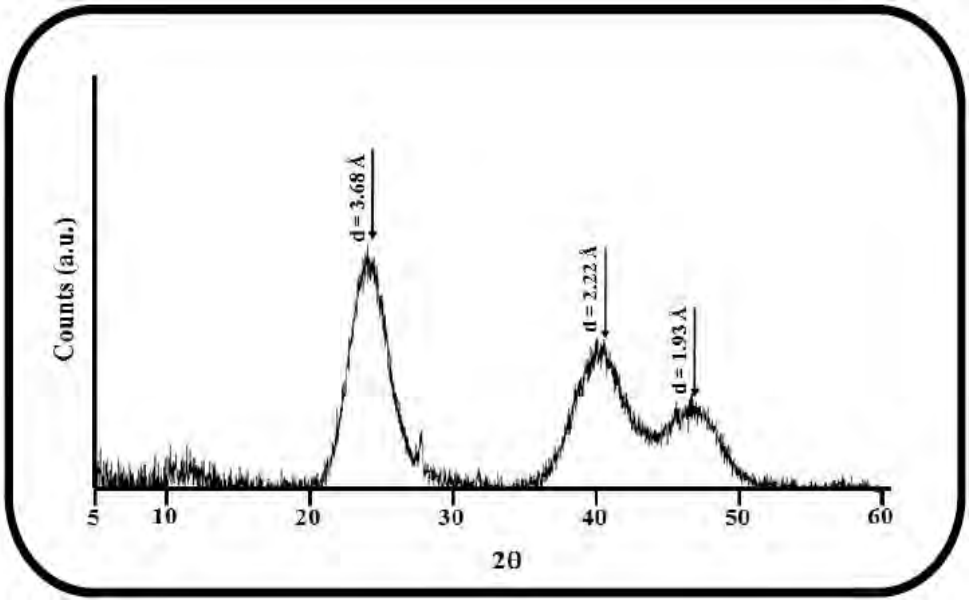

Figure 1.10: A representative XRD spectra of CdTe QDs [53].

AFM (CdTe QDs only), FT-IR, XRD, UV-Vis and PL (except AuNPs) spectroscopies were used to characterize the QDs in this work. These methods were also employed to evaluate the behaviour of these nanoparticles in the presence of MPcs. TEM was also used to characterize AuNPs.

1.1.5 Absorbance and Fluorescence Spectroscopy of Quantum Dots

Quantum dots display unique and exceptional optical properties and these result from quantum confinement effects explained at the onset [54]. The absorbance and emission spectra vary with the size of QDs. As QDs increase in size, the absorbance and emission spectra shift from the visible to the infra-red region [2,14,15]. This is because as QDs grow the band gap in these semiconductor nanocrystals gets smaller hence the emission will appear at longer wavelengths. On the contrary, smaller QDs have larger band gaps and so they have emissions occurring at shorter wavelengths, Figure 1.11 [55]. It is for this reason that the desired optical properties of QDs can be size tuned. The Stokes shift values obtained for QDs are usually quite high as a result of the fairly large separation between their excitation and emission spectra.

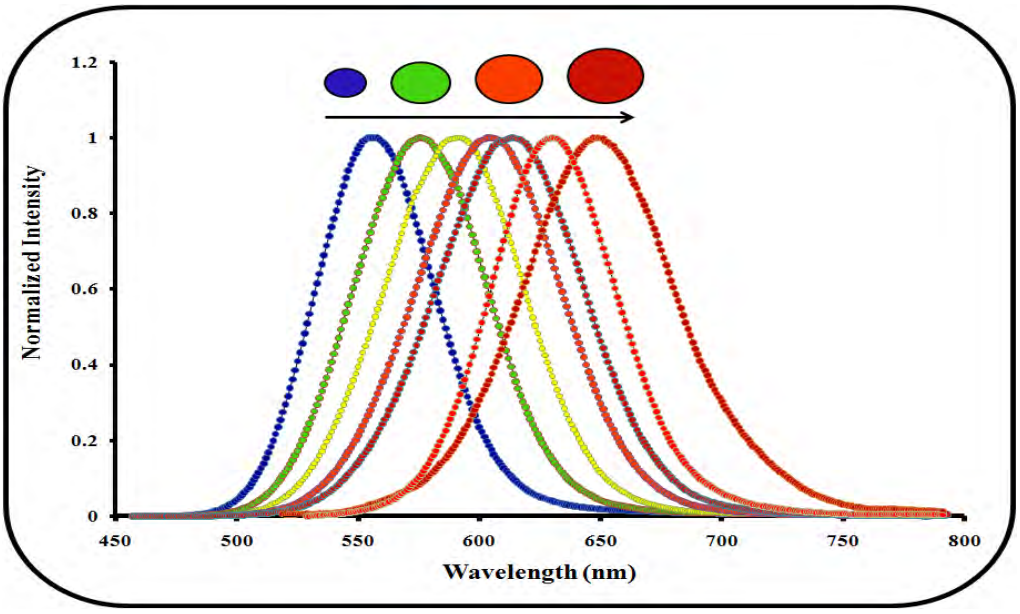

Figure 1.11: Variation of emission spectra with increase in QD size [55].

QDs are characterized by symmetrical narrow emission spectra. The emission spectra however has a tendency to broaden with increase in size and this is brought about by the difference in size and shape distribution of the QDs, but may also be

influenced by the presence of defect sites, as well as the temperature and pH conditions used during the growth of QDs [56,57].

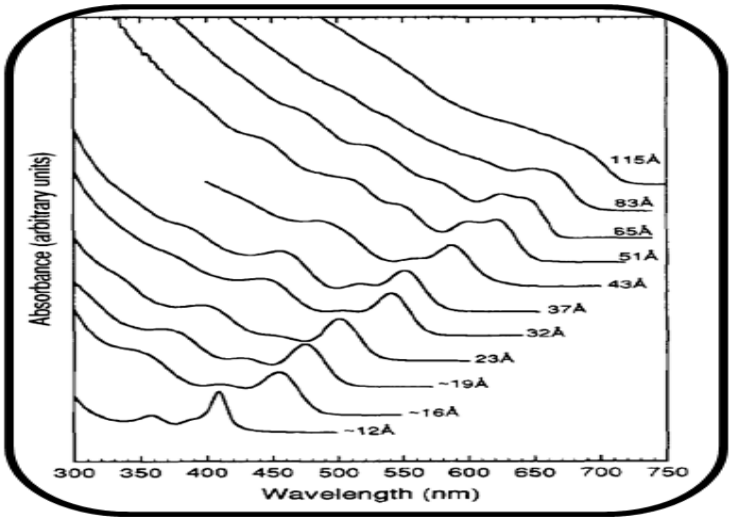

Figure 1.12: Variation of absorption spectra with increase in CdSe QD size [58].

The QDs absorption spectra, Figure 1.12, are also quite sensitive to the size and shape distribution, presence of defect sites, degree of quantum confinement as well as growth conditions employed in the synthesis of QDs [58]. Stable QDs and of fine quality are characterized by the presence of one or more electronic transitions in the absorbance spectrum but as the QDs grow, the distinct nature of the peaks is usually lost as they merge into one peak or as they flatten off, Figure 1.12 [58,59].

1.1.6 Fluorescence Lifetimes of CdTe Quantum Dots

The studies for fluorescence lifetimes were carried out only for CdTe and a select number of photosensitizers synthesized in this work. Studies on the effect of photosensitizers on the fluorescence lifetimes of CdTe QDs are scanty and so these studies are carried out in this work. Fluorescence lifetimes of QDs still remain a heated topic of debate and as such there exist different views on the interpretation of the sets of lifetimes that may be obtained. The fluorescence lifetimes of QDs vary

with size, solvent used, stabilizer agent used and the makeup of the QD [60,61]. Biexponential and triexponential decay kinetics are quite common for CdTe QDs [62-64]. In the biexponential decay kinetics setting, the much longer lifetimes (slow decay component, τ_{F1}) have been ascribed to excitonic recombination from the surface defect sites because it is well established that defect states trap excitons thereby leading to increased radiative lifetimes [63]. The shorter lifetime (fast decay component, τ_{F2}) has been attributed to the excitonic recombination within the core of the QDs [62,63]. For the triexponential decay kinetics, the much longer lifetimes τ_{F1} have been suggested to involve carrier recombination processes in the defects sites while the intermediate fluorescence lifetime component τ_{F2} is attributed to the radiative electron-hole recombination processes at the surface states [64]. The shorter lifetime τ_{F3} has been suggested to be for the excitonic recombination at the band edge or surface of the core of the QDs [64]. Due to the controversy about the origin of the slow and fast decay component lifetimes, bold assertions as to the assignments of these lifetimes cannot be made as yet. A typical fluorescence decay curve for CdTe QDs is shown in Figure 1.13 [53].

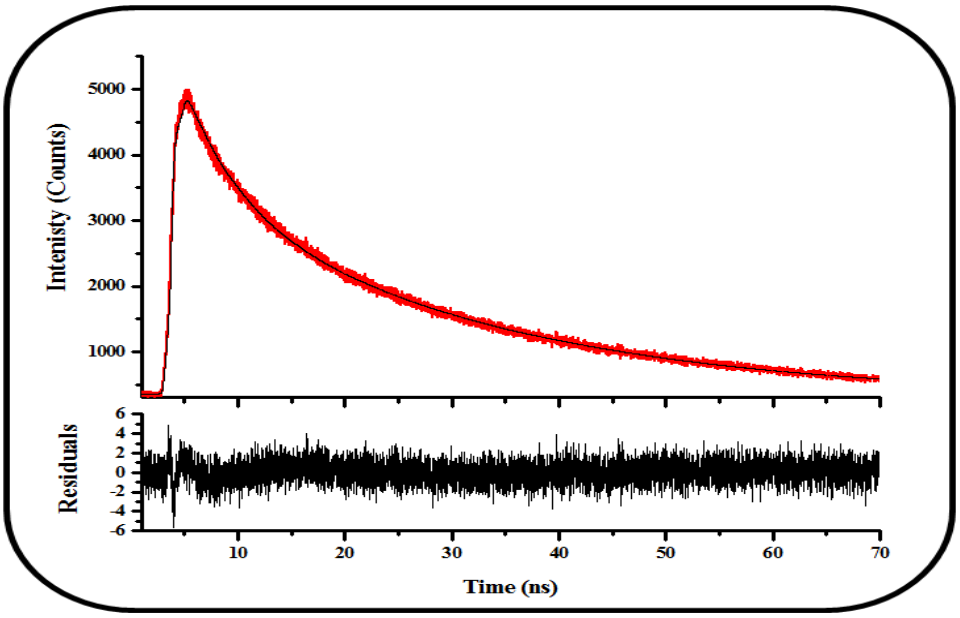

Figure 1.13: A representative fluorescence decay curve for MPA CdTe QDs in 0.1 M NaOH [53].

1.1.7 Electrochemistry of CdTe QDs

Electrochemical studies were only carried out on CdTe QDs for the purpose of this work. Electrochemical studies have been carried out on CdTe QDs of different sizes and hence of different optical properties [9,65]. A typical cyclic voltammogram (CV) of CdTe QDs is shown in Figure 1.14. The CV studies of CdTe QDs were done in this thesis with a view to drawing a relationship between the electrochemical properties of QDs and their corresponding sizes, stability and optical properties. Correlations of this kind are very important, especially since QDs are currently an exciting subject in bioapplications [66]. The CV studies are employed to obtain information of great value about the redox properties of QDs as well as information about the surface of QDs and the electrochemical degradation of these semiconductor nanomaterials [65]. A typical overall oxidation process for CdTe QDs has been shown to result in free cadmium ions in solution as well as tellurium oxides, equation 1.3 [67].

$$CdTe + 6\ OH^- \rightarrow Cd^{2+} + TeO_3^{2-} + 3H_2O + 6e^- \qquad (1.3)$$

There is a direct relationship between the QD redox properties and their band gap energies.

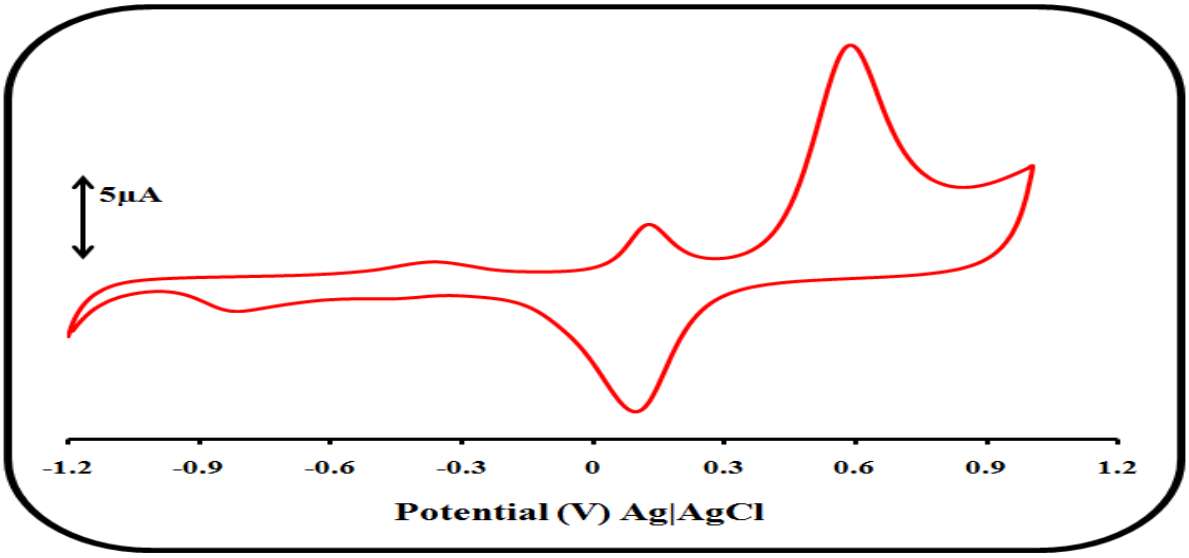

Figure 1.14: A representative cyclic voltammogram for TGA CdTe QDs in pH 9 solution using a gold electrode.

1.2 Metallophthalocyanines

1.2.1 Discovery of Phthalocyanines

Phthalocyanines were first serendipitously synthesized by Braun and Tscherniac in 1907 [68]. The insoluble bluish compound (free-base Pc) then unknown to them had been obtained as a by-product during a synthetic procedure involving the use of phthalamide to make *o*-cyanobenzamide [69,70]. Pc derivatives were encountered by many others but the correct formulation of the complex was achieved by Linstead and co-workers following his unexpected discovery of an iron Pc [71-73]. Linstead conjured up the name phthalocyanine for the bluish complex he had accidentally come across. The root 'phthalo' depicts the structural building block from the phthalic acid precursor while 'cyanine' is from a word (with Greek roots) meaning blue [71-74]. X-ray crystallography characterization of the complex was later carried out to confirm the chemical formula of the metal free Pc to be $C_{32}H_{18}N_8$ by Robertson [75]. These complexes possess intense blue-green colours and this has led to their use in industries as dyes [76]. Due to their robust physical and chemical properties, Pcs find application in various fields such as electrocatalysis [77-79], photocatalysis [80,81], nonlinear optics [82], information storage [83], light emitting diodes [84], as liquid crystals [74,85], semiconductor materials [86] and as photosensitizers in photodynamic therapy of cancer (PDT) [87,88].

The robust physical and chemical properties of Pcs make them desirable for PDT purposes. The use of MPcs for PDT has been approved in a number of countries for selective tumours e.g. oesophageal and gastric cancers. Photosensitizers that have been permitted for use in PDT up to date include Photofrin® and Photosens®, Figure 1.15 [89-92].

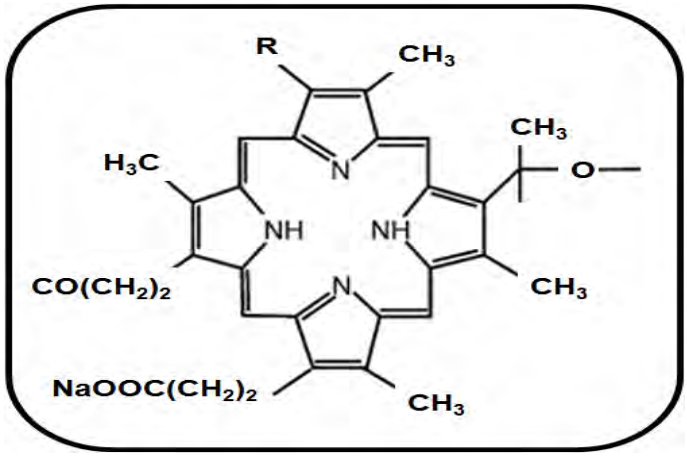

Figure 1.15: Structure of Photofrin® photosensitizer (exists as a mixture of oligomers) [92].

1.2.2 Phthalocyanine Structure

A phthalocyanine molecule is made up of four isoindole subunits which are linked to each other by nitrogen (N) atoms resulting in a closed phthalocyanine ring structure (Figure 1.16) thus rendering these molecules thermally stable [93]. The fused Pc ring by virtue of the four interlinking N atoms possesses a highly conjugated 18 π electron system which is also a major contributing factor in the photophysicochemical stability of Pcs.

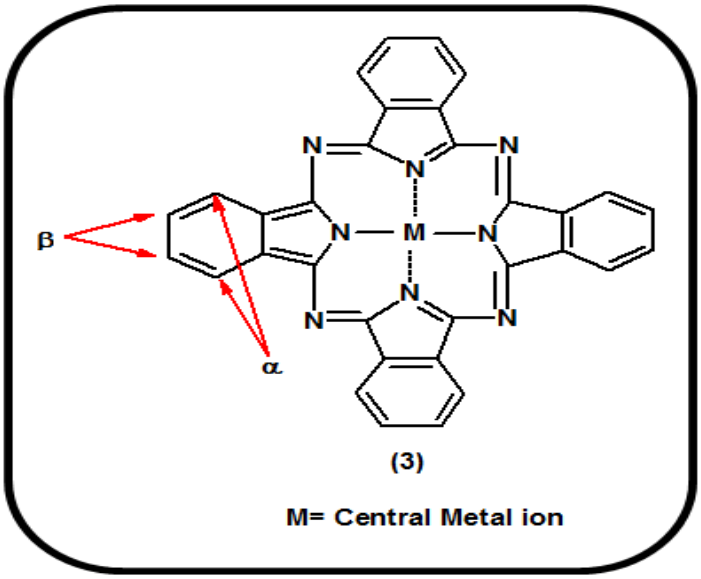

Figure 1.16: Structure of a typical metallophthalocyanine (MPc).

The Pc ring can house a variety of metals resulting in different physical properties e.g. colour of the metallated Pc (MPc), Figure 1.17 [94-96]. Insertion of a metal ion in the Pc cavity has a positive impact on the complex in that the symmetry of the Pc is raised to D_{4h} (for a metallophthalocyanine (MPc **(3)**, Figure 1.16)) from D_{2h} (for an H_2Pc), and the photophysicochemical properties of Pcs are enhanced in the presence of a central metal ion [94].

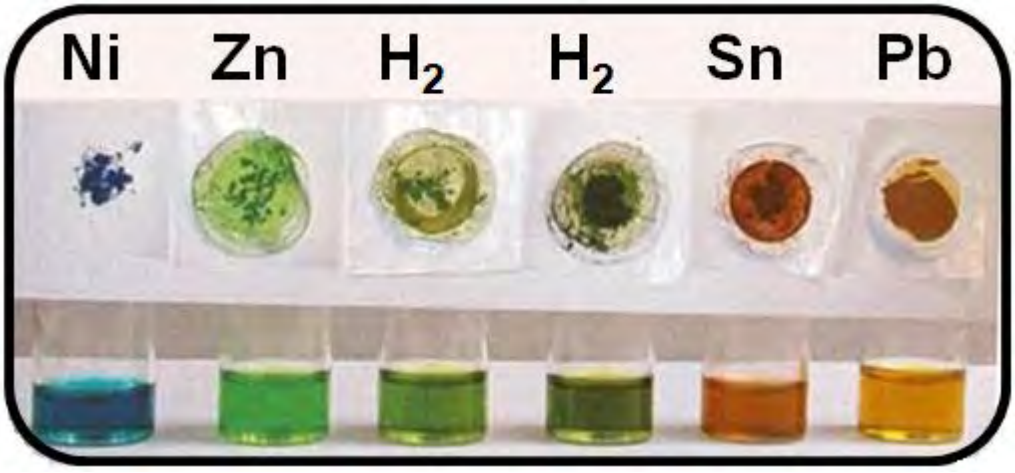

Figure 1.17: A variation of phthalocyanine colours with change in central metal [96].

The variation in the central metal ion, axial substitution on central metal ion, ring substitution, the number of substituents on the Pc ring and their position on the ring (peripheral (β) or non peripheral (α)) greatly affect the inherent properties of MPcs [94,95]. The distance between the two diagonal N atoms in the cavity of the Pc ring is 396 pm, thus because of its small size some large metal ions e.g. In^{3+}, Ge^{2+}, Sn^{2+}, Pb^{2+} do not fit well in to the centre of the ring [94]. As a result the MPc D_{4h} symmetry may be reduced in such cases to C_{4v} symmetry, but this loss in symmetry may be balanced in Pcs whose central metal ions have axial ligands e.g. Cl_2SnPc thus allowing the MPc to retain the D_{4h} symmetry [97].

As stated above phthalocyanines are tetrapyrrolic aromatic macrocycles with a highly conjugated system of 18 π electrons and for this reason they absorb very strongly in the red region of the visible spectrum. The tetrapyrrolic aromatic class of

macrocycles also includes naturally occurring porphyrins **(4)** and tetrabenzoporphyrins **(5)** which are constituted of four pyrrolic units linked by four methine bridging groups, porphyrazines **(6)** as well as tetrabenzotetraazaporphyrins **(7)** (phthalocyanines) whose four pyrrolic units are bridged by azamethine bridges (N atoms), Figure 1.18 [98,99]. Unlike porphyrins, porphyrazines and phthalocyanines are synthetic molecules because they are not naturally occurring. The benzo subunits on Pcs allow for functionalization of these molecules since substituents can be added to the periphery of the respective macrocyclic units.

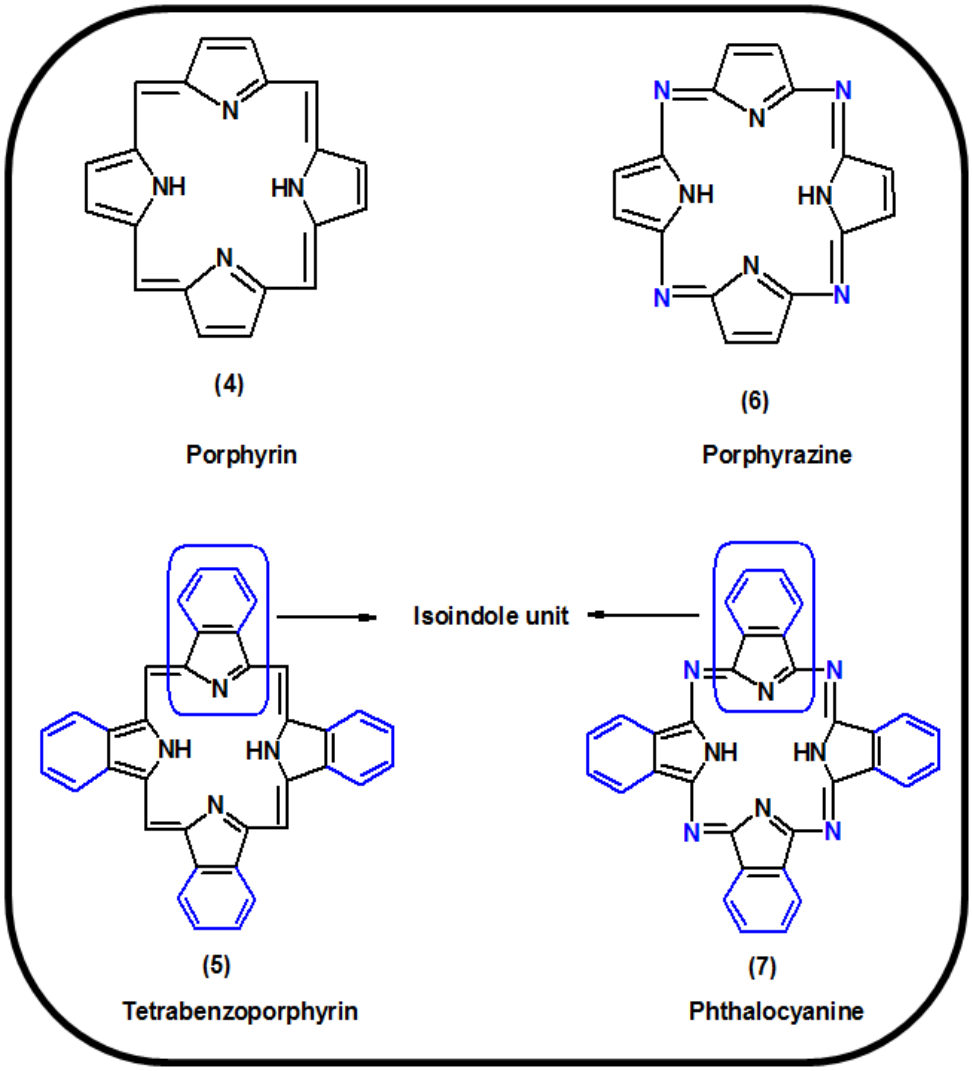

Figure 1.18: Structures of macrocycles included in the tetrapyrrolic class of compounds.

1.2.3 Phthalocyanine Syntheses

There are different routes used for the synthesis of phthalocyanines, be it metallated or metal free, symmetrical or assymetrical. The conditions (e.g. temperature, solvent, catalyst) of a synthetic procedure may be changed so as to optimize yields or the purity of the product sought. Cyclotetramerization of the precursor molecules leads to the formation of Pc macrocyclic complexes.

1.2.3.1 Unsubstituted Phthalocyanines

The synthesis of Pcs may be carried out via different routes involving the use of phthalimide **(8)**, phthalonitrile **(9)**, phthalic acid **(10)**, phthalic anhydride **(11)**, 1,3-diiminoisoindole **(12)** or *o*-cyanobenzamide **(13)** in the absence or presence of a metal salt to afford a metal free or metallated Pc respectively (Scheme 1.1) [100-104]. The synthetic strategy that makes use of the phthalonitrile **(9)** starting material is the simplest and affords a much purer product and also in appreciable quantity [105]. A typical reaction employing the use of phthalonitrile **(9)** usually involves the use of a high boiling point solvent e.g. quinoline and trichlorobenzene but other solvents like 1-pentanol and dimethylaminoethanol (DMAE) may also be used in the presence of a strong base like 1,8-diazabicyclo[5.4.0]undec-7-ene (DBU), or 1,5-diazabicyclo[4.3.0]non-5-ene (DBN) [101]. When there is a need for a catalyst, ammonium molybdate is the most commonly used catalyst of choice especially when using phthalimide **(8)** or phthalic anhydride **(11)** as precursors while urea is mainly used as a source of nitrogen. Labile metal ions may be employed in the cyclotetramerization of the Pc and can be exchanged at a later time for the desired central metal ion or a free base Pc may be synthesized and can then be metallated later [106]. The metallation of this free base Pc **(**H_2Pc, **7)** is achieved by refluxing the H_2Pc in an appropriate solvent in the presence of the metal salt, whose metal ion can fit into the cavity of the Pc ring [107].

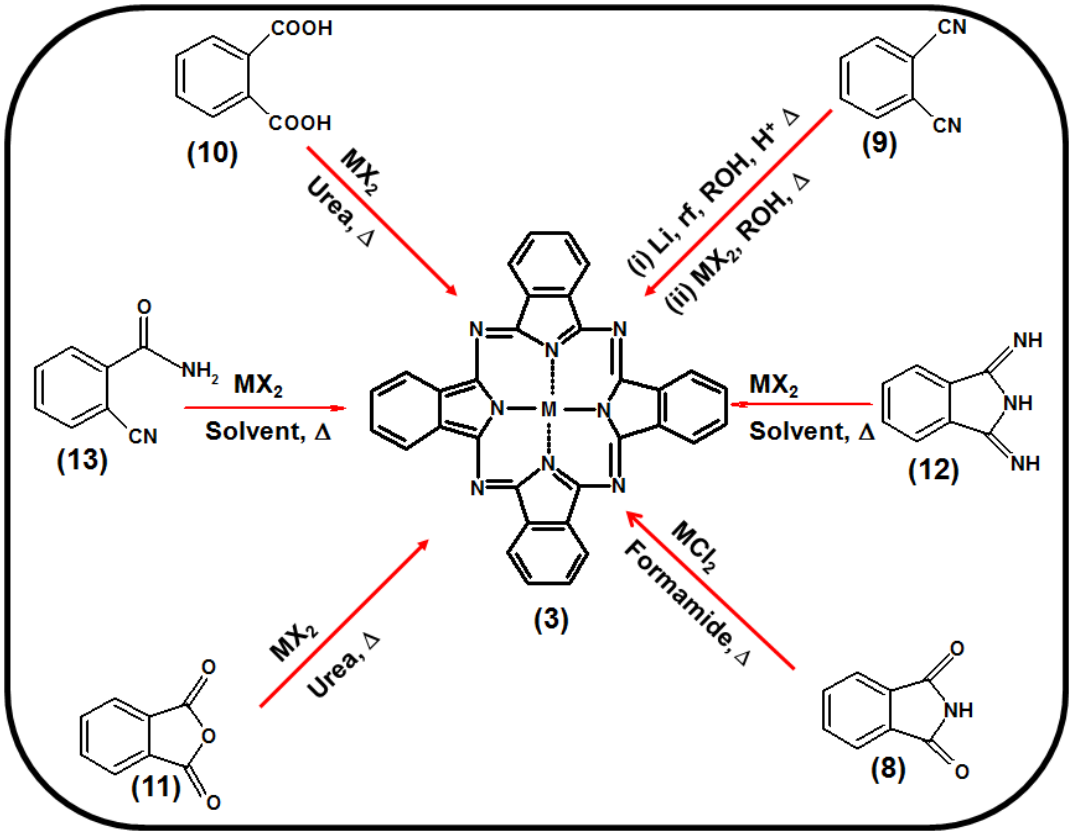

Scheme 1.1: Typical approaches for the synthesis of MPcs.

1.2.3.2 Substituted Phthalocyanines

Unsubstituted Pcs generally have limited solubility in most organic solvents and aqueous media. The main reason for this behaviour stems from the high degree of hydrophobicity that is demonstrated by the highly conjugated Pc macrocycle. These unsubstituted Pc structures result in highly stable crystallographic configurations accompanied by high molecular lattice energies. Substitution on the periphery of the Pc as well as on the central metal ion (axial ligation for multivalent metal ions) has been shown to aid the solubilization of the Pc. The benzo subunits that are present in phthalocyanines provide 16 positions for substitution on the periphery (both peripheral (**β**) and non peripheral (**α**) positions) of the Pc macrocycle, Figure 1.16.

Substitution may be achieved by the use of an appropriately substituted precursor e.g. mono-, di- or tetra substituted phthalonitrile which would result in tetra-

(Scheme 1.2), octa- (Scheme 1.2) or hexadeca substituted Pc or it may be carried out on a preformed Pc [108,109]. Various groups may be used in substitution and these include alkyl chains, aromatics, amines, thio groups and halides. Substitution of Pcs has been demonstrated to somewhat alter the electronic properties of the macrocyle [110,111]. Another important reason for the necessity of substitution is to tackle the problem of aggregation of Pcs and this problem is solved by incorporation of bulky or long chain substituents into the framework of Pcs [112,113].

Tetra substituted Pc derivatives generally have greater degree of solubility than octa substituted derivatives. The solubility of the tetra substituted Pcs is mainly enhanced because the synthesis of such a Pc results in the formation of constitutional isomers while the octa substituted Pcs only have one isomer [108,110]. Some of these constitutional isomers have an unsymmetrical arrangement of substituents on the periphery of the Pc ring resulting in a change in the centrosymmetry of the Pc leading to a high dipole moment that leads to increased solubility. The tetra β-substituted constitutional isomers obtained are of C_{4h}, D_{2h}, C_{2v}, and C_s symmetry with 12.5 %, 12.5 %, 25 % and 50 % distributions respectively and they can be separated with the use of high performance liquid chromatography (HPLC) [114,115].

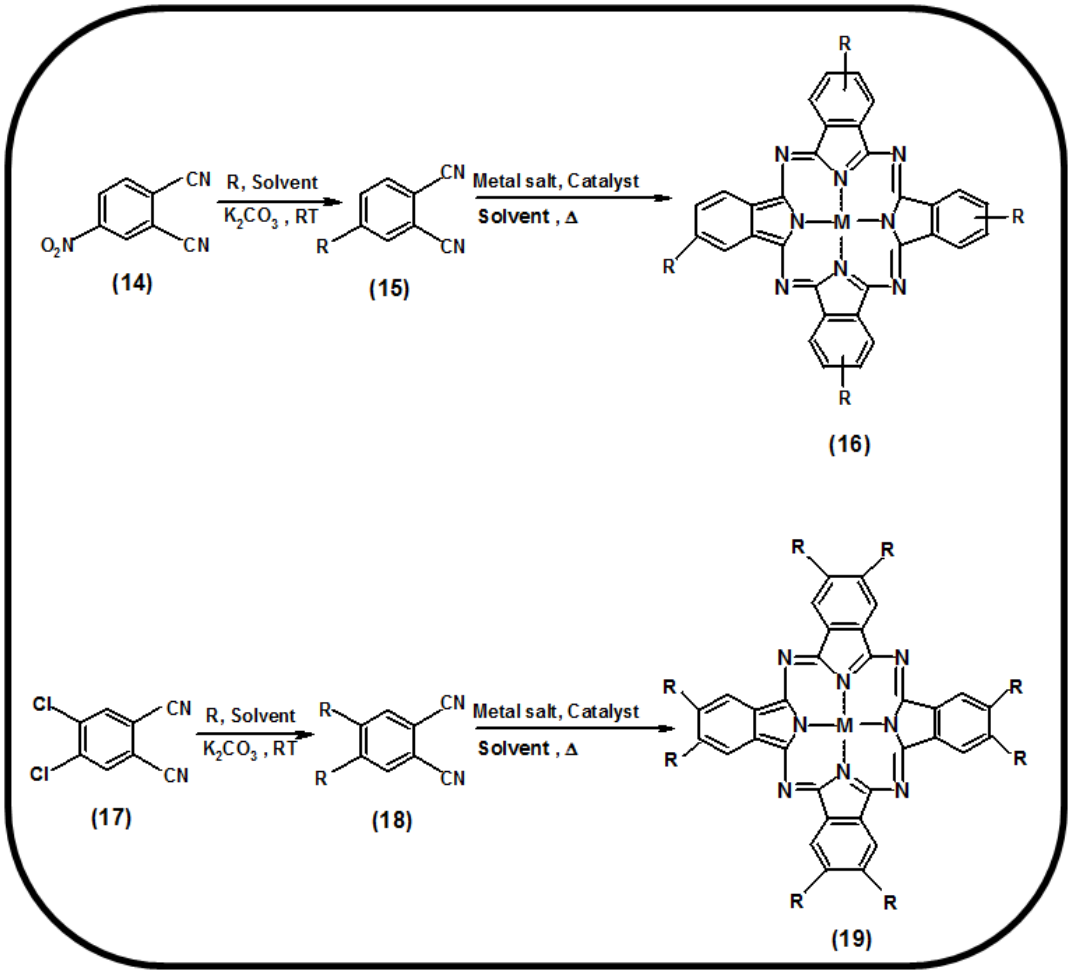

Scheme 1.2: Synthetic approach to tetrasubstituted (16) and octasubstituted (19) MPcs from peripherally monosubstituted (15) and disubstituted (18) phthalonitriles.

1.2.3.3 Water soluble phthalocyanines

Water solubility in phthalocyanines may be accomplished by introducing hydrophilic substituents like carboxy, sulphonate and phosphono groups onto the Pc framework [116-119]. The sulphonate and carboxy groups are the most commonly used to confer solubility in aqueous media. One of the most widely used methods of sulphonation is by Weber and Busch, which employs a monosodium salt of sulphonic acid and involves heating this salt in the presence of a metal salt, catalyst and urea in nitrobenzene to form a tetrasulphonated MPc (MTSPc) [117]. However, simpler methods for tetrasulphonation of MPcs have been realized, Scheme 1.3 [120]. Sulphonation may also be carried out on preformed Pcs, although this would result

in a mixture of sulphonated Pcs: mono-, di,-, tri- and even tetra sulphonates which all would show different degrees of solubility due to the minor differences in polarity in the sulphonate mixture ($MPcS_{mix}$) [121].

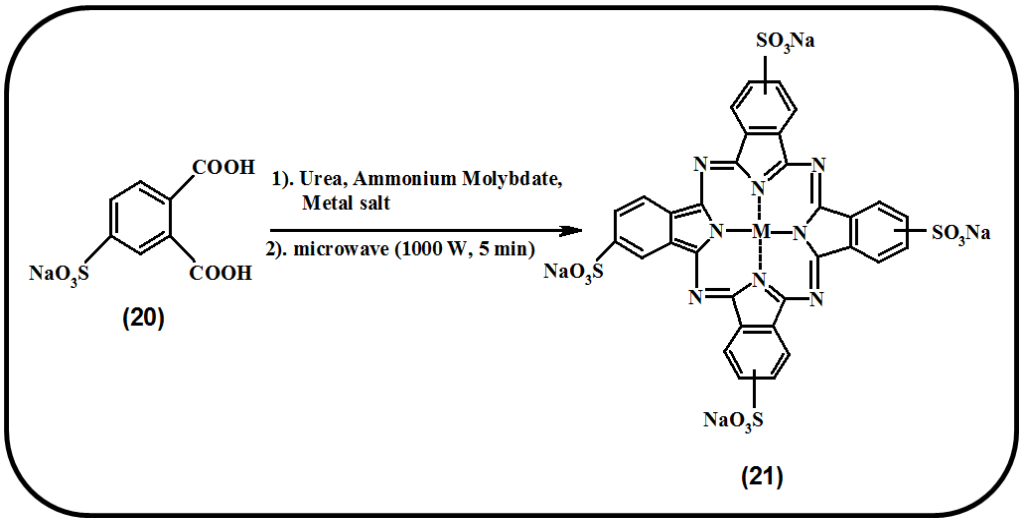

Scheme 1.3: Synthesis of tetrasulphonated MPc (MTSPc, (21)) using a microwave method [120].

The introduction of carboxy substituents onto the Pc ring proceeds via formation of Pc intermediates for both the tetra and octa substituted MPcs [118,122,123]. In Scheme 1.4 the preparation of tetracarboxymetallophthalocyanine (TCMPc, **23a**) from trimellytic anhydride **(22a)** in the presence of urea and ammonium molybdate as a catalyst is shown [118,123]. The final step involving hydrolysis using 10 % potassium hydroxide solution yields the tetracaboxy MPc complex. Included in Scheme 1.4 is the preparation of octacarboxymetallophthalocyanine (OCMPc, **23b**) from Benzene-1,2,4,5-tetracaboxylic dianhydride (**22b**) and the final step involves hydrolysis of the octacarboxy Pc intermediate with 20 % aqueous HCl solution.

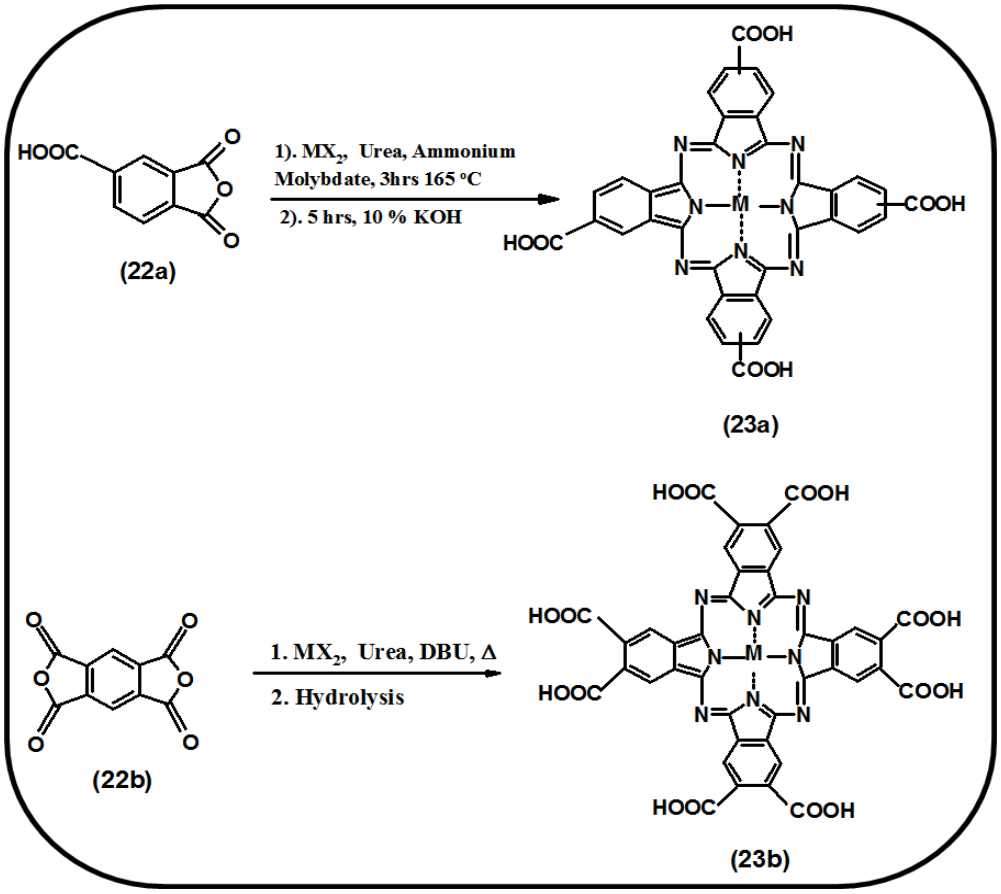

Scheme 1.4: Synthesis of tetracarboxymetallophthalocyanine (TCMPc, (23a)) and octacarboxymetallophthalocyanine (OCMPc, (23b)).

In addition to sulphonation and carboxylation of the Pc framework, Pcs can be made water soluble by quaternization. For this to be possible, the benzo ring in Pcs may either be replaced with a pyridine ring or the pyridine ring may be introduced as a substituent, after which methylation of the nitrogen atom of the pyridine ring may then be carried out thus conferring a positive charge on the Pc, (Scheme 1.5) [124-126]. The preparation of a tetrapyridinometalloporphyrazine **(25)** and its subsequent quaternization to give a tetra cationic tetrapyridinoporphyrazine **(26)** is shown in Scheme 1.5.

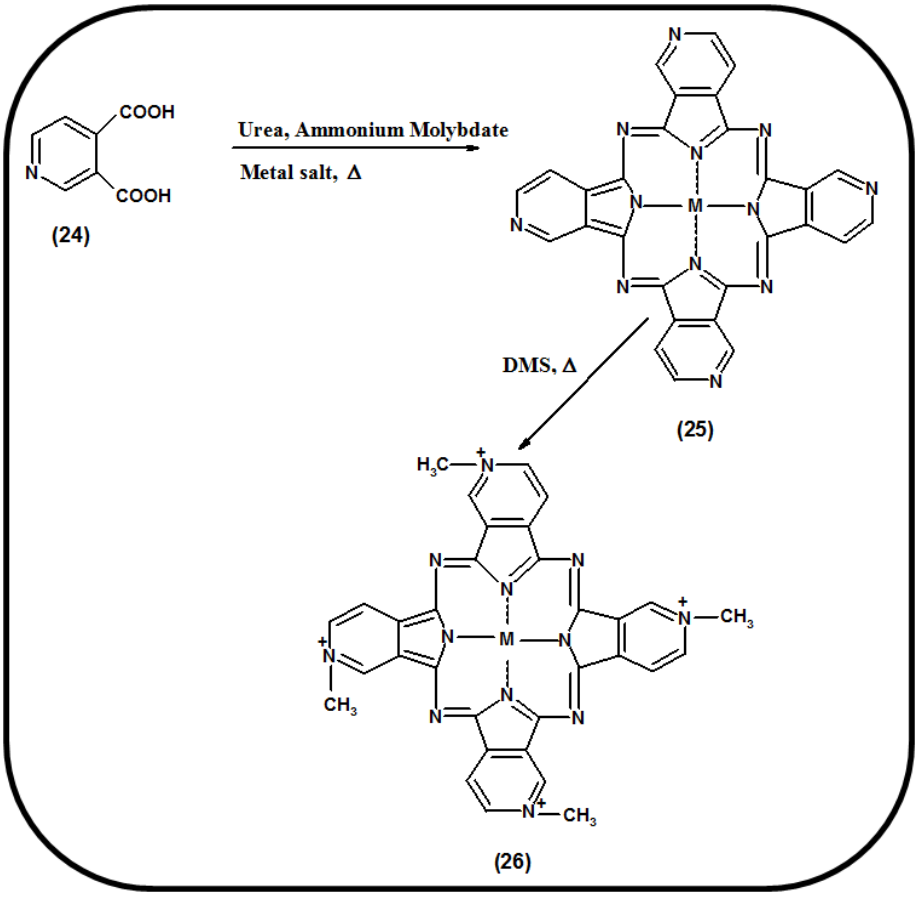

Scheme 1.5: Synthesis of tetra methyl tetrapyridinometalloporphyrazine (TmTPMPz, (26)).

Quaternization is accomplished through the use of reagents such as methyl iodide (CH_3I), dimethyl sulphate (DMS), and diethyl sulphate (DES) [126,127].

1.2.3.4 Phthalocyanines synthesized and studied in this work.

All the MPcs synthesized and studied in this work are shown in Figure 1.19 and Figure 1.20. A few MPcs in this work are soluble in organic solvents, while most of the MPcs are soluble in aqueous media. The main focus on water soluble MPcs was inspired by the proposed line of application which is PDT. In PDT applications, preference is given to water soluble MPcs because these will not elicit solubility problems when intravenously injected into the bloodstream of cancer patients under treatment [26]. Aqueous media soluble MPcs are also known to show less toxicity than their organic soluble counterparts because these can readily be excreted and

cleared from the body [128]. Peripherally tetrasubstituted MPcs are substituted at the positions: 2, 9(10), 16(17), 23(24) of the phthalocyanine ring. In octasubstituted MPcs the peripheral positions of substitution are: 2, 3, 9, 10, 16, 17, 23 and 24 of the phthalocyanine ring. The MPcs shown in Figure 1.19 have been reported on previously. These are tetramethyltetrakis-2,(3)-{pyridinoporphyrazine}zinc(II) **(**TmTPZnPz, **27b)**, zinc(II)tetrasulfonatephthalocyanine **(**ZnTSPc, **28)**, zinc(II)tetracarboxyphthalocyanine **(**ZnTCPc, **29)**, zinc(II)octacarboxyphthalocyanine **(**ZnOCPc, **30)**, tetramethyltetrakis-2,(3)-{2-pyridyloxyphthalocyanine}zinc(II) **(**TmTPyZnPc, **31b)** and tetramethyltetrakis-2,(3)-{2-mercaptopyridinephthalocyanine}zinc(II) **(**TmTMPyZnPc, **32b)**, Figure 1.19 [129,130]. Complexes **27b**, **31b** and **32b** were obtained from the quaternization of complexes **27a**, **31a** and **32a** ((tetrakis-2,(3)-{pyridinoporphyrazine}zinc(II) **(**TPZnPz, **27a),** tetrakis-2,(3)-{2-pyridyloxyphthalocyanine}zinc(II) **(**TPyZnPc, **31a)** and tetrakis-2,(3)-{2-mercaptopyridinephthalocyanine}zinc(II) **(**TMPyZnPc, **32a)**) shown in the first row of Figure 1.19. Although the properties of these Pcs had already been studied and elucidated, their behaviour and properties in the presence of semiconductor quantum dots such as CdTe QDs has not been fully explored. For all these Pcs that were already known, an investigation on their interactions with CdTe QDs with different cappings will be carried out in order to determine the effect of these nanoparticles on the physicochemical properties of the MPcs. Studies on MPc-QD interactions on the photophysical properties of Pcs are necessary since they shed light on whether the combination of Pc and QDs would result in enhanced photophysical properties of the former as has been shown to be the case in several reports [131-134]. These studies of the different forms of interaction between MPcs and QDs yielded intriguing results that would call for further studies employing similar molecules.

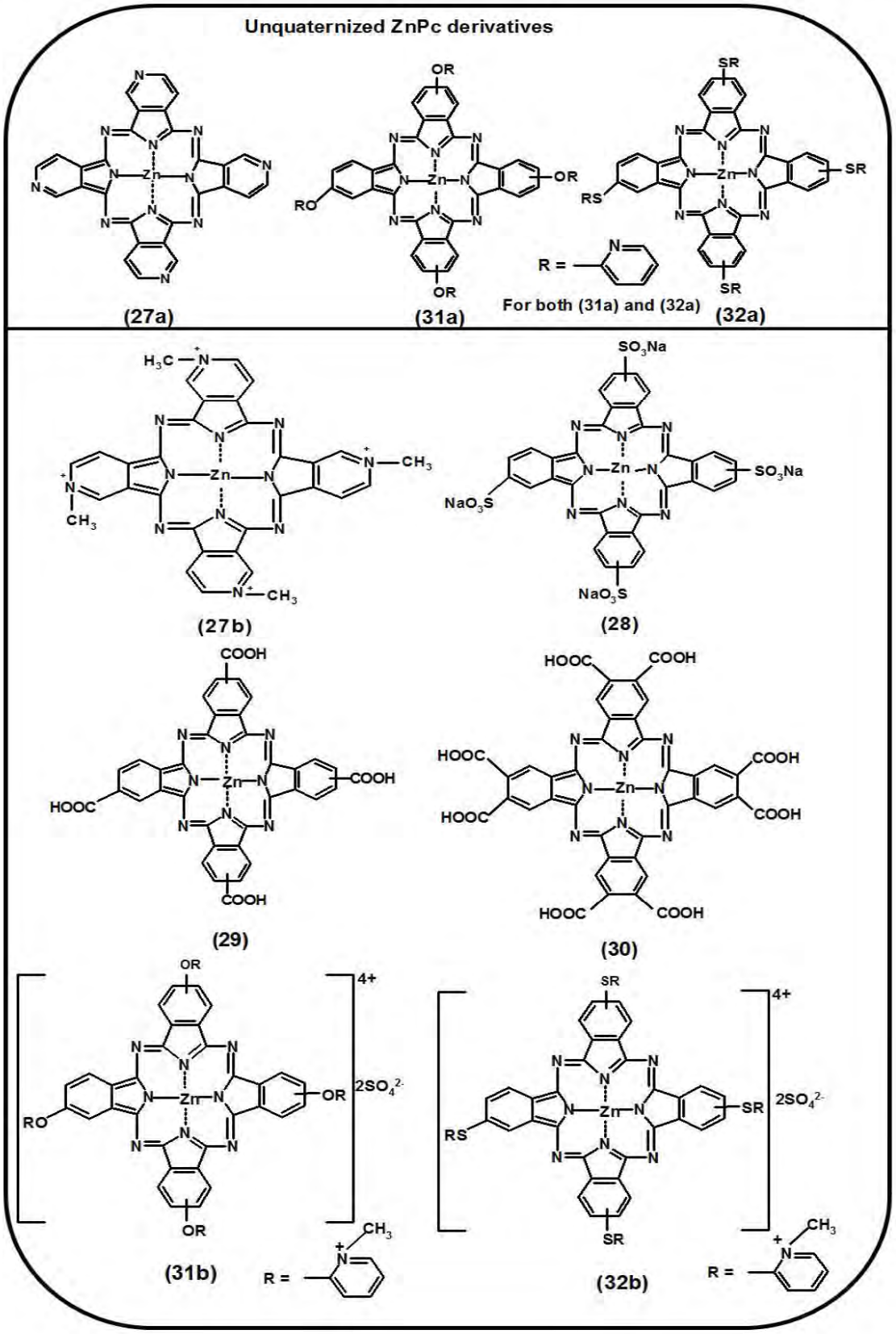

Figure 1.19: Structures of non novel MPcs synthesized and studied in the presence of CdTe QDs in this work.

Novel organic soluble MPcs that will be synthesized in this thesis are shown in Figure 1.20. These MPcs include tetrakis-2,(3)-{2-mercaptopyridinephthalocyanine}Ga(III)Cl ((Cl)GaTMPyPc, **33a**), tetrakis-2,(3)-{2-mercaptopyridinephthalocyanine}In(III)Cl ((Cl)InTMPyPc, **33b**), tetrakis-2,(3)-{2-mercaptopyridinephthalocyanine}Si(III)Cl_2 $((Cl)_2$SiTMPyPc, **33c**), and tetrakis-2,(3)-{2-mercaptopyridinephthalocyanine}Sn(II) (SnTMPyPc, **33d**). The 2-mercaptopyridine substituent is favourable because it allows for quaternization of the MPcs. Quaternization of the complexes **(33a)** and **(33b)** could thus be carried out affording tetramethyltetrakis-2,(3)-{2-mercaptopyridinephthalocyanine}Ga(III)Cl ((Cl)GaTmTMPyPc, **34**) and tetramethyltetrakis-2,(3)-{2-mercaptopyridine phthalocyanine}In(III)Cl ((Cl)InTmTMPyPc, **35**) which can be solubilised in aqueous media. Two novel anionic MPcs bearing the 2-mercapto-4-methyl-5-thiazoleacetic acid (MmTAA) substituent; tetrakis-2,(3)-{2-mercapto-4-methyl-5-thiazoleaceticacidphthalocyanine}zinc(II) (TMmTAAZnPc, **36**) and octakis-2,3-{2-mercapto-4-methyl-5-thiazoleaceticacidphthalocyanine}zinc(II) (OMmTAAZnPc, **37**) are synthesized. Another novel group of MPcs bearing mercaptoacetic acid (MAA) and mercaptopropionic acid (MPA) substituents: tetrakis-2,(3)-{mercaptoaceticacidphthalocyanine}Ga(III)OH ((OH)GaTMAAPc, **38a**), tetrakis-2,(3)-{mercaptoaceticacidphthalocyanine}In(III)OH ((OH)InTMAAPc, **38b**), tetrakis-2,(3)-{mercaptoaceticacidphthalocyanine}Si(IV)(OH)(Me) **(**(OH)(Me)SiTMAAPc, **38c**), tetrakis-2,(3)-{mercaptoaceticacidphthalocyanine}zinc(II) **(**TMAAZnPc, **38d**)**,** tetrakis-2,(3)-{3-mercaptopropionicacidphthalocyanine}Ga(III)OH ((OH)GaTMPAPc, **39a**), tetrakis-2,(3)-{3-mercaptopropionicacidphthalocyanine}In(III)OH ((OH)InTMPAPc, **39b**), tetrakis-2,(3)-{3-mercaptopropionicacidphthalocyanine}Si(IV)(OH)(Me) ((OH)(Me)SiTMPAPc, **39c**) and tetrakis-2,(3)-{3-mercaptopropionicacidphthalocyanine}Zn(II) (TMPAZnPc **39d**), are also synthesized, Figure 1.20.

The chemistry of silicon (Si) and tin (Sn) Pcs has received a lot of attention recently since using Si and Sn as central metals has been shown to result in improved physicochemical properties of the corresponding photosensitizer. Central metals ions

like Si (Si^{4+}), zinc (Zn^{2+}), aluminium (Al^{3+}), and indium (In^{3+}) are diamagnetic in nature and thus have a closed shell structure which results in improved photophysical properties (increased triplet state quantum yields (Φ_T) and relatively long triplet lifetimes (τ_T)) [135-137]. The spectroscopic and photophysicochemical properties of all the MPcs synthesized are explored in the absence and presence of QDs and reported in this work. The effect of the interaction of CdTe QDs and MPcs on the QD fluorescence lifetimes is also studied and reported in this work.

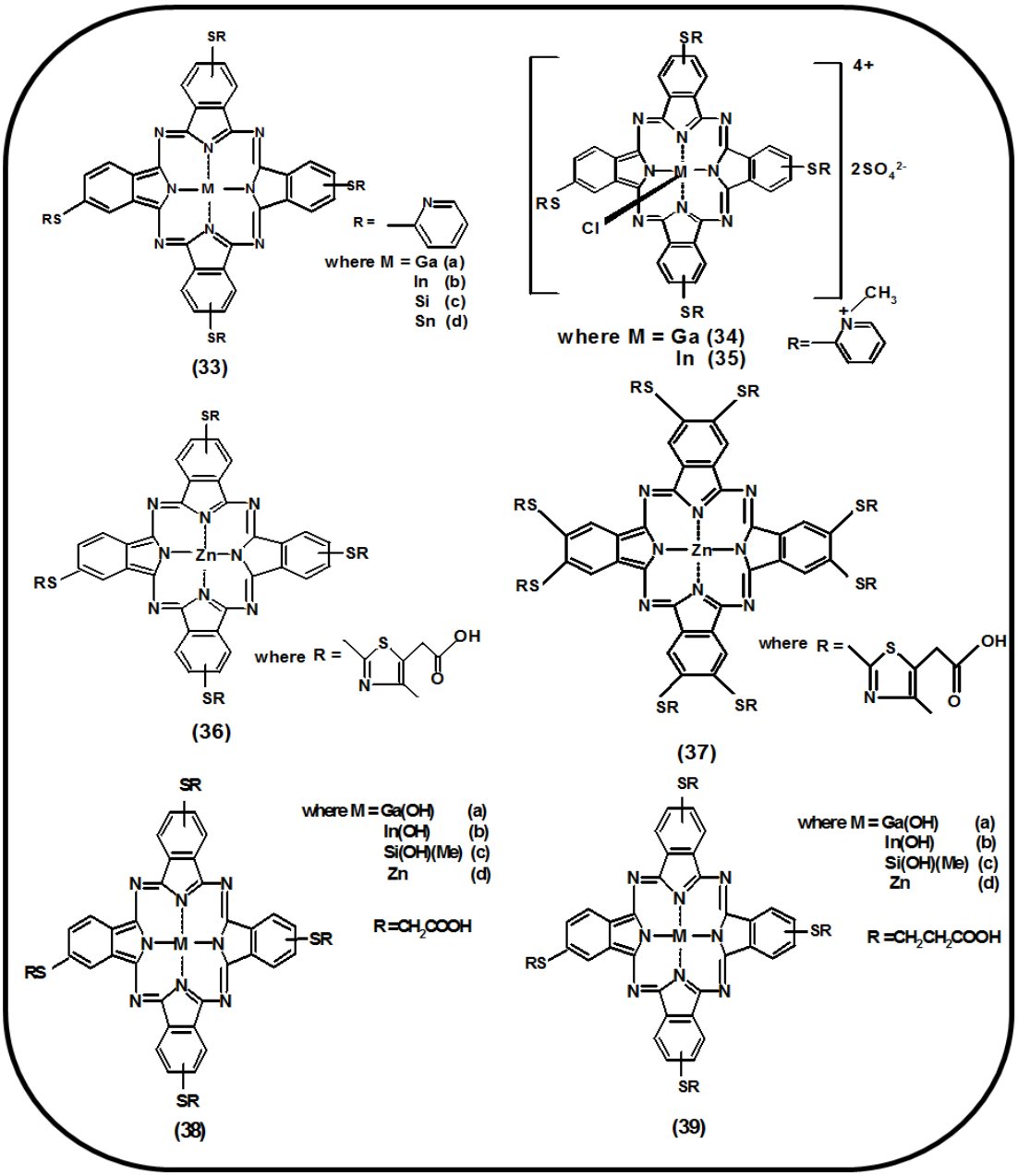

Figure 1.20: Structures of novel MPcs synthesized and studied in this work.

The complexes tetrakis-2,(3)-[5-(trifluoromethyl)-2-pyridyloxyphthalocyaninato] zinc(II) **(**TtfmPyZnPc, **40)**, tetrakis-2,(3)-[5-(trifluoromethyl)-2-mercaptopyridinephthalocyaninato] zinc(II) **(**TtfmMPyZnPc, **41)** were donated by a fellow researcher (Dr. Ali Erdogmŭs) and the MPc complex 2,(3)-tetra-[1,6-hexanedithiolphthalocyaninato] zinc(II) **(**THdTZnPc, **42)** was donated by a fellow researcher (Dr. Edith Antunes) and the structures of these complexes are shown in Figure 1.21. The synthesis of these molecules is however reported here for the first time. The interaction of the quaternizable complexes (**40** and **41)** mentioned above shall be studied in organic solvents in the presence of CdTe QDs. Complex **42** will be attached to AuNPs (gold nanoparticles) through the use of the free thiol terminal groups which are known to have a high affinity for gold and the **42**-AuNP conjugate shall be studied accordingly. The photophysicochemical properties of all MPcs studied will be determined with reference to ZnPc **(43)**.

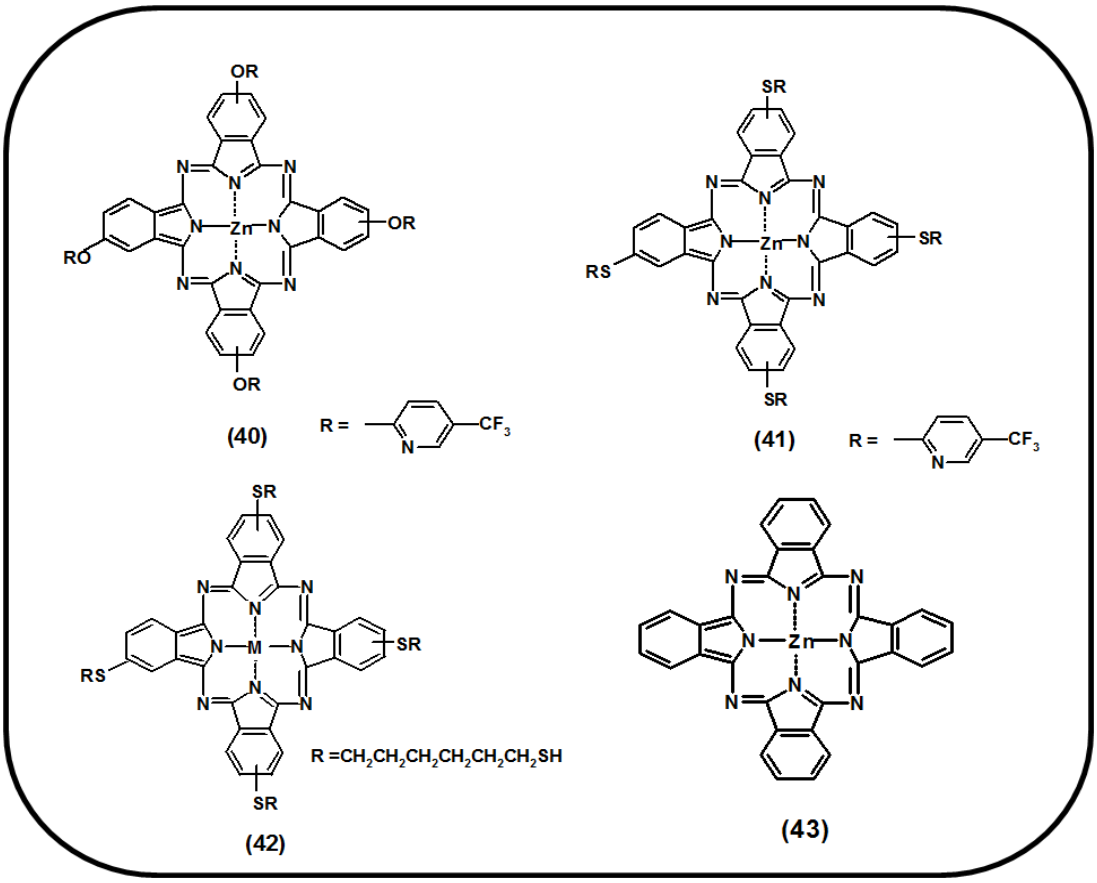

Figure 1.21: Structures of ZnPc (43) and some novel MPcs donated and used for NP interaction studies in this work.

1.2.4 Preparation of MPc-AuNP nanoconjugates

It has been well established that nanoparticles are responsible for improved photosensitizing properties of Pcs [138]. Conjugates of QDs and Pcs may be formed via adsorptive interactions or they may result from a chemical linkage between the two species. Complex **42** by virtue of the four terminal thio groups allows for conjugation with AuNPs. This is because gold surfaces have a high affinity for the lone pair of electrons on the sulphur thereby allowing the formation of a coordinate covalent bond between the MPc complex (**42**) and the AuNPs.

A similar form of interaction has been reported but the studies were carried out with different Pc complexes [138,139]. However for most of the work that has been carried out, the Pcs used only had one or two mercaptoalkyl tethers for attachment onto the gold nanoparticles while in this work there are four thio groups allowing for attachment of MPcs onto the AuNPs. As a result different forms of Pc arrangement on the AuNP are envisaged, where the binding of all four tethers would result in a flat or dome shaped arrangement of the MPc onto the NP, while the binding of only two mercaptoalkyl groups would allow the MPc to be positioned in such a way that the rest of the molecule has freedom of movement, Figure 1.22 [139].

In this work semiconductor QDs (CdTe and ZnS QDs) were studied in a mixture with MPcs in solution. These QDs mainly interacted with the MPc complexes via adsorption or electrostatic forces. However the study conducted with AuNPs involved attachment of the MPc of choice onto the AuNPs through alkyl thio tethers thereby forging a chemical bond. A considerable number of studies have been conducted with CdTe QDs conjugated to Pc complexes but very few studies have been conducted for Pc-AuNP conjugates hence the study carried out with AuNPs in this work.

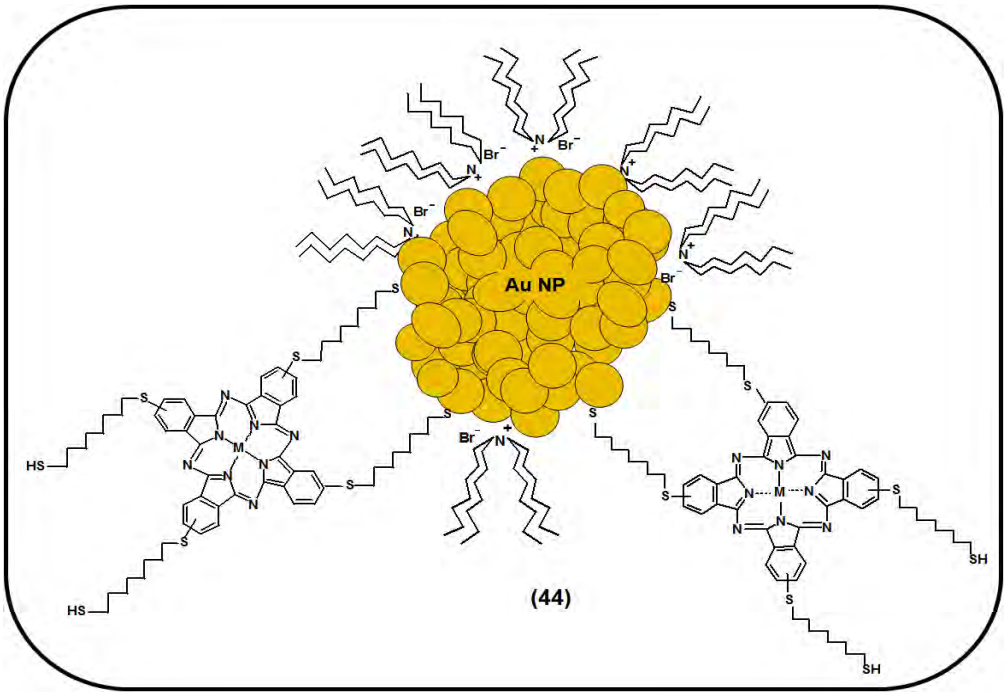

Figure 1.22: A schematic representation of a phthalocyanine functionalized AuNP (MPc-AuNP, (44)). The AuNP is not drawn in proportion to the size of the TOAB and MPcs, and the loading capacity of the MPcs and TOAB is not accurately illustrated [139].

1.2.5. Phthalocyanine Spectroscopy

1.2.5.1 Electronic absorption of phthalocyanines at ground state

The absorption spectra of Pcs are highly influenced by a number of factors which include presence or absence of central metal ion, substituents, the number of substituents and their relative positions, solvent used and aggregation tendencies [140]. Figure 1.23 shows a typical ground state absorption spectrum of a metallated Pc. MPcs show a characteristic sharp, intense absorption band known as a Q-band (Q_{00}) and at ~ 700 nm and this band usually demonstrates high molar extinction coefficients (ε_s) that are generally above 10^5 $M^{-1}cm^{-1}$ [140,141]. The vibrational Q bands [Q_{vib}, (Q_{01}, Q_{02})] are found along with the main Q-band and results from electronic transitions from vibrational levels of the Q-band electronic states. There is also the presence of much weaker bands (Figure 1.23) and these are observed at much higher energies. The B or Soret band is found at ~ 340 nm and it is quite broad

in Pcs because it consists of the B_1 and B_2 bands that are superimposed with one another [142,143]. There is also the presence of the N, L and C bands listed in order of increasing energy and they are readily observed with the use of UV transparent solvents e.g. dichloromethane (DCM) [142,144]. Charge transfer (CT) bands on the other hand occur as modest absorptions in the 400-500 nm regions, Figure 1.23. A CT may take place from a ligand to metal (LMCT) in which case it is termed a ligand to metal CT, or they may be from metal to ligand and are thus referred to as metal to ligand CT (MLCT).

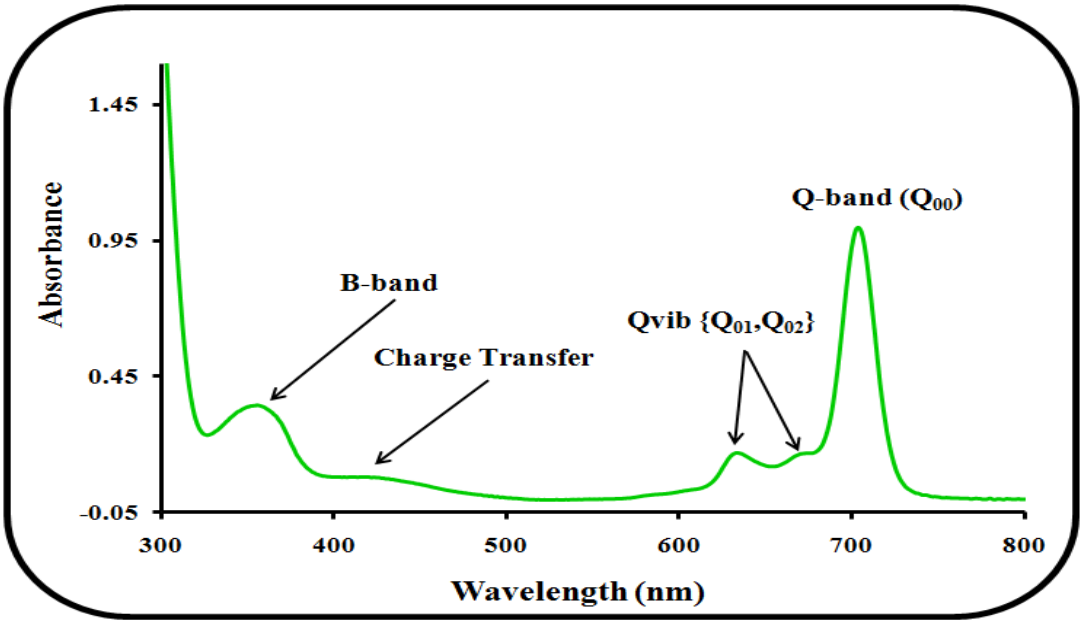

Figure 1.23: A typical electronic ground state absorption of a metallated phthalocyanine (MPc).

CT transitions are generally observed when metal d-orbitals lie within the HOMO-LUMO gap of the Pc [94,145]. Gouterman's theory involving a four orbital model is one of the theories used to explain the origin of the Q and B bands [94,146,147]. The Gouterman model is composed of a four-orbital linear combination of atomic orbitals, Figure 1.24. This model consists of the top two highest occupied molecular orbitals (HOMO) and the lowest unoccupied molecular orbital (LUMO) [94].

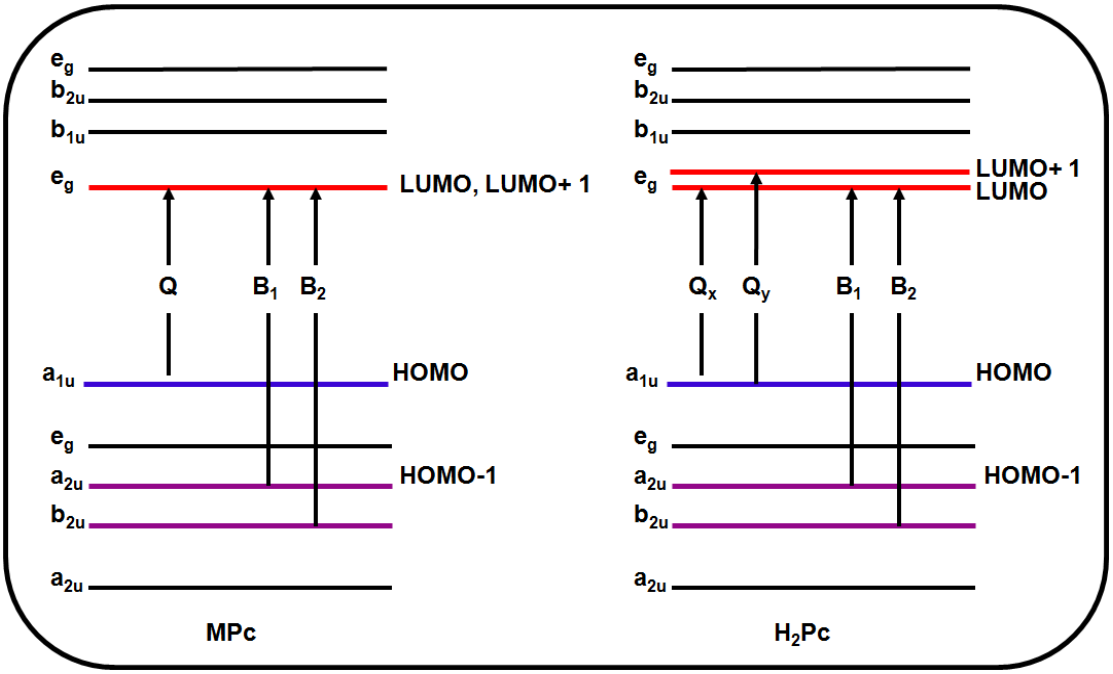

Figure 1.24: Representation of electronic transitions in (a) metallated (MPc) and (b) metal free (H_2Pc) phthalocyanines showing the origin of the Q and B-bands [94].

A transition from the a_{1u} (HOMO) orbital to the degenerate e_g (LUMO) orbital results in the Q-band for a metallated Pc complex whereas for an H_2Pc, the e_g (LUMO) orbital is doubly degenerate resulting in a split Q-band absorption (Q_x and Q_y), Figure 1.25. On the other hand the B-bands result from a transition from the a_{2u} and b_{2u} (HOMO) orbitals to the e_g (LUMO) orbital suggesting a split B-band into two components (B_1 and B_2). However the B_1 and B_2 bands have similar energies and so they merge into a single broad B-band instead.

Substitution at the non-peripheral (α) position of the Pc ring with electron donating groups causes a more pronounced red shift of the Q-band indicative of a reduction in the HOMO-LUMO energy gap of the Pc when compared to the peripherally (β) substituted counterparts [148]. However, substitution with electron withdrawing groups elicits the opposite effect with regard to the non-peripheral and peripheral positions in that a blue shift is realized [149,150]. The type of solvent used in solubilizing the Pc also influences the position of the Q-band. Aromatic solvents, solvents with relatively high refractive indices and those showing a degree of

conjugation have all been proven to cause red-shifting of the Q-band position [151,152].

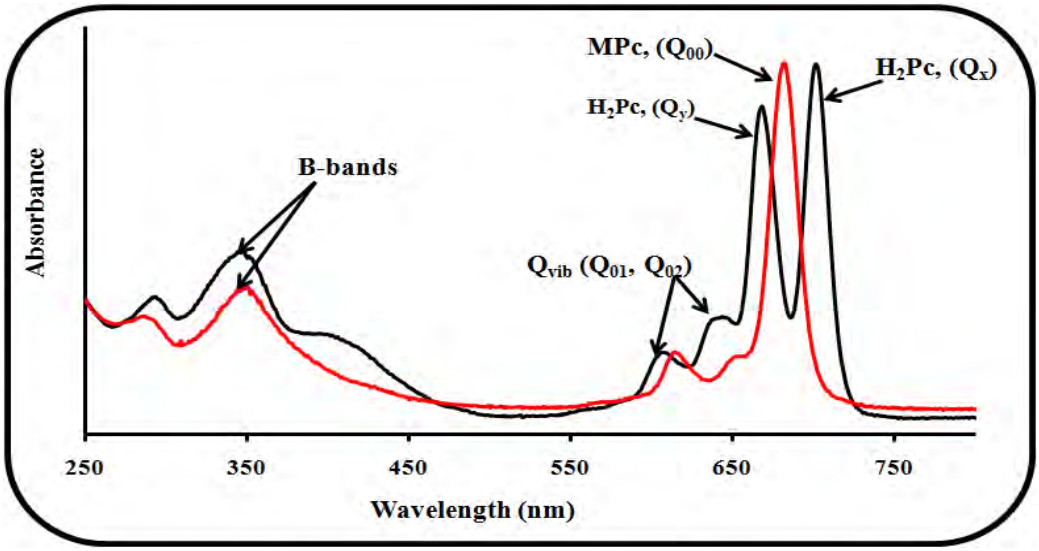

Figure 1.25: Overlaid electronic ground state absorption of a metal free and metallated phthalocyanine.

1.2.5.2 Aggregation effects on phthalocyanine spectra

Phthalocyanines are predisposed to forming aggregates in solution but more especially at higher solution concentrations. These aggregation tendencies are governed by a number of factors including the nature of: the central metal, the substituents and their relative positions and lastly the solvent used in terms of its polarity and coordinating capacity [150,153-158]. The type of interactions of the Pc macrocycles and their arrangement in solution influences to a great degree the spectroscopic behaviour of any resulting aggregates. A co-facial arrangement of Pc macrocycles results in a hypsochromic (blue) shift (with parallel dipole moments) of the Q-band absorption and these aggregates are more commonly referred to as H-aggregates and an edge to edge arrangement of Pc macrocycles forms aggregates that cause a bathochromic (red) shift and are known as J-aggregates (with head to tail dipole moments), Figure 1.26 [159-161]. The formation of H-aggregates is fuelled by the inherent hydrophobic nature of aromatic benzene rings which facilitates the stacking of the Pcs, one on top of the other leading to π-π interactions which are a

result of the overlapping electron clouds of the benzene rings in the Pcs [162,163]. H-aggregates are characterized by a broadened Q-band, with a typical blue-shifted absorption band around 630 nm [164]. The exciton coupling theory is usually used to explain the incidences of H and J-aggregates. This theory holds that the only allowed transitions are those to the higher energy state (^1E_u) hence the significant blue-shifted absorption while transitions to the lower energy state (^1E_g) are forbidden but can to a small degree still take place and these result in a broad absorption in H-aggregates while the opposite applies for J-aggregates, Figure 1.26 [165-167].

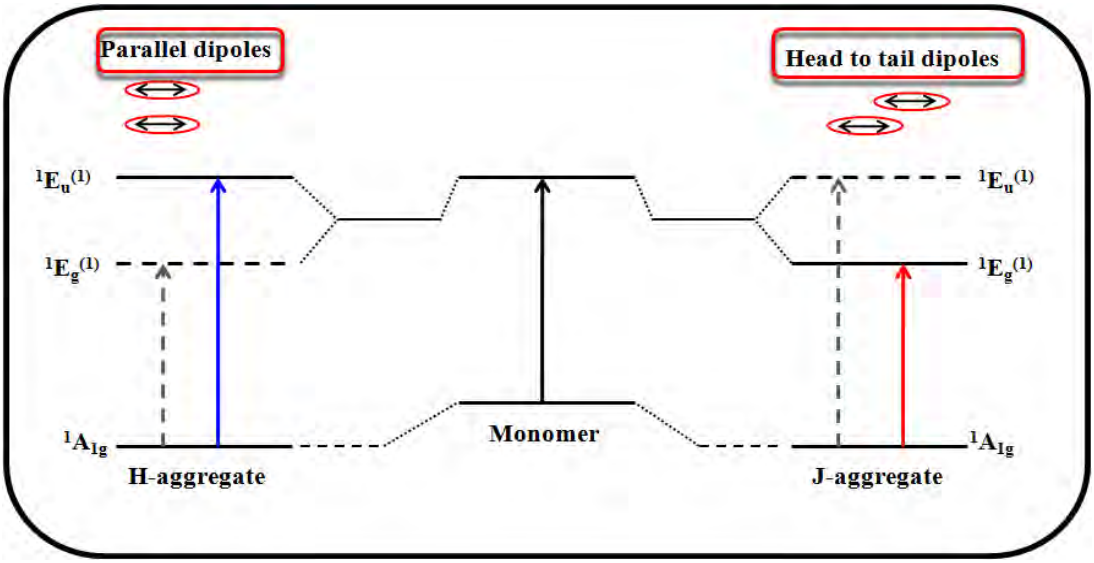

Figure 1.26: A representation of electronic transitions for H and J aggregates based on the molecular exciton theory (with the grey dashed arrows indicative of forbidden transitions) [167].

The work reported on in this thesis is mainly on MPcs that are soluble in aqueous media. MPcs that are water soluble tend to exhibit intense aggregation in water [153]. Disaggregation of these MPcs in aqueous media is usually achieved by employing neutral surfactants e.g. Triton-X 100, cremophore EL (CEL) or by the addition of organic solvents that are miscible with water e.g. methanol, ethanol, dimethylsulfoxide (DMSO) or even pyridine [164]. Aggregation may also be hindered by the incorporation of bulky substituents onto the MPc framework or using central metal ions that possess axial ligands [168-171].

1.3 Photophysicochemical properties of phthalocyanines

The determination of photophysical and photochemical properties of phthalocyanines is of utmost significance in elucidating the competence of these complexes as photosensitizers e.g. for PDT purposes. A Jablonski diagram is usually used to explain all the possible photoprocesses for an MPc undergoing excitation, Figure 1.27.

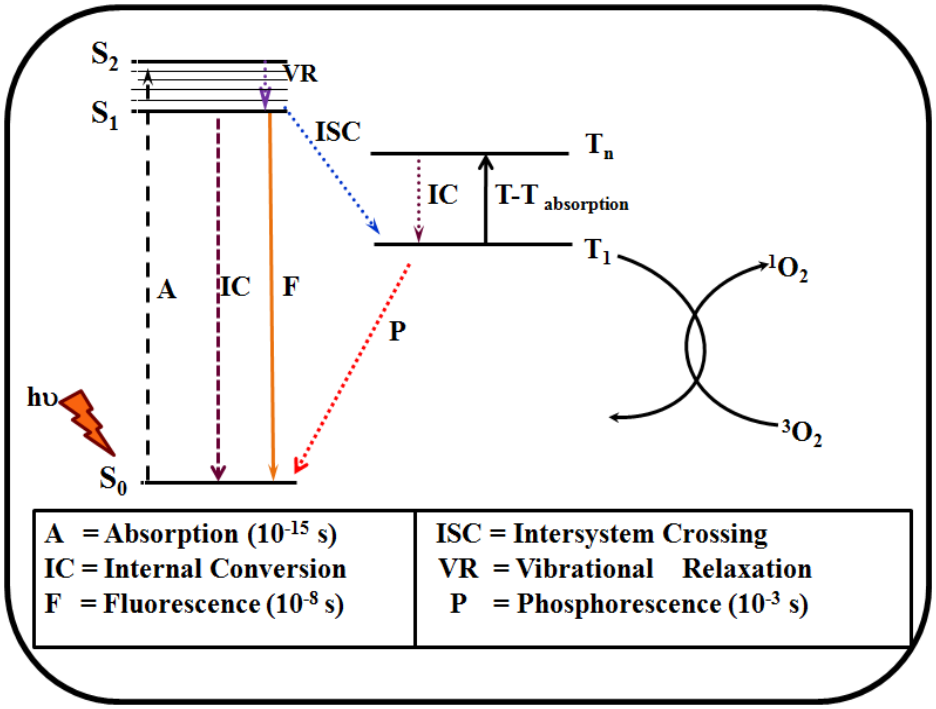

Figure 1.27: A simplified Jablonski diagram showing the possible photoprocesses between ground and excited electronic states.

1.3.1. Fluorescence spectra, quantum yields and lifetimes

In general the fluorescence of MPcs is affected by factors such as: the central metal ion, substituents, solvent used, aggregation, electron transfer, energy transfer and also some structural features of the MPc [91,137,172]. It has been widely established that monomeric forms of Pcs are fluorescent while their aggregated forms e.g. Pc dimers are generally non-fluorescent [173]. A comparison of the fluorescence emission spectrum of an MPc to its absorption spectrum (Figure 1.28) shows that the

emission is red-shifted and a mirror image of the absorption and excitation spectra [135]. The relative difference between the emission and excitation band wavelengths gives the corresponding values of the Stokes shift [174]. The excitation spectrum is usually very similar to the absorption spectrum and is obtained by scanning for the fluorescence at a preset emission wavelength. A difference in the excitation spectra in comparison to the absorbance may however be brought about by processes such as demetallation (for MPcs with large central metal ions) in the excited state and aggregation since only the monomer fluoresces [152,173,175,].

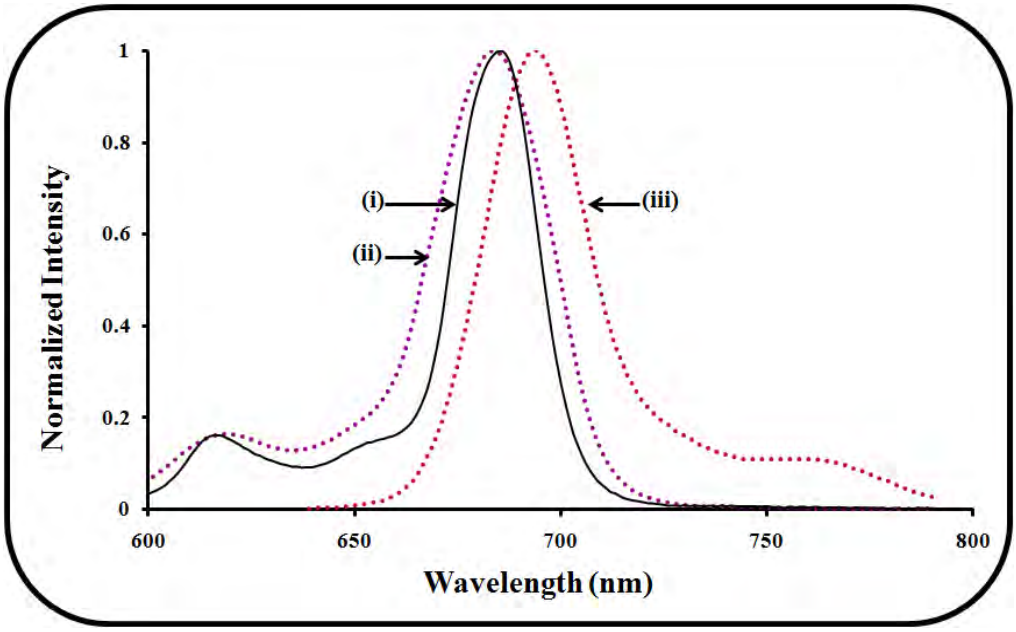

Figure 1.28: A typical MPc (D_{4h}) absorption (i) excitation (ii) and emission (iii) spectra [135].

Paramagnetic metals and metals with high atomic number significantly reduce the fluorescence of MPcs due to spin orbit coupling which encourages an otherwise spin-forbidden process, referred to as intersystem crossing (ISC), Figure 1.27. The determination of quantum yields is for the sole purpose of giving a measure of the overall efficiency of a photophysical or photochemical process [176]. Steady state fluorescence measurements are employed to determine the efficiency of a respective emission process (**F**, Figure 1.27). By definition, the fluorescence quantum yield (Φ_F)

is a ratio of the number of emitted photons to the number absorbed photons. Φ_F values of MPcs are determined via a comparative method that makes use of a standard reference of known Φ_F to which unknown samples can be measured against, using equation 1.4 [177,178]

$$\Phi_F = \Phi_{F(Std)} \frac{F \,.\, A_{Std.}\, n^2}{F_{Std.}\, A \,.\, n_{Std}^2} \qquad (1.4)$$

where F and F_{Std} are the areas under the fluorescence curves of the photosensitizer and the reference, respectively. A and A_{Std} are the absorbances of the sample and reference at the excitation wavelength, and n and n_{Std} are the refractive indices of solvents used for the sample and standard, respectively. ZnPc in DMSO is usually used as a standard for Pc Φ_F determinations, Φ_F = 0.20 [179]. Rhodamine 6G in ethanol with Φ_F = 0.94 is generally employed as a standard for CdTe quantum dots [180,181]. The sample and the standard are both excited at the same relevant wavelength and to avoid inner filter effects (result in self quenching and reduced Φ_F values) the absorbance at the wavelength of excitation is kept low [182].

MPc fluorescence lifetimes (τ_F) are usually in the nanosecond range (< 10 ns) and are very sensitive to the presence of other species in solution that may be interacting with MPcs. Fluorescence lifetimes may mainly be obtained by using either the time or frequency domains [183-185]. The time correlated single photon counting (TCSPC) equipment is used for time domain measurements and was the most used technique for fluorescence lifetime determinations in this work [184,185]. Fluorescence lifetimes may also be determined from the PhotochemCAD software by employing the absorbance and emission spectra of MPcs and fitting in all that is required. The fluorescence lifetime determination through the use of the PhotochemCAD program involves application of the Strickler-Berg equation [186-188].

1.3.2 Fluorescence studies of the interaction of QDs and MPcs

MPcs and QDs in solution are liable to various forms of interaction depending on the Pc substituent and the QDs stabilizer groups used [8]. Adsorption and electrostatic forces may be encouraged at the interface of QDs and Pcs depending on the ligands on either QDs or Pcs. The interaction between the two species in solution may result in quenching effects on the photoluminescence of the QDs and MPcs or it could also lead to Förster resonance energy transfer (FRET) [181,189].

1.3.2.1 Fluorescence Quenching

Fluorescence quenching causes the reduction of the fluorescence intensity for a photoluminescent sample. A number of molecular interactions e.g. energy transfer, charge transfer, ground state complex formation and many other excited state interactions lead to the drop in fluorescence intensity. The decline observed in the fluorescence intensity results from a depopulation of the excited state without the emission of fluorescence. This usually comes about due to the diffusion of a quencher to the surface of the fluorophore in the excited state and when contact between the two is established, the fluorophore goes back to the ground state without the emission of a photon [181,189]. Collisional interactions between the excited state fluorophore and the quencher results in dynamic quenching while formation of a ground state complex results in static quenching. It has been shown by Stern and Volmer that the decrease in fluorescence intensity has a linear relationship with the quencher concentration, equation 1.5 [189]

$$\frac{F_0}{F} = 1 + K_{SV}[Q] \qquad (1.5)$$

where K_{SV} represents the Stern-Volmer quenching constant, F_0 and F are the fluorescence intensities of the fluorophore in the absence and presence of the respective quencher (Q). K_{SV} is obtained as the slope from the linear plot of F_0/F

against [Q] which has an intercept of 1. K_{SV} is better explained by the use of equation 1.6 which shows that K_{SV} is obtained as the product of the bimolecular quenching constant (k_Q) and the fluorophore fluorescence lifetime (τ_F) in the absence of the quencher.

$$K_{SV} = k_Q \tau_F \tag{1.6}$$

The binding constant (k_b) and the number of binding sites (n) on the fluorophore may be estimated by employing equation 1.7 [189].

$$\log\left[\frac{(F_0 - F)}{F - F_\infty}\right] = \log k_b + n\log[Q] \tag{1.7}$$

where F_0 and F are the fluorescence intensities of the fluorophore in the absence and presence of the quencher (Q); F_∞, the fluorescence intensity of the fluorophore saturated with quencher (MPc). Plots of log $((F_0\text{-}F)/(F\text{-}F_\infty))$ against log [Q] provide the values of n (from slope) and log k_b (from the intercept).

1.3.2.2 Förster resonance energy transfer (FRET)

FRET may be described as the non radiative transfer of energy from a donor fluorophore in the excited state to an acceptor fluorophore in its ground state, Figure 1.29 [189-191]. This photoprocess is facilitated by weak dipole-dipole interactions of the donor and acceptor chromophores (or fluorophores in the event that both donor (QD) and acceptor (MPc) pair are fluorescent). The evidence of FRET is demonstrated by the quenching of the donor photoluminescence or excited state lifetime and results in the sensitized emission of the acceptor [189].

The occurrence of FRET is dependent on the spectral overlap between the donor emission and acceptor absorption, the donor quantum yield, the orientation between

the donor and acceptor dipole moments and it is also reliant on the distance between the donor and acceptor chromophores [192-194].

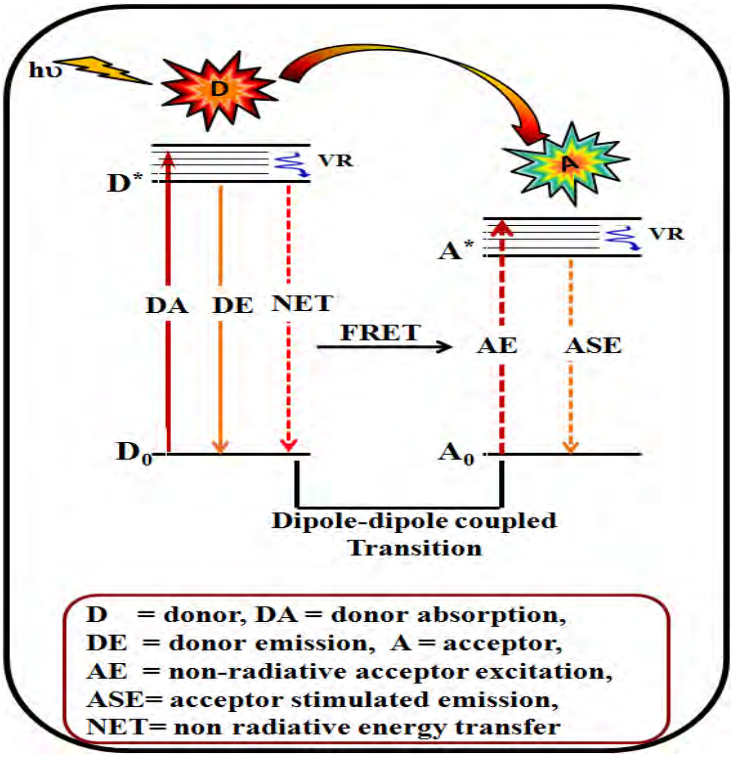

Figure 1.29: A modified Jablonski diagram illustrating the FRET photoprocess [190].

The efficiency of FRET may be experimentally determined from the fluorescence quantum yield of the donor in the presence ($\Phi_{F(DA)}$) and absence ($\Phi_{F(D)}$) of the acceptor using equation 1.8 [189,194,195].

$$Eff = 1 - \frac{\Phi_{F(DA)}}{\Phi_{F(D)}} \qquad (1.8)$$

The FRET efficiency (*Eff*) is related to centre to centre distance between the donor and acceptor chromophores (r) by equation 1.9. The equation shows that because of the weak dipole-dipole coupling mechanism of the donor-acceptor pair, there is a an inverse 6th order law dependence of *Eff* on r (Å) [189,191].

$$Eff = \frac{R_0^{\,6}}{R_0^{\,6} + r^6} \qquad (1.9)$$

where R_0 (the Förster distance, Å) is the critical distance between the donor and acceptor chromophores at which the efficiency of energy transfer is 50%. R_0 depends on the fluorescence quantum yield of the donor, dipole orientation, and spectral overlap (J) equation 1.10 [189,191]

$$R_0^6 = 8.8 \times 10^{23} \kappa^2 n^{-4} \Phi_{F(D)} J \qquad (1.10)$$

where n, is the refractive index of the medium; $\Phi_{F(D)}$, the fluorescence quantum yield of the donor in the absence of the acceptor; J is the Förster overlap integral and κ^2 is the dipole orientation factor. It is assumed that κ^2 is 2/3 in this thesis. This assumption is often made for donor-acceptor pairs in a liquid medium, since their dipole moments are considered to be isotropically oriented during the excited state lifetimes. The use of the isotropic dynamical average (κ^2= 2/3) is more appropriate than the static isotropic average (κ^2= 0.476) because the donor-acceptor pair is not in a rigid medium. FRET parameters were computed using the program PhotochemCAD in this thesis [187,196]. J, the Förster overlap integral, is better defined with the use of equation 1.11.

$$J = \int f_D(\lambda)\, \varepsilon_A(\lambda)\, \lambda^4\, \partial\lambda \qquad (1.11)$$

where f_D is the normalized donor emission spectrum; and ε_A, the molar extinction coefficient of the acceptor and λ is the wavelength of the acceptor.

Interactions of QDs and Pcs through FRET have only recently garnered the much deserved attention [24,134,138]. The nature of capping agent used to passivate the surface of QDs usually facilitates various interactions (e.g. hydrophobic, hydrogen bonding, covalent and adsorptive interactions) between QDs and other molecules. Some of the reports to date focus on Pcs adsorbed onto QDs while others specifically centre their attention on chemically linked QD-Pc conjugates [61,134,197-200]. Although there have been a few research studies on QD-MPc interactions, most of

the MPcs used in these studies are organic solvent soluble and thus not biocompatible (not suitable for PDT studies). Our research group though, has recently reported on interactions of water soluble MPcs and QDs and the focus was mainly on the FRET photoprocess, and this involved the use of aluminium tetrasulfonatephthalocyanine (AlTSPc, **45**) and octacarboxy MPcs ($(OH)_2$SiOCPc **(46)**, $(OH)_2$GeOCPc **(47)**, (OH)AlOCPc **(48)** and ZnOCPc **(30)**) studied in the presence of MPA and L-cysteine (L-cys) stabilized CdTe QDs, Table 1.1 [131,201,202]. The studies carried out for the water soluble tetrasulfonate complex AlTSPc (**45**) and the octacarboxy complexes ($(OH)_2$SiOCPc **(46)**, $(OH)_2$GeOCPc **(47)**, (OH)AlOCPc **(48)** and ZnOCPc **(30)**) suggest adsorptive interactions between the MPcs and the water soluble CdTe QDs employed [131,202]. Organic solvent soluble MPcs used recently in FRET studies allowed for conjugation to QDs by covalent attachment and they include the tetraamino substituted ZnPc (ZnTAPc, **49**) and the low symmetry tertiarybutyl substituted imido ZnPc (ZnttbIPc, **50**) from our research group, SiPc analogues by Burda's group with different axial ligands: SiPc4 (**51**) and SiPc158 (**52**) and a low symmetry tertiarybutyl substituted H_2Pc with thioacetate linkers by another group (**53**) [53,61,132,139,199,200,203]. The covalent attachment of low symmetry phthalocyanines to QDs is gaining recognition and has been suggested to be highly desirable since it would render the determination of the number of Pc units coordinated to the QD surface easier than would be possible with a tetrasubstituted Pc [53]. The coordinate covalent attachment of Pcs to AuNPs has also earned considerable attention, especially attachment through single thio tethers [139]. In this work, the sensitized emission of water soluble MPcs by the highly photoluminescent CdTe QDs with different cappings via FRET shall also be explored. In addition to the FRET photoprocess, other processes involving charge transfer and MPc ring reduction by the QDs and the effect of the stabilizer group on ring reduction will also be explored for the first time. The effect of attachment of an MPc bearing tetra thio tethers onto AuNPs will be explored as well.

Table 1.1: MPcs adsorbed or chemically linked to QDs for FRET studies

MPc	Structure	QD	*Eff*	Ref
AlTSPc (45)	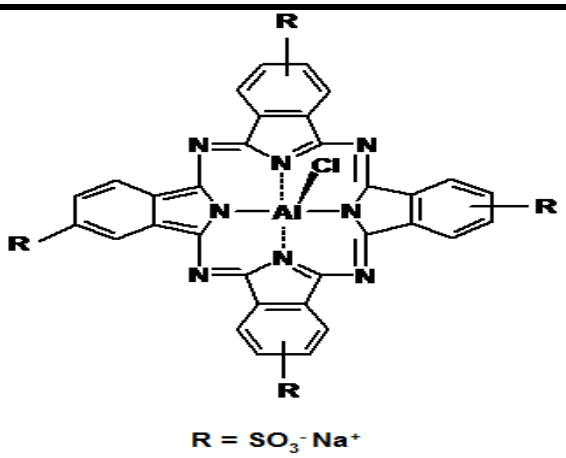 R = $SO_3^-Na^+$	CdTe MPA CdTe TGA CdTe L-cys	0.58 0.35 0.97	[131]
OCMPcs	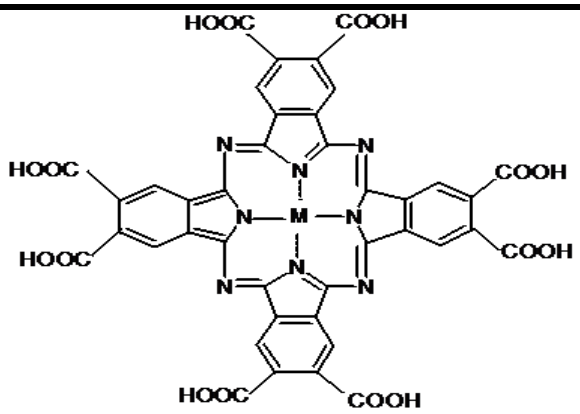 M = Zn (30), $Si(OH)_2$ (46), $Ge(OH)_2$ (47), Al(OH) (48)	CdTe L-cys (SiPc-QD) (GePc-QD) (AlPc-QD) (ZnPc-QD)	 0.80 0.76 0.73 0.54	[202]
ZnTAPc (49)	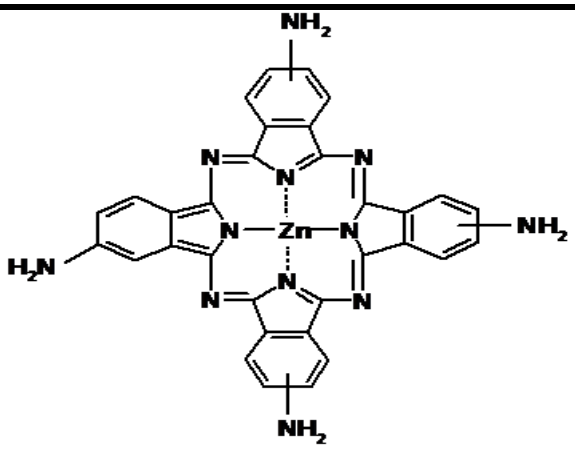	CdTe MPA	-	[132,203]

Table 1.1 Contd.

MPc	Structure	QD	*Eff*	Ref
ZnttbIPc (50)	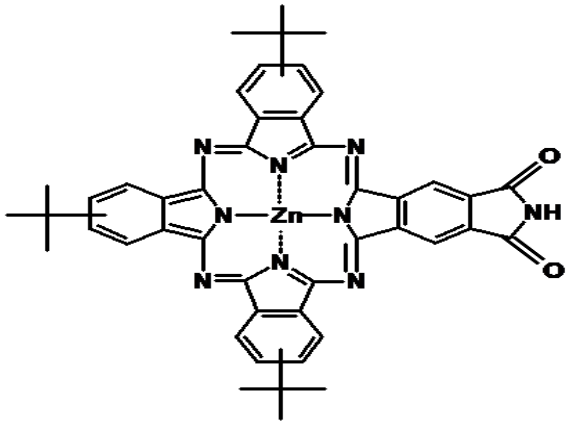	CdTe MPA (Pc-QD$_{mixed}$) (Pc-QD$_{linked}$)	 0.52 0.82	[53]
SiPc	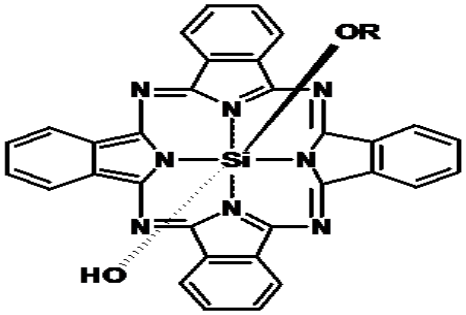 (51) SiPc4 R = 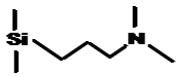 (52)SiPc158 R = 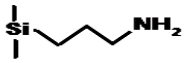	CdSe TOPO CdTe TBPO	-	[199,200]
H_2Pc (53)	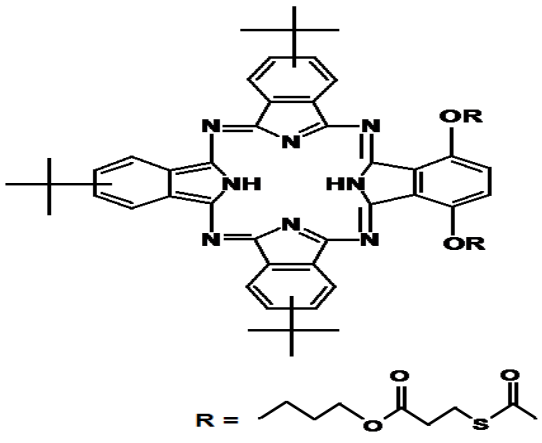 R =	Au TOAB	-	[139]

1.3.3 Triplet state quantum yields and lifetimes

The triplet state quantum yields (Φ_T) and lifetimes (τ_T) of MPc solutions are obtained through the use of laser flash photolysis which basically screens the absorption from the T_1 state to higher T_n states, Figure 1.27 [137,190]. Φ_T values give the relative population of the triplet state while the τ_T gives time spent in the triplet state. Figure 1.30 shows a typical triplet state decay curve and Table 1.2 shows photophysical parameters of several MPcs in the presence of CdTe QDs [202].

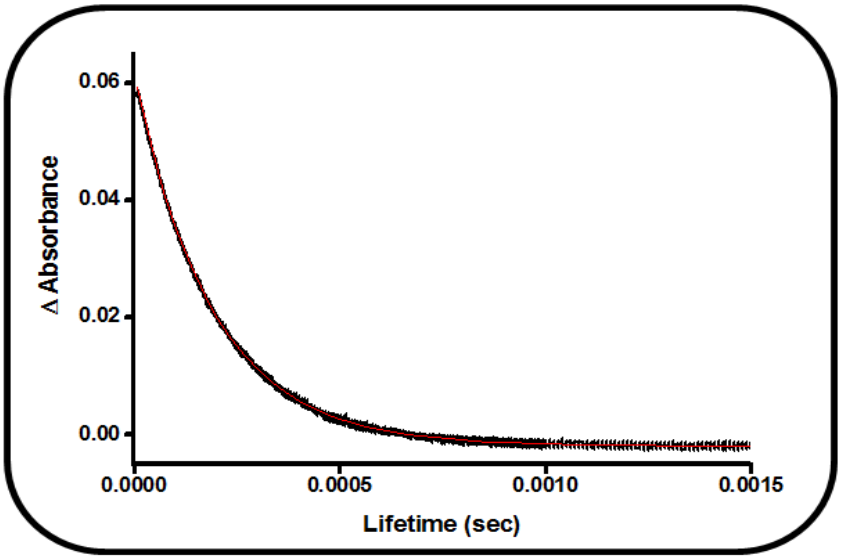

Figure 1.30: A representative MPc triplet state decay curve [202].

The triplet state quantum yield (Φ_T) is determined via a comparative method which employs equation 1.12 [204].

$$\Phi_T^{Sample} = \Phi_T^{Std} \frac{\Delta A_T^{Sample}}{\Delta A_T^{Std}} \frac{\varepsilon_T^{Std}}{\varepsilon_T^{Sample}} \qquad (1.12)$$

where ΔA_T^{Sample} and ΔA_T^{Std} are the changes in the triplet state absorbance of the MPc derivatives and the standard respectively. Φ_T^{Std} is the triplet state quantum yield for the standard (e.g. ZnPc). ε_T^{Sample} and ε_T^{Std} are the triplet state extinction coefficients for

the MPc derivative and standard (ZnPc), respectively and are determined with the use of equation 1.13 [205].

$$\varepsilon_T = \varepsilon_S \frac{\Delta A_T}{\Delta A_S} \qquad (1.13)$$

where ΔA_S and ΔA_T are the changes in the absorbance of the ground singlet states and the triplet state respectively. In order to determine the excited state lifetime of the transient species in the triplet state, the data obtained from the time-resolved absorption measurements is fitted using OriginPro 7.0. This fitting affords the triplet lifetime of the transient MPc species. Due to the forbidden nature of the $T_1 \rightarrow S_0$ transition, the triplet state lifetimes of MPcs range from microseconds (μs) to milliseconds (ms).

It is well-known that high triplet state quantum yields (Φ_T) are to be expected at the expense of fluorescence quantum yields (Φ_F), (Table 1.2). Triplet state quantum yields (Φ_T) are enhanced by the use of either heavy diamagnetic metal ions or paramagnetic metal ions. Heavy and diamagnetic central metal ions encourage spin orbit coupling which favours intersystem crossing (ISC) from the lowest excited singlet state to the triplet state and this then allows for increased energy transfer from the MPc species in the triplet state to ground state molecular oxygen with subsequent production of cytotoxic species [95,96]. Long lived lifetimes are encountered with the use of diamagnetic metal ions e.g. Zn^{2+}, but the lifetime is shortened in the presence of heavy metal ions e.g. Sn^{2+} and paramagnetic metal ions e.g. Pd^{2+}. MPcs with paramagnetic metal ions demonstrate short lifetimes in the triplet state because the paramagnetic metal ions possess low lying d-orbitals which allow for the quenching of the triplet state. The reduction in the triplet state lifetime results in decreased efficiency of energy transfer to ground state molecular oxygen ($^3O_2$) and hence minimal generation of the cytotoxic singlet oxygen ($^1O_2$) species which is responsible for the necrosis of tumour cells.

Table 1.2: Photophysicochemical properties of MPcs in the presence and absence of CdTe QDs.

MPc	Solvent	Φ_F	Φ_T	Φ_Δ	τ_T (μs)	Ref
ZnPc	DMSO	0.20	0.65	0.67	350	[179,205,207,215]
ZnPc	DMF	0.30	0.58	0.56	330	[179,206,216]
ZnOCPc	Aqueous [a]	0.23	0.50 (0.55)	0.32 (0.60)	160 (190)	[202]
SiOCPc	Aqueous [a]	0.24	0.34 (0.32)	0.22 (0.21)	90 (130)	[202]
ZnttbIPc (50)	DMF:H_2O[b]	0.08	0.77	0.45	70	[53]
ZnttbIPc (50)-QD_{mix}	DMF:H_2O[b]	-	0.81	0.53	15	[53]
ZnttbIPc (50)-QD_{linked}	DMF:H_2O[b]	-	0.73	0.48	48	[53]

[a] **The values in brackets are for the MPc in the presence of L-cysteine capped QDs.**

[b]**The solvent mixture is a ratio of 4:1 (DMF:H_2O, v/v) and studies were carried out with MPA capped QDs.**

The photophysicochemical properties of MPcs have been studied in detail over the past two decades [149,173,175,176,206-216]. However, there is still a need for the determination of the photophysical and photochemical properties of novel MPcs whose parameters are yet unknown. In this work a study of the photophysicochemical properties of several novel water soluble and organic soluble MPcs (complexes **33-42**) is carried out. The effect of the central metal, substituent and the solvents used is investigated on in this work. Furthermore very little work has been done on the effect of QD-MPc interactions on the photophysical and photochemical properties of the MPcs in the mixture with QDs or in the conjugate

species [25,53,131,197-203,217]. This work embarks on the elucidation of these photophysical properties in the QD-MPc mixture so as to determine whether the combination of QDs and MPcs will result in superior photosensitizers for PDT.

1.3.4 Singlet oxygen

Singlet oxygen ($^1O_2$) is the chief cytotoxic species in PDT responsible for the apoptosis of cancerous cells and is produced as a result of a transfer of the excited state from an MPc in the triplet state (^{3}MPc*) to ground state oxygen ($^3O_2$, or $^3\Sigma_g^-$). The generation of singlet oxygen is independent of the concentration of the MPc and it can be generated repeatedly from the same solution if molecular oxygen is still available in the solution hence the reason why MPcs degrade with prolonged photosensitization times. In order for MPcs to generate singlet oxygen successfully, the energy of the MPc in the triplet state (T_1) must be well over 94 kJ mol^{-1} so as to foster efficient energy transfer to ground state oxygen to produce $^1O_2$ ($^1\Delta_g$) [81,91]. Photosensitization of MPcs can occur through either one of the two main pathways generally referred to as Type I and Type II mechanisms, Scheme 1.6.

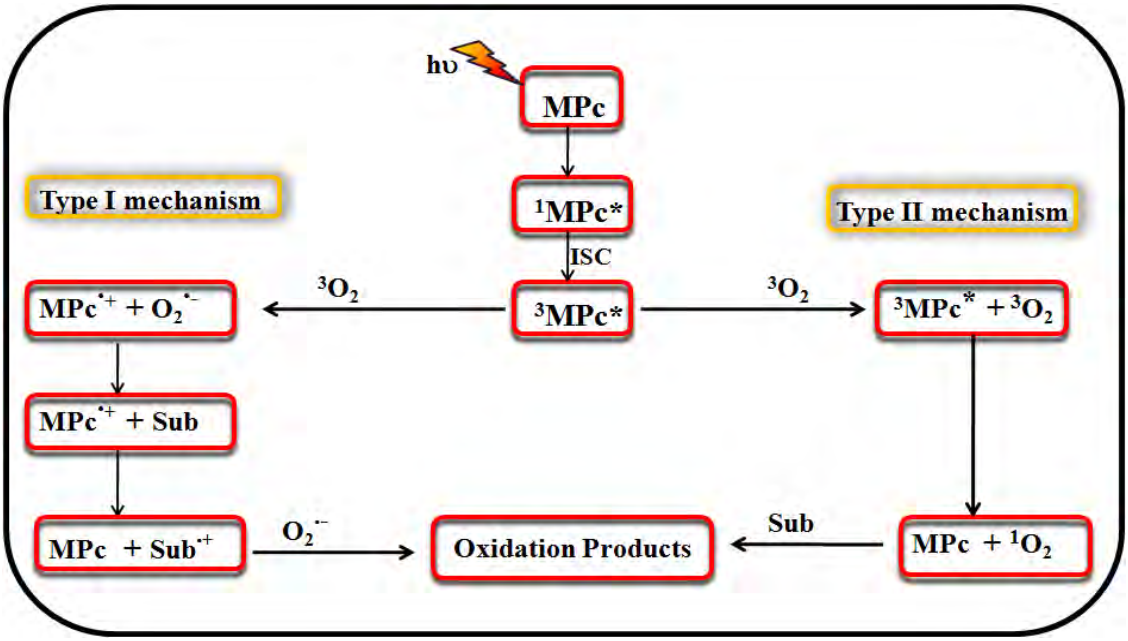

Scheme 1.6: A representation of Type I and Type II photochemical mechanisms.

The Type I mechanism proceeds via hydrogen atom abstraction resulting in photo-initiated autoxidation which leads to formation of radical species while the Type II mechanism is encouraged in environments rich in oxygen and results in the production of $^1O_2$ [95,143,218]. Of the two photosensitization mechanisms, the Type II mechanism has been suggested to take precedence over the Type I mechanism with both mechanisms leading to the formation of oxidation products, Scheme 1.6 [91].

Singlet oxygen quantum yields (Φ_Δ) give a measure of the efficiency of singlet oxygen production by the respective photosensitizers in solution. The Φ_Δ values may be determined via a comparative method using equation 1.14 [219].

$$\Phi_\Delta = \Phi_\Delta^{Std} \frac{W_{DPBF} \cdot I_{abs}^{Std}}{W_{DPBF}^{Std} \cdot I_{abs}} \qquad (1.14)$$

where Φ_Δ^{Std} is the singlet oxygen quantum yield for the standard and W_{DPBF} and W_{DPBF}^{Std} are the singlet oxygen scavenger photobleaching rates in the presence of the photosensitizer under investigation or the standard respectively. I_{abs} and I_{abs}^{Std} are the rates of light absorption by the photosensitizer and the standard respectively and were determined using known methods [219]. The energy transfer efficiency from the MPc in the triplet state to ground state oxygen is determined with the use of equation 1.15

$$S_\Delta = \frac{\Phi_\Delta}{\Phi_T} \qquad (1.15)$$

The S_Δ values give the fraction of the excited triplet state quenched by ground state molecular oxygen.

The most common singlet oxygen scavengers or quenchers used are 1,3-diphenylisobenzofuran (DPBF), 1,4-diazabicyclo-octane (DABCO), sodium azide, tetrasodium-α,α-(anthracene-9,10-diyl)dimethylmalonate (ADMA) and bis 9,10-

anthracene-(4-trimethylphenylammonium)dichloride (BPAA). The singlet oxygen quenchers DPBF and DABCO are used in organic solvents while the rest are employed in aqueous media. In order to determine the efficiency of singlet oxygen production by a given MPc, the quencher e.g. DPBF is mixed with the photosensitizer solution and this mixture is then irradiated for a set amount of time and then the absorption of the quencher is monitored spectroscopically, Figure 1.31 [220]. The method which employs singlet oxygen scavengers is used in this work for the determination of singlet oxygen quantum yields. It has been well documented in literature, that the aforementioned quenchers act solely as chemical quenchers in the respective solvent media in which they are used [221-223]. There is another method for the detection of singlet oxygen and it involves the detection of the characteristic luminescence of singlet oxygen at 1270 nm, however this method was not employed in this work [224,225].

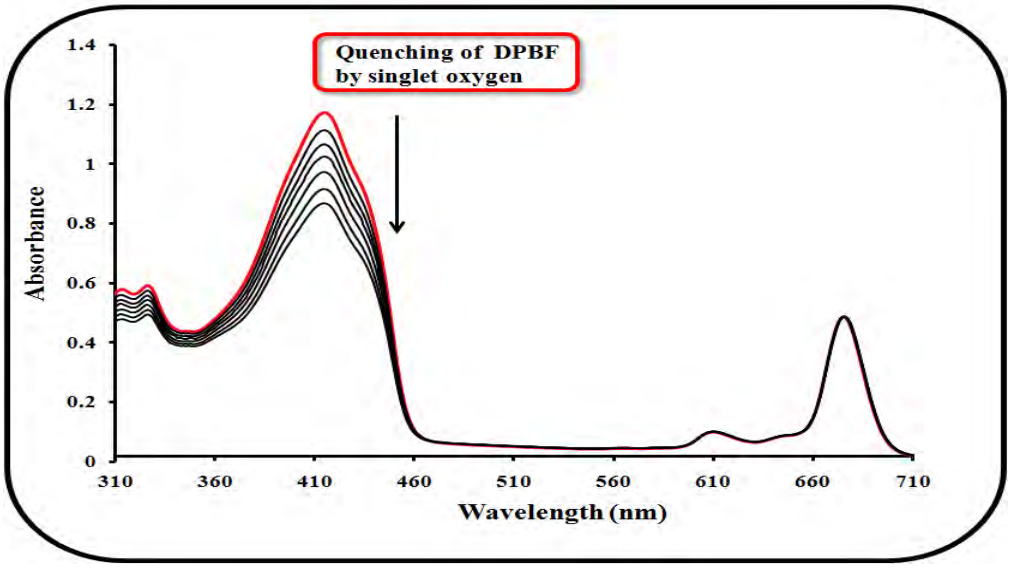

Figure 1.31: An absorption decay profile of DPBF with generation of singlet oxygen by MPc over time [220].

Singlet oxygen quantum yields heavily depend on the triplet quantum yield (Φ_T), triplet lifetime (τ_T), efficiency of energy transfer to $^3O_2$ (S_Δ) and the quenching

capabilities of the substituents borne by the photosensitizer. In general, MPcs that boast high Φ_T values also tend to show high to moderate Φ_Δ values as shown in Table 1.2. It is clear from Table 1.2 that the Φ_Δ values of the MPcs are generally enhanced (except for SiOCPc) in the presence of QDs. The lower Φ_Δ value with SiOCPc suggests that the central metal and the substituents affect the Φ_Δ values significantly with the result that more work is called for in this area.

1.4 Summary of Aims of Thesis

The aims of the work in this thesis are listed as follows:

1. Synthesis of ZnS QDs **(1a)**, CdTe QDs **(1b)** with mercapto ligand stabilizers and TOAB stabilized AuNPs **(2)** and their characterization ((a) spectroscopic: absorption, fluorescence, IR, XRD, (b) microscopy: AFM (for CdTe QDs) and TEM (for AuNPs) (c) time resolved lifetime measurements (for CdTe QDs) and (d) electrochemistry (for CdTe QDs)).

2. The photophysical properties of complexes TmTPZnPz (**27b**) {from quaternization of TPZnPz, **27a**}, ZnTSPc (**28**), ZnTCPc (**29**), ZnOCPc (**30**), TmTPyZnPc (**31b**) {from quaternization of TPyZnPc, **31a**}, TmTMPyZnPc (**32b**) {from quaternization of TMPyZnPc, **32a**} were studied in the presence of QDs.

3. Synthesis of novel neutral and positively charged MPcs: (Cl)GaTMPyPc **(33a)**, (Cl)InTMPyPc **(33b)**, $(Cl)_2$TMPySiPc **(33c)**, TMPySnPc **(33d)** and the quaternization of **33a** and **33b** to give **34** and **35** and the study of their spectroscopic, photophysical, and photochemical properties and the determination of solvent effects on these new MPcs. The photophysical properties of the novel positively charged MPcs (Cl)GaTmTMPyPc **(34)**, (Cl)InTmTMPyPc **(35)** and the donated complexes TtfmPyZnPc **(40)**, and TtfmMPyZnPc **(41)** were also studied in the presence of CdTe QDs.

4. Synthesis of novel negatively charged MPcs: TMmTAAZnPc **(36)**, OMmTAAZnPc **(37)**, (OH)GaTMAAPc **(38a)**, (OH)InTMAAPc **(38b)**, (OH)(Me)SiTMAAPc **(38c)**, TMAAZnPc **(38d),** (OH)GaTMPAPc **(39a)**, (OH)InTMPAPc **(39b)**, (OH)(Me)SiTMPAPc **(39c)** and TMPAZnPc **(39d)** and their photophysical behaviour in the presence and absence of CdTe QDs.

5. Spectroscopic characterization, determination of the photophysical and photochemical properties of THdTZnPc **(42)**, attachment of the MPc complex to AuNPs and the investigation of time resolved measurements and photophysical properties of the **42**-AuNP conjugate.

Experimental

2

In this chapter all the experiments carried out are listed, as well as the characterization methods employed for the complexes synthesized and studied in this thesis.

2.1 Materials

Thioglycolic acid (TGA), 2-mercaptoethanol (2-ME), 3-mercaptopropionic acid (MPA) 98%, L-cysteine, 4,5-pyridine dicarboxylic acid, urea, tellurium powder (200 mesh) and zinc acetate dihydrate, 4-sulphophthalic acid, nitrobenzene, trimellitic anhydride, phthalimide, quinoline, 2-mercaptopyridine, 2-hydroxypyridine, chlorophyll a, 1,3-diphenylisobenzofuran (DPBF), 1-pentanol, 2-mercaptopyridine, silicon tetrachloride, gallium(III)chloride, indium(III)chloride, tin(II) chloride, 4-nitrophthalic acid, Triton-X 100, 2-mercapto-4-methyl-5-thiazoleacetic acid, and pyromellitic anhydride were obtained from Sigma- Aldrich.

Cadmium chloride monohydrate, sodium borohydride, ammonium chloride, ammonium molybdate, dimethylformamide (DMF), urea, sodium hydroxide, sulphuric acid, hydrochloric acid, dimethyl sulphoxide (DMSO), potassium carbonate, ferric chloride, nitric acid, ethanol, tetrahydrofuran (THF), chloroform, hexane, diethylether, acetone, chlorotrimethylsilane, sodium hydrogen phosphate, potasium hydrogen phosphate, sodium chloride, potassium chloride and sodium sulphide, were obtained from Saarchem.

Dimethyl sulphate (DMS), ZnPc, ZnPcSmix, deuterated chloroform ($CDCl_3$), deuterated DMSO (DMSO-d_6), deuterated cpyridine (pyridine-d_5) ammonia (32%), formamide, acetic anhydride, silica gel 60 (0.04-0.063) and neutral alumina were obtained from Merk. Size exclusion chromatography biobeads Sx-2 were obtained from BIO-RAD laboratories. Pyridine, anthracene-9,10-bis-methylmalonate (ADMA), trifluoroacetic acid (TFA), 1,8-Diazabicyclo[5,4,0]undec-7-ene (DBU) was obtained from Fluka. Ultra pure water was obtained from a Milli-Q Water System (Millipore Corp, Bedford, MA, USA). Phosphate buffer saline (PBS) solution (0.01M, pH 7.4) were prepared using adequate amounts of Na_2HPO_4 and K_2HPO_4, KCl and NaCl in ultra pure water. The solvents used for studies in this work, were dried as explained in literature [226].

2.2 Instrumentation

1. The ground state electronic spectra were recorded on a Varian 500 UV-Vis/NIR spectrophotometer or Shimadzu 2550 UV-Vis/NIR.
2. Fluorescence excitation and emission spectra were recorded on a Varian Eclipse spectrofluorimeter.
3. FT- IR data (KBr) pellets was obtained using the Perkin-Elmer spectrum 2000 FTIR spectrometer.
4. ^{1}H-nuclear magnetic resonance (^{1}H NMR) spectra were recorded using the Bruker AMX 400 MHz or Bruker AVANCE II 600 MHz spectrometers.
5. Elemental analyses were carried out on a Vario EL III MicroCube CHNS Analyzer.
6. Mass spectra data were collected with a Bruker AutoFLEX III Smartbeam TOF/TOF Mass spectrometer. The instrument was operated in positive ion mode using an m/z range of 400 – 3000. The voltage of the ion sources were set at 19 and 16.7 kV for ion sources 1 and 2 respectively, while the lens was set at 8.50 kV. The reflector 1 and 2 voltages were set at 21 and 9.7 kV respectively. The spectra were acquired using dithranol as the MALDI matrix, using a 354 nm Nd:YAG laser.

7. X-ray powder diffraction patterns were recorded on a Bruker D8, Discover equipped with a proportional counter, using Cu-Kα radiation (λ = 1.5405 Å, nickel filter). Data were collected in the range from $2\theta = 5^{o}$ to 60^{o}, scanning at 1^{o} min^{-1} with a filter time-constant of 2.5 s per step and a slit width of 6.0 mm. Samples were placed on a silicon wafer slide. The X-ray diffraction data were treated using the freely-available Eva (evaluation curve fitting) software. Baseline correction was performed on each diffraction pattern by subtracting a spline fitted to the curved background and the full-width at half-maximum values used in this study were obtained from the fitted curves.
8. Fluorescence lifetimes were measured using a time correlated single photon counting (TCSPC) setup (FluoTime 200, Picoquant GmbH). The excitation source was a diode laser (LDH-P-C-485 with 10 MHz repetition rate, 88 ps pulse width). However, some lifetime measurements were carried out with a light emitting diode

(LED) and a linear polariser (PLS-500 with PDL 800-B, Picoquant GmbH 497 nm, with 10 MHz repetition rate). Fluorescence was detected under the magic angle with a peltier cooled photomultiplier tube (PMT) (PMA-C 192-N-M, Picoquant) and integrated electronics (PicoHarp 300E, Picoquant GmbH). A monochromator with a spectral width of about 8 nm was used to select the required emission wavelength band (Figure 2.1). The response function of the system, which was measured with a scattering Ludox solution (DuPont), had a full width at half-maximum (FWHM) of about 300 ps. The ratio of stop to start pulses was kept low (below 0.05) to ensure good statistics. All luminescence decay curves were measured at the maximum of the emission peak. The data were analysed with the program FluoFit (Picoquant). The support plane approach was used to estimate the errors of the decay times [181].

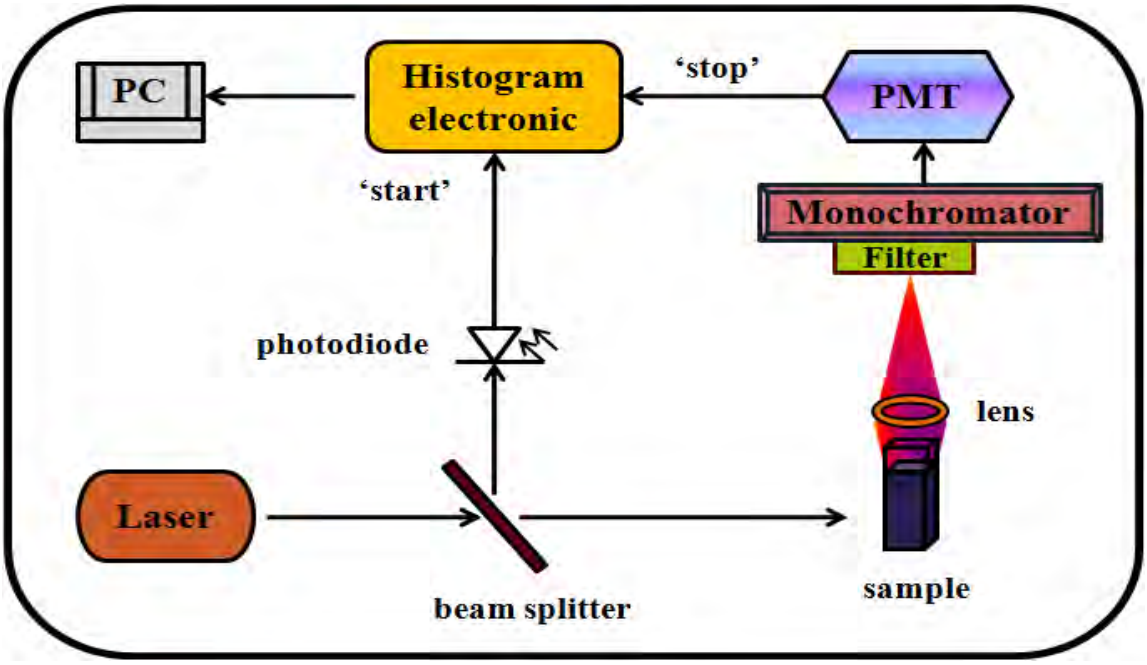

Figure 2.1: A schematic diagram of the setup of the TCSPC equipment.

9. Photo-irradiations for singlet oxygen quantum yields were done using a General Electric Quartz line lamp (300W). A 600 nm glass cut off filter (Schott) and a water filter were used to filter off ultraviolet and infrared radiations respectively. An

interference filter (Intor, 670 nm with a band width of 40 nm) was additionally placed in the light path before the sample (Figure 2.2).

10. Light intensities were measured with a POWER MAX5100 (Mol-electron detector incorporated) power meter and were found to be 1.25 × 10^{16} photons s^{-1} cm^{-2} for singlet oxygen studies.

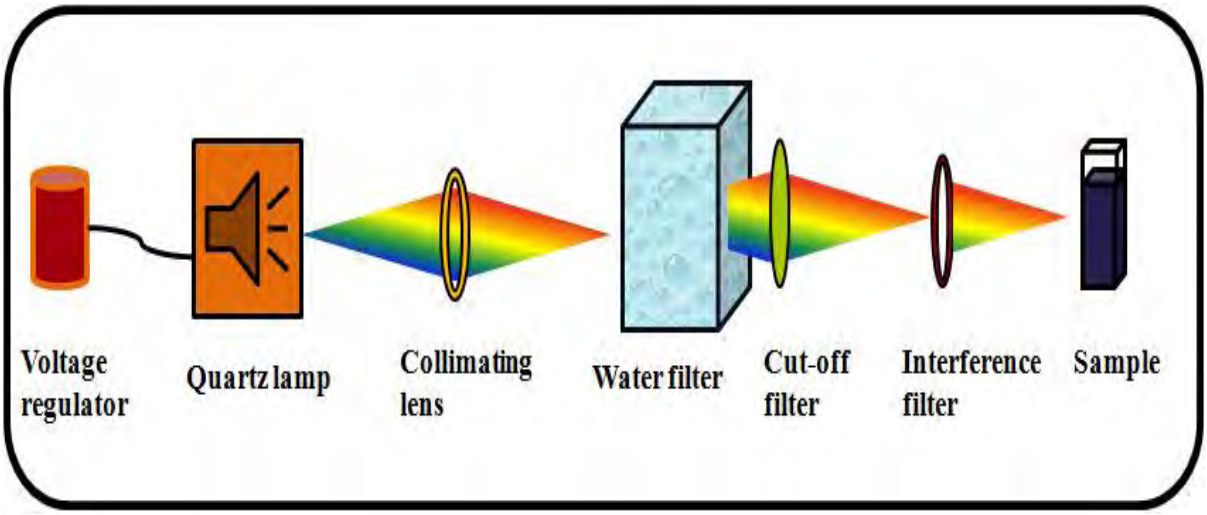

Figure 2.2: Schematic diagram for a photochemical setup.

10. Laser flash photolysis experiments were performed with light pulses produced by a Quanta-Ray Nd:YAG laser providing 400 mJ, 9 ns pulses of laser light at 10 Hz, pumping a Lambda-Physik FL3002 dye (Pyridin 1 dye in methanol). Single pulse energy ranged from 2 to 7 mJ. The analyzing beam source was from a Thermo Oriel xenon arc lamp, and a photomultiplier tube was used as a detector (Figure 2.3). Signals were recorded with a digital real-time oscilloscope (Tektronix TDS 360). The triplet life times were determined by exponential fitting of the kinetic curves using the program OriginPro 7.0.

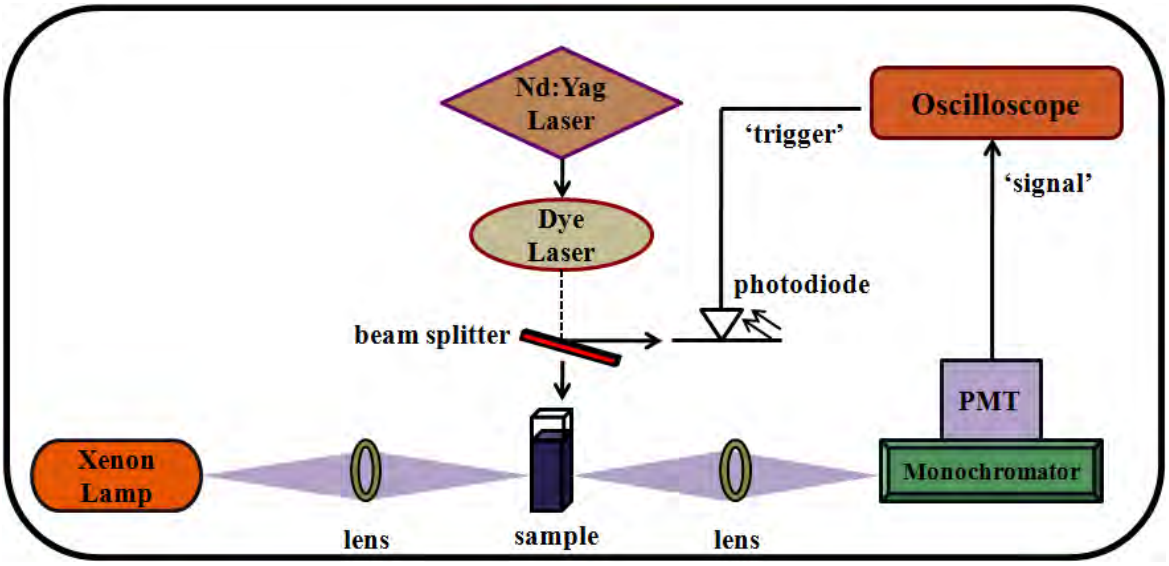

Figure 2.3: Schematic diagram for a laser flash photolysis setup.

2.3 Methods

2.3.1 Absorption and Fluorescence studies

In this work the interactions between MPcs and the different nanoparticles were studied spectroscopically. The absorbance and emission spectra of QDs were generally obtained in aqueous media. However, their interaction with MPcs was studied in a mixture of solvents such as pyridine: water (1:1 v/v) and ethanol: NaOH 0.01 M (1:1 v/v) solvent mixtures. These solvent mixtures allow for the solubilization of QDs and MPcs and they in turn preserve the monomericity of the MPc. The absorption spectra of the MPcs alone have been acquired in different solvents and all measurements were carried out at ambient conditions in a 1 cm quartz cell. For fluorescence studies, the solutions of the standards, QDs and MPcs under investigation were prepared such that the absorbance at the excitation wavelength was ~ 0.05. In order to determine the fluorescence quantum yields, the area under the curves was determined and used in equation 1.4. When different solvents were used for the sample and standard respectively, the refractive indices were corrected for. The standard commonly used for MPcs is ZnPc in DMSO for Φ_F determinations,

Φ_F = 0.20 while Rhodamine 6G in ethanol with Φ_F = 0.94 is generally used as a standard for Φ_F determinations for quantum dots [179-181].

2.3.2 Förster Resonance Energy Transfer (FRET) studies

FRET interactions between QDs and MPcs were studied at ambient conditions by adding a solution of QDs of known concentration (~10^{-6} M) to a solution of MPc with known concentration (~6 × 10^{-6} M). The changes in absorbance and fluorescence spectra from the QD and MPc solutions alone and when mixed are then recorded. The fluorescence data obtained is then used to calculate for the fluorescence quantum yield of the QDs in the presence of the donor ($\Phi_{F(DA)}$) which is then used to calculate for the efficiency (*Eff*) of energy transfer using equation 1.8. FRET results in the quenching of QDs due to the non radiative energy transfer to MPcs in the vicinity of QDs.

2.3.3 Quenching studies

The fluorescence quenching of QDs by MPcs was also carried out at room temperature by titrating QDs in solution (with a fixed concentration 10^{-6} M) with the respective MPc (quencher) solution of varying concentrations (from 0 to 8 × 10^{-6} M). The QD solutions during the titration were excited at 500 nm and the fluorescence was recorded between 510 nm and 800 nm in the absence or presence of the respective MPc serving as a quencher.

2.3.4 Fluorescence lifetimes studies

Fluorescence lifetimes (τ_F) for QDs in the absence and the presence of MPcs were determined through the use of time correlated single photon counting (TCSPC) setup (Figure 2.1). The solutions of the samples to be measured had optical densities below

0.1. In addition, the ratio of the stop to start pulses was kept below 0.05 in order to ensure good statistics. The decay curves were all measured at the maximum of the emission peak and the matching lifetimes were obtained by using the FluorFit software program to deconvolute the decay curves. Time resolved emission spectra for some MPcs were also obtained using the TCSPC setup at 4 nm steps.

2.3.5 Triplet quantum yields and lifetimes

The studies of triplet quantum yields (Φ_T) and the corresponding triplet lifetimes (τ_T) were obtained by recording the triplet absorption and decay kinetics during laser flash photolysis (from the setup shown in Figure 2.3). The optical density of the MPc solutions to be investigated was set to ~1.5 and placed in a 1 cm path length spectrophotometric quartz cell and were deaerated with argon gas for about 20 min and were then irradiated at the wavelength where the standard and sample Q-bands crossed with Nd:YAG laser light. The Φ_T were calculated from equation 1.12 using ZnPc in DMSO (Φ_T = 0.65, [205]), in DMF (Φ_T = 0.58, [206]) or $ZnPcS_4$ in aqueous media (Φ_T = 0.56, [227]) as standards. Triplet lifetimes were attained from an exponential fitting of kinetic curves using OriginPro 7.0 software.

2.3.6 Singlet oxygen quantum yields

Quantum yields of singlet oxygen (Φ_Δ) were determined with the use of the setup shown in Figure 2.2. The Φ_Δ values were determined using air saturated solutions of the MPcs (2 mL) mixed with the respective singlet oxygen quencher (DPBF in organic media or ADMA in aqueous media) in a 1 cm pathlength spectrophotometric quartz cell with a stopper that fits well. This mixture is then photolysed at the Q-band position using the setup described above. The absorbance decay of the quencher at 416 nm for DPBF in DMSO or 380 nm for ADMA in aqueous media was monitored with time and the resulting data used in calculating for the Φ_Δ values

using equation 1.14. The concentration of DPBF was kept at about 3 x 10^{-5} M and that of ADMA was kept at about 6 x 10^{-5} M in order to avoid chain reactions involving the quencher [216]. The same quencher concentration (at an absorbance ~ 0.6) was used for both the MPc sample and the respective standard. ZnPc in DMSO (Φ_Δ = 0.67 [215]), in DMF (Φ_Δ = 0.56 [216]) or $ZnPcS_{mix}$ in aqueous media (Φ_Δ = 0.45 [228]) were employed as standards.

2.4 Synthesis

2.4.1 Synthesis of ZnS (1a) quantum dots (ME-ZnS, Scheme 3.1)

ZnS quantum dots were synthesized using the wet chemical method using 2-mercaptoethanol as a capping agent. The synthesis was carried out following previously mentioned methods [34]. Zinc acetate dihydrate ($ZnAc_2.2H_2O$) (0.44g, 2 mmol) and the capping agent 2-mercaptoethanol (0.19g, 2.39 mmol) were dissolved in 25 mL deionised water under inert atmosphere. A 10 mL solution of sodium sulphide (0.2 M) was then added to the reaction mixture. The white suspension formed was left stirring for 6 days while heating at 100 ^oC. Centrifugation of the white suspension afforded the particles which were then washed with distilled water and once with ethanol. The white powder was then left to dry in a vacuum dessicator for 24 hours. The ZnS quantum dots powder was redispersed in a pH 7.4 phosphate buffer solution. The sizes of the ZnS quantum dots were determined through the use of XRD to be 2.90 nm.

ME stabilized ZnS QDs (1a): IR [(KBr) υ_{max}/cm^{-1}]: 3332 (O-H), 2930 (C-H), 1632, 1556 (C-O), 1414 (C-H), 940 (C-S). UV/Vis (PBS pH 7.4): λ_{max} nm (log ε): 370 nm.

2.4.2 Synthesis of CdTe (1b) quantum dots (Scheme 3.2)

CdTe quantum dots were synthesized using wet chemical routes with thioglycolic acid (TGA), 3-mercaptopropionic acid (MPA) and 2-mercaptoethanol (ME) cappings, using reported methods [4]. Briefly, $CdCl_2$ (0.22g, 1.18 mmol) was dissolved in 65 mL of deionized water and (2.6g, 2.86 mmol) TGA, MPA or 2-ME was added to the $CdCl_2$ solution. The pH of this precursor solution was adjusted to 11.5 with 1 M NaOH and left under a flow of nitrogen gas for half an hour. The solution of NaHTe was prepared by modified literature methods as follows: 0.05 M NaOH was reacted with H_2Te gas (the latter generated by reaction of $NaBH_4$ (0.035g, 0.9 mmol) with Te powder (0.091g, 0.7 mmol) in the presence of 0.5 M H_2SO_4 under a flow of nitrogen gas). This reaction employed a molar ratio of Cd^{2+}:Te^{2-}:Thiol capping group of 1:0.5:2.4. The freshly prepared NaHTe was then added to the precursor solution. The solution was refluxed under air at 100 ^oC for 3 days (until the desired size was reached). Aliquots from the growth solution were frequently sampled and the absorbance and emission spectra were recorded. Precipitation of the QDs from the aqueous colloidal solution was achieved by using propan-2-ol yielding a yellow to orange colour for the ME capped CdTe QDs and orange to maroon colour for the TGA and MPA capped CdTe QDs. The sizes of the CdTe quantum dots were determined using a polynomial fitting function explained by equation 1.1 and XRD.

ME stabilized CdTe QDs (1b, i): IR [(KBr) υ_{max}/cm^{-1}]: 3335 (O-H), 2933, 2874 (C-H), 1458, 1416 (C-O), 761 (C-S). UV/Vis (PBS pH 7.4): λ_{max} nm (log ε): 570 nm (4.4).

TGA stabilized CdTe QDs (1b, ii): IR [(KBr) υ_{max}/cm^{-1}]: 3252 (O-H), 2957 (C-H), 1552, 1377 (C=O), 774, 692 (C-S). UV/Vis (PBS pH 7.4): λ_{max} nm (log ε): 570 nm (5.1).

MPA stabilized CdTe QDs (1b, iii): IR [(KBr) υ_{max}/cm^{-1}]: 3326 (O-H), 2903 (C-H), 1552, 1392 (C=O), 850 (C-S). UV/Vis (PBS pH 7.4): λ_{max} nm (log ε): 570 nm (4.9).

2.4.3 Gold Nanoparticles

2.4.3.1 Synthesis of Gold Nanoparticles (AuNPs (2), Scheme 3.3)

Gold nanoparticles (**2**) were prepared following literature methods by dissolving gold (III) chloride in water (25 mM, 2 mL) and then added to tetraoctylammonium bromide solution (85 mM, 3 mL) in toluene under vigorous stirring until all the gold chloride was transferred into the organic phase [40]. A reducing agent $NaBH_4$ in an aqueous media (36 mM, 2mL) was added dropwise over a period of 10 min after which the mixture was stirred vigorously for 20 min. The resulting organic phase was separated and washed with water and was left to dry under vacuum. The gold nanoparticles obtained as a yellow powder were characterized using XRD, TEM and AFM and were found to have an average size of 5 nm.

Au NPs (**2**)**:** IR [(KBr) υ_{max}/cm^{-1}]: 3023 (N-H), 2927, 2860 (C-H), 1215 (C-N), 746, 668 (N-H). UV/Vis ($CHCl_3$): λ_{max} nm (log ε): 389 nm (7.04) [139].

2.4.3.2 Synthesis of the MPc-AuNP conjugate (42-AuNP (44), Scheme 3.3)

The novel MPc-AuNP conjugate **44** was prepared according to reported procedures [138,139]. The complex THdTZnPc (**42**) (0.020 g, 0.016mmol) and TOAB-AuNPs (0.050 g) in toluene 5 mL were mixed and stirred for 72 hrs for the ligand exchange to take place and to attach the Pc onto AuNPs. After the ligand exchange, the unreacted MPc was separated in a size exclusion column: Biobeads S-X1 using toluene as an eluent. The MPc-AuNP conjugate comes off first, followed by unreacted AuNPs and finally the unreacted MPc. The THdTZnPc-Au NP conjugate was characterized using XRD, TEM and AFM.

THdTZnPc-AuNP (**44**)**:** IR [(KBr) υ_{max}/cm^{-1}]: 3018 (N-H), 2932 (C-H), 1517 (C=C), 1213 (C-N), 1039 (C-C), 749, 667 (N-H). UV/Vis ($CHCl_3$): λ_{max} nm (log ε): 426 (7.28) [139].

The syntheses of complexes **27a** [229,230], **27b** [126], **28** [117,120], **29** [123], **30** [118,122], **31a** [129,231,232] and **32a** and **32b** [130] have been reported before (Schemes 3.4 and 3.5).

2.4.4 Synthesis of substituted phthalonitriles (Scheme 3.6).

The syntheses of complexes **54a** [129] and **54b** [233] have been reported before (Scheme 3.6).

4-(2-Pyridyloxy) phthalonitrile (54a): 2-hydroxypyridine (3.90 g, 41 mmol) and 4-nitrophthalonitrile (**14**) (5.00 g, 29 mmol) were dissolved in DMF (30 ml) under argon according to reported methods [129,231,232]. After stirring for 30 min at room temperature, finely ground anhydrous potassium carbonate (9.70 g, 70 mmol) was added in portions during 4 h with efficient stirring. The reaction mixture was stirred under argon atmosphere at room temperature for 3 days. Then the mixture was poured into 200 ml iced water, and the precipitate was filtered off, washed with water and then dried. The crude product was recrystallized from ethanol. Finally the pure product was dried in vacuum to give a brown-yellow solid. Yield: 6.09 g (95 %). IR [(KBr) υ_{max}/cm^{-1}]: 2239 (C≡N), 1290 (C-O-C), 1210, 1183, 1162 (C-N). ^{1}H NMR (DMSO-d_6); δ, ppm: 8.28-26 (1H, d, Ar-H), 8.12-7.93 (2H, m, Ar-H), 7.78-7.72 (1H, d, Ar-H), 7.65-7.61 (1H, t, Ar-H), 6.60-6.58 (1H, d, Ar-H), 6.46-6.44 (1H, t, Ar-H).

4-(2-Mercaptopyridine) phthalonitrile (54b): The synthesis of **54b** was similar to that of **54a**, except 2-mercaptopyridine (2.33 g, 21 mmol) was employed instead of 2-hydroxypyridine [233]. The amount of 4-nitrophthalonitrile (**14**) used was (3.63 g, 21 mmol). The quantity of anhydrous potassium carbonate used was (7.5 g, 54.0 mmol). The crude product was recrystallized from ethanol. Finally the pure product was dried in vacuum to give a brownish yellow solid. Yield: 3.79 g (76 %). IR [(KBr) υ_{max}/cm^{-1}]: 2231 (C≡N), 643 (C-S-C), 1282, 1157, 1130 (C-N). ^{1}H NMR (DMSO-d_6); δ,

ppm: 8.50 (1H, d, Ar-H), 8.28 (1H, s, Ar-H), 8.09 (1H, d, Ar-H), 7.91 (1H, dd, Ar-H), 7.81-7.68 (1H, m, Ar-H), 7.46 (1H, d, Ar-H), 7.35 (1H, m, Ar-H).

4-(2-Mercapto-4-methyl-5-thiazoleaceticacid) phthalonitrile (54c): 2-Mercapto-4-methyl-5-thiazoleaceticacid (3.98 g, 21mmol) and 4-nitrophthalonitrile (**14**) (3.64 g, 21 mmol) were dissolved in DMF (80 mL) under a stream of nitrogen and the mixture was stirred at room temperature for 15 min. Thereafter, finely ground K_2CO_3 (7.5g, 54 mmol) was added portion-wise over a period of 4 h and the reaction mixture left to stir for a further 72 h at room temperature. The mixture was then added to diethyl ether (150 mL) and stirred for 15 min. The resulting precipitate was filtered, thoroughly washed with diethyl ether and acetone, dried and recrystallized from an ethanol: chloroform mixture (5:1). Yield: 5.95 g (90 %) IR [(KBr) ν_{max}/cm^{-1}]: 3434 (COOH), 2223 (C≡N), 1591 (C=C), 1379 (C-OH), 1270 (C-O). ^{1}H NMR (400 MHz, D_2O) δ ppm: 8.04 (1H, s, OH), 7.92-7.89 (2H, d, Ar-H), 7.83 (1H, s, Ar-H), 3.39 (2H, s, CH_2), 2.28 (3H, s, CH_3).

4,5-(2-Mercapto-4-methyl-5-thiazoleaceticacid) phthalonitrile (54d): The synthesis of **54d** was the same as for **54c**, except 4,5-dichlorophthalonitrile (**17)** (1.99g, 10 mmol) was employed instead of **14**. The amounts of the other reagents and reaction conditions were the same as for **54c**. Yield: 5.86 g (55 %). IR[(KBr) ν_{max}/cm^{-1}]: 3278 (COOH), 2231 (C≡N), 1617 (C=C), 1383 (C-OH), 1278 (C-O). ^{1}H NMR (400 MHz, D_2O) δ ppm: 8.09 (2H, s, OH), 8.00 (2H, s, Ar-H), 3.80 (s, 4H, CH_2), 2.93 (6H, s, CH_3).

4-(2-Mercaptoacetic acid) phthalonitrile (54e)*:* 2-Mercaptoacetic acid (1.93 g, 21 mmol) and 4-nitrophthalonitrile (**14**) (3.63 g, 21 mmol) were dissolved in DMF (80 mL) under a stream of nitrogen and the mixture stirred at room temperature for 15 min. Thereafter, finely ground K_2CO_3 (4.5g, 33 mmol) was added portion wise over a period of 4 h and the reaction mixture left to stir for a further 72 h at room temperature. The mixture was then added to diethyl ether (150 mL) and stirred for

15 min. The resulting precipitate was filtered off, thoroughly washed with diethyl ether and acetone, dried and recrystallized from an ethanol: chloroform mixture (5:1). Yield: 10.1 g (93 %) IR [(KBr) ν_{max}/cm^{-1}]: 3397 (COOH), 2222 (C≡N), 1641-1603 (C=C), 1448-1381 (C-OH), 1310-1113 (C-O) 910-827 (C-S-C). ^{1}H NMR (600 MHz, DMSO-d_6); δ ppm: 10.01 (1H, m, Carboxyl-H), 7.92 (1H, d, Ar-H), 7.89 (1H, d, Ar-H), 7.66 (1H, dd, Ar-H), 3.71 (2H, m, Methylene-H).

4-(2-Mercaptopropionic acid) phthalonitrile (54f)*:* The synthesis for **54f** was the same as for **54e** except 3-mercaptopropionic acid (2.2 g, 21 mmol) was employed instead of mercaptoacetic acid. The amounts of the reagents were the same as for **54e**. Yield: 10.7g (92 %) IR [(KBr) ν_{max}/cm^{-1}]: 3324 (COOH), 2263 (C≡N), 1664-1582 (C=C), 1455-1380 (C-OH), 1331-1274 (C-O), 880-803 (C-S-C). ^{1}H NMR (600 MHz, DMSO-d_6); δ ppm: 9.91(1H, s, Carboxyl-H), 7.98 (1H, d, Ar-H), 7.71 (1H, dd, Ar-H), 7.64 (1H, d, Ar-H), 3.41 (2H, m, methine-H), 3.21 (2H, m, Methylene-H).

The phthalonitriles **54g**, **54h** and **54i** were synthesized by the researchers who donated the MPc complexes **40**, **41** and **42** respectively and the details of their synthesis are shown below, since they are reported for the first time.

4-[5-(trifluoromethyl)-2-pyridyloxy] phthalonitrile (54g): The synthesis of **54g** was carried out by dissolving 4-nitrophthalonitrile (**14**) (0.97 g, 5.58 mmol) in DMF (10 ml) under argon followed by the addition of 2-hydroxy-5-(trifluoromethyl)pyridine (1.00 g, 5.58 mmol). After stirring for 30 min at room temperature, finely ground anhydrous potassium carbonate (2.30 g, 16.7 mmol) was added in portions during 4 h with efficient stirring. The reaction mixture was stirred under argon atmosphere at room temperature for 3 days. Then the mixture was poured into 200 ml iced water, and the precipitate was filtered off, washed with water and then dried. The crude product was recrystallized from ethanol. Finally the pure product was dried in vacuum. Yield: 1.40 g (85 %). IR spectrum (cm^{-1}): 3092, 3057 (Ar-CH), 2235 (C≡N),

1599 (C=C), 1581 (C=N), 1476, 1379 (C-F), 1330, 1247, 1215, 1113, 1007, 939, 849, 742, 688 (C-S-C). ^{1}H NMR ($CDCl_3$): δ = 8.71 (1H, s, Ar-H), 8.04 (1H, s, Ar-H), 7.94-7.82 (3H, m, Ar-H), 7.44 (1H, d, Ar-H).

4-[5-(trifluoromethyl)-2-mercaptopyridine]-phthalonitrile (54h): The synthesis of **54h** was similar to that of **54g** except 5-(trifluoromethyl)-2-mercaptopyridine (1.00 g, 6.13 mmol) instead of 2-hydroxy-5-(trifluoromethyl)pyridine was employed. The amounts of the other reagents were: 4-nitrophthalonitrile (**14**) (1.06 g, 6.13 mmol) and anhydrous potassium carbonate (2.38 g, 18.0 mmol). Yield: 1.0 g (56 %). IR spectrum (cm^{-1}): 3076, 3053 (Ar-CH), 2238 (C≡N), 1597 (C=C), 1578 (C=N), 1492, 1384 (C-F), 1336, 1250 (C-O-C), 1169, 1116, 1065, 917, 853, 774, 616. ^{1}H NMR ($CDCl_3$): δ = 8.02 (d, 1H, Ar-H), 7.97 (1H, s, Ar-H), 7.88-7.85 (2H, m, Ar-H), 7.62-7.59 (1H, m, Ar-H), 6.81 (d, 1H, Ar-H).

4-(1,6-hexanedithiol) phthalonitrile (54i): The synthesis of **54i** was carried out by the dissolving 1,6-hexanedithiol (1.6 mL, 11 mmol) and 4-nitrophthalonitrile (**14**) (1.68 g, 9 mmol) in DMF (80 mL) under a stream of nitrogen and the mixture stirred at room temperature for 15 min. Thereafter, finely ground K_2CO_3 (2.12g, 15mmol) was added portion wise over a period of 4 h and the reaction mixture left to stir for a further 24 h at room temperature. The mixture was then added to water (150 mL) and stirred for 30 min. The resulting precipitate was filtered off, thoroughly washed with diethyl ether and acetone, dried and recrystallized from an ethanol. Yield: 2.7 g (90 %) IR [(KBr) ν_{max}/cm^{-1}]: 3007 (C-H), 2230 (C≡N), 1668, 1583 (C=C), 1437, 1408, 1387 (C-H) 884, 666 (C-S-C). ^{1}H NMR (600 MHz, DMSO-d_6 δ ppm: 7.64-7.62 (m, 1H, Ar-H), 7.53 (d, 1H, Ar-H), 7.48-7.47 (dd, 1H, Ar-H), 3.02-3.00 (m, 6H, Methylene-H), 1.67-1.42 (m, 6H, Methylene-H), not observed (m, 1H, SH).

2.4.5 Synthesis of substituted phthalocyanines (Schemes 3.4 and 3.7 to 3.12).

The synthesis of **31a** has been reported before but its quaternization was not reported [129]. In this thesis the quaternization of **31a** is attempted and reported (Scheme 3.4).

Quaternized tetrakis-2,(3)-[(2-pyridyloxy)phthalocyanine]zinc(II) (TmTPyZnPc (31b), Scheme 3.4).

This complex was prepared by the quaternization of Tetrakis-2,(3)-[(2-pyridyloxy)phthalocyanine]zinc(II) (**31a**) according reported methods [126] as follows: complex **31a** (0.2 g, 0.21 mmol) was heated to 120 ^{o}C in freshly distilled DMF (1 mL) and dimethyl sulphate (5 mL) was added dropwise. The mixture was stirred at 120 ^{o}C for 12 h, cooled to room temperature and the product was precipitated with hot acetone and collected by filtration. The greenish blue product was washed successively with hot ethanol, ethyl acetate, THF, $CHCl_3$, n-hexane, and diethyl ether. The resulting product was dried over phosphorous pentoxide. Yield: 0.12 g, (58 %) UV/vis (DMSO): λ_{max} nm (log ε); 681 (4.60), 615 (3.87), 348 (4.02); IR (KBr): ν_{max}/cm^{-1}; 3145 (ν_{Ar-H}), 1560, 1577, 1597 ($\nu_{C=C}$), 1190-1250 (ν_{C-O}), 1090, 1096, 1120 (ν_{C-O-C}). ^{1}H NMR: (D_2O): δ ppm 6.8-10.2 (28H, m, Pc-H and Pyridyl H), 3.7-4.7 (12H, m, CH_3). $C_{56}H_{40}N_{12}O_4Zn.2SO_4$: C 65.55, H 3.90, N 16.27, Found: C 64.45, H 3.72, N 16.52. MALDI-TOF-MS m/z: Calc. 1202.61 amu; Found: 1202.76 $[M]^{+}$.

Tetrakis-2,(3)-[(2-mercaptopyridine)phthalocyanine]gallium(III) ((Cl)GaTMPyPc (33a), Scheme 3.7).

A mixture of $GaCl_3$ (0.25 g, 1.5 mmol), 4-(2-mercaptopyridine)phthalonitrile **(54b)** (0.5 g, 2.1 mmol), DBU (1.66 mL, 12 mmol) and 1-pentanol (10 mL) was stirred at 160 ^{o}C for 5 h under nitrogen atmosphere. After cooling, the solution was mixed with n-hexane. The green solid product was precipitated and collected by filtration and washed with n-hexane. The crude product was re-dissolved in DMF. After concentrating, the green product was precipitated with hot ethanol and filtered then washed with ethanol, acetone, n-hexane and diethyl ether. The green product was further purified by passing through a column of biobeads Sx-1 using DCM as the eluting solvent. Yield: 0.215g (39 %). UV/vis (DMSO): λ_{max} nm (log ε); 691 (5.43), 624 (4.65), 363 (4.68); IR (KBr): ν_{max}/cm^{-1}; 3061 (ν_{Ar-H}), 1312 ($\nu_{C=C}$), 1077 (ν_{C-S-C}). ^{1}H NMR

(400 MHz, DMSO-d_6) δ ppm: 9.86-9.76 (d, 4H, Pyridyl-H), 9.7-8.56 (d, 8H, Pc-H), 7.89-7.82 (dd, 4H, Pyridyl-H), 7.61-7.46 (m, 8H, Pyridyl-H), 7.36-7.33 (bs, 4H, Pc-H). Calc. for $C_{52}H_{28}N_{12}S_4GaCl$: C 59.24, H 2.68, N 15.95, S 12.16 Found: C 58.99, H 3.61, N 15.95, S 10.47. MALDI-TOF-MS m/z: Calc. 1052 amu; Found: 1054.03 $[M+2H]^+$.

Tetrakis-2,(3)-[(2-mercaptopyridine)phthalocyanine]indium(III) ((Cl)InTMPyPc (33b), Scheme 3.7).

The method employed for synthesis of **33b** was the same as used for **33a**, except $InCl_3$ instead of $GaCl_3$ was employed. The amounts of all the reagents were the same (in terms of mmol) as for **33a**. Yield: 0.126g (54 %). UV/vis (DMSO): λ_{max} nm (log ε); 698 (5.09), 630 (4.47), 360 (4.65); IR (KBr): ν_{max}/cm^{-1}; 3067 (ν_{Ar-H}), 1335 ($\nu_{C=C}$), 1091 (ν_{C-S-C}). ^1H NMR (400 MHz, DMSO-d_6) δ ppm: 9.25 (m, 8H, Pyridyl-H), 8.58 (d, 8H, Pc-H), 7.45 (dd, 4H, Pyridyl-H), 7.3 (s, 4H, Pc-H), 7.07 (d, 4H, Pyridyl-H). Calc. for $C_{52}H_{28}N_{12}S_4InCl$: C 56.81, H 2.57, N 15.29, S 11.67; Found: C 57.51, H 2.96, N 14.53, S 11.10. MALDI-TOF-MS m/z: Calc. 1098 amu; Found: 1099.38 $[M+H]^+$.

Tetrakis-2,(3)-[(2-mercaptopyridine)phthalocyanine]silicon(IV) ($(Cl)_2$SiTMPyPc (33c), Scheme 3.7).

The method employed for synthesis of **33c** was the same as used for **33a**, except $SiCl_4$ instead of $GaCl_3$ was employed. The amounts of all the reagents were the same (in terms of mmol) as for **33a** Yield: 0.298 g (50 %). UV/vis (DMSO): λ_{max} nm (log ε); 692 (5.07), 623 (4.39), 368 (4.66); IR (KBr): ν_{max}/cm^{-1}; 3052 (ν_{Ar-H}), 1337 ($\nu_{C=C}$), 1093 (ν_{C-S-C}). ^1H NMR (400 MHz, DMSO-d_6) δ ppm: 8.52-8.48 (dd, 4H, Pyridyl-H), 8.12-8.09 (s, 4H, Pc-H), 7.94-7.88 (d, 4H, Pyridyl-H), 7.85 (m, 8H, Pyridyl-H), 7.83-7.77 (d, 8H, Pc-H). Calc. for $C_{52}H_{28}N_{12}S_4SiCl_2$: C 58.31, H 2.69, N 15.69, S 11.97 Found: C 58.75, H 3.22, N 14.95, S 11.41. MALDI-TOF-MS m/z: Calc. 1046 amu; Found: 1048.11 $[M+2H]^+$.

Tetrakis-2,(3)-[(2-mercaptopyridine)phthalocyanine]tin(II) (SnTMPyPc (33d), Scheme 3.7).

The method employed for synthesis of **33d** was the same as used for **33a**, except $SnCl_2$ instead of $GaCl_3$ was employed. The amounts of all the reagents were the same (in terms of mmol) as for **33a**. Yield: 0.137g (48 %). UV/vis (DMSO): λ_{max} nm (log ε); 711 (4.32), 636 (3.63), 373 (3.84); IR (KBr): ν_{max}/cm^{-1}; 3050 (ν_{Ar-H}), 1336 ($\nu_{C=C}$), 1080 (ν_{C-S-C}). ^1H NMR (400 MHz, DMSO-d_6) δ ppm: 8.50-8.47 (m, 8H, Pyridyl-H), 7.95-7.79 (d, 8H, Pc-H), 7.86-7.11 (s, 4H, Pc-H), 7.32-7.29 (d, 8H, Pyridyl-H). Calc. for $C_{52}H_{28}N_{12}S_4Sn$: C 58.49, H 2.64, N 15.73, S 12.01 Found: C 58.8, H 3.39, N 14.2, S 10.83. MALDI-TOF-MS m/z: Calc. 1068 amu; Found: 1069.04 $[M+H]^+$.

Quarternized tetrakis-2,(3)-[(2-mercaptopyridine)phthalocyanine]gallium(III) ((Cl)GaTmTMPyPc (34), Scheme 3.8).

The quaternization of complexes **33c** and **33d** were not attempted due to the low yields obtained for these complexes and was only carried out for complexes **33a** and **33b** as follows: complex **33a** (0.12 g, 0.11 mmol) was added to DMF (5 mL) and to this solution dimethyl sulphate was added (5 mL). The mixture was then left stirring and heated to 120 ^oC for 12 h under nitrogen. The dark green product was precipitated from the DMF with hot acetone, and the precipitate was then washed further with hot acetone, hexane, ethanol and diethyl ether. Yield: 0.041g (33 %). UV/vis (DMSO): λ_{max} nm (log ε); 361 (4.79), 620 (4.56), 691 (5.31); IR (KBr): ν_{max}/cm^{-1}; 2997, 2913 (ν_{C-H}), 1663, 1436, 1406 ($\nu_{C=C}$), 1311 (ν_{C-S-C}). ^1H NMR (600 MHz, DMSO-d_6) δ ppm: 9.29-9.26 (4H, m, Pyridyl-H), 8.74-8.68 (8H, t, Pyridyl-H), 8.27-8.21 (4H, d, Pc-H), 7.97-7.93 (4H, d, Pyridyl-H), 7.60-7.45 (dd, 4H, Pc-H), 7.26 (4H, s, Pc-H), 1.29 (12H, s, Pyridyl-H). Calcd for $C_{56}H_{40}N_{12}S_4GaCl{\cdot}2SO_4{\cdot}H_2O$: C 45.55, H 4.09, N 11.38, S 13.04 %. Found: C 44.78, H 3.95, N 11.05, S 17.83 %**.** MALDI-TOF-MS *m/z*: Calc.; 1306.55 Found: 1078.90 $[M-2(SO_4)-Cl]^+$.

Quarternized tetrakis-2,(3)-[2-mercaptopyridine)phthalocyanine]indium(III) ((Cl)InTmTMPyPc (35), Scheme 3.8).

The method employed for synthesis of **35** was the same as the one used for **34**, except compound **33b** instead of **33a** was employed. The amounts of all the reagents were the same as those used for **34** except for the amount of compound **33b** (0.095 g, 0.086 mmol). Yield: 0.033 g (38 %). UV/vis (DMSO): λ_{max} nm (log ε); 366 (4.75), 626 (4.46), 698 (5.19); IR (KBr): ν_{max}/cm^{-1}; 2998, 2914 (ν_{C-H}), 1709, 1662, 1436, 1407 ($\nu_{C=C}$), 1311 (ν_{C-S-C}). ^{1}H NMR (600 MHz, DMSO-d_6) δ ppm: 9.15-9.13 (4H, m, Pyridyl-H), 9.04-9.03 (4H, d, Pyridyl-H), 8.25-8.22 (4H, t, Pyridyl-H), 8.18 (4H, s, Pc-H), 8.05-8.04 (d, 4H, Pc-H), 7.46-7.44 (4H, d, Pc-H), 7.42-7.39 (4H, t, Pyridyl-H), 1.22 (12H, s, Pyridyl-H). Calcd for $C_{56}H_{40}N_{12}S_4InCl{\cdot}2SO_4{\cdot}H_2O$: C, 43.91; H, 3.95; N, 10.97 %. Found: C, 45.36; H, 3.81; N, 11.21%. MALDI-TOF-MS *m/z*: Calc. 1351.177; Found: 1124.60 $[M-2(SO_4)-Cl]^+$.

Tetrakis-2,(3)-[(2-mercapto-4-methyl-5-thiazoleaceticacid)phthalocyanine] zinc(II) (TMmTAAZnPc (36), Scheme 3.10).

A mixture of anhydrous zinc (II) acetate (0.6 g, 2.8 mmol), 4-(2-mercapto-4-methyl-5-thiazoleaceticacid) phthalonitrile (**54c**) (1. g, 3.17 mmol), DBU (0.55 mL, 4 mmol) and pentanol (15 mL) was stirred at 160 ^{o}C for 5 h under nitrogen atmosphere. After cooling, the solution was mixed with n-hexane. The green solid product was precipitated and collected by filtration and washed with n-hexane. The crude product was purified by passing through a silica gel column using ethanol to elute the impurities and then 2% NaOH solution was used to elute the product. Precipitation of the product from solution was achieved with the use of 20% HCl solution (150 mL). The product was centrifuged and dried in the oven at 80 ^{o}C overnight. Yield: 0.068 g (6.8 %) UV/vis (DMSO): λ_{max} nm (log ε); 687 (4.33), 619 (3.41), 343 (4.01); IR (KBr): ν_{max}/cm^{-1}; 3447 (COOH), 1639 (C=C), 1384 (C-OH). ^{1}H NMR (400 MHz, Pyridine-d_5) δ ppm: 9.97 (m, 4H, OH), 8.09 (s, 4H, Ar-H), 7.91-7.89 (dd, 4H, Ar-H), 7.14-7.10 (d, 4H, Ar-H), 4.22 (s, 8H, CH_2), 0.96 (s, 12H, CH_3).

Calc. for $C_{56}H_{36}N_{12}S_8Zn$: C 48.84, H 2.84, N 13.14. Found: C 48.38, H 2.9, N 12.57. MALDI-TOF-MS *m/z*: Calc.1326.98 ; Found: 1325.9 $[M]^+$.

Octakis-2,3-[(2-mercapto-4-methyl-5-thiazoleaceticacid)phthalocyanine]zinc(II) (OMmTAAZnPc (37), Scheme 3.10).

The synthesis of **37** was the same as for **36** except **54d** (1.5 g, 3 mmol) instead of **54c** was employed. The amounts of the other reagents and reaction conditions were the same as for **36**.Yield: 0.088 g (5.79 %) UV/vis (DMSO): λ_{max} nm (log ε); 698 (4.42), 619 (4.33), 343 (4.51); IR (KBr): ν_{max}/cm^{-1}; 3416 (COOH), 1619 (C=C), 1400 (C-OH). ^1H NMR (400 MHz, pyridine–d_5) δ ppm: 10.78 (m, 8H, OH), 9.65 (s, 4H, Ar-H), 9.56 (s, 4H, Ar-H), 4.20 (s, 8H, CH_2), 4.11 (s, 8H, CH_2), 2.41 (s, 12H, CH_3), 2.39 (s, 12H, CH_3). Calc. for $C_{80}H_{60}N_{16}S_{16}Zn$: C 44.93, H 2.98, N 11.03. Found: C 43.77, H 2.84, N 10.44. MALDI-TOF-MS *m/z*: Calc. 2079.9 ; Found: 1040 $[M/2]^+$.

Tetrakis-2,(3)-[(mercaptoaceticacid)phthalocyanine)]gallium(III) ((OH)GaTMAAPc (38a), Scheme 3.11)

A mixture of anhydrous gallium (III) chloride (0.49 g, 2.8 mmol), 4-(mercaptoacetic acid*)* phthalonitrile (**54e**) (0.50 g, 2.34 mmol), DBU (0.55 mL, 4 mmol) and pentanol (15 mL) was stirred at 160 ^oC for 5 h. After cooling, the solution was mixed with n-hexane. The green solid product was precipitated and collected by filtration and washed with n-hexane. The crude product was purified with chloroform, acetone and ethanol. The phthalocyanine was then dissolved in 5 mL of 0.1 M NaOH solution and precipitation of the product from solution was achieved with the use of (100 mL) of 20% HCl solution and this was repeated several times and the product was finally dissolved in THF and left to dry. Yield: 0.11 g (20 %) UV/vis (0.01 M NaOH): λ_{max} nm (log ε); 684, 640, 334. IR (KBr): ν_{max}/cm^{-1}; 3457 (COOH), 1708 (C=C), 1436-1407 (C-OH), 697 (C-S-C). ^1H NMR (600 MHz, DMSO-d_6) δ ppm: 9.49 (m, 4H, Carboxyl-H), 8.18 (m, 8H, Ar-H), 6.87 (s, 4H, Ar-H), 4.22 (m, 8H, Methylene-H). Calc. for $C_{40}H_{24}N_8S_4O_8Ga{\cdot}OH.3H_2O$: C 50.07, H 2.50, N 11.68, S 13.35, Found: C 49.85, H

3.03, N 12.25, S 13.31 %. MS (ES-MS) m/z: Calc.; 960.73, Found: 962.23 [M+2H] for $C_{40}H_{24}N_8S_4O_8Ga{\cdot}OH$.

Tetrakis-2,(3)-[(mercaptoaceticacid)phthalocyanine]indium(III) ((OH)InTMAAPc (38b), Scheme 3.11)

The method employed for synthesis and purification of **38b** was the same as the one used for **38a** except anhydrous indium (III) chloride (0.62 g, 2.8 mmol) was used as metal salt. The amounts of all the reagents were the same as those used for **38a** Yield: 0.065 g (12%) UV/vis (0.01 M NaOH): λ_{max} nm; 689, 653, 349. IR (KBr): ν_{max}/cm^{-1}; 3451 (COOH), 1697 (C=C), 1436 (C-OH), 697 (C-S-C). ^{1}H NMR (600 MHz, DMSO-d_6) δ ppm: 9.32 (m, 4H, Carboxyl-H), 7.89 (m, 8H, Ar-H), 6.88 (s, 4H, Ar-H), 4.33 (m, 8H, Methylene-H). Calc. for $C_{40}H_{24}N_8S_4O_8In{\cdot}OH(THF)$: C 49.09, H 2.99, N 10.41, S 11.91, Found: C 49.17, H 2.42, N 9.86, S 11.98 %. MS (ES-MS) m/z: Calc.; 1004.7 Found: 1006.19 [M+2H] for $C_{40}H_{24}N_8S_4O_8In{\cdot}OH$

Tetrakis-2,(3)-[(mercaptoaceticacid) phthalocyanine]silicon(IV)](OH)(Me)

((OH)(Me)SiTMAAPc (38c), Scheme 3.11)

The method employed for synthesis and purification of **38c** was the same as the one used for **38a** except chlorotrimethylsilane(IV) (0.38 g, 2.8 mmol) was used as metal source. The amounts of all the reagents were the same as those used for **38a** Yield: 0.05 g (10%) UV/vis (0.01 M NaOH): λ_{max} nm; 685, 645, 340. IR (KBr): ν_{max}/cm^{-1}; 3459 (COOH), 1709 (C=C), 1436 (C-OH), 697 (C-S-C). ^{1}H NMR (600 MHz, DMSO-d_6) δ ppm: 8.02-7.78 (m, 4H, Carboxyl-H), 7.41-7.04 (m, 8H, Ar-H), 6.93(m, 4H, Ar-H), 3.99-3.97 (m, 8H, Methylene-H), 1.23 (s, 3H, Axial methyl-H). Calc. for $C_{40}H_{24}N_8S_4O_8Si{\cdot}(OH)(Me)$: C 51.38, H 2.68, N 11.99, S 13.70, Found: C52.51, H 2.94, N 10.74, S 14.10 %. MS (ES-MS) m/z: Calc.; 933.08, Found: 934.63 [M+H] for $C_{40}H_{24}N_8S_4O_8Si{\cdot}(OH)(Me)$.

Tetrakis-2,(3)-[(mercaptoaceticacid) phthalocyanine]zinc(II) (ZnTMAAPc (38d), Scheme 3.11)

The method employed for synthesis and purification of **38d** was the same as the one used for **38a** except anhydrous zinc (II) acetate (0.51 g, 2.8 mmol) was used as metal source. The amounts of all the reagents were the same as those used for **38a** Yield: 0.019 g (5%) UV/vis (0.01 M NaOH): λ_{max} nm; 692, 628, 351. IR (KBr): ν_{max}/cm^{-1}; 3444 (COOH), 1662 (C=C), 1437-1407 (C-OH), 698 (C-S-C). ^{1}H NMR (600 MHz, DMSO-d_6) δ ppm: 8.34 (m, 4H, Carboxyl-H), 7.84-7.06 (m, 8H, Ar-H), 6.88 (s, 4H, Ar-H), 4.25 (m, 8H, Methylene-H). Calc. for $C_{40}H_{24}N_8S_4O_8Zn$: C; 51.20 H; 2.70 N; 12.61 S; 14.42 Found: C; 50.98 H; 2.99 N; 11.89 S; 13.61. MS (ES-MS) m/z: Calc.; 938.29 Found: 940.09 [M+2H] for $C_{40}H_{24}N_8S_4O_8Zn$.

Tetrakis-2,(3)-[(mercaptopropionicacid)phthalocyanine]gallium(III) ((OH)GaTMPAPc (39a), Scheme 3.11)

The method employed for synthesis of **39a** was the same as the one used for **38a** and anhydrous gallium (III) chloride (0.49 g, 2.8 mmol) was used as metal salt, and compound **54f** was employed instead of **54e**. The amounts of all the other reagents were the same as those used for **38a.** Yield: 0.017 g (5 %) UV/vis (0.01 M NaOH): λ_{max} nm; 687, 650, 345. IR (KBr): ν_{max}/cm^{-1}; 3449 (COOH), 1709 (C=C), 1437-1407 (C-OH), 697 (C-S-C). ^{1}H NMR (600 MHz, DMSO-d_6) δ ppm: 7.99 (m, 4H, Carboxyl-H), 7.72-7.53 (m, 8H, Ar-H), 6.86 (s, 4H, Ar-H), 6.64 (s, 1H, Axial-H) 2.92 (m, 16H, Methylene-H). Calc. for $C_{44}H_{32}N_8S_4O_8Ga{\cdot}OH.2H_2O$: C 50.24, H 3.45, N 10.66, S 12.19, Found: C 50.68, H 2.38, N 10.28, S 13.97 %. MS (ES-MS) m/z: Calc.; 1015.79 Found: 1016.23 [M+H] for $C_{44}H_{32}N_8S_4O_8Ga{\cdot}OH$.

Tetrakis-2,(3)-[(mercaptopropionic)acidphthalocyanine]indium(III) ((OH)InTMPAPc (39b), Scheme 3.11)

The method employed for synthesis of **39b** was the same as the one used for **38a** except anhydrous indium (III) chloride (0.62 g, 2.8 mmol) was used as metal salt, and compound **54f** was employed instead of **54e**. The amounts of all the reagents were the same as those used for **38a.** Yield: 0.015 g (5%) UV/vis (0.01 M NaOH): λ_{max} nm; 689, 651. IR (KBr): ν_{max}/cm^{-1}; 3450 (COOH), 1709 (C=C), 1437 (C-OH), 697 (C-S-C). ^{1}H NMR (600 MHz, DMSO-d_6) δ ppm: 7.99-7.92 (m, 4H, Carboxyl-H), 7.71-7.65 (d, 8H, Ar-H), 6.86 (s, 4H, Ar-H), 6.65 (s, 1H, Axial-H), 2.92 (m, 16H, Methylene-H). Calc. for $C_{44}H_{32}N_8S_4O_8In{\cdot}OH.2H_2O$: C 49.82, H 3.14, N 10.56, S 12.09, Found: C 48.26, H 3.36, N 10.24, S 11.72 %. MS (ES-MS) m/z: Calc.; 1060.89, Found: 1062.21 [M+2H] for $C_{44}H_{32}N_8S_4O_8In{\cdot}OH$.

Tetrakis-2,(3)-[(mercaptopropionicacid)phthalocyanine]silicon(IV) (OH)(Me) ((OH)(Me)SiTMPAPc (39c), Scheme 3.11)

The method employed for synthesis of **39c** was the same as the one used for **38a** except chlorotrimethylsilane(IV) (0.39 g, 2.8 mmol) was used as metal source, and compound **54f** was employed instead of **54e**. The amounts of all the reagents were the same as those used for **38a.** Yield: 0.11 g (19. 4 %) UV/vis (0.01 M NaOH): λ_{max} nm 692, 644, 345. IR (KBr): ν_{max}/cm^{-1}; 3445 (COOH), 1707 (C=C), 1437 (C-OH), 698 (C-S-C). ^{1}H NMR (600 MHz, DMSO-d_6) δ ppm: 7.52 (m, 4H, Carboxyl-H), 7.18-7.08 (m, 8H, Ar-H), 7.00 (s, 4H, Ar-H), 6.53 (s, 1H, Axial-H), 4.05 (m, 16H, Methylene-H) 1.35 (s, 3H, Axial methyl-H). Calc. for $C_{44}H_{32}N_8S_4O_8Si{\cdot}(OH)(Me){\cdot}2H_2O$: C 51.55, H 3.54, N 10.93, S 12.51, Found: C 52.64, H 3.66, N 9.71, S 13.10 %. MS (ES-MS) m/z: Calc.; 989.18, Found: 990.61 [M+H] for $C_{44}H_{32}N_8S_4O_8Si{\cdot}(OH)(Me)$.

Tetrakis-2,(3)-[(mercaptopropanoicacid)phthalocyanine]zinc(II) ((TMPAZnPc (39d), Scheme 3.11)

The method employed for synthesis of **39d** was the same as the one used for **38a** except anhydrous zinc (II) acetate (0.51 g, 2.8 mmol) was used as metal source and compound **54f** was employed instead of **54e**. The amounts of all the reagents were the same as those used for **38a**. Yield: 0.38 g (72 %) UV/vis (0.01 M NaOH:methanol): λ_{max} nm (log ε); 693 (3.98), 628 (3.64), 353 (4.11); IR (KBr): ν_{max}/cm^{-1}; 3452 (COOH), 1709 (C=C), 1436-1407 (C-OH), 697 (C-S-C). ^{1}H NMR (600 MHz, DMSO-d_6) δ ppm: 8.80 (m, 4H, Carboxyl-H), 8.01 (m, 8H, Ar-H), 6.87 (s, 4H, Ar-H), 2.65 (m, 16H, Methylene-H). Calc. for $C_{44}H_{32}N_8S_4O_8Zn.3H_2O$: C; 50.40 H; 3.62 N; 10.69 S; 12.21 Found: C; 50.54 H; 2.65 N; 10.04 S; 13.32. MS (ES-MS) m/z: Calc.; 994.44 Found: 995.3 [M+H] for $C_{44}H_{32}N_8S_4O_8Zn$.

The complexes **40**, **41** and **42** were donated but their synthetic details are provided below, since they had not been reported before.

Tetrakis-2,(3)-[(5-trifluoromethyl-2-pyridyloxy)phthalocyanine]zinc(II)

(TtfmPyZnPc (40), Scheme 3.9)

Complex **40** was prepared from compound **54g** (0.40 g, 1.31 mmol), anhydrous zinc acetate (0.28 g, 1.31 mmol) and 2.5 ml of dry pentanol which were placed in a standard Schlenk tube in the presence of 1,8-diazabicyclo[5.4.0] undec-7-ene (DBU) (0.31 ml, 0.20 mmol) under an argon atmosphere and held at a reflux temperature for 12 h. After cooling to room temperature, the reaction mixture was precipitated by adding it drop-wise into n-hexane. The crude product was precipitated, collected by filtration and washed with hot hexane. The crude green product was further purified by a silica gel column using THF and then a mixture of $CHCl_3$: MeOH (100/5 v/v) as eluents. Yield: 140 mg (30%). Uv/vis (DMSO): λ_{max} nm (log ε) 366 (4.75), 619 (4.55), 685 (5.21). IR spectrum (cm^{-1}): 3064 (Ar-CH), 1594 (C=C), 1574 (C=N), 1489, 1442,

1400, 1332 (C-F), 1326, 1247, 1074, 1009, 908, 830, 765, 743, 685 (C-S-C), 649 (Pc skeletal). ^{1}H NMR (DMSO-*d6*) δ: 8.65 (4H, s, Ar-H), 8.11-7.70 (16H, m, Ar-H), 7.34 (d, 4H, Ar-H). Calcd for $C_{52}H_{24}F_{12}N_{12}S_4Zn$: C; 52.28 H; 1.88 N; 13.06 S; 9.97%. Found: C; 52.33 H; 2.21 N; 12.88 S; 10.51 %. MS (ES-MS) m/z: Calc.; 1222 Found: 1223.34 $[M+H]^+$.

Tetrakis-2,(3)-[(5-trifluoromethyl-2-mercaptopyridine)phthalocyanine]zinc(II) (TtfmMPyZnPc (41), Scheme 3.9)

The synthesis of **41** was as outlined for **40**, except compound **54h** (0.30 g, 1.04 mmol) instead of compound **54g** was employed. The amounts of the other reagents were as follows: anhydrous zinc acetate (0.23 g, 1.04 mmol), dry pentanol (2 ml) and DBU (0.25 ml, 0.16 mmol). A dark green product was obtained following purification. Yield: 85 mg (27%). Uv/vis (DMSO): λ_{max} nm (log ε) 359 (4.82), 612 (4.60), 678 (5.28). IR spectrum (cm^{-1}): 3064 (Ar-CH), 1594 (C=C), 1571 (C=N) 1489, 1442, 1332 (C-F), 1292, 1061 (C-O-C), 923, 835, 751, 706, 630 (Pc skeletal). ^{1}H NMR (DMSO-*d6*) δ: 7.97-7.51 (21H, m, Ar-H), 7.03-6.99 (3H, bs, Ar-H). Calcd for $C_{52}H_{24}F_{12}N_{12}O_4Zn$: C; 55.03 H; 1.98 N; 13.75 %. Found: C; 54.62 H; 2.12 N; 13.58 %. MS (ES-MS) m/z: Calc.; 1287 Found: 1287.86 $[M+H]^+$.

Tetrakis-2,(3)-[(1,6-hexanedithiol)phthalocyanine]zinc(II) (THdTZnPc (42), Scheme 3.12)

Complex **42** was prepared through the use of a mixture of anhydrous zinc (II) acetate (0.51 g, 2.8 mmol), 4-(1,6-hexanedithiol)phthalonitrile (**54i**) (0.5 g, 1.6 mmol), DBU (0.55 mL, 4 mmol) and pentanol (15 mL) which was stirred at 160 ^oC for 5 h. After cooling, the solution was mixed with n-hexane. The green solid product was precipitated and collected by filtration and washed with hot n-hexane. The crude product was purified by column chromatography using silica gel and eluting with

chloroform. Yield: 0.048 g (12 %) UV/vis (DMSO): λ_{max} nm; 706 (4.64), 638 (4.08), 364 (4.33). IR (KBr): ν_{max}/cm^{-1}; 2997 (C-H), 1436, 1406 (C=C), 1307 (C-H), 667 (C-S-C). ^{1}H NMR (600 MHz, DMSO-d_6) δ ppm: 7.70-7.69 (dd, 4H, Ar-H), 7.53-7.51 (dd, 4H, Ar-H), 6.97 (s, 4H, Ar-H), 4.30-4.11 (m, 24H, Methylene-H), 1.68-1.39 (m, 24, Methylene-H), not observed (s, 4H, S-H). Calc. for $C_{56}H_{64}N_8S_8Zn$: C; 57.38, H; 5.59, N; 9.56, Found: C; 56.35, H; 5.44, N; 10.65. MALDI-TOF-MS m/z: Calc.; 1171.08 Found: 1170.56 $[M]^+$ for $C_{56}H_{64}N_8S_8Zn$.

Results and Discussion

3. Synthesis and Spectroscopic Characterization

4. Photophysical and Photochemical Characterization

5. The Interaction of Metallophthalocyanines with Nanoparticles

Publications

The results which are to be considered in the following chapters have been presented in the list of articles shown below. These articles have either been published or submitted for publication in peer-reviewed journals and have not been referenced in this thesis:

1. The Interaction of CdTe quantum dots with negatively charged zinc phthalocyanines, S. Moeno and T. Nyokong, *Polyhedron*, 2008, **27**, 1953-1958.

2. Spontaneous charge transfer between zinc tetramethyl-tetra-2,(3)-pyridinoporphyrazine and CdTe and ZnS quantum dots, S. Moeno, M. Idowu and T. Nyokong, *Inorganica Chimica Acta,* 2008, **361**, 2950-2956.

3. Solvent and central metal effects on the photophysical and photochemical properties of peripherally tetramercaptopyridine substituted metallophthalocyanines, S. Moeno and T. Nyokong, *Journal of Photochemistry and Photobiology A: Chem.,* 2009, **203**, 204-210.

4. Opposing responses elicited by positively charged phthalocyanines in the presence of CdTe quantum dots, S. Moeno and T. Nyokong, *Journal of Photochemistry and Photobiology A: Chem.,* 2009, **201**, 228-236.

5. Photophysical properties of newly synthesized fluorinated zinc phthalocyanines in the presence CdTe quantum dots and the accompanying energy transfer processes, A. Erdoğmuş, S. Moeno, C. Litwinski and T. Nyokong, *Journal of Photochemistry and Photobiology A: Chem.,* 2010 , **210**, 200-208.

6. Photoinduced energy transfer between CdTe quantum dots and new zinc phthalocyanine derivatives peripherally substituted with mercapto methylthiazoleacetic acid, S. Moeno, E. Antunes, S. Khene, C. Litwinski and T. Nyokong, *Dalton Transactions.,* 2010, **39**, 3460-3471.

7. An investigation of the behaviour of quaternized peripherally tetra mercaptopyridine substituted metallophthalocyanines in the presence of quantum dots, S. Moeno, and T. Nyokong, *Journal of Photochemistry and Photobiology. A: Chem.*, 2010, **215**, 196-204.

8. The determination of the photosensitizing properties of mercapto substituted phthalocyanine derivatives in the presence of quantum dots capped with mercaptopropionic acid, S. Moeno, E. Antunes and T. Nyokong, *Journal of Photochemistry and Photobiology. A: Chem.*, 2011, **218**, 101-110.

9. Synthesis and photophysical properties of a novel zinc photosensitizer and its gold nanoparticle conjugate, S. Moeno, E. Antunes and T. Nyokong, In Progress.

Synthesis and Spectroscopic Characterization

3

All the syntheses and spectroscopic characterizations of the nanoparticles and metallophthalocyanines used in this work are contained in this chapter.

Three different nanoparticles were synthesized in this work and they are listed below in Table 3.1.

Table 3.1: List of Synthesized Nanoparticles

Nanoparticle	[a]Capping	Abs max (nm)	Size(nm) polynomial	Size(nm) XRD	Abb.	No.
ZnS	ME	280	--	2.90	ME-ZnS	1a
CdTe	ME	462	3.19	3.25	[b]ME-CdTe	1b(i)
CdTe	TGA	630	4.09	4.19	[c]TGA-CdTe	1b(ii)
CdTe	MPA	645	4.24	4.54	MPA-CdTe	1b(iii)
AuNP	TOAB	389	--	4.96	TOABAuNP	2

[a]ME=Mercaptoethanol, [a]TGA=Thioglycolic acid, [a]MPA=Mercaptopropionic acid, [a]TOAB=Tetraoctylammonium bromide.

[b] The following ME-CdTe QDs were also used: 3.25 nm and 3.29 nm.

[c] The following TGA-CdTe QDs were also used: 2.95 nm, 3.20 nm, 3.45 nm, and 3.73 nm.

3.1 Synthesis and Characterization of Nanoparticles

The ZnS QDs, CdTe QDs and AuNPs used in this thesis were synthesized according to reported methods and their spectroscopy and microscopic characterizations were consistent with those reported in literature.

3.1.1 Mercaptoethanol capped ZnS QDs

These QDs were prepared using a well known method from literature, (Scheme 3.1) [34] as previously explained in the experimental section.

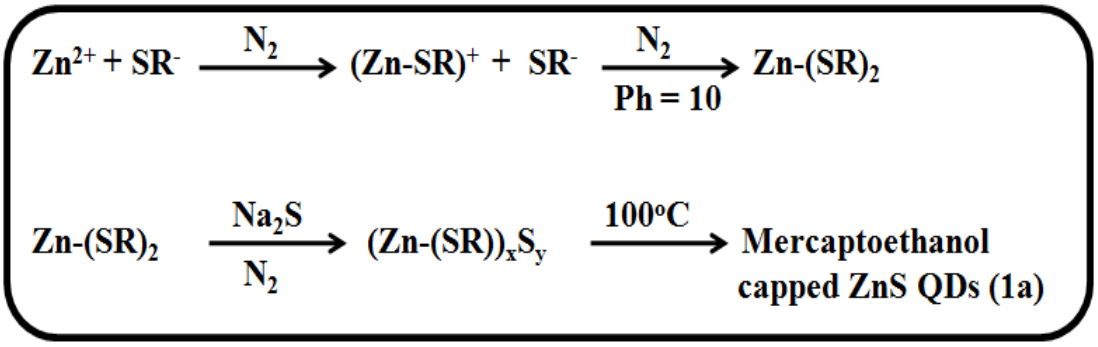

Scheme 3.1: Synthesis of mercaptoethanol capped ZnS QDs (1a). (SR= 2-Mercaptoethanol)

The absorption and emission spectra of ZnS QDs capped with 2-ME are shown in Figure 3.1. The absorption spectrum for ZnS has been reported [34,234,235] to show a broad absorption peak at about 280 nm, and this band was observed as shown in Figure 3.1. The emission spectral peak was relatively well resolved though it was broad, with peaks ranging from 395 to 537 nm, as has been reported in literature [34].

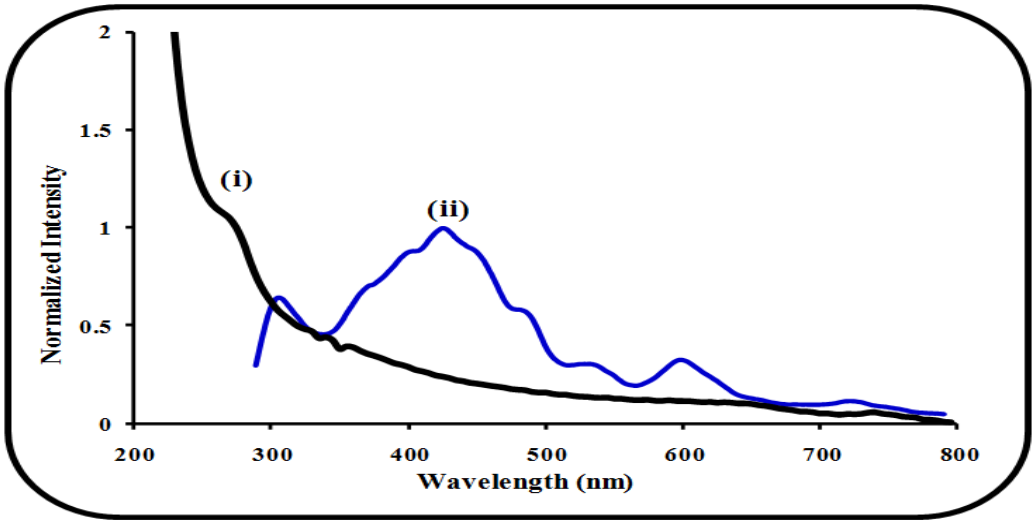

Figure 3.1: Normalized ground state absorbance (i) and emission spectra of ME ZnS QDs (1a) (ii) in pH 7.4 buffer ($\lambda_{excitation}$= 270 nm).

The first peak at 395 nm has been attributed to excess zinc in ZnS nanoparticles, while the second peak at 426 nm is due to sulfur vacancies (S^{-2}) [34]. The peak at 480

nm results from luminescence of zinc (Zn^{2+}) vacancies in the quantum dots [34,234,235]. Another peak at 531 nm is observed and the cause for this luminescence is not known. The estimated full width at half maximum (FWHM) is about 143 nm for the emission peak in Figure 3.1. FT-IR measurements showed a spectrum with a characteristic broad O-H band at 3332 cm^{-1}, C-H vibrations at 2930 and 1414 cm^{-1}, asymmetric C-O stretches at 1632 and 1556 cm^{-1} and C-S stretches at 940 cm^{-1}.

XRD was used to determine the size of the ME capped ZnS QDs, Figure 3.2. The XRD pattern obtained showed three characteristic peaks at 29° (111), 48.3° (220) and at 56° (331) at the planes indicated corresponding to the zinc blende structure [236]. The QD diameter was determined through the use of software that calculates for the size using the Debye-Scherrer equation 3.1, (same as Equation 1.2).

$$d(\text{Å}) = \frac{k\lambda}{\beta Cos\theta} \qquad (3.1)$$

The width of the main peak at 29° was used to compute the size of ME ZnS QDs. The size was determined to be 2.90 nm. The peaks are broadened because of the nanocrystalline nature of the particles.

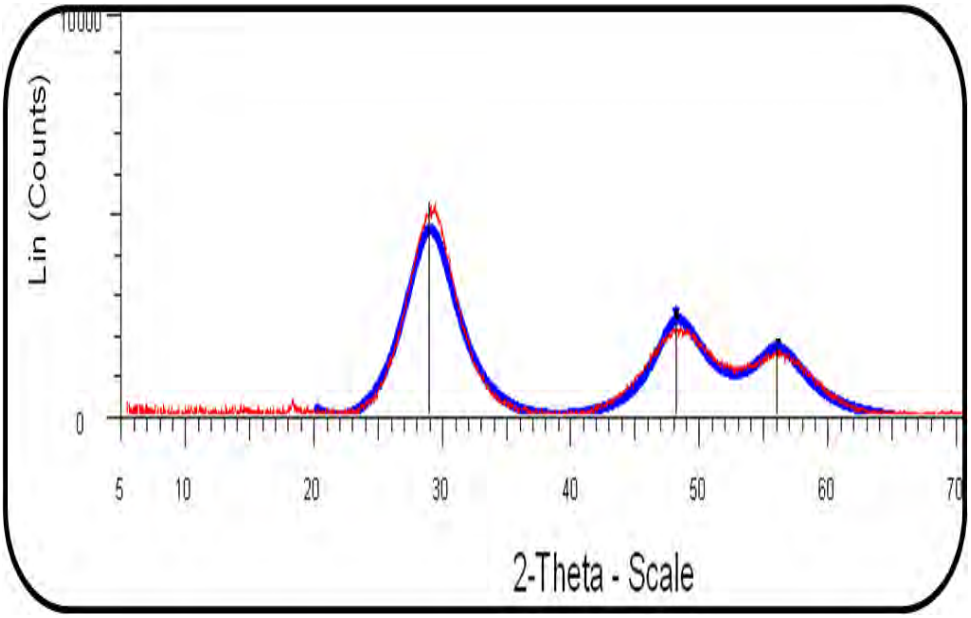

Figure 3.2: XRD diffractogram of ME ZnS QDs (1a).

3.1.2 Mercaptoalkanoic acid capped CdTe QDs

3.1.2.1 Synthesis and Spectra

CdTe QDs were synthesized using a conventional method from literature as explained in the experimental section, (Scheme 3.2) [4].

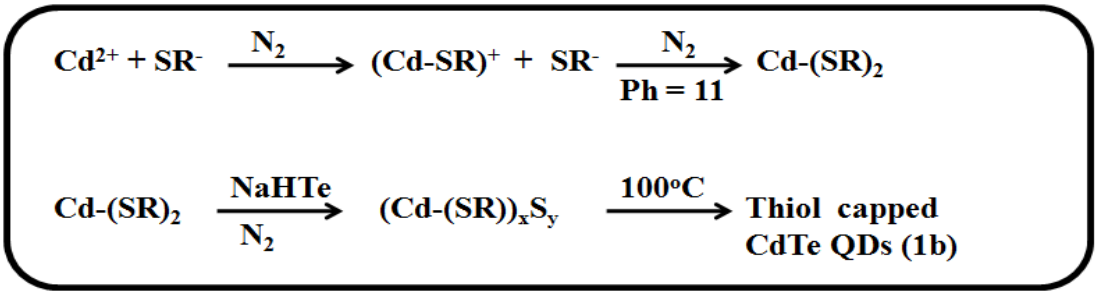

Scheme 3.2: Synthesis of thiol stabilizer capped CdTe QDs (1b). (SR= mercaptocalkanoic stabilizer)

The ME, TGA and MPA capped CdTe QDs synthesized in this work are all characterized by broad absorption peaks, Figure 3.3. The solubility of cadmium thiolate precursor complexes was ensured by using pH 12 aqueous solutions for the synthesis of CdTe QDs with all the thiol stabilizer groups that were employed.

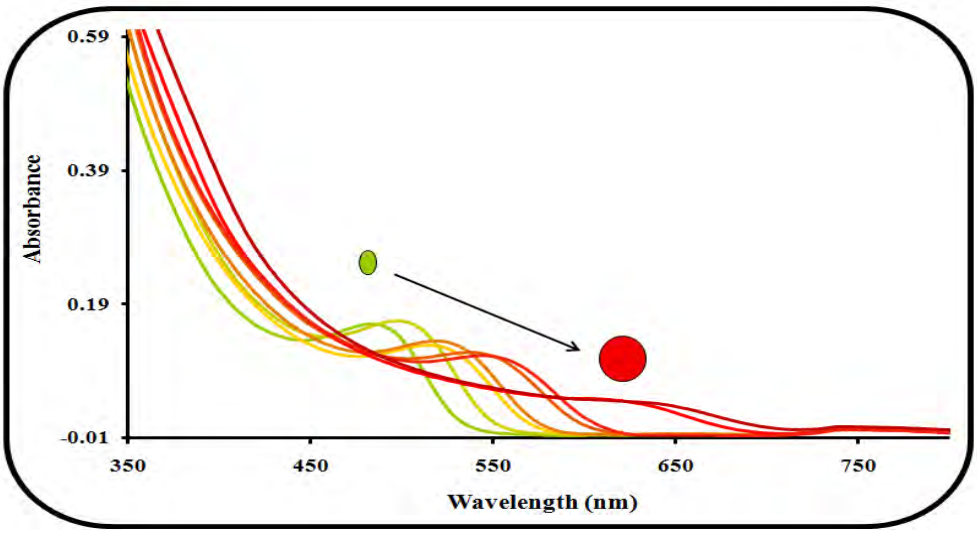

Figure 3.3: Ground state absorption spectra of MPA CdTe QDs with increasing size in aqueous medium.

As the CdTe QDs grow through the Ostwald ripening process both the absorption and the emission spectra continue to get red shifted [4]. The CdTe-QDs displayed characteristic emission spectral behaviour with smaller QDs showing narrower emission and thus smaller values of the full width at half maximum (FWHM), Figure 3.4.

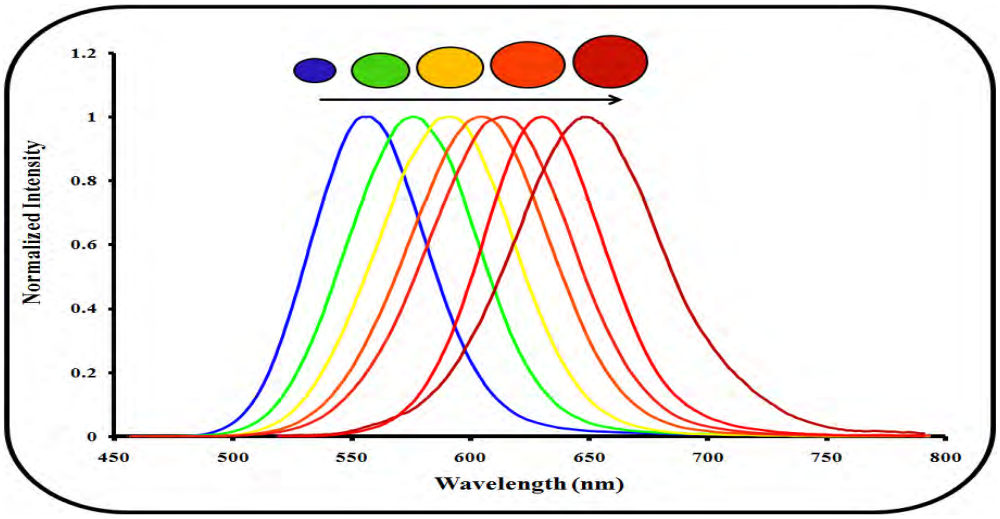

Figure 3.4: Emission spectra of MPA CdTe QDs (1b, iii) in aqueous media. ($\lambda_{excitation}$= 450 nm).

The observed growth in size of the QDs is accompanied by changes in colour of the CdTe QDs. These colour changes for the CdTe QDs with increase in size are shown in Figure 3.5.

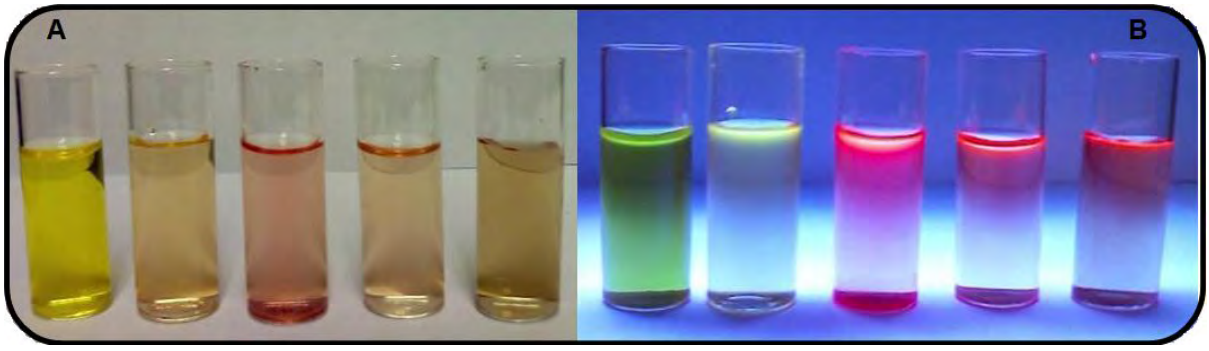

Figure 3.5: Colour changes with increase in size of TGA CdTe QDs without UV radiation (A) and under UV radiation (B).

The FT-IR spectra for CdTe QDs with all three thiol cappings (ME, TGA and MPA) showed characteristic O-H vibrations between 3250 and 3330 cm^{-1}, C-H vibrations between 2900 and 2870 cm^{-1}, C=O stretches between 1550 and 1370 cm^{-1} for TGA and MPA capped QDs while a C-O stretch for ME capped QDs were between 1460-1400 cm^{-1}, C-S stretches for all QDs were observed between 850-690 cm^{-1}.

The sizes of the CdTe QDs were determined using two different methods. One method makes use of a polynomial fitting function and this polynomial is only applicable to CdTe and CdSe QDs with sizes between 1 and 9 nm [50]. This polynomial fitting function is shown as equation 3.2 (same as Equation 1.1).

$$D = (9.8127\times10^{-7})\lambda^3 - (1.7147\times10^{-3})\lambda^2 + (1.0064)\lambda - (194.84) \qquad (3.2)$$

The average error in the size determination of the QDs using the polynomial fitting function was ± 0.1 nm. XRD was also employed to ascertain the sizes of the CdTe QDs, where the generated data was fed into a programme that uses equation 3.1 shown above. The diffractograms for ME, TGA and MPA QDs were very similar, Figure 3.6. There are three peaks observed for each QD diffractogram between 24.1° and 25.2°, 40.5° and 42.9°, 48.9° and 49.9°, all corresponding to the 111, 220 and 311 planes respectively suggesting that the QDs have a zinc blende structure. The sizes of QDs obtained from XRD are more accurate than those from the polynomial fitting function and are thus employed.

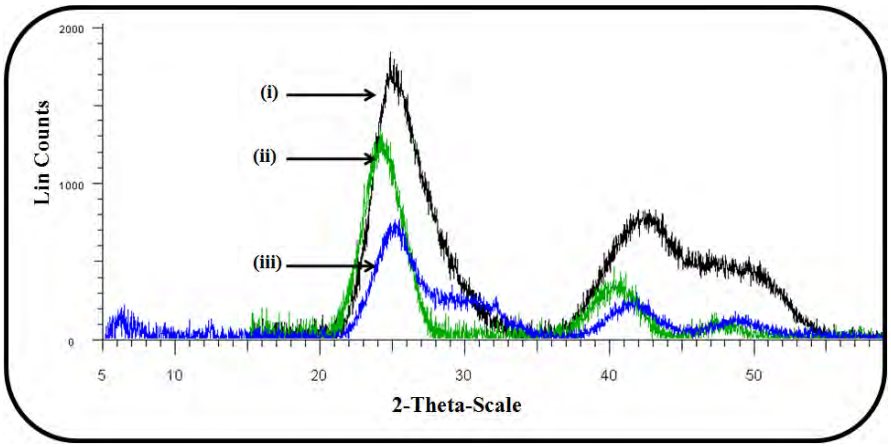

Figure 3.6: XRD diffractograms of ME (i), TGA (ii) and MPA (iii) CdTe QDs (1b).

3.1.2.2 CdTe Quantum Dot Cyclic Voltammetry

A typical cyclic voltammogram of TGA stabilized CdTe QDs is as shown in Figure 3.7.

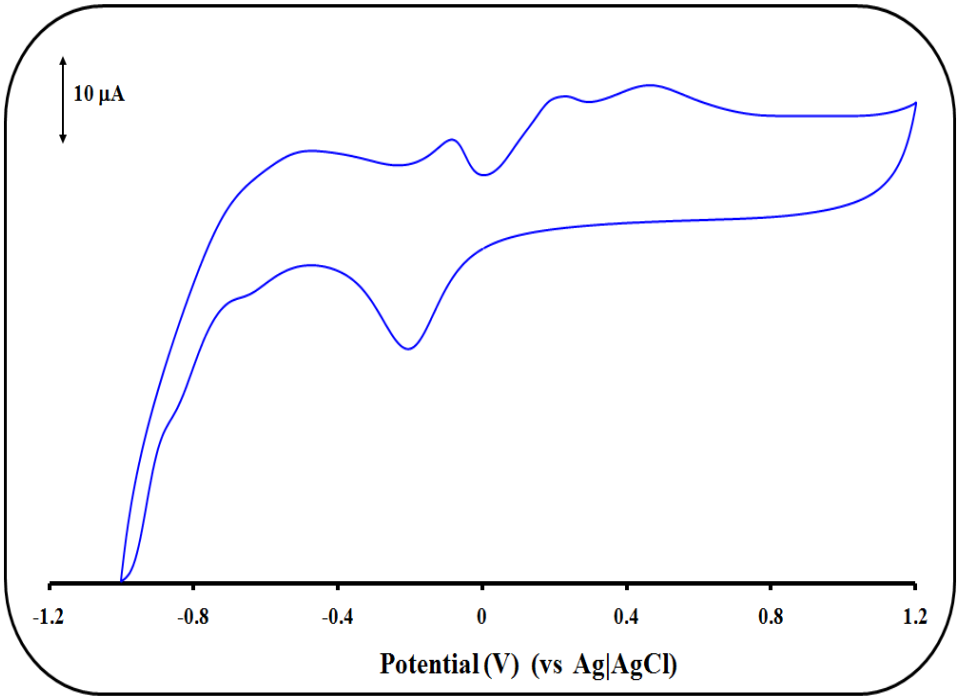

Figure 3.7: Cyclic Voltammogram for TGA CdTe QD (3.94 nm) in a pH 9.2 buffer using a platinum electrode.

The oxidation and reduction potentials of the TGA capped QDs of different sizes are shown in Table 3.2. The CV shown in Figure 3.7 suggests that the QDs studied show an irreversible system.

Table 3.2 shows that the oxidation and reduction potentials of CdTe QDs are dependent on the size of the QDs. According to the tabulated results, as the size of the QDs increases, the oxidation potential becomes less positive (with the exception of 4.09 nm QDs) while the reduction potential becomes less negative as observed in the literature [67].

Table 3.2: Anodic and cathodic potential variations for TGA CdTe QDs with different QD sizes.

[a]Emission wavelength λ (nm)	Size/nm (D)	E_P (V) Oxidation	E_P (V) reduction
528	**2.95**	**0.66**	**-0.86**
546	**3.20**	**0.63**	**-1.02**
573	**3.45**	**0.63**	**-0.81**
608	**3.73**	**0.59**	**-0.87**
626	**3.94**	**0.48**	**-0.85**
636	**4.09**	**0.57**	**-0.7**

[a]A pH 9.2 buffer solution was used for all cyclic voltammetry measurements.

3.1.3 Tetraoctylammonium bromide (TOAB) and MPc stabilized AuNPs

AuNPs were synthesized according to a well known procedure from literature as explained in the experimental section, (Scheme 3.3 (A)) [40].The replacement of the TOAB capping by the novel tetrakis-2,(3)-[(1,6-hexanedithiol)phthalocyanine]zinc(II) (THdTZnPc, **42**) was carried out according to a known method (Scheme 3.3 (B)) [138,139].

In metallic NPs an intense absorption is observed when the frequency of the collective dipolar oscillation of the electron cloud of the nanoparticles matches that of the incident radiation. This intense absorption is called surface plasmon absorption. The AuNPs showed broad surface plasmon absorption bands in both $CHCl_3$ and toluene, Figure 3.8. The surface plasmon band for TOAB Au NPs is shown to be around 389 nm in $CHCl_3$ and is at 375 nm in toluene.

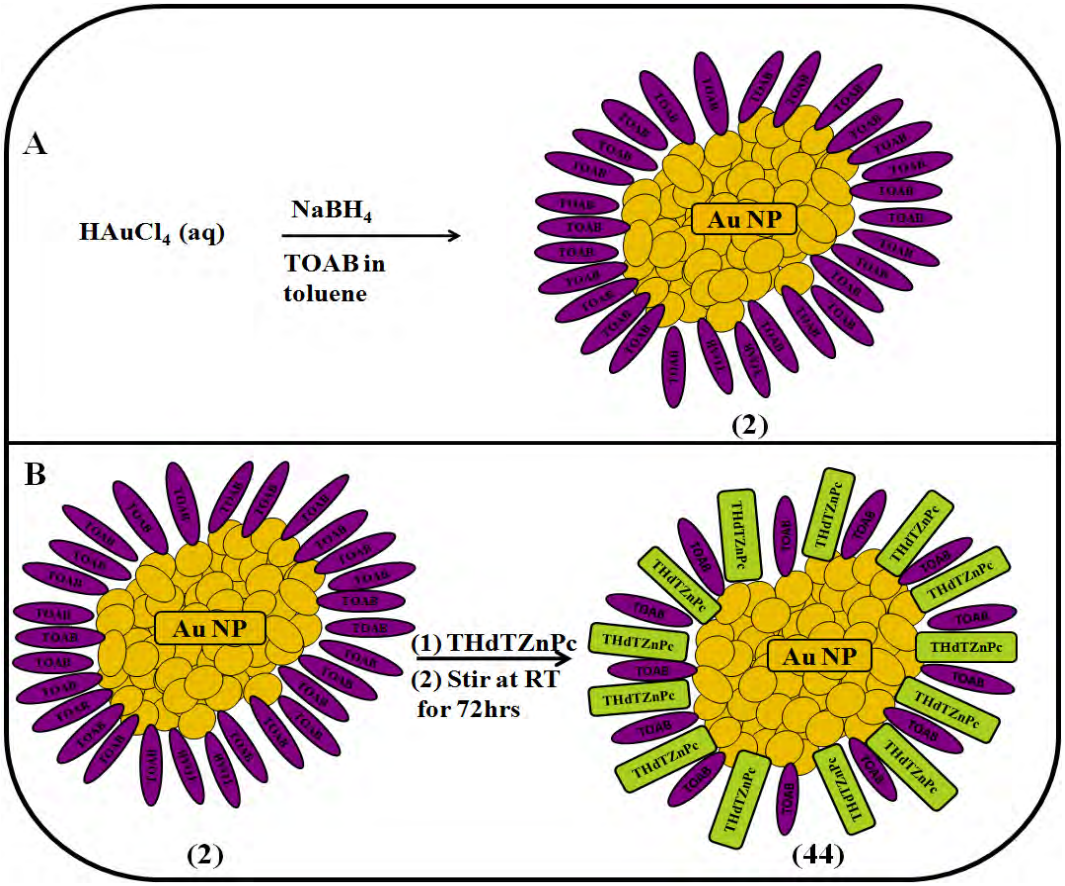

Scheme 3.3: Synthesis of TOAB capped AuNPs (2) in (A) and the 42-AuNP conjugate in (B). (The loading capacity of TOAB and MPc onto AuNP is not accurately illustrated).

A change in the position of the surface plasmon absorption band is indicative of (i) modification of NPs and (ii) differences in size of the AuNPs with smaller AuNPs having bands in the blue region of the visible spectrum [237,238]. In addition to the effect of the NP size on the surface plasmon bands, these bands may also appear at different positions based on the shape of the NPs, and solvents used since these possess different dielectric constants, Figure 3.8(curves (i) and (ii)) [239]. The TOAB stabilizer used to passivate the AuNPs was replaced with an MPc complex terminating with thiol groups (THdTZnPc (**42**)) to give AuNPs covalently attached to the MPc complex **44**. The surface plasmon band of the AuNPs in the MPc-AuNP conjugate is red-shifted in comparison to the parent TOAB AuNPs, Figure 3.8(curve

iii). The synthesized TOAB stabilized AuNPs and the **42**-AuNP conjugate were non fluorescent.

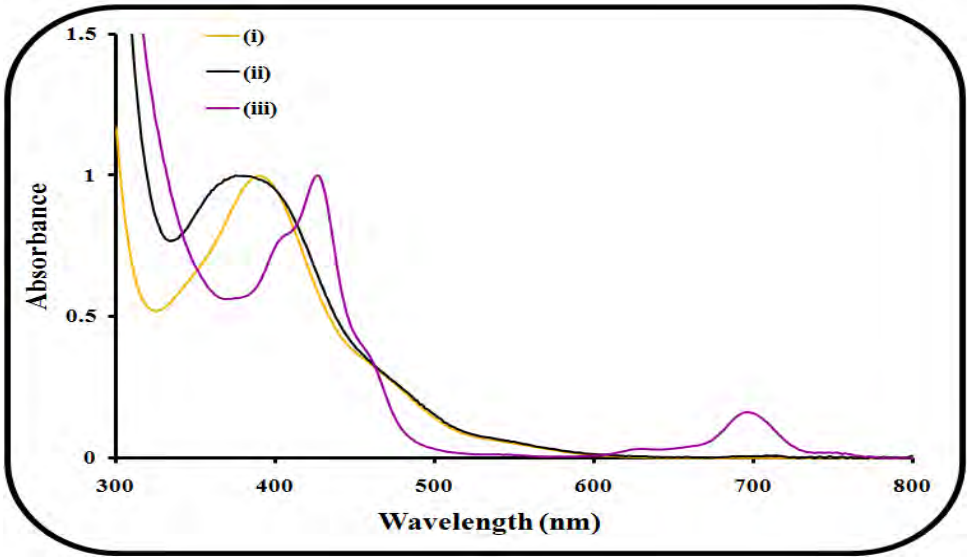

Figure 3.8: Ground state absorbance of TOAB AuNPs in $CHCl_3$ (i), in toluene (ii) and 42-AuNP conjugate (iii) in $CHCl_3$.

The TOAB stabilized AuNPs showed FT-IR spectra with characteristic C-H vibrations at 2927 and 2860 cm^{-1}, and C-N stretches at 1215 cm^{-1}.

The attachment of complex **42** onto AuNPs was also evident from the FT-IR spectra which showed C=C stretches at ~1517 cm^{-1}, and C-C stretches at ~1039 cm^{-1} (that are likely due to the MPc complex **42**) in addition to the vibrations mentioned for TOAB AuNPs. XRD was also used to determine the TOAB AuNPs and **42**-AuNP conjugate sizes. The fitting of the XRD data established the TOAB AuNPs to have an average size of 4.96 nm while the **42**-AuNP conjugate had a size of 5.96 nm. The AuNP XRD diffractograms obtained for this work showed the expected Bragg reflections at 2θ values of 39.1°, 45.3° and 65.2° which are assigned to the (111), (200), (220) reflections of cubic face centred nanoparticles. However many other reflections were observed and these may be due to the TOAB stabilizer used on the parent AuNPs as well as local structural disorders and defects of the AuNPs, Figure 3.9 [240,241]. The Pc

functionalized AuNPs show less Bragg reflections and these as expected are slightly shifted in comparison to those of the parent AuNPs, Figure 3.9.

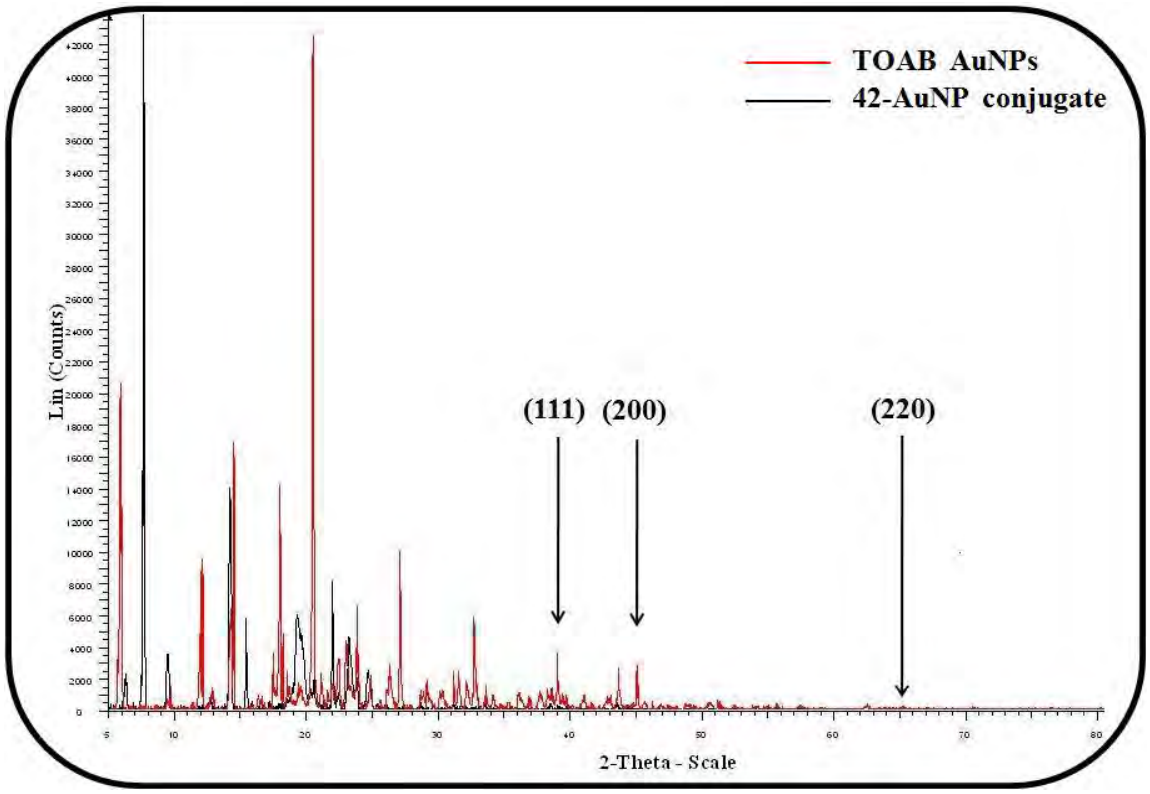

Figure 3.9: XRD diffractogram for TOAB capped AuNPs (2) (i) and 42-AuNP conjugate (ii).

The TOAB and MPc stabilized AuNPs were further characterized with transmission electron microscopy (TEM) [242,243]. The TEM images of the AuNPs show that the TOAB AuNPs have the tendency to form aggregates, Figure 3.10(A). The TEM pictures showed in Figure 3.10 are at the same magnification (2000 nm) and they show a clear distinction between the TOAB AuNPs (**2**) and the **42**-AuNP conjugate (**44**), where TOAB stabilized AuNPs are light and clear whereas the **42**-AuNP conjugate is dark and not as clear as their non MPc-functionalized counterparts indicative that complex **42** has been successfully attached (assembled) onto the AuNPs. As a result of the functionalization of the AuNPs, the MPc-AuNP conjugates

do not reflect light as well as AuNPs that are TOAB stabilized and so they appear as dark black spherical particles, Figure 3.10(B).

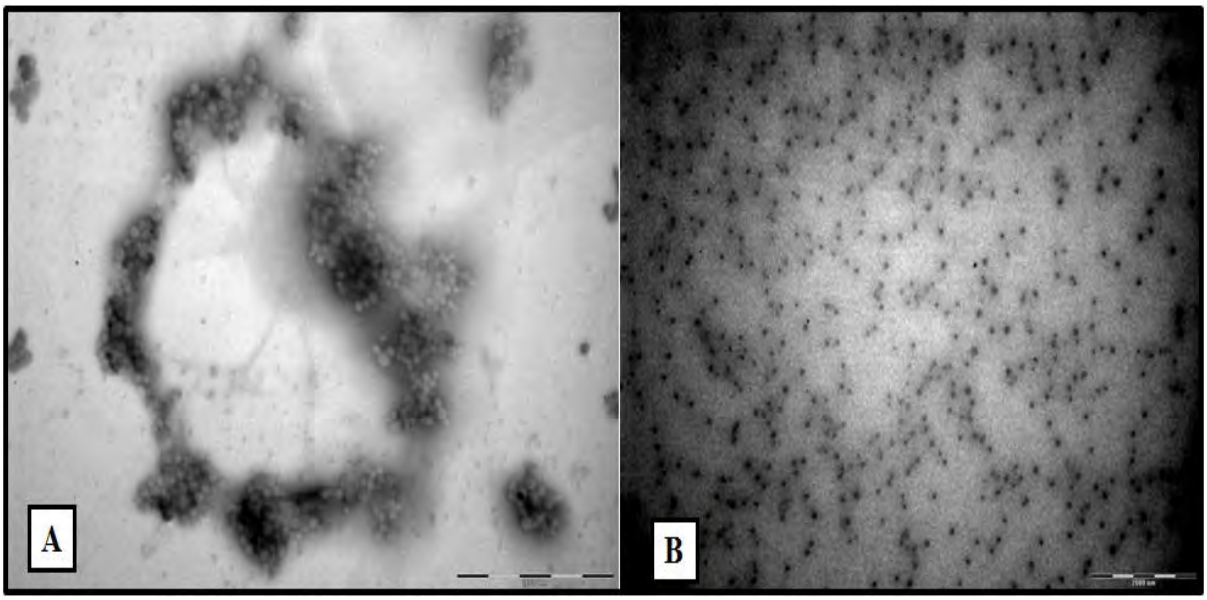

Figure 3.10: TEM picture for TOAB stabilized AuNPs (2) in (A) and the 42-AuNP conjugate (44) in (B). (The scale bar for A and B is 2000 nm).

3.2 Synthesis and Characterization of Metallophthalocyanines (MPcs)

The compounds that were synthesized and employed for studies in this work are listed in Table 3.3. Also included are the complexes that were donated by fellow researchers as mentioned at the onset.

Table 3.3: MPc complexes synthesized and used in this thesis

MPc complex	Abbreviation	No.
TetramethylTetrakis-2,(3)-{pyridinoporphyrazine}zinc(II)	TmTPyZnPz	27b
Zinc(II)tetrasulfonatephthalocyanine	ZnTSPc	28
Zinc(II)tetracarboxyphthalocyanine	ZnTCPc	29
Zinc(II)octacarboxyphthalocyanine	ZnOCPc	30
TetramethylTetrakis-2,(3)-{2-pyridyloxyphthalocyanine} zinc(II)	TmTPyZnPc	31b
TetramethylTetrakis-2,(3)-{2-mercaptopyridine phthalocyanine}zinc(II)	TmTMPyZnPc	32b
Tetrakis-2,(3)-{2-mercaptopyridinephthalocyanine} Ga(III)Cl	(Cl)GaTMPyPc	33a
Tetrakis-2,(3)-{2-mercaptopyridinephthalocyanine} In(III)Cl	(Cl)InTMPyPc	33b
Tetrakis-2,(3)-{2-mercaptopyridinephthalocyanine} $Si(III)Cl_2$	$(Cl)_2$SiTMPyPc	33c
Tetrakis-2,(3)-{2-mercaptopyridinephthalocyanine} Sn(II)	SnTMPyPc	33d
TetramethylTetrakis-2,(3)-{2-mercaptopyridine phthalocyanine} Ga(III)Cl	(Cl)GaTmTMPyPc	34
TetramethylTetrakis-2,(3)-{2-mercaptopyridine phthalocyanine} In(III)Cl	(Cl)InTmTMPyPc	35
Tetrakis-2,(3)-{2-mercapto-4-methyl-5-thiazoleaceticacid phthalocyanine}zinc(II)	TMmTAAZnPc	36
Octakis-2,3-{2-mercapto-4-methyl-5-thiazoleaceticacid phthalocyanine}zinc(II)	OMmTAAZnPc	37
Tetrakis-2,(3)-{mercaptoaceticacidphthalocyanine} Ga(III)OH	(OH)GaTMAAPc	38a
Tetrakis-2,(3)-{mercaptoaceticacidphthalocyanine} In(III)OH	(OH)InTMAAPc	38b
Tetrakis-2,(3)-{mercaptoaceticacidphthalocyanine}Si(IV) (OH)(Me)	(OH)(Me)SiTMAAPc	38c

Table 3.3 contd.

MPc complex	Abbreviation	No.
Tetrakis-2,(3)-{mercaptoaceticacidphthalocyanine}zinc(II)	TMAAZnPc	38d
Tetrakis-2,(3)-{3-mercaptopropionicacidphthalocyanine} Ga(III)OH	(OH)GaTMPAPc	39a
Tetrakis-2,(3)-{3-mercaptopropionicacidphthalocyanine} In(III)OH	(OH)InTMPAPc	39b
Tetrakis-2,(3)-{3-mercaptopropionicacidphthalocyanine} Si(IV)OH	(OH)(Me)SiTMPAPc	39c
Tetrakis-2,(3)-{3-mercaptopropionicacidphthalocyanine} zinc(II)	TMPAZnPc	39d
Tetrakis-2,(3)-{(5-trifluoromethyl)-2-pyridyloxy phthalocyanine}zinc(II)	TmtfTPyZnPc[a]	40
Tetrakis-2,(3)-{(5-trifluoromethyl)-2-mercaptopyridine phthalocyanine}zinc(II)	TmtfTMPyZnPc[a]	41
Tetrakis-2,(3)-{(1,6-hexanedithiol)phthalocyanine} zinc(II)	THdTZnPc[a]	42

[a]Complexes donated by fellow researchers (Dr. Ali Erdogmŭs and Dr. Edith Antunes).

3.2.1 Spectroscopic characterization of known complexes

3.2.1.1 Positively charged complexes

The complexes **27b**, **31b** and **32b** were synthesized using well known literature methods (Scheme 3.4). Since these MPc complexes are not new, their characterization is well established and documented in literature [126,129,130,229-231]. The quaternization of these compounds is carried out by using over a 2.5 molar excess of the alkylating agent and heating the compound in the presence of an alkylating agent for more than 10 hours. This is done to avoid obtaining a mixture of di, tri and tetraalkylated products and it allows for the formation of the tetraalkylated product as the main product. The FT-IR, NMR and elemental analysis characterization carried out on these complexes in this work was in line with that documented in

literature. The synthetic routes of the complexes **27b**, **31b** and **32b** are shown in Scheme 3.4.

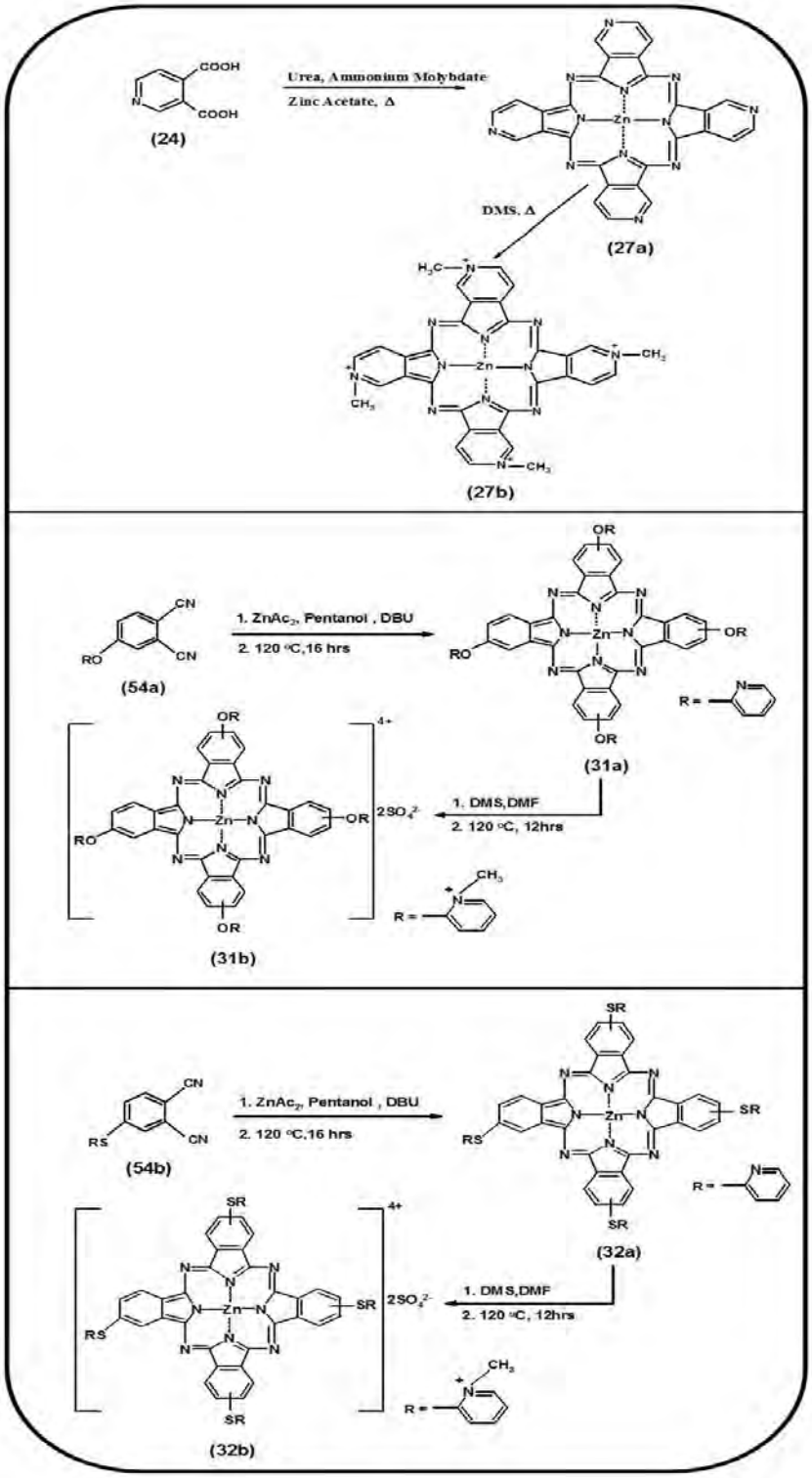

Scheme 3.4: Synthetic route of well known MPcs (27b, 31b and 32b) used in this work [126,129,130,229,230].

The quaternized zinc porphyrazine **27b**, and the quaternized MPc complexes **31b** and **32b** are soluble in aqueous media by virtue of the tetra cationic charge inferred onto them by the methyl groups on the pyridine ring of the macrocycle.

Figure 3.11 shows the electronic ground state absorption spectrum of TmTPZnPz (**27b**) in pH 7.4 phosphate buffer. Complex **27b** is known not to form aggregates in aqueous solutions [229,244]. However, the spectra of this complex in water have been shown to show slight splitting of the Q band of the quaternized porphyrazine. This split is attributed to the presence of symmetrical and unsymmetrical constitutional isomers of the porphyrazine [229]. The absorption maximum for TmTPZnPz (**27b**) was observed at ~ 648 nm in pH 7.4 phosphate buffer, Table 3.4.

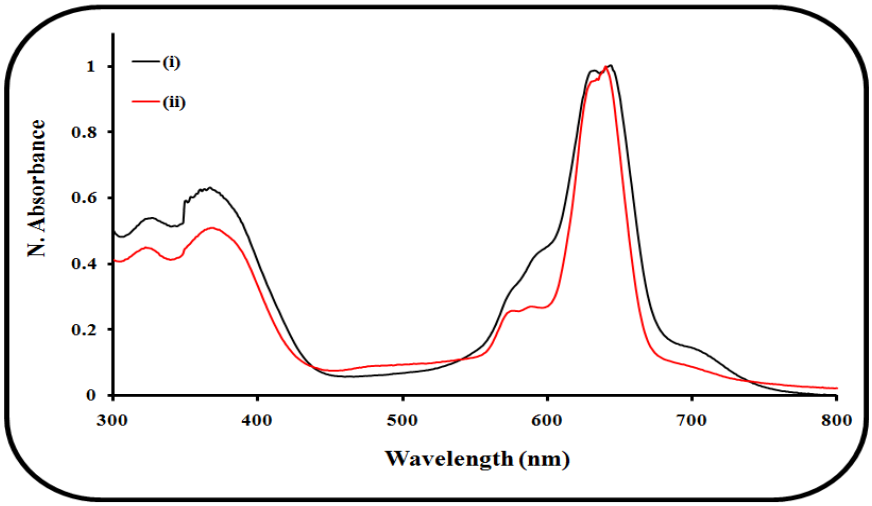

Figure 3.11: Ground state absorption spectrum of TmTPZnPz (27b) in pH 7.4 buffer (i) and in DMSO (ii). {[TmTPZnPz] = 7 × 10^{-6} M}

As shown in Figure 3.12 the Q-bands of the mercaptopyridine substituted zinc Pcs (TMPyZnPc (**32a**) and TmTMPyZnPc (**32b**)) are slightly red-shifted compared to those of the pyridyloxy substituted zinc Pcs (TPyZnPc (**31a**) and TmTPyZnPc (**31b**)), Table 3.4. The reason for this observed behaviour results from the thio group in the mercaptopyridine substituents. Alkylthio or arylthio substituents result in red-shifting of the Q-band since they are electron donating in nature more so than their alkyloxo or aryloxo counterparts.

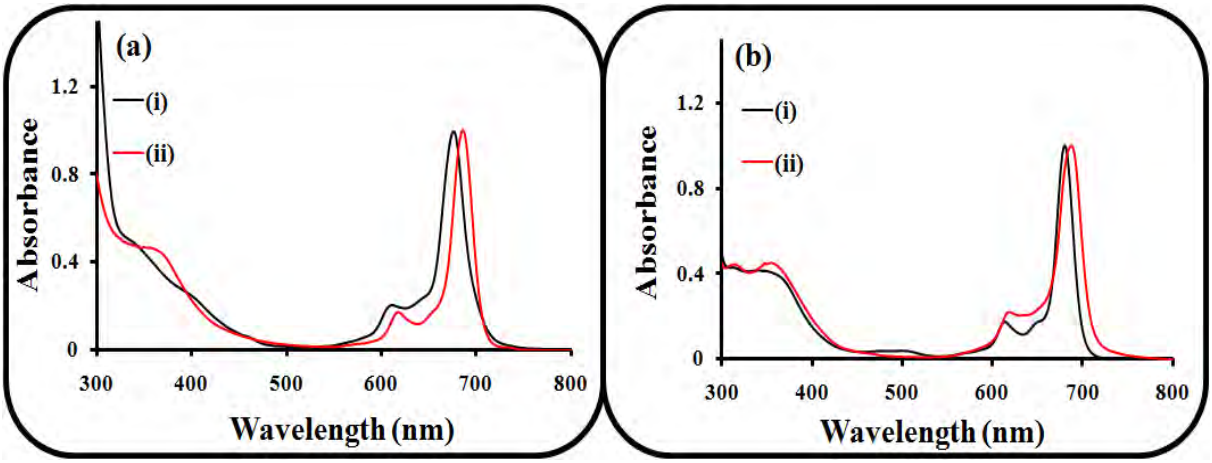

Figure 3.12: Normalized ground state absorption spectra for (a) TPyZnPc (31a) (i) and TMPyZnPc (32a) (ii) in DMSO and (b) TmTPyZnPc (31b) (i) and TmTMPyZnPc (32b) (ii) in DMSO. { [MPc] = ~6 × 10^{-6} M}

Table 3.4: Absorbance data for well known water soluble MPc complexes in different solvents.

MPc	Solvent	Q band, λ_{max} (nm)	Log ε
TmTPZnPz (27b)	pH 7.4 buffer	648	4.94
ZnTSPc (28)	DMSO	680	4.54
	[a](1:1)EtOH:NaOH	676	4.95
ZnTCPc (29)	DMSO	690	4.98
	[a](1:1)EtOH:NaOH	694	4.82
ZnOCPc (30)	DMSO	706	5.12
	[a](1:1)EtOH:NaOH	694	5.20
TPyZnPc (31a)	DMSO	676	5.36
TmTPyZnPc (31b)	DMSO	680	4.61
TMPyZnPc (32a)	DMSO	685	5.52
TmTMPyZnPc (32b)	DMSO	688	4.91

[a]A (1:1) ethanol:NaOH 0.01M solvent mixture was used.

3.2.1.2 Negatively charged MPc complexes

The tetra sulfonated (**28**) [117,120], tetracarboxy (**29)** [123] and the octacarboxy (**30**) zinc (II) phthalocyanines [118, 122] are also not new complexes, as their full characterization is documented in literature. These tetrasulfonated, tetracarboxy and octacarboxy zinc phthalocyanines are negatively charged due to the ionizable sulfonate and carboxyl moieties on the peripheral positions of the Pc ring. The synthetic routes to these negatively charged MPcs are shown in Scheme 3.5 [118,122].

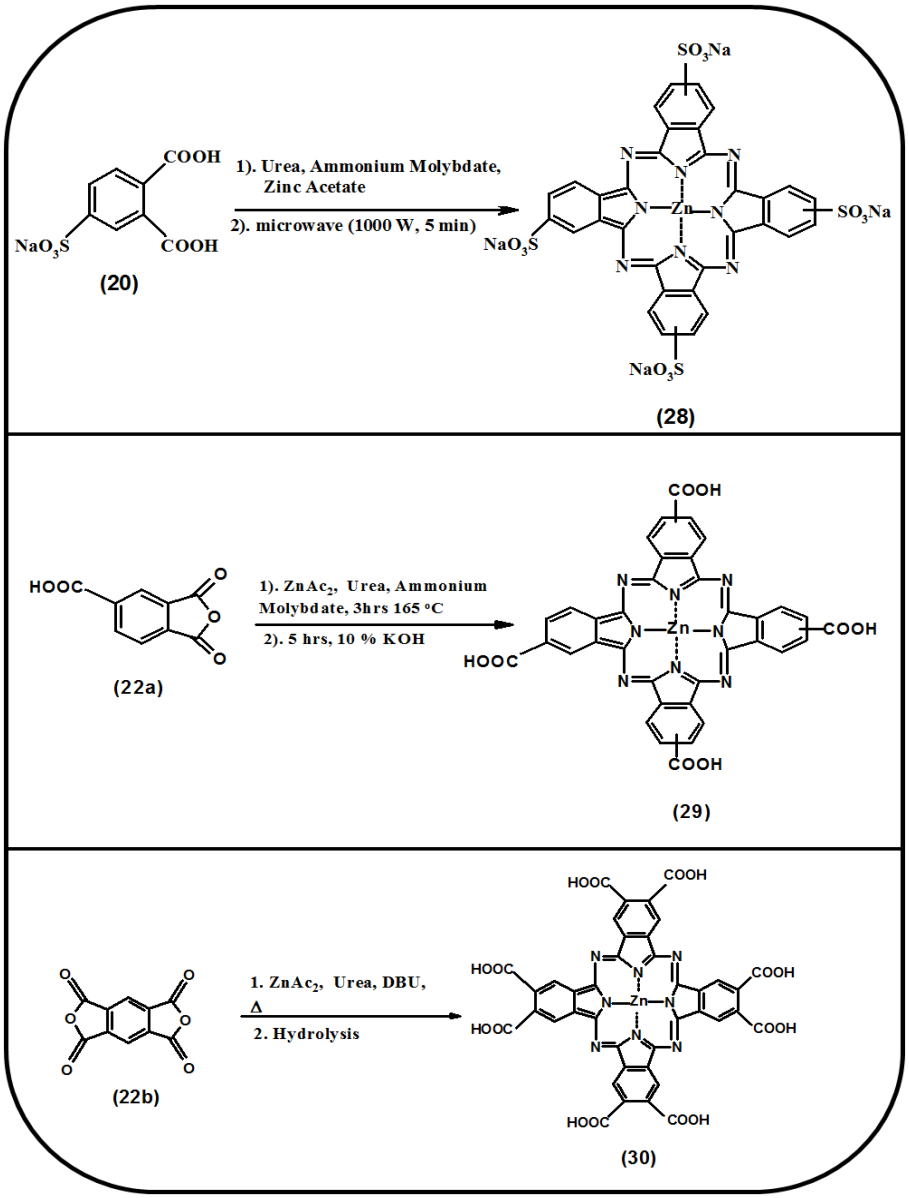

Scheme 3.5: Synthetic route of well known MPcs (28, 29 and 30) used in this work [117,118,120,122,123].

The water soluble ZnPc complexes generally exist as aggregates in equilibrium with monomers in aqueous media. Figure 3.13 shows the ground state electronic absorption spectra of the negatively charged MPcs in aqueous solutions. As shown in Figure 3.13, the spectra of the negatively charged tetra substituted Pcs **28** and **29** give evidence of aggregation from the band observed ~640 nm besides the main Q-band of the monomeric species that appears ~680 nm in pH 7.4 buffer solution. Aggregation in MPc complexes is due to a coplanar association of rings, resulting in splitting and broadening of spectra, with the blue-shifted peak at ~ 630 nm being due to the aggregate. Addition of organic solvents normally breaks the aggregates, resulting in monomeric species. As a result, a (1:1) ethanol:NaOH (0.01M) solvent mixture was employed to break aggregation in this work for the negatively charged MPcs. However complex **30** did not show any aggregation in the pH 7.4 buffer solution. The ZnPc derivatives obeyed Beer's law for concentrations less than 1×10^{-5} M in this solvent mixture.

Octacarboxyl MPc complexes generally display monomeric sharp Q-bands in organic solvents as well as in aqueous media (within pH ranges of 6-10) [245,246]. This behaviour of octacarboxy MPcs has been attributed to (i) the complete ionization of the carboxylate moieties on the Pc ring at the specified pH ranges above and (ii) the plurality of the carboxyl substituents (eight carboxylate groups in ZnOCPc compared to four in ZnTCPc) [246]. In the (1:1) ethanol: NaOH (0.01M) solvent mixture complexes **28** and **29** show complete monomericity.

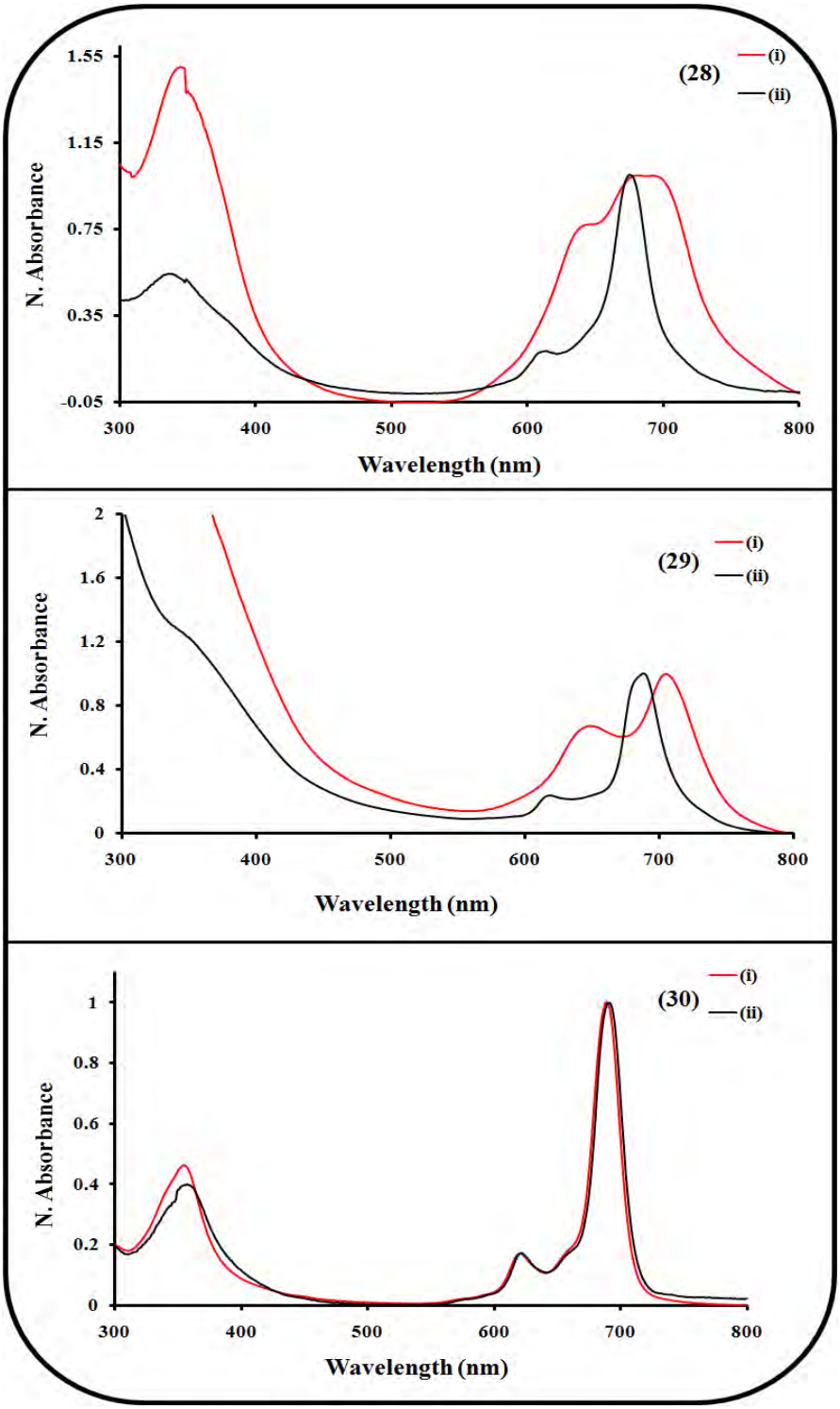

Figure 3.13: Ground state absorption spectra in pH 7.4 phosphate buffer solution (i) and in a (1:1) ethanol:NaOH (0.01M) solvent mixture (ii) for ZnTSPc (28), ZnTCPc (29) and ZnOCPc (30) respectively. {[ZnTSPc] = 1 × 10^{-5} M, [ZnTCPc] = 8 × 10^{-6} M and [ZnOCPc] = 7.5 × 10^{-6} M}

3.2.2 Synthesis and characterization of novel MPc complexes

3.2.2.1 Synthesis of peripherally substituted phthalonitriles

The syntheses of 4-[2-pyridyloxy] (**54a**), 4-[2-mercaptopyridine] (**54b**), 4-[2-Mercapto-4-methyl-5-thiazoleaceticacid] (**54c** and **54d**), 4-[2-mercaptoacetic acid] (**54e**), 4-[2-mercaptopropionic acid] (**54f**), 4-[5-(trifluoromethyl)-2-pyridyloxy] (**54g**), 4-[5-(trifluoromethyl)-2-mercaptopyridine] (**54h**) and 4-[1,6-hexanedithiol] (**54i**) substituted phthalonitriles were all carried out at room temperature, under inert atmospheric conditions (using nitrogen or argon) and in the presence of a base, Scheme 3.6. The base has been shown to catalyze the nucleophilic displacement reaction during the formation of the phthalonitriles [247]. The synthesis and characterization of the 2-pyridyloxy (**54a**) and 2-mercaptopyridine (**54b**) substituted phthalonitriles have been previously reported in literature [129,231-233], while the rest of the phthalonitriles are all new.

The phthalonitriles were characterized by FT-IR and NMR spectra. All phthalonitriles synthesized showed a characteristic C≡N stretch in the IR spectra at ~ 2230 cm^{-1}. The yields obtained for all synthesized phthalonitriles were satisfactory.The phthalonitriles **54a** to **54i** also proved to be pure by ^{1}H-NMR as shown in the experimental section with their proton NMR corresponding well to the expected number of protons.

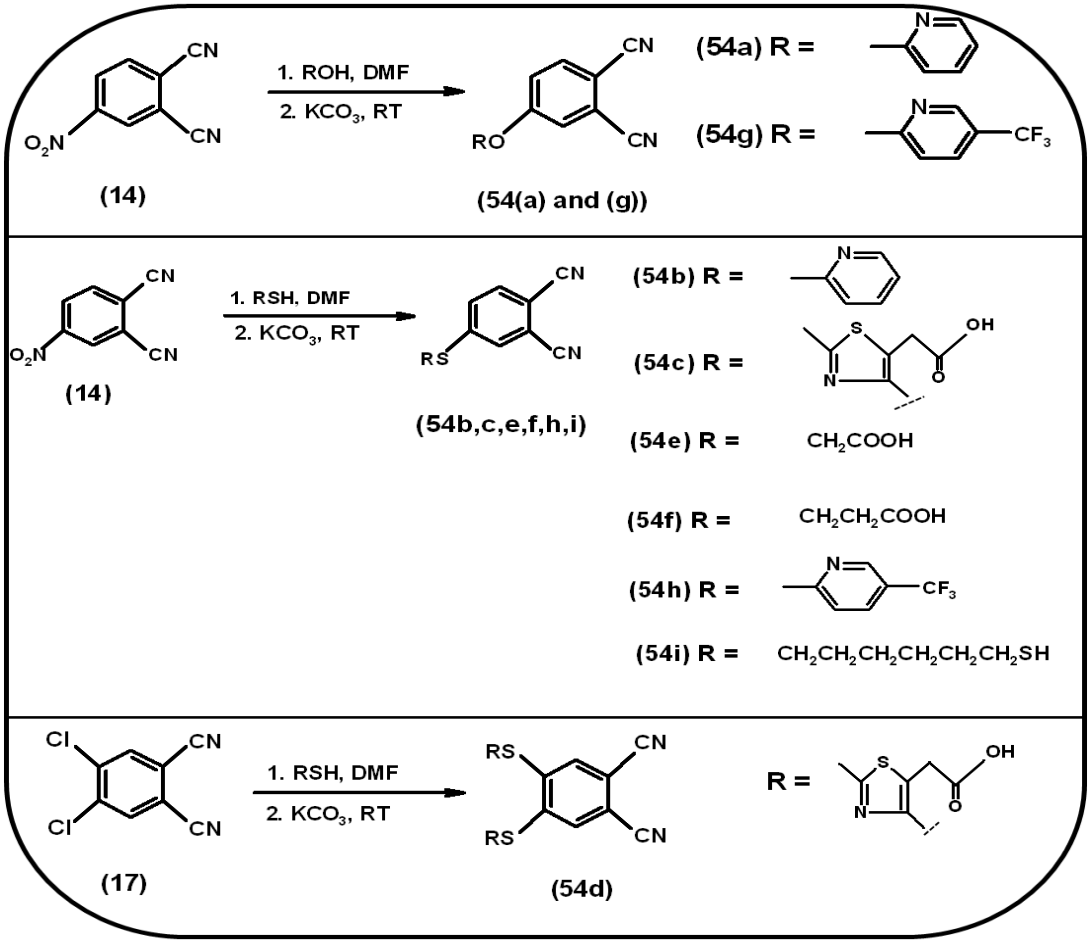

Scheme 3.6: Synthesis of peripherally substituted phthalonitriles (54a-i).

3.2.2.2 Synthesis of quaternized MPcs and their quaternizable precursors

Neutral quaternizable complexes 33(a-d)

Following the synthesis of the zinc phthalocyanines above, novel tetra-2,(3)-[2-mercaptopyridine] substituted Pcs with different metal centres were synthesized, Scheme 3.7. In this work Pcs with Ga^{3+}, In^{3+}, Si^{4+} and Sn^{2+} as central metal ions of choice were synthesized. After conversion into gallium, indium, silicon or tin phthalocyanines, the characteristic C≡N stretch at ~2230 cm^{-1} of 4-(2-mercaptopyridinephthalonitrile) disappeared, thus giving an indication of metallophthalocyanine formation. In general, the synthesis of SnPc complexes using $SnCl_2$ may result in the formation of either the Sn(II)Pc or $(Cl)_2$Sn(IV)Pc

species depending on the amount of $SnCl_2$ used in the reaction [248,249]. When excess $SnCl_2$ is used, Sn(II)Pc derivatives (SnTMPyPc, **33d**) are formed as is the case in this work. For the rest of the complexes: (Cl)GaTMPyPc (**33a**), (Cl)InTMPyPc (**33b**) and $(Cl)_2$SiTMPyPc (**33c**), the central metals have their usual oxidation states. $SiCl_4$ used as a metal source is known to easily react with alcohols leading to the formation of pentylorthosilicates thus inert solvents (e.g. quinoline) are always employed for synthesis involving $SiCl_4$. However in this work by heating the phthalonitrile until it had fully dissolved in pentanol, the quick ejection of $SiCl_4$ into the hot solution allowed formation of $(Cl)_2$SiTMPyPc (**33c**) as the main product, SiPc with axial pentoxy substituents and pentylorthosilicates were formed as minor products (negligible).

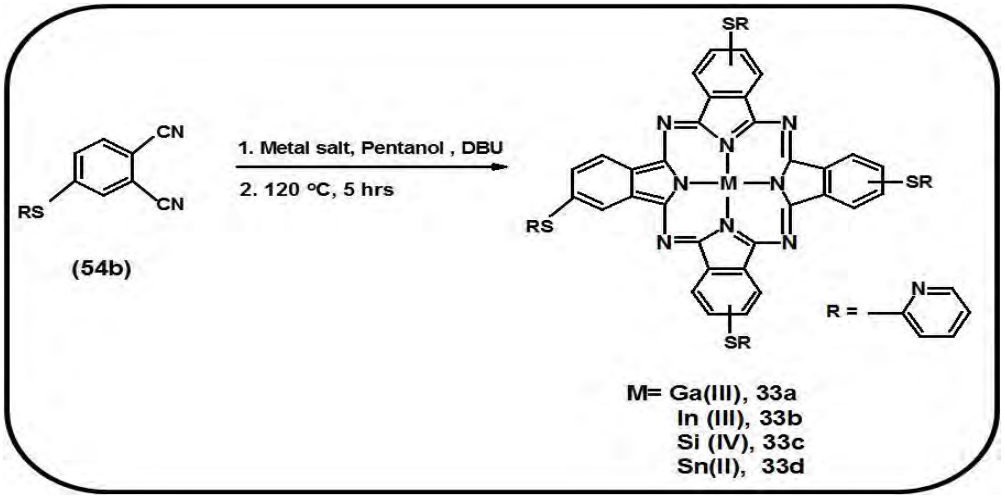

Scheme 3.7: Synthesis of mercaptopyridine substituted MPcs 33a-33d.

The presence of chloride axial ligands (with weak metal-halide vibrations in the 320 to 350 cm^{-1} region) was confirmed by IR spectroscopy. The complexes showed charateristic C-H stretches at ~ 3050 cm^{-1}, C=C stretches at ~ 1330 cm^{-1} and C-S-C stretches at 1080 cm^{-1}. Generally, phthalocyanine complexes are insoluble in most organic solvents; however introduction of substituents on the ring increases the solubility. All complexes (**33a-d**) exhibited excellent solubility in organic solvents such as dichloromethane, chloroform, THF, DMF, and DMSO with absorption spectra shown in Figure 3.14. The new compounds were characterized by UV-Vis, IR, NMR spectroscopies, and elemental analysis. The analyses are consistent with

the predicted structures as shown in the experimental section, with the percent carbon values differing by less than 1% from the calculated values. The ^{1}H NMR spectra of tetrasubstituted phthalocyanine derivatives (**33a-d**) show complex patterns owing to the mixed isomer character of these compounds. The complexes were found to be pure by ^{1}H NMR with all the substituents and ring protons observed in their respective regions as shown in the experimental section. The protons for the Pc ring and the pyridine ring were generally observed between 9.86 and 7.07 ppm for the 2-mercaptopyridine substituted MPcs integrating for all 28 protons of the Pc ring and pyridine ring of the substituent.

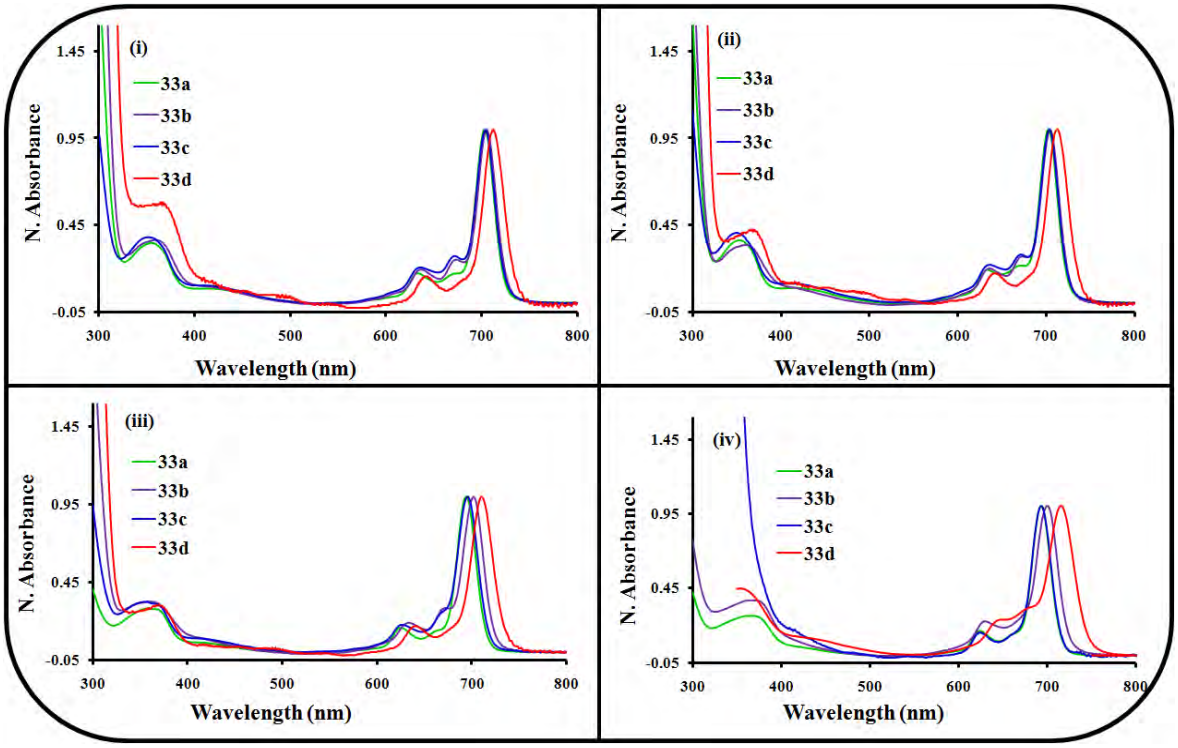

Figure 3.14: Normalized ground state absorption spectra of complexes 33a-d in $CHCl_3$ (i), DCM (ii), THF (iii) and DMSO (iv). {[MPc] = ~8.5 × 10^{-6} M}

The MPc complexes **33a-d** obeyed Beer's law for concentrations ranging up to 1 x 10^{-5} M and all showed a monomeric behaviour in DMSO, DMF, THF, $CHCl_3$, and DCM. It has been reported that a shift in the Q band to the red occurs with increase in the refractive index of the solvent [152]. The order of increase of the refractive indices of the solvents is DMSO > $CHCl_3$ > DMF > DCM > THF. The red-shifting of the Q band with an increase in the refractive index of the solvent is not obvious in Table 3.5 as

well as in the absorption spectra shown in Figure 3.14. However a general red-shift in the Q band was observed with increase in size of the central metal and the order of the Q band positions is **33d** (Sn) > **33b** (In) > **33a** (Ga) ≅ **33c** (Si). This trend in Q band positions can be explained through a consideration of the degree of destabilization of the highest occupied molecular orbital (HOMO) in the MPc complexes. Since tin has more electrons in its atomic structure it has greater reducing properties than the rest of the central metal ions and thus will destabilize the HOMO more than the In^{3+}, Ga^{3+} and Si^{4+} central metal ions. Consequently, the greater destabilization resulting from tin will result in a smaller HOMO-LUMO separation, hence the largest red-shifted spectra as readily discernible in Figure 3.14. The Q-band positions and molar extinction coefficients of the Pc complexes with different metal centres are shown in Table 3.5. Generally, the complexes **33a** and **33c** had the higher molar extinction coefficient values compared to their heavy metal ion counterparts.

Quaternized complexes 34 and 35

The mercaptopyridine substituent in the newly synthesized MPc complexes above allows for quaternization of the MPcs. However for this work only two MPcs were used for the quaternization procedure and studies with QDs, these being **33a** and **33b**, Scheme 3.8. The quaternization of the MPc complexes **33c** and **33d** was not attempted as mentioned earlier.

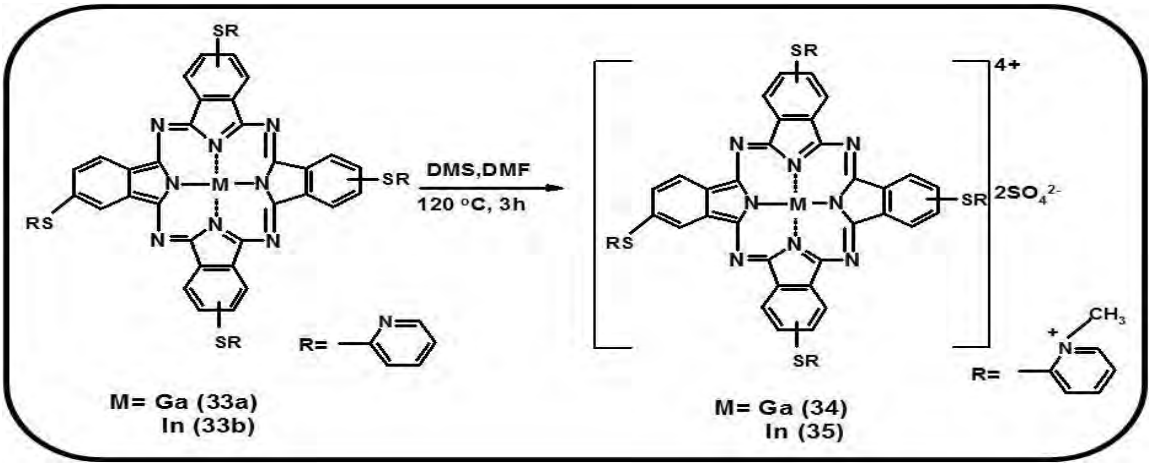

Scheme 3.8: The quaternization procedure for complexes 34 and 35.

Table 3.5: Absorbance data for novel quaternizable and quaternized MPc complexes in different solvents

MPc	Solvent	Q band, λ_{max} (nm)	Log ε
(Cl)GaTMPyPc (33a)	DMSO	691	5.43
	DMF	688	5.20
	$CHCl_3$	702	5.13
	DCM	702	5.17
	THF	693	5.22
(Cl)InTMPyPc (33b)	DMSO	698	5.09
	DMF	690	4.96
	$CHCl_3$	704	5.08
	DCM	703	4.99
	THF	701	4.98
$(Cl)_2$SiTMPyPc (33c)	DMSO	692	5.07
	DMF	689	5.06
	$CHCl_3$	702	5.20
	DCM	702	5.09
	THF	694	5.17
SnTMPyPc (33d)	DMSO	711	4.32
	DMF	705	4.23
	$CHCl_3$	710	4.37
	DCM	710	4.5
	THF	709	4.55
(Cl)TmGaTMPyPc (34)	DMSO	691	5.31
	EtOH:H_2O (1:1)	686	5.36

Table 3.5 contd.

MPc	Solvent	Q band, λ_{max} (nm)	Log ε
(Cl)TmInTMPyPc (35)	DMSO	698	5.19
	EtOH:H_2O (1:1)	694	5.16
TtfmPyZnPc (40)	DMSO	678	5.28
TtfmMPyZnPc (41)	DMSO	685	5.21

The FT-IR, elemental and NMR characterization results were in line with what was expected as shown in the experimental section. As expected, the quaternized MPcs: (Cl)GaTmTMPyPc (**34**) and (Cl)InTmTMPyPc (**35**) are water soluble and showed considerable aggregation in water as judged by the broad band at 643 nm (for **34**) and 651 nm (for **35**) due to the formation of H-aggregates, with the monomer peak being observed at 686 nm for **34** (as a shoulder) and at 694 nm for **35**. However, the aggregation was broken by the addition of ethanol and the Q-bands were typical monomeric species. The monomerization of the Q-band is evidenced by the sharp increase in the intensity of the monomer peaks accompanied by a decrease in the intensity of the dimer peaks as shown in Figure 3.15. In addition to their solubility in aqueous solution, both complexes exhibited excellent solubility in organic solvents such as DMF and DMSO and showed monomeric behaviour and obeyed Beer's law for concentrations up to 1×10^{-5} M.

The mass spectra of the phthalocyanines were obtained by the relatively soft ionization MALDI-TOF technique with the molecular ion peaks observed at m/z 1078.90 for **34** and 1124.60 for **35** with chlorine as the axial atom for both complexes. In solution, the chloride axial ligand can easily be displaced by another on the central metal (e.g. hydroxyl ligand). The complexes were found to be pure by ^{1}H NMR with all the substituent and ring protons observed in their respective regions. There is a slight red-shift in the Q-band with increase in size of the central metal, thus the Q-band position of complex **35** is more red-shifted than that of complex **34**.

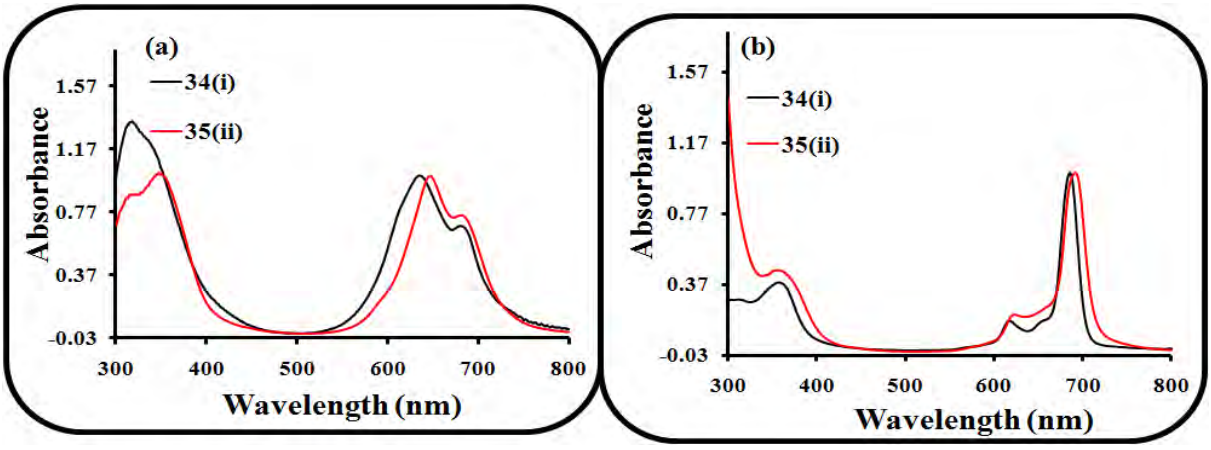

Figure 3.15: Ground state absorbance of (a) complexes 34 (i) and 35 (ii) in water, (b) complexes 34 (i) and 35 (ii) in (1:1) ethanol: water solvent mixture. {The same concentration was used for both MPc complexes [MPc] = ~8 × 10^{-6} M}

Neutral quaternizable complexes 40 and 41

The characterization of quaternizable MPc complexes TtfmPyZnPc **(40)** and TtfmMPyZnPc (**41**) (Scheme 3.9) is also reported in this thesis. Complex **41** bearing a thio bridge once again shows a typical red-shift in the Q-band when compared to complex **40** bearing an oxo bridge as shown in Table 3.5. Figure 3.16 shows the respective absorption spectra for TtfmPyZnPc **(40)** and TtfmMPyZnPc (**41**) in DMSO with the latter being more red-shifted than the former.

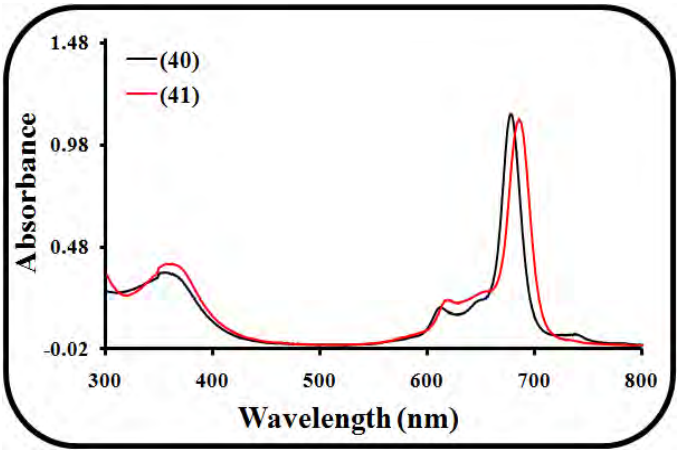

Figure 3.16: Ground state absorbance of TtfmPyZnPc (40) and TtfmMPyZnPc (41) in DMSO. ([MPc] = ~1.5 × 10^{-5} M}

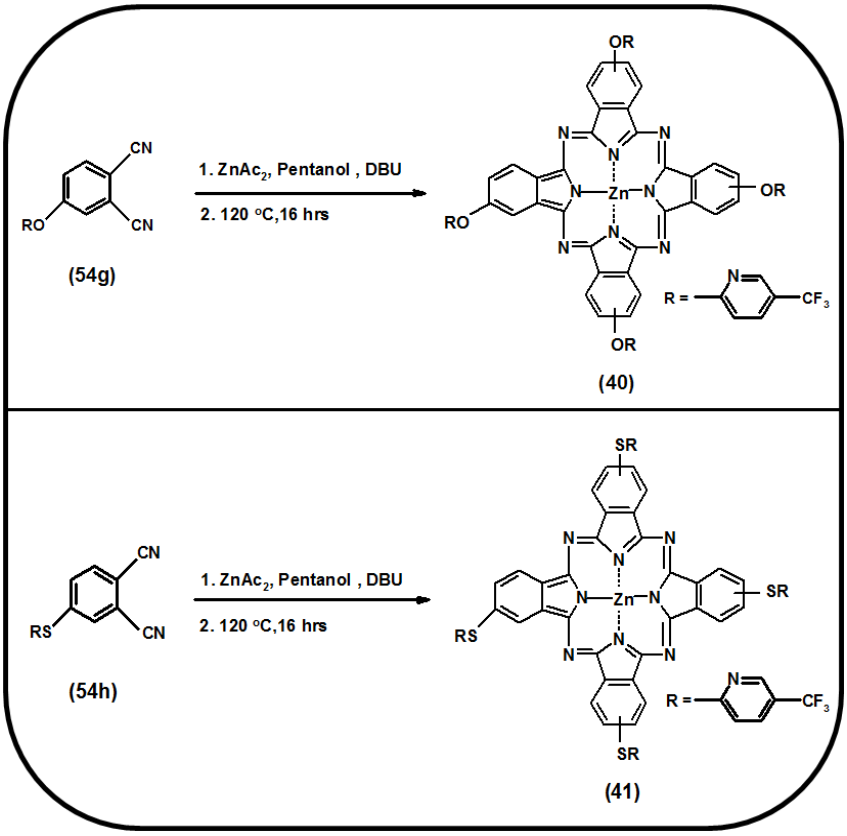

Scheme 3.9: Synthetic route for complexes TtfmPyZnPc (40) and TtfmMPyZnPc (41).

3.2.2.3 Synthesis of negatively charged MPcs

Complexes 36 and 37

The new complexes TMmTAAZnPc (**36)** and OMmTAAZnPc (**37)** were synthesized by the cyclotetramerization of the corresponding phthalonitrile **54c** and **54d** respectively Scheme 3.10. These complexes were characterized by UV-Vis, FT-IR, NMR spectroscopies and elemental analyses. All the analyses are consistent with the expected results as shown in the experimental section. The complexes showed characteristic COOH vibrations between 3410 and 3450 cm^{-1}, C=C stretches between 1615 and 1640 cm^{-1} and C-OH stretches between 1380 and 1400 cm^{-1}.

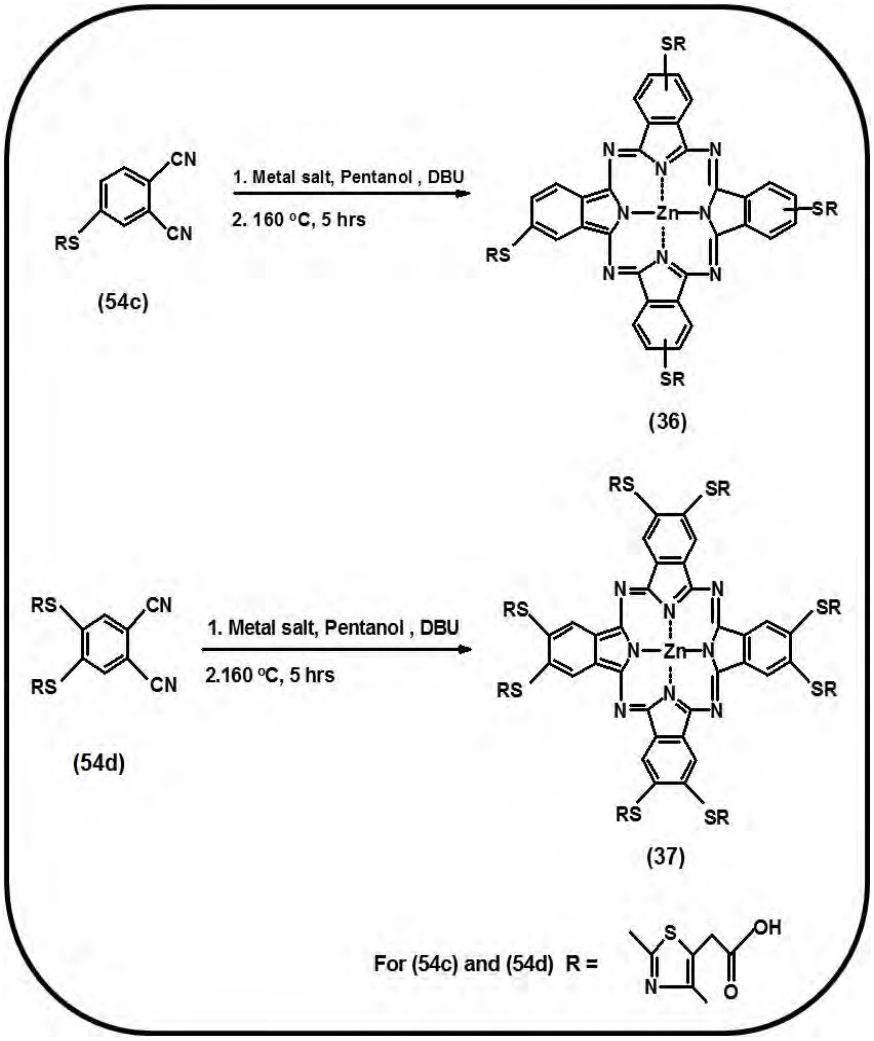

Scheme 3.10: Synthesis of water soluble tetra and octa substituted ZnPcs 36 and 37.

The Q band absorption maxima for **36** ranged from 683 to 687 nm, and for **37** the spectra ranged from 693 to 698 nm in different solvents, Table 3.6. Thus the latter is more red-shifted than the former. The presence of sulphur atoms will result in red shifting of the Q band compared to unsubstituted ZnPc [250]. The plurality of the substituents in the octasubstituted derivative (**37**) results in more red-shifting, Table 3.6. The complexes are soluble in organic solvents: DMSO and DMF, but they also show solubility in basic aqueous media. The ZnPc derivatives (**36** and **37**) are highly aggregated in the basic media alone but the addition of ethanol reduces the aggregation significantly, Figure 3.17. However, the presence of

ethanol could not break the aggregates completely for complexes **36** and **37**, Figure 3.17. Slight aggregation is also evident in DMSO or DMF for **37** and to a lesser degree for complex **36**.

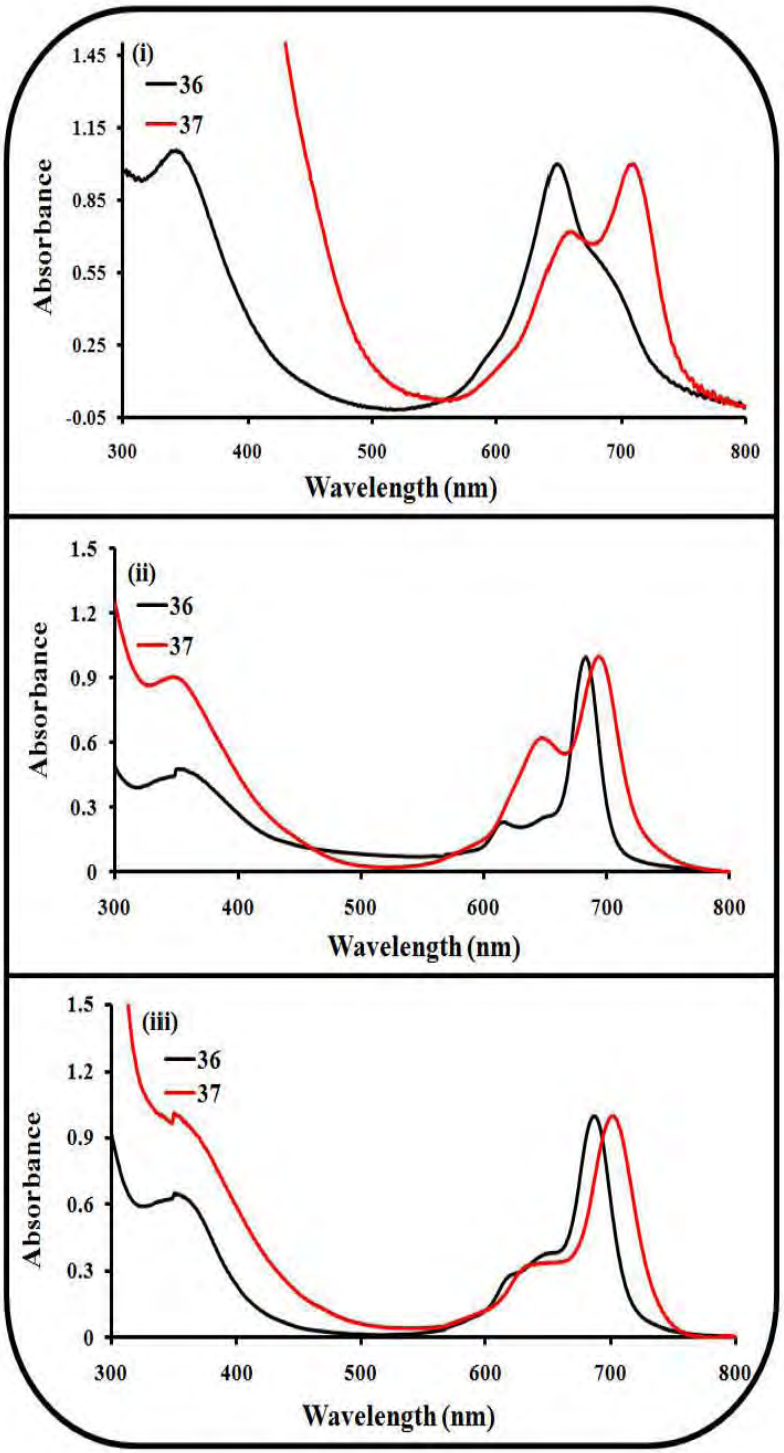

Figure 3.17: Ground state absorption spectra of 36 and 37 in 0.01 M NaOH (i), (1:1) ethanol:NaOH 0.01 M solvent mixture (ii) and DMSO (iii). {[MPc] = ~8 × 10^{-6} M}

Table 3.6: Absorbance data for novel negatively charged MPc complexes in different solvents.

MPc	Solvent	Q band, λ_{max} (nm)	Log ε
TMmTAAZnPc (36)	DMSO	687	4.33
	DMF	685	4.31
	[a](1:1)EtOH:NaOH	683	4.59
OMmTAAZnPc (37)	DMSO	698	4.42
	DMF	693	4.43
	[a](1:1)EtOH:NaOH	696	4.45
(OH)GaTMAAPc (38a)	DMSO	654, 687, 709	-
(OH)GaTMPAPc (39a)	DMSO	653, 686, 712	-
(OH)InTMAAPc (38b)	DMSO	643, 680, 705	-
(OH)InTMPAPc (39b)	DMSO	655, 687, 713	-
(OH)(Me) SiTMAAPc (38c)	DMSO	641, 684, 708	-
(OH)(Me) SiTMPAPc (39c)	DMSO	652, 685, 715	-
TMAAZnPc (38d)	DMSO	658, 691, 714	-
TMPAZnPc (39d)	DMSO	692	4.26

[a]A (1:1) ethanol:NaOH 0.01M solvent mixture was used.

Complexes 38(a-d) and 39(a-d)

A number of novel water soluble MPc complexes with mercaptoacetic acid and mercaptopropionic acid substituents were synthesized, Scheme 3.11. The central metal ions used in the synthesis of these MPcs include Ga^{3+}, In^{3+}, Si^{4+} and Zn^{2+} complexes to afford (OH)GaTMAAPc (**38a**), (OH)InTMAAPc (**38b**), (OH)(Me)SiTMAAPc (**38c**) and TMAAZnPc (**38d**) for the mercaptoacetic acid substituted Pcs. The mercaptopropionic acid on the other hand yielded the

following complexes: (OH)GaTMPAPc (**39a**), (OH)InTMPAPc (**39b**), (OH)(Me)SiTMPAPc (**39c**) and TMPAZnPc (**39d**).

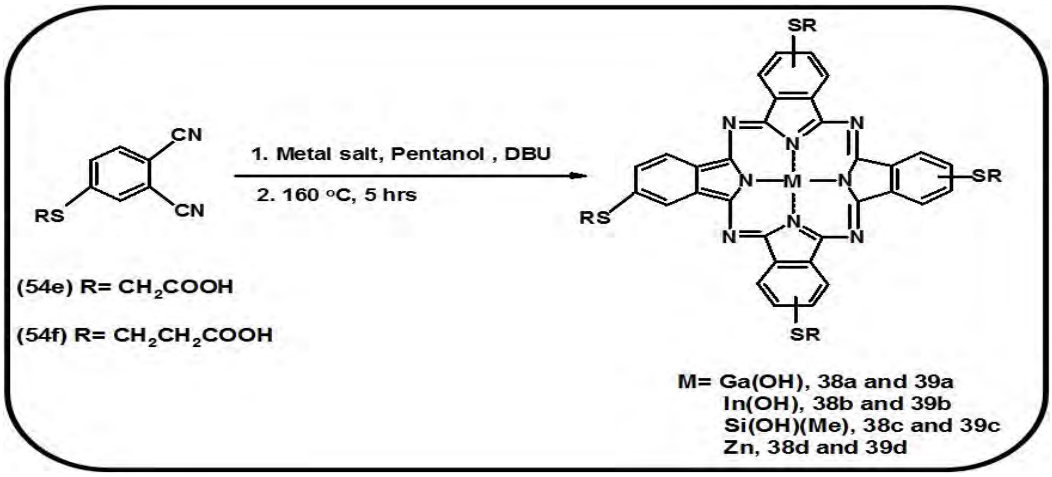

Scheme 3.11: Synthesis of novel water soluble complexes 38a-d and 39a-d.

The mass spectra of the phthalocyanines **38(a-d)** and **39(a-d)** gave molecular ion peaks observed at m/z, 962.23 (**38a**), 1016.23 (**39a**), 1006.19 (**38b**), 1062.01 (**39b**), 934.63 (**38c**), 990.61 (**39c**), 940.09 (**38d**) and 995.31 for (**39d**) as shown in the experimental section. Hydroxyl axial ligands are expected due to the use of sodium hydroxide solution during the purification process.

The complexes **38(a-d)** and **39(a-d)** were found to be pure by ^{1}H NMR with all the substituents and ring protons observed in their respective regions. However, because of the broad nature of the ^{1}H NMR spectra, proton signals due to axial ligands (for complexes **38a-c** and **39a-c**, containing axial ligands) were not observed. Hydrogen bonding will also affect the ^{1}H NMR spectra since the MPc complexes have substituents with terminal carboxyl moieties and complexes **38a-c** and **39a-c** have hydroxyl axial ligands. However, mass spectra and elemental analyses confirmed the formation of the complexes. The complexes showed charateristic COOH vibrations between 3400 and 3455 cm^{-1}, C=C stretches between 1710 and 1600 cm^{-1} and C-OH stretches between 1390 and 1460 cm^{-1}.

These complexes exhibited moderate solubility in organic solvents such as DMF and DMSO as well as in aqueous solution. The complexes **38(a-d)** and **39(a-d)** are generally highly aggregated in the solvents employed: DMSO, DMF and aqueous media, Figure 3.18. The spectral data for these MPc complexes are listed in Table 3.6. The addition of ethanol breaks the aggregation only for the **39d** MPc complex but the rest of the MPcs remain highly aggregated even upon addition of Triton-X 100 (surfactant). As stated above, it is probable that the aggregation observed includes effects from hydrogen bonding since the MPc complexes have substituents with terminal carboxyl moieties and some of the complexes also have hydroxyl axial ligands (Ga^{3+}, In^{3+} and Si^{4+} complexes). Due to the aggregation encountered for these complexes, molar extinction coefficients could only be determined for complex **39d**.

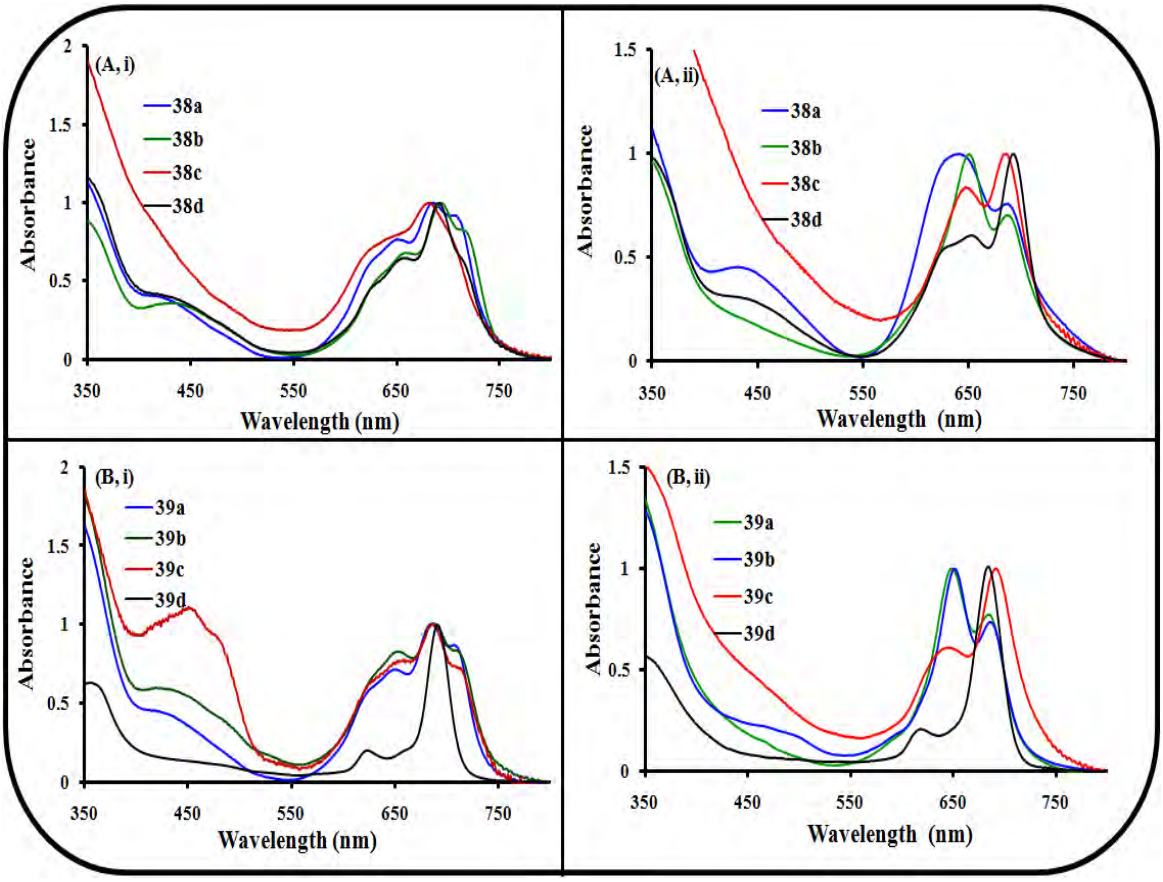

Figure 3.18: Normalized absorption spectra for 38a-d (A) and 39a-d (B) in DMSO (i) and in a (1:1) ethanol:NaOH 0.01M solvent mixture (ii). { [MPc] = ~9 × 10^{-6} M}

3.2.2.4 Neutral MPc complex

The new MPc complex **42** was characterized using UV-Vis, IR, NMR spectroscopies, MALDI-TOF mass spectra and elemental analysis. The analyses are all consistent with the expected as shown in the experimental section. The mass spectra of complex **42** gave a molecular ion peak observed at m/z 1170.56 for complex **42** as shown in the experimental section. Complex **42** exhibited moderate solubility in organic solvents such as $CHCl_3$, DCM, THF, DMF and DMSO. The newly synthesized complex **42** exhibited slight aggregation of the absorption spectra in the solvents employed; $CHCl_3$, DMSO and DMF, Figure 3.19.

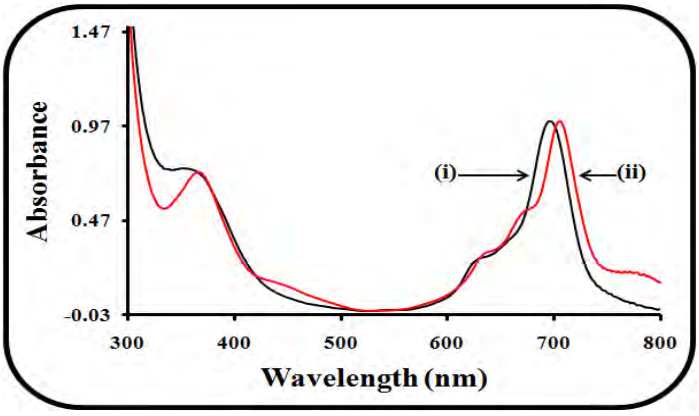

Figure 3.19: Ground state absorption spectra of THdTZnPc (42) in DMSO (i) and $CHCl_3$ (ii). {[THdTZnPc] = ~7.5 × 10^{-6} M}

The synthesis of complex **42** via the cyclotetramerization of the phthalonitrile **54i** is shown in Scheme 3.12.

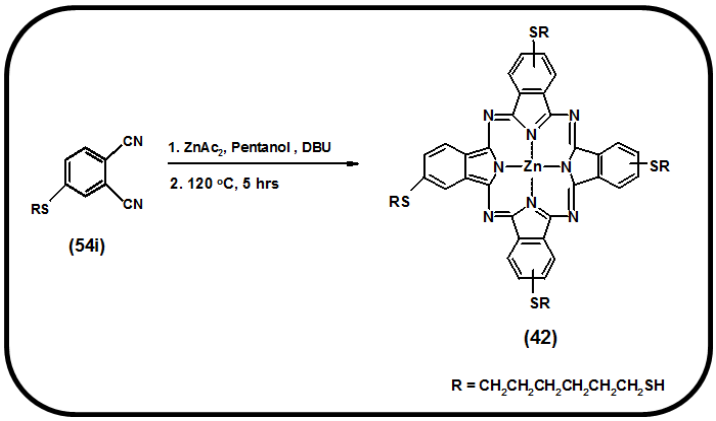

Scheme 3.12: Synthetic route for complex 42.

3.3 Conclusions

In this work, tetra negatively charged phthalocyanines bearing sulfonate groups (zinc), carboxy groups (zinc), mercaptomethylthiazoleacetic acid (zinc), mercaptoacetic acid and mercaptopropionic acid (zinc, gallium, indium, silicon) were successfully synthesized. These MPc complexes were characterized via spectroscopic methods. The negatively charged complexes are soluble in aqueous media, DMSO and DMF. In addition to the MPcs bearing negative charges, positively charged MPcs were synthesized. Mercaptopyridine substituted phthalocyanines (zinc, gallium, indium, silicon and tin), and hydroxypyridine substituted Pcs (zinc) were also synthesized. These MPc complexes were soluble in $CHCl_3$, DCM, THF, DMF and DMSO. The 2-hydroxypyridine substituted ZnPc and several of the 2-mercaptopyridine substituted Pcs (zinc, gallium and indium) were quaternized. Quaternization was also carried out on the zinc tetrapyridino porphyrazine. The tetra positively charged MPcs were soluble in aqueous media, DMSO and DMF and were likewise characterized spectroscopically. The spectroscopic measurements confirmed the formation of the MPcs, as well as their purity. The neutral MPc complexes **40**, **41** (both quaternizable) and **42** which were obtained from fellow researchers were also characterized spectroscopically.

Photophysical and Photochemical Characterization

4

In this chapter the photophysicochemical properties of QDs and the MPcs synthesized for this work are considered. Furthermore, the effects of the use of different central metal ions, substituents and solvents on the photophysicochemical properties of MPcs are also examined.

4.1 Fluorescence spectra and quantum yields

4.1.1 Nanoparticles (CdTe QDs)

In Figure 4.1, the normalized fluorescence spectra of MPA stabilized CdTe QDs (similar to other thiol capped CdTe QDs spectra) are shown in different solvents. They are shown to possess good spectral symmetry as is characteristic for good quality QDs. The stabilizers used for passivating the QDs are known to foster monodispersity of the QDs in solution [4-8]. Solvents affect the aggregation tendencies of QDs to different extents. Aggregation of QDs brought about by solvents sometimes causes a broadening and red-shift in their emission spectrum [251]. As shown in Figure 4.1, the (1:1) pyridine:NaOH 0.01 M solvent mixture resulted in the greatest red-shifting (hence aggregation) of the QDs emission but with negligible broadening. The greatest broadening of the QD emission is evident in DMF and DMSO, Figure 4.1.

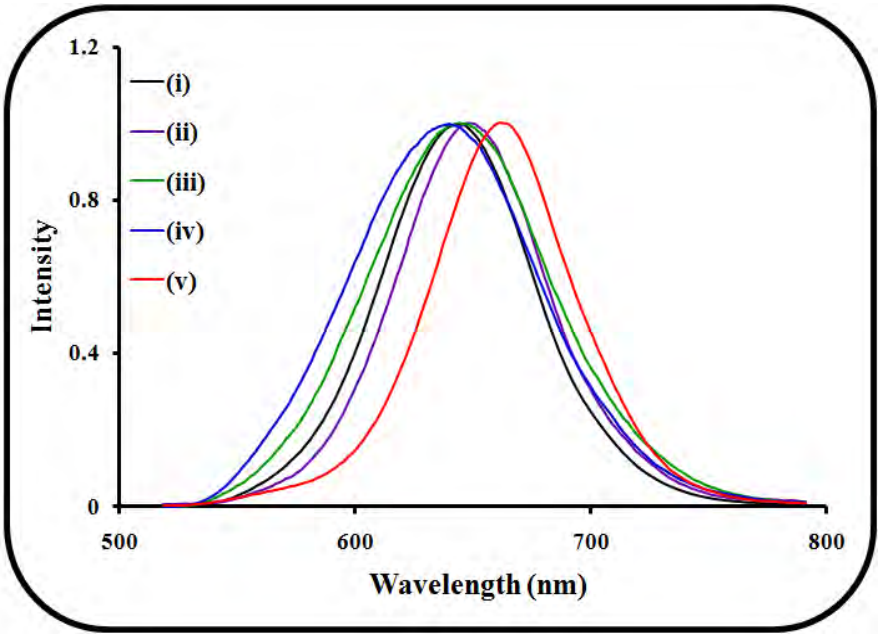

Figure 4.1: Emission spectra for MPA CdTe QDs in water (i), (1:1) ethanol:NaOH 0.01 M solvent mixture (ii), DMF (iii), DMSO (iv) and (1:1) pyridine:NaOH 0.01 M solvent mixture (v).{[QDs] = 1mg/1mL}

Fluorescence quantum yields were determined for CdTe QDs (and not for ZnS QDs or AuNPs, Table 4.1) which are shown to possess high photoluminescence. The fluorescence quantum yield values (Φ_F) for the CdTe QDs were calculated using equation 1.4 shown here as equation 4.1.

$$\Phi_F = \Phi_{F(Std)} \frac{F \,.\, A_{Std.} \, n^2}{F_{Std.} \, A \,.\, n^2_{Std}} \qquad (4.1)$$

It has been clearly shown in literature that QDs possess excellent photostability compared to some conventional organic fluorophores [20].

Table 4.1: The spectral properties, fluorescence quantum yields and lifetimes of MPA stabilized CdTe QDs in different solvents.

[a]Solvent	Refractive Index (n_D)	[b]Emission λ_{max} (nm)	$\Phi_{F\,(QD)}$ (± 0.01)	τ_{F1} (ns) (± 0.6)	τ_{F2} (ns) (± 0.3)	τ_{F3} (ns) (± 0.2)
water	1.339	640	0.35	33.56	4.97	--
NaOH (0.01 M)	1.339	642	0.25	25.22	4.87	--
Ethanol:NaOH (1:1)	1.349	645	0.22	24.31	17.58	1.63
Pyridine:NaOH (1:1)	1.4246	657	0.11	30.3	8.4	--
DMF	1.4305	641	0.26	32.57	7.22	1.72
DMSO	1.4793	638	0.32	30.86	11.45	2.05

[a]All the results shown are for MPA CdTe QDs of the size 4.54 nm.

[b]The excitation wavelength ($\lambda_{excitation}$) = 500 nm.

Table 4.1 shows that Φ_F values for the MPA QDs are highest in water, but are slightly decreased in other solvent media e.g. DMF, basic aqueous media and in DMSO. The MPA QDs Φ_F value was lowest in the (1:1) pyridine:NaOH 0.01M solvent mixture

and this may be brought about by the pyridine molecules. This is because pyridine molecules are most likely to displace the thiol stabilizers (that enrich the surface of QDs) which are responsible for the relatively high Φ_F values of the CdTe QDs.

The effect of changing the solvent used is most likely to be evidenced in a variation of the fluorescence lifetimes originating from the surface states or defect sites which correspond to longer lifetimes according to literature (τ_{F1} for biexponential kinetics and τ_{F1} and τ_{F2} for triexponential kinetics) [63,64]. CdTe QDs may exhibit biexponential or triexponential kinetic models depending on which of the two models most accurately fits the experimental decay signal. QDs in water, basic media and the pyridine:NaOH 0.01M solvent mixture displayed biexcitonic kinetics while QDs in the ethanol:NaOH 0.01M solvent mixture, DMSO and DMF exhibited triexponential decay kinetics. There is a clear change in τ_{F1} (for the biexcitonic models) and τ_{F1} and τ_{F2} (for the triexponential models) with a change in the solvent used suggesting an involvement of surface defects and states. This observed decrease in the lifetimes from surface defects and states indicates the susceptibility of QDs to aggregation in solvents other than water. The τ_{F1} value was highest in water (biexponential) while that for τ_{F2} was highest in the ethanol:NaOH 0.01M solvent mixture (triexponential). The fluorescence lifetimes were determined through the use of a time correlated single photon counting setup (TCSPC). A typical photoluminescence decay curve of MPA QDs is shown in Figure 4.2.

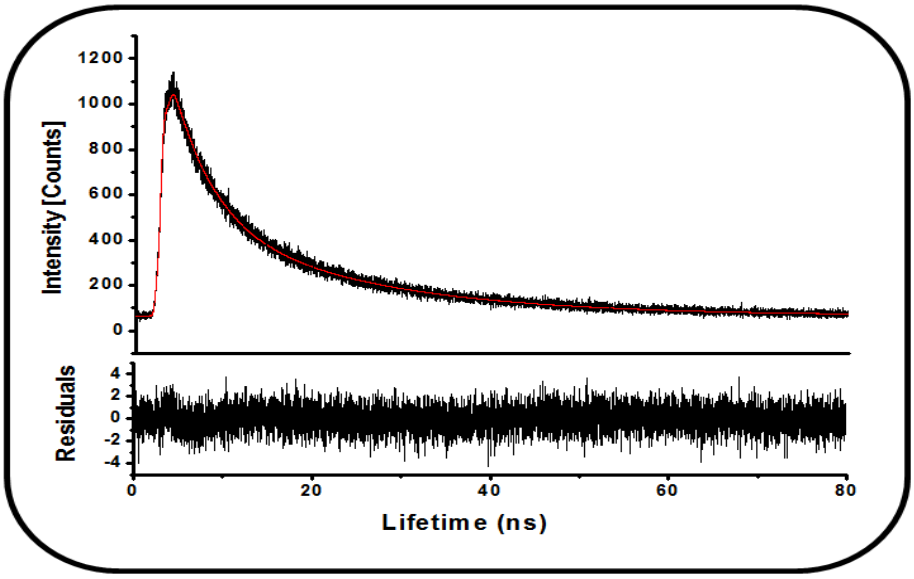

Figure 4.2: Photoluminescence decay curve of MPA CdTe QDs in water ($\lambda_{excitation}$ = 640 nm).

4.1.2 Metallophthalocyanines

4.1.2.1 Monomerized MPc complexes in aqueous solvent mixtures

The water soluble complexes **27b, 28, 29, 30**, **34**, **35, 36** and **39d** were monomerized by the (1:1) ethanol:NaOH 0.01M solvent mixture used in this work. These water soluble Pc complexes are generally aggregated in aqueous media, but they were fully disaggregated upon the addition of ethanol to the basic aqueous medium and showed complete monomericity. For all these Pc complexes the absorbance and fluorescence excitation spectra in both the aqueous solvent mixture and in DMSO were similar and mirror images of the fluorescence emission spectra as expected for monomeric MPcs, as shown for ZnTSPc (**28**) and ZnOCPc (**30**) in Figure 4.3. The emission spectra occur at longer wavelengths than the absorption spectra, with Stokes shifts that range from 3-20 nm (Table 4.2) which is typical of MPcs [252]. The proximity of the Q-band maxima for the absorption and excitation spectra suggests that the configuration of Pc molecules in the ground and excited states remains the same.

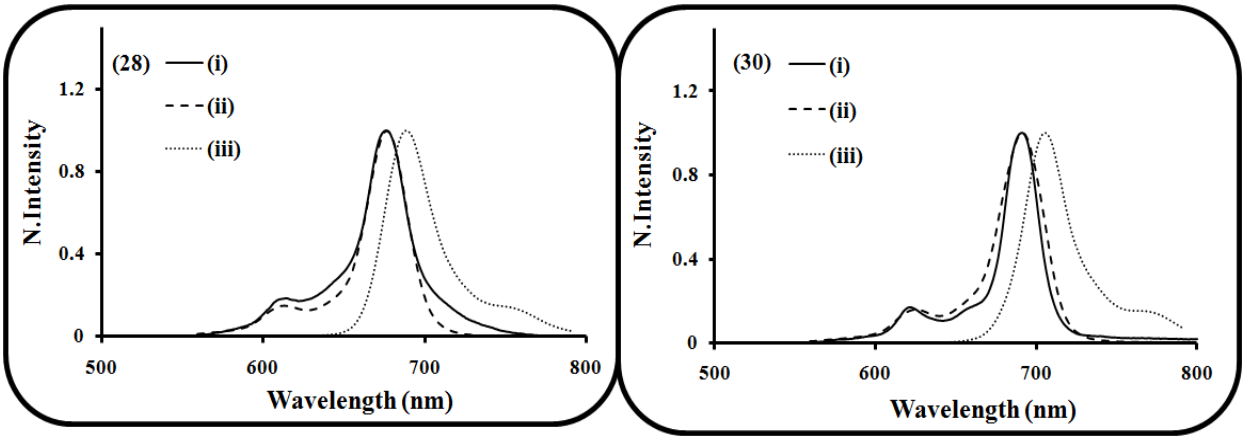

Figure 4.3: The ground state absorbance (i), excitation (ii) and emission (iii) of ZnTSPc (28), and ZnOCPc (30) in a (1:1) ethanol:NaOH 0.01M solvent mixture. {($\lambda_{excitation}$= 610 nm), [MPc] = 7.5 × 10^{-6} M}

Fluorescence quantum yield (Φ_F) values were determined for MPcs using equation 4.1 and are listed in Table 4.2. The Φ_F values calculated for the MPc complexes are within the acceptable ranges for such complexes [252].

4.1.2.2 Quaternizable monomeric non-water soluble MPcs in organic media

Complexes 33(a-d)

The non-water soluble phthalocyanines (Cl)GaTMPyPc (**33a**), (Cl)InTMPyPc (**33b**), $(Cl)_2$SiTMPyPc (**33c**) and SnTMPyPc (**33d**) spectra in DMSO is shown in Figure 4.4. The absorption spectra and fluorescence excitation spectra were mirror images of the fluorescence emission spectra for (Cl)GaTMPyPc (**33a**), (Cl)InTMPyPc (**33b**) and $(Cl)_2$SiTMPyPc (**33c**) MPc complexes. The complex SnTMPyPc (**33d**) showed an excitation spectrum that was different from the absorption spectrum in that the excitation spectrum of the Q-band had a shoulder to the blue. In addition, the excitation spectrum appears to be blue-shifted from the absorption spectrum, indicating a change of symmetry on excitation, most likely due to demetallation [253]. The loss of symmetry upon excitation for MPc complexes containing large central metals has been encountered in literature [254].

Table 4.2: Fluorescence data of all MPcs studied in aqueous and non-aqueous media

Abbreviation MPc	[b]Solvent	Q-band λ_{max} (nm)	[c]Ems. λ_{ems} (nm)	[d]Exc. λ_{exc} (nm)	Φ_F (± 0.01)
TmTPyZnPz (27b)	DMSO	641,655	682	655	--
ZnTSPc (28)	DMSO	680	692	680	0.08
	EtOH+NaOH	675	681	676	0.21
ZnTCPc (29)	DMSO	690	702	690	0.15
	EtOH+NaOH	695	697	694	0.02
ZnOCPc (30)	DMSO	705	714	706	0.23
	EtOH+NaOH	694	702	694	0.21
TmTPyZnPc (31b)	Pyr + H_2O	672	680	672	0.17
TmTMPyZnPc (32b)	Pyr + H_2O	678	687	678	0.11
(Cl)GaTMPyPc (33a)	DMSO	691	703	691	0.30
(Cl)InTMPyPc (33b)	DMSO	698	710	698	0.03
$(Cl)_2$SiTMPyPc (33c)	DMSO	692	705	692	0.20
SnTMPyPc (33d)	DMSO	711	711	706	0.01
(Cl)GaTmTMPyPc (34)	DMSO	691	697	692	0.25
	EtOH+NaOH	686	692	686	0.27
(Cl)InTmTMPyPc (35)	DMSO	698	702	698	0.02
	EtOH+NaOH	694	698	694	0.02
TMmTAAZnPc (36)	DMSO	687	698	687	0.09
	EtOH+NaOH	683	693	683	0.06

Table 4.2 contd.

MPc	[b]Solvent	Q-band λ_{max} (nm)	[c]Ems. λ_{ems}(nm)	[d]Exc. λ_{exc}(nm)	Φ_F (± 0.01)
OMmTAAZnPc (37)	DMSO	698	709	698	0.05
	EtOH+NaOH	696	701	696	0.04
(OH)GaTMAAPc (38a)	DMSO	654,687,709	721	714	0.04
(OH)InTMAAPc (38b)	DMSO	643,680,705	716	717	0.03
(OH)(Me)SiTMAAPc(38c)	DMSO	641, 684, 708	713	708	0.02
TMAAZnPc (38d)	DMSO	658,691,714	723	717	0.02
(OH)GaTMPAPc (39a)	DMSO	653,686,712	722	715	0.07
(OH)InTMPAPc (39b)	DMSO	655,687,713	725	718	0.01
(OH)(Me)SiTMPAPc (39c)	DMSO	652,685,715	724	717	0.04
TMPAZnPc (39d)	DMSO	692	706	694	0.13
	EtOH+NaOH	683	691	682	0.19
TtfmPyZnPc[a] (40)	DMSO	678	689	677	0.13
	Pyridine	678	690	678	0.18
TtfmMPyZnPc[a] (41)	DMSO	685	698	686	0.10
	Pyridine	685	697	685	0.17
THdTZnPc[a] (42)	DMSO	706	718	705	0.06
	DMF	702	712	703	0.08
ZnPc (43)	DMSO	672	679	673	0.2

[a] MPcs donated by fellow researchers.

[b] The ethanol:NaOH 0.01M solvent mixture and the pyridine:water solvent mixture had a 1:1 (v/v) composition.

[c] Ems = emission; λ_{ems}= fluorescence emission wavelength.

[d] Exc = excitation; λ_{exc}= fluorescence excitation wavelength.

In DMF, (Cl)GaTMPyPc (**33a**) and $(Cl)_2$SiTMPyPc (**33c**) complexes showed absorption and excitation spectra that were similar and they were mirror images of fluorescence emission spectra (similar to spectra in Figure 4.4). However, for the (Cl)InTMPyPc (**33b**) and SnTMPyPc (**33d**) complexes, there was broadening or splitting in the Q band of the excitation spectra. The excitation spectra for **33b** and **33d** was slightly blue-shifted compared to absorption spectra. The Stokes shifts observed as shown in Table 4.2 ranged from 0 to 14 nm.

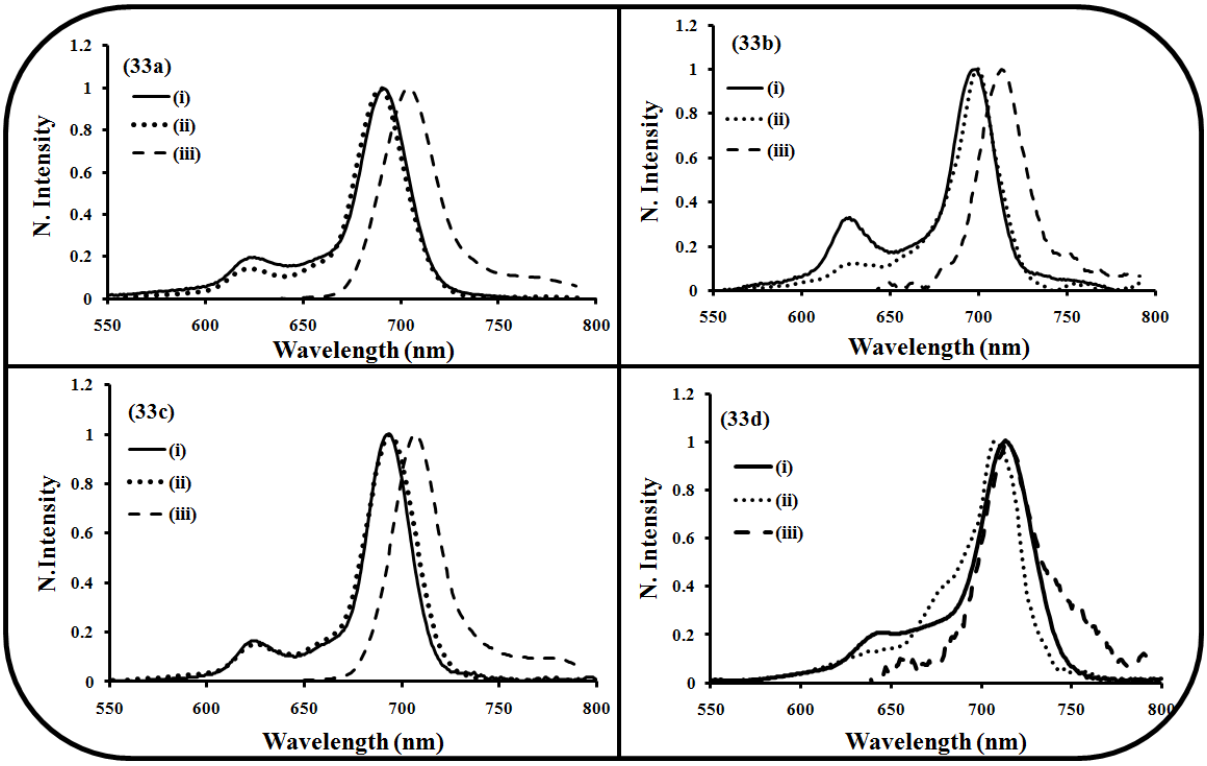

Figure 4.4: Absorbance (i), excitation (ii) and emission (iii) spectra for complexes 33a-d in DMSO. {[MPc] = 7 × 10^{-6} M}

The splitting in the Q band of the fluorescence excitation spectra has been reported for InPc derivatives (but not for corresponding GaPc derivatives) [213]. The observed difference in the behaviours of **33a** and **33b** on excitation was attributed to the larger In metal being more displaced from the core of the Pc ring, and the displacement being more pronounced on excitation hence the loss of symmetry [213]. Similarly in this work, the differences in the fluorescence behaviour of **33b** and **33d** compared to

33a and **33c** respectively, could be attributed to the large sizes of the former pair. The observation of the emission spectra occurring at shorter wavelengths compared to absorption, could be a result of the loss of symmetry on excitation due to demetallation, thus emission occurs from the demetallated species, hence the blue-shift.

A split in the Q band of the excitation spectra for **33b** and **33d** in DMF is clearer when the solution is left to stand for a while before recording the spectra, Figure 4.5 (for complex **33b** and **33d** in DMF). Broadening of the emission spectra is observed coupled to the clear splitting of the excitation spectra for complex **33d**, while the excitation spectrum of complex **33b** gets blue-shifted and shows slight splitting compared to the absorbance spectrum. As stated above, the split of the Q band in the excitation spectra may be attributed to the lowering of symmetry following excitation of the complexes [253]. The Sn^{2+} and In^{3+} central metal ions are quite large and as a result these central metal ions in the MPc molecules protrude out of the planar phthalocyanine ring, making the molecules prone to loss of symmetry.

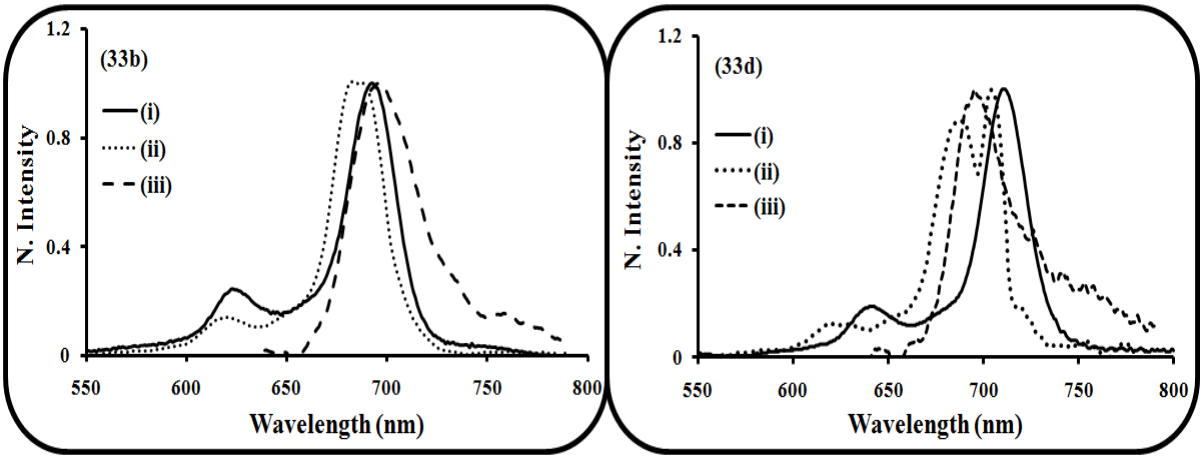

Figure 4.5: Absorbance (i), excitation (ii) and emission (iii) spectra for complexes 33b and 33d in DMF. {[MPc] = 7 × 10^{-6} M}

In DCM, $CHCl_3$ and THF, complexes **33a**, **33c** and **33d** showed excitation spectra similar to absorption spectra and were mirror images of the emission spectra

(figure not shown). However, the fluorescence excitation spectra were split or broad for complex **33b** for the same reasons given above.

The Φ_F values decreased with increase in atomic number of the central metal ion of the MPc complexes **33b** and **33d** (In^{3+} and Sn^{2+} respectively). This is because an increase in the atomic number (hence increased atomic weight), of the metal ion centre would encourage spin orbit coupling of the MPc complexes thus lowering the fluorescing capacity and thereby reducing the Φ_F values of the MPcs, Table 4.2. Complexes **33a** and **33c** however showed high fluorescence quantum yield values since the central metal ions (Ga^{3+} and Si^{4+}) are not as heavy as their counterparts in **33b** and **33d**.

Complexes 40 and 41

The spectra for unquaternized phthalocyanine complexes TtfmPyZnPc (**40**) and TtfmMPyZnPc (**41**) in DMSO are shown in Figure 4.6. The absorption spectra and fluorescence excitation spectra were mirror images of the fluorescence emission spectra for these complexes. Fluorescence quantum yields were typical [252] of MPc complexes, Table 4.2.

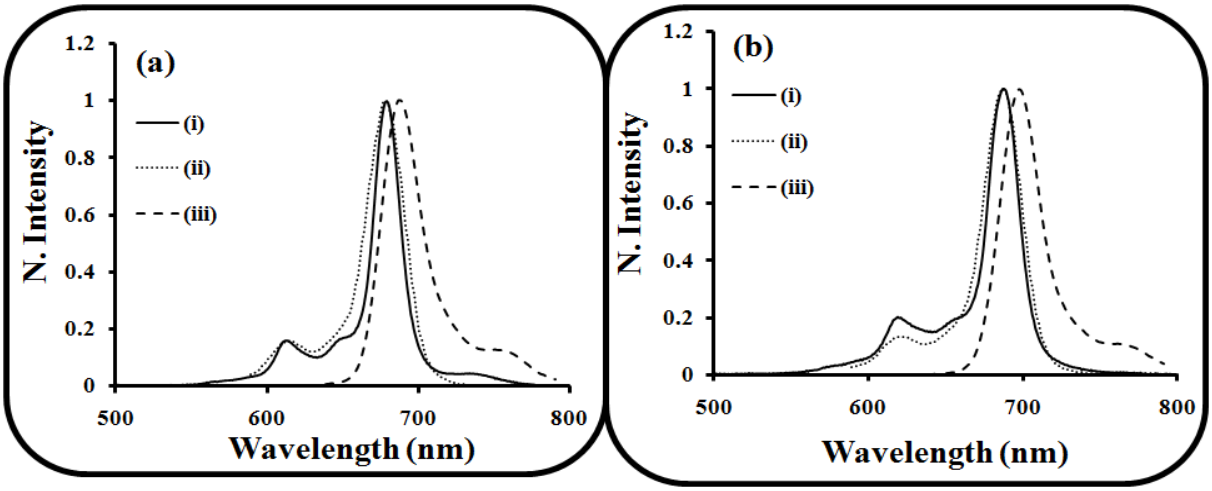

Figure 4.6: Absorbance (i), excitation (ii) and emission (iii) spectra for complexes TtfmPyZnPc (40) and TtfmMPyZnPc (41) in DMSO. {[MPc] = 6.5 × 10^{-6} M}

4.1.2.3 Aggregated MPcs in aqueous solvent mixtures

The water soluble MPc complexes **31b**, **32b**, **37**, **38a-d** and **39a-c** are highly aggregated in aqueous media. Addition of ethanol to the aqueous media allows for partial disaggregation of some of the Pcs (TmTPyZnPc (**31b)**, TmTMPyZnPc **(32b)** and OMmTAAZnPc **37**), but they are not completely monomerized. As shown in Figure 4.7 for complexes **31b**, **32b**, **37** and **38d** (representative of **38a-c** and **39a-c**), the dimer bands at ~ 640 nm in the absorption spectra are not observed in the fluorescence excitation spectra indicating that only the monomer is fluorescent. This observation is in line with what is expected theoretically, since it is well established that dimers are non photoactive [227]. Complete monomeric behaviour however was observed for complexes TmTPyZnPc (**31b)**, TmTMPyZnPc **(32b)** in DMSO where the fluorescence excitation and absorption spectra are mirror images of the respective emission spectra.

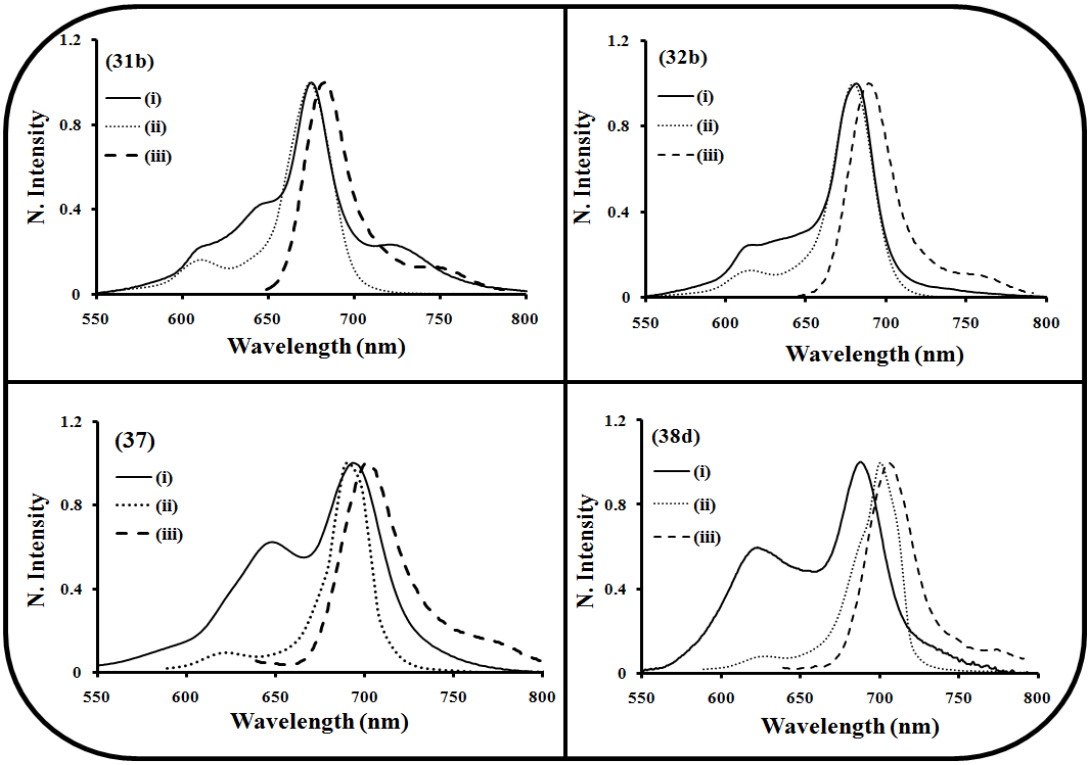

Figure 4.7: Absorbance (i), excitation (ii) and emission (iii) spectra for complexes 31b, 32b, 37 and 38d in a ((1:1) ethanol:NaOH 0.01M solvent mixture). {[MPc] = 7 × 10^{-6} M}

The absorption maxima are approximately the same as the fluorescence excitation spectra maxima for the complexes **31b**, **32b** and **37** suggesting that the ground state species is not different from the excited state species for these MPc complexes, Table 4.2. The fluorescence excitation spectra maxima were different from the absorption maxima for the complexes **38a-d** and **39a-c** indicative of the heavy extent of aggregation. The Φ_F values of the complexes in aqueous solvent mixtures and in DMSO are shown in Table 4.2. The Φ_F values of complexes **38a-d, 39a-c** and **37** are very low (< 0.1) due to extensive aggregation, Table 4.2.

4.1.2.4 Aggregated neutral MPc complex in organic media

The slightly aggregated complex THdTZnPc (**42**) showed absorption and fluorescence excitation spectra that were mirror images of the fluorescence emission spectra in DMSO, Figure 4.8. The absorption spectra for complex **42** showed aggregation tendencies in DMF, $CHCl_3$ and DCM similar to those observed in DMSO, Figure 4.8(curve i). As a result of aggregation, the Φ_F values for complex **42** are very low (< 0.1), Table 4.2.

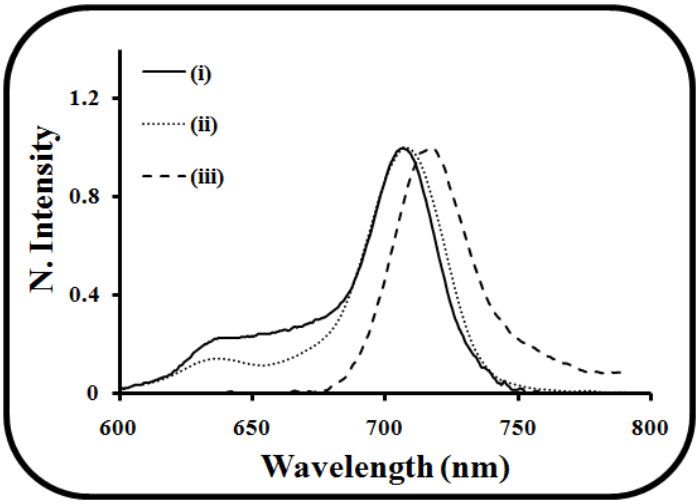

Figure 4.8: Absorbance (i), excitation (ii) and emission (iii) spectra for THdTZnPc (42) in DMSO. {[THdTZnPc] = 7 × 10^{-6} M}

4.2. Triplet state quantum yields and lifetimes of MPcs

4.2.1 Positively charged MPcs and their neutral quarternizable precursors

The triplet state quantum yields (Φ_T) and the lifetimes (τ_T) of phthalocyanines are used to evaluate the efficiency of the Pc complexes as photosensitizers. In Table 4.3 the Φ_T and τ_T values of the MPcs (in different solvents) studied in this thesis are shown. The Φ_T values were calculated with the use of equation 4.2, which is the same as equation 1.12.

$$\Phi_T^{Sample} = \Phi_T^{Std} \frac{\Delta A_T^{Sample}}{\Delta A_T^{Std}} \frac{\varepsilon_T^{Std}}{\varepsilon_T^{Sample}} \qquad (4.2)$$

The transient absorption spectrum and triplet decay curve (inset (i)) for complex **35** are shown in Figure 4.9 (and are typical of all MPc complexes). Figure 4.9 shows that the transient Q-band is similar to that in the ground state of the complex suggesting that there is no change in the geometry of the complex upon excitation.

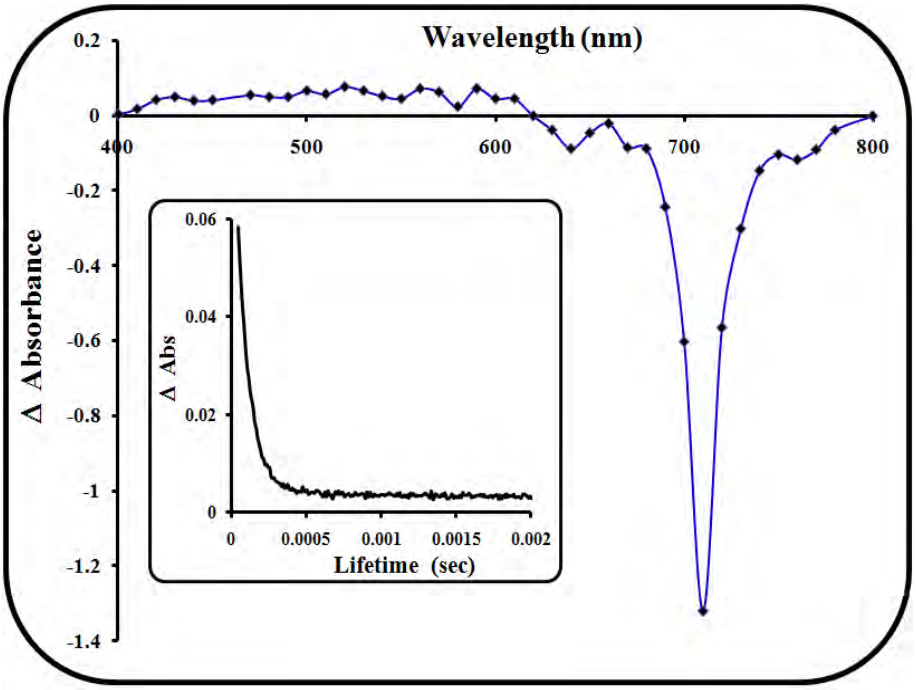

Figure 4.9: Transient absorption spectra of complex 35 and the corresponding triplet decay curve (inset).

Table 4.3: Photophysical and photochemical data of all MPcs studied in aqueous and non-aqueous media

Abbreviation MPc	[b]Solvent	Φ_F	[a]Φ_T	[a]Φ_{IC}	[a]Φ_Δ	[a]S_Δ	[a]τ_T (μs)
TmTPyZnPz (27b)	DMSO	--	--	--	0.06[c]	--	170[d]
ZnTSPc (28)	[e]DMSO	0.08	0.88	0.04	0.46	0.52	460
	[f]EtOH+NaOH	0.21	0.56	0.23	--	--	170
ZnTCPc (29)	[g]DMSO	0.15	0.82	0.03	0.84	1.02	220
	EtOH+NaOH	0.02	0.50	0.48	--	--	600
ZnOCPc (30)	[g]DMSO	0.23	0.62	0.15	0.56	0.90	450
	EtOH+NaOH	0.21	0.75	0.04	--	--	140
TmTPyZnPc (31b)	Pyr + H_2O	0.17	0.78	0.05	--	--	30
TmTMPyZnPc (32b)	Pyr + H_2O	0.11	0.43	0.46	--	--	10
(Cl)GaTMPyPc (33a)	DMSO	0.30	0.65	0.05	0.34	0.52	110
(Cl)InTMPyPc (33b)	DMSO	0.03	0.93	0.04	0.33	0.35	60
$(Cl)_2$SiTMPyPc (33c)	DMSO	0.20	0.80	~0	0.62	0.78	130
SnTMPyPc (33d)	DMSO	0.01	0.88	0.11	0.59	0.67	40
(Cl)GaTmTMPyPc(34)	DMSO	0.25	0.63	0.12	0.28	0.44	650
	EtOH+H_2O	0.27	0.75	~0	--	--	40
(Cl)InTmTMPyPc (35)	DMSO	0.02	0.68	0.30	0.26	0.38	80
	EtOH+H_2O	0.02	0.84	0.14	--	--	20
TMmTAAZnPc (36)	DMSO	0.09	0.63	0.28	0.46	0.73	280
	EtOH+NaOH	0.06	0.54	0.4	0.51	0.94	160
OMmTAAZnPc (37)	DMSO	0.05	0.76	0.19	0.49	0.64	50
	EtOH+NaOH	0.04	0.67	0.29	0.55	0.82	50

Table 4.3 contd.

MPc	[b]Solvent	Φ_F	[a]Φ_T	[a]Φ_{IC}	[a]Φ_Δ	[a]S_Δ	[a]τ_T(μs)
(OH)GaTMAAPc (38a)	DMSO	0.04	--	--	--	--	--
(OH)InTMAAPc (38b)	DMSO	0.03	--	--	--	--	--
(OH)(Me)SiTMAAPc(38c)	DMSO	0.02	--	--	--	--	--
TMAAZnPc (38d)	DMSO	0.02	--	--	--	--	--
(OH)GaTMPAPc (39a)	DMSO	0.07	--	--	--	--	--
(OH)InTMPAPc (39b)	DMSO	0.01	--	--	--	--	--
(OH)(Me)SiTMPAPc(39c)	DMSO	0.04	--	--	--	--	--
TMPAZnPc (39d)	DMSO	0.13	0.88	~0	0.86	0.98	230
	EtOH+NaOH	0.19	0.63	0.18	0.33	0.52	13
TtfmPyZnPc (40)	DMSO	0.13	0.74	0.13	0.63	0.85	210
	Pyridine	0.18	0.76	0.06	--	--	11
TtfmMPyZnPc (41)	DMSO	0.10	0.86	0.04	0.68	0.79	140
	Pyridine	0.17	0.83	~0	--	--	5
THdTZnPc (42)	DMSO	0.06	0.67	0.27	0.59	0.88	76
	DMF	0.08	0.63	0.29	0.59	0.94	210
ZnPc (43)	DMSO	0.2[e]	0.65[h]	0.15	0.67[i]	1.03	350[h]
	DMF	0.3[e]	0.58[j]	0.12	0.56[k]	0.96	330[e]

[a] **Values not obtained for complexes 38(a-d) and 39(a-c) due to aggregation.**

[b] **The ethanol:NaOH 0.01M solvent mixture and the pyridine:water solvent mixture had a 1:1 (v/v) composition.**

[c][255],[d][229],[e] [179], [f][227],[g][253],[h][205],[i][207],[j][206],[k][216].

The points at which maximum triplet absorption are observed range between 490 and 550 nm for the complexes studied. The transient spectra and triplet decay curve shown in Figure 4.9 are typical of MPc complexes. The fitting of the triplet decay data with appropriate software (Origin 7.0) gives triplet decay curves which obey second order decay kinetics. This behaviour is expected for MPc complexes at the concentrations (>1 × 10^{-5} M) employed for laser flash photolysis. These concentrations are known to result in triplet-triplet recombination and since concentrations in the range given above were used, triplet-triplet recombination was expected [254]. The laser flash photolysis studies were carried out in DMSO, DMF and aqueous solvent mixtures ((1:1) ethanol:NaOH 0.01M, (1:1) ethanol:water and (1:1) pyridine:water solvent mixtures) that allowed for monomericity of the water soluble MPc complexes. The MPc complexes which by virtue of the heavy atom effect encourage the strongest spin-orbit coupling are expected to have the highest triplet quantum yield values (Φ_T). The trend observed for triplet quantum yields of the quaternizable neutral MPc complexes was in the order (Cl)InTMPyPc (**33b**) > SnTMPyPc (**33d**) > TtfmMPyZnPc (**41**) > $(Cl)_2$SiTMPyPc (**33c**) > TtfmPyZnPc (**40**) > (Cl)GaTMPyPc (**33a**) in DMSO. The quaternized MPc complexes showed the triplet quantum yield trend in the order; (Cl)InTmTMPyPc (**34**) > TmTPyZnPc (**31b**) > (Cl)GaTmTMPyPc (**35**) > TmTMPyZnPc (**32b**) in the respective aqueous solvent mixtures. Although the Zn(II) complexes would be expected to have lower Φ_T values compared to the Sn(II) and In(III) complexes, they generally showed moderate to high Φ_T values and these changed with the substituents employed.

Generally higher Φ_T values were obtained in organic solvents e.g. DMSO, DMF and pyridine than in aqueous solvent mixtures ((1:1) ethanol:water and (1:1) pyridine:water solvent mixtures) employed in this thesis with the exception of complexes **34** and **35** in the respective aqueous solvent mixtures. The reason for the decreased Φ_T values in DMSO for complexes **34** and **35** compared to those obtained in the aqueous solvent mixture is attributed to ring reduction with the formation of the anionic Pc^{-3} species following laser flash experiments, Figure 4.10. Weak

absorption bands in the 500 to 650 nm area in phthalocyanine spectra are typical of ring reduction with the formation of Pc^{-3} species [255]. These bands were observed following laser flash photolysis suggesting that the complexes undergo phototransformation to the anionic Pc^{-3} species. The phototransformation observed for the complexes in DMSO was not observed in the (1:1) ethanol:water solvent mixture. Consequently the phototransformation in DMSO affected the triplet quantum yield values in that they were found to be lower than in the (1:1) ethanol:water solvent mixture for the complexes **34** and **35**.

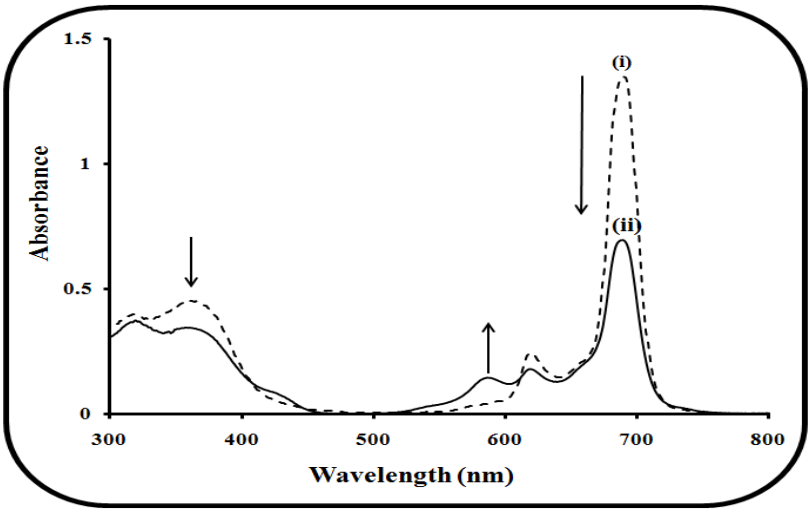

Figure 4.10: Absorbance before (i) and after (ii) laser flash photolysis for complex 35 in DMSO. {[35] = 2 x 10^{-5} M}

The photoreduction mechanism of complexes **34** and **35** has been shown to involve H atoms of the solvent (S-H) in the presence of light. This photoreduction of MPc complexes results in the formation of anionic Pc^{-3} species, Scheme 4.1(equations (i) to (iii)) [213,255].

$$MPc + h\upsilon \longrightarrow {}^3MPc^* \quad \text{(i)}$$

$$^3MPc^* + S\text{-}H \longrightarrow MPc^{\bullet -} + S\text{-}H^{\bullet +} \quad \text{(ii)}$$

$$MPc^{\bullet -} + O_2 \longrightarrow MPc + O_2^{\bullet -} \quad \text{(iii)}$$

Scheme 4.1: A photoreduction mechanism of MPcs in the presence of light [213].

Triplet lifetimes (τ_T) have been established to vary linearly with the logarithms of solvent viscosities for some MPc complexes [256]. This is observed in Table 4.3 where the study of MPcs in less viscous pyridine shows shorter triplet lifetime values. DMSO however has a viscous nature and thus triplet lifetimes are long lived in this solvent compared to others. The triplet lifetime values ranged from fairly short for complexes **33b** and **33d** in DMSO, **40** and **41** in pyridine, **34** and **35** in aqueous media to fairly long for complexes **33a**, **33c**, **34, 40** and **41** in DMSO.

4.2.2 Neutral MPc complex 42

The neutral complex THdTZnPc (**42**) as shown in Table 4.3 exhibited moderate Φ_T values in both DMSO and DMF. This complex (**42**) had higher triplet lifetime values in DMF than in DMSO. Due to the low Φ_F values obtained, higher Φ_T values were anticipated but triplet quatum yield values just above average were obtained instead. This observed behaviour implies that the excited state of complex **42** could be deactivated by radiationless transitions as demonstrated in Table 4.3.

4.2.3 Negatively charged MPc complexes

Complexes **38(a-d)** and **39(a-c)** were highly aggregated in solution in both organic and aqueous media. The results obtained suggest that H-bonding in solution encouraged by the carboxy terminal moieties and the axial hydroxyl ligands on the In^{3+}, Ga^{3+} and Si^{4+} central metal ions may have contributed in worsening the aggregation of these complexes**.** The heavy aggregation of complexes **38(a-d)** and **39(a-c)** did not allow for the determination of the photophysicochemical properties of these negatively charged complexes. The trend observed for triplet quantum yields of the negatively charged MPc complexes was in the order ZnOCPc (**30**) > OMmTAAZnPc (**37**) > TMPAZnPc (**39d**) > ZnTSPc (**28**) > TMmTAAZnPc (**36**) > ZnTCPc (**29**) in the aqueous solvent mixtures used. In DMSO the trend observed for triplet quantum yields of the negatively charged MPcs was of the order: ZnTSPc (**28**) ≅ TMPAZnPc (**39d**) > ZnTCPc (**29**) > OMmTAAZnPc (**37**) > TMmTAAZnPc (**36**) ≥ ZnOCPc (**30**). The high Φ_T values are obtained at the expense of Φ_F values (due to the

complementary nature of the fluorescence and triplet quantum yields) as shown from the data in Table 4.3. Higher Φ_T values were obtained in DMSO than in the aqueous solvent mixtures used for the negatively charged MPc complexes (with the exception of ZnOCPc (**30)**).

Triplet lifetimes (τ_T) were generally longer in DMSO but shorter in the aqueous solvent mixtures employed in this work with the exception of ZnTCPc (**29**) and OMmTAAZnPc (**37**) in the (1:1) ethanol:NaOH 0.01M solvent mixture. Complex **29** showed relatively longer triplet lifetime (in the aqueous solvent mixture) than that in DMSO while **37** had the same value to that in DMSO. The triplet lifetime values in aqueous media ranged from short (for complexes **37** and **39d)** to long (for complexes **28**, **29**, **30** and **36)**.

Quantum yields of internal conversion (Φ_{IC}) were determined with the use of equation 4.3. The internal conversion quantum yields are responsible for the deactivation of the excited singlet states via non-radiative pathways and the calculated values are also shown in Table 4.3.

$$\Phi_{IC} = 1 - (\Phi_F + \Phi_T) \qquad (4.3)$$

This equation is based on the assumption that only fluorescence, intersystem crossing and internal conversion cause the deactivation of the excited singlet state of an MPc molecule. The general observation was that the Φ_{IC} values were higher in aqueous solvent mixtures but there was no clear trend among the MPc complexes as shown in Table 4.3. The higher Φ_{IC} values in aqueous solvent mixtures compared to organic solvents may be the result of the lower viscosity of aqueous media compared to DMSO and DMF which tends to encourage deactivation of the excited singlet state via non-radiative pathways.

4.3 Singlet oxygen quantum yields

Singlet oxygen ($^1O_2$) is a cytotoxic species that is produced by the energy transfer process from the triplet excited state of the metallophthalocyanine (^{3}MPc*) to ground state oxygen ($^3O_2$). In order to produce considerable amounts of singlet oxygen, the energy transfer between the triplet state of the excited MPc and oxygen in the ground state has to be highly efficient. As a result the triplet state quantum yield (Φ_T), lifetimes (τ_T) and the efficiency of energy transfer from the excited triplet state MPc to oxygen in the ground state have a bearing on the singlet oxygen quantum yield (Φ_Δ). The singlet oxygen quantum yield gives a measure of the efficiency of generation of singlet oxygen and is determined with the use of equation 4.4, which is the same as equation 1.14.

$$\Phi_\Delta = \Phi_\Delta^{Std} \frac{W_{DPBF} \cdot I_{abs}^{Std}}{W_{DPBF}^{Std} \cdot I_{abs}} \qquad (4.4)$$

The singlet oxygen quenchers diphenylisobenzofuran (DPBF) in DMSO, and tetrasodium-α,α-(anthracene-9,10-diyl)dimethylmalonate (ADMA) in aqueous media were used in the determination of singlet oxygen. The absorption decays (at ~317 nm for DPBF in DMSO and ~380 nm for ADMA in aqueous media) of the singlet oxygen quenchers in the presence of singlet oxygen were monitored over time and the data was used to calculate for Φ_Δ values which are shown in Table 4.3. Figure 4.11 shows the quenching of DPBF by the singlet oxygen species generated by the photoexcited complex **40**. All the MPc complexes whose photochemical properties were studied did not show photobleaching effects in the Q-band region of the MPcs, during Φ_Δ determinations.

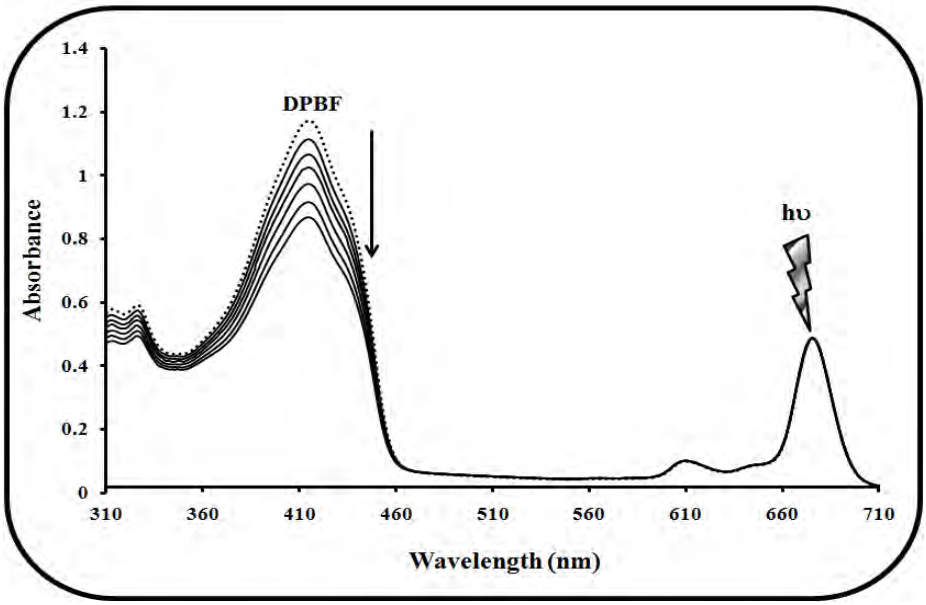

Figure 4.11: Absorption spectra TtfmPyZnPc (40) in the presence of DPBF for the determination of singlet oxygen in DMSO. ([TtfmPyZnPc] = 3 × 10^{-6} M, [DPBF] =~5 × 10^{-5} M Irradiation wavelength = 670 ± 20 nm).

Since Φ_Δ values depend on triplet state quantum yields and lifetimes, the trend observed was such that high Φ_T values generally resulted in moderate to high Φ_Δ values with a few exceptions. The complexes TMPAZnPc (**39d**) and ZnTCPc (**29**) showed the greatest efficiency of singlet oxygen production and these correlated well with the Φ_T values of these complexes. Complex ZnTCPc (**29**) exhibited Φ_Δ (0.82) and Φ_T (0.84) values which within experimental error (± 0.02) are the same. Complexes **30**, **33c**, **33d**, **36, 37** and **40-42**, also showed reasonably moderate values of Φ_Δ in DMSO but they were considerably lower than their Φ_T values. However complex **33b** which had a very high Φ_T value gave a very low Φ_Δ value. Other MPc complexes which showed low singlet oxygen generation efficiencies relative to their Φ_T values include **33a**, **34** and **35** in DMSO. The complexes **33a** and **33b** are the unquaternized forms of complexes **34** (Ga^{3+}) and **35** (In^{3+}) and the results from Table 4.3 show that these MPc complexes generally had low singlet oxygen quantum yields. The reason for this observation could be attributed to the relatively short triplet lifetimes [**33a** (110 μs), **33b** (60 μs), **35** (80 μs)] that these MPcs had with the exception of complex **34** (650 μs)

which had a rather long lived triplet state. Short triplet lifetimes do not allow time for efficient transfer of energy from the excited triplet state of the MPcs to ground state oxygen hence lower Φ_Δ values are anticipated for MPcs with short triplet lifetimes. Longer triplet lifetimes however cause increased molecular interactions between the photosensitizer molecules in the triplet state and the ground state oxygen $^3O_2(^3\Sigma_g^-)$ thus producing more singlet oxygen $^1O_2(^1\Sigma_g^-)$ as shown in Table 4.3 for complexes **39d** and **29** in DMSO.

It was also observed that singlet oxygen quantum yields in the aqueous solvent mixtures employed in this thesis were lower for **39d** than those obtained in DMSO. It has been established that solvents (such as water) that absorb around 1100 nm (triplet energy level of Pcs) and around 1270 nm (singlet oxygen energy level) quench the triplet state of the MPc derivative as well as singlet oxygen, hence the low value of Φ_Δ in aqueous media is not unexpected [179]. However the Φ_Δ values of complexes **36** and **37** (in aqueous media) were slightly higher than those obtained in DMSO, contradicting the explanation above.

The efficiency of the quenching of the triplet state by singlet oxygen represented by S_Δ was calculated with the use of equation 4.5 (same as equation 1.15).

$$S_\Delta = \frac{\Phi_\Delta}{\Phi_T} \qquad (4.5)$$

The values of S_Δ determined through the use of equation 4.5 are shown in Table 4.3. As shown in Table 4.3 the S_Δ values range from 0.35 to 0.98 for the MPc complexes whose photophysicochemical properties are studied in this thesis. The S_Δ values closest to unity were obtained for complexes **39d**, **40**, **41**, and **42** in DMSO (and DMF for the latter) indicating that the quenching of the triplet state by singlet oxygen was efficient for these complexes. Complexes **33c**, **33d**, **36** and **37** showed modest S_Δ values less than unity in DMSO while low values for S_Δ were obtained for complexes **33a**, **33b**, **34** and **35**. The S_Δ values for complexes **36** and **37** in aqueous media were much closer to unity than those obtained in DMSO.

4.4 Fluorescence lifetime measurements for highly aggregated MPcs

Time resolved emission spectroscopy (TRES) measurements were carried out for the complexes **38(a-d)** and **39(a-d)** using time correlated single photon counting equipment. Complexes **38(a-d)** and **39(a-c)** were all highly aggregated and the results of the MPc lifetime measurements are shown in Table 4.4. An example of TRES spectra is shown for **39a** in Figure 4.12. The inset in Figure 4.12(a) shows the emission spectra of the monomeric (Figure 4.12(a) inset (i)) and aggregated (Figure 4.12(a) inset (ii)) forms of the Pc, with the aggregated specie of the Pc having shorter fluorescence lifetime τ_{F1} whereas the monomeric specie exhibits longer fluorescence lifetime τ_{F2}. The amplitude values (α) give the abundance of species with different lifetimes (with α_1 and α_2 corresponding to τ_{F1} and τ_{F2} respectively). The MPcs studied indicated the same trend where the monomeric specie was in greater abundance except for **38a** where the aggregated specie was in greater abundance in solution. The monomeric specie corresponds to the emission peak with higher intensity while the aggregated specie corresponds to the lower intensity peak in Figure 4.12(a) (inset).

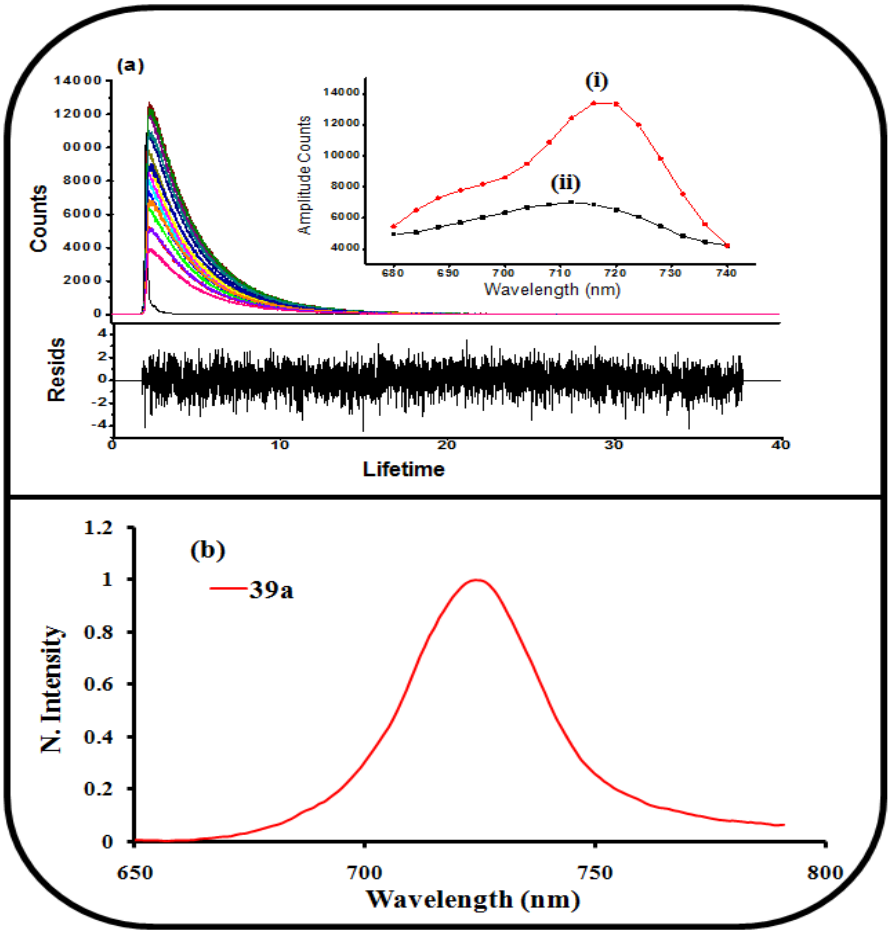

Figure 4.12: TRES spectra with inset (i) for monomeric species and (ii) for aggregated species in (a) and emission spectra in (b) for complex 39a. ($\lambda_{excitation}$= 722 nm)

The peak of higher intensity (monomeric specie at 722 nm) is rather red-shifted from the lower intensity (aggregated specie at 712 nm). A comparison of the inset with the steady state emission spectrum of **39a** in Figure 4.12(b) shows that the emission spectrum of monomeric specie shown in the inset (Figure 4.12(a) inset (i)) lies at the same wavelength as the emission maxima of the complex in steady state emission (722 nm as shown in Table 4.2).

Table 4.4: Fluorescence lifetimes of complexes 38a-d and 39a-d in DMSO.

Sample	$^{a}\tau_{F1}$ (ns)	$^{b}\alpha_{1}$	$^{a}\tau_{F2}$ (ns)	$^{b}\alpha_{2}$
(OH)GaTMAAPc (38a)	2.27 ± 0.02	0.77	4.59 ± 0.04	0.23
(OH)InTMAAPc (38b)	2.51 ± 0.06	0.38	4.97 ± 0.02	0.62
(OH)(Me)SiTMAAPc (38c)	1.95 ± 0.05	0.34	4.74 ± 0.02	0.66
TMPAZnPc (38d)	1.99 ± 0.03	0.35	3.75 ± 0.02	0.65
(OH)GaTMPAPc (39a)	1.99 ± 0.05	0.33	4.58 ± 0.05	0.67
(OH)InTMAAPc (39b)	1.87 ± 0.06	0.28	4.35 ± 0.02	0.72
(OH)(Me)SiTMPAPc (39c)	2.09 ± 0.02	0.49	3.85 ± 0.02	0.51
TMPAZnPc (39d)	2.40 ± 0.02	0.28	3.73 ± 0.04	0.72

[a] Fluorescence lifetimes at MPc emission.

[b] α denotes the amplitude fraction.

4.5 Conclusions

The photophysicochemical properties of the MPc complexes synthesized in this work were determined and they were found to depend on the central metal, substituents and the solvents used for the study. Complexes **33b** and **33d** displayed molecular geometries in their excited states that were different from those in the ground state due to the large central metal ions which tend to be displaced from the core of the phthalocyanine ring upon excitation. This displacement of the metal ion from the core of the Pc ring on excitation resulting in loss of symmetry lead to a change in geometry of the MPc compared to that in the ground state. Complexes **34** and **35** underwent phototransformation following laser irradiation resulting in ring reduced anionic specie (Pc^{-3}) in DMSO. This phototransformation resulted in low triplet state and singlet oxygen quantum yields. The photophysical and photochemical parameters that were determined in this work demonstrate the MPc complexes to have potential as photosensitizers in biomedical applications such as PDT, photocatalysis, and other varied applications involving the use of photosensitizers.

The Interaction of Metallophthalocyanines With Nanoparticles

5

This chapter focuses on the interactions between metallophthalocyanines synthesized in this thesis and the nanoparticles used in this work (ZnS QDs, CdTe QDs and AuNPs). The effect of these interactions on the spectroscopic and photophysicochemical properties of the metallophthalocyanines is also considered.

5.1 Interaction of Metallophthalocyanines with Quantum Dots

The studies on the interaction of MPcs with QDs were carried out with all water soluble MPc complexes whose photophysicochemical properties had been determined and also with neutral quaternizable complexes **40** and **41**. These studies were carried out in aqueous solvent mixtures ((1:1) ethanol:NaOH 0.01M, (1:1) ethanol:water or (1:1) pyridine:water solvent mixtures) that rendered the MPcs monomeric in solution, as well as in pyridine, DMSO and DMF. Complete monomericity of the MPcs is a prerequisite in order to gain an accurate determination of their photophysicochemical properties in the presence of QDs. Two categories of water soluble MPcs were employed for the studies carried out in this work, these being negatively charged and positively charged MPcs.

5.1.1 Interaction of neutral and positively charged complexes with QDs

5.1.1.1 Absorption spectral changes of quaternized complexes in the presence of QDs

Quaternized Porphyrazine complex 27b

Complex **27b** is treated separately since it is not a phthalocyanine like the rest and it also undergoes major spectral changes without photolysis in the presence of QDs. The studies of the interaction between the negatively charged QDs (ME ZnS QDs, ME CdTe QDs and TGA CdTe QDs) and the positively charged zinc porphyrazine (**27b**) were carried out in aqueous media. The QDs are negatively charged by virtue of the stabilizer groups while the porphyrazine complex bears a tetra positive charge on the macrocycle. As a result of the different charges for QDs and the quaternized porphyrazine (**27b**), electrostatic interactions are anticipated between the QDs and the **27b**.

Spectroscopic studies were carried out on complex **27b** (in pH 7.4 buffer solution) in the presence of ME ZnS (2.90 nm), ME CdTe QDs (3.19, 3.25 and 3.29 nm) and TGA

CdTe QDs (3.20, 3.73 and 3.94 nm). The quaternized zinc porphyrazine is monomeric in the buffer solution employed. The overlaid absorption and emission spectra of the QDs used in the interaction with the positively charged zinc porphyrazine are shown in Figure 5.1.

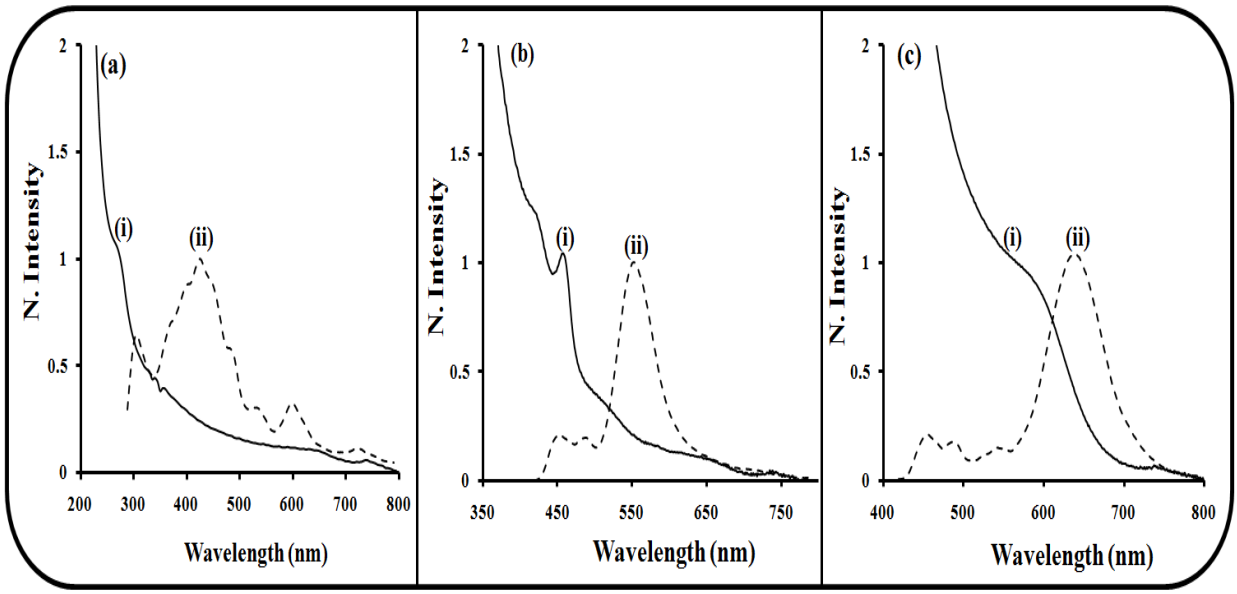

Figure 5.1: Absorption (i) and emission (ii) spectra for ME ZnS QDs (a), ME CdTe QDs (b) and TGA CdTe QDs. {[QD] = 1mg/1mL}

All the QDs used in the study of the interaction of QDs with the porphyrazine complex demonstrated an adequate overlap of the QD emission spectra with the absorption spectra of complex **27b**, Figure 5.2(a). The addition of QDs (ZnS or CdTe) to TmTPZnPz (**27b**) in aqueous media resulted in the absorption spectral changes shown in Figure 5.2(b).

The changes observed upon addition of QDs to the complex **27b** in buffer solution occurred without photolysis and consisted of a gradual decrease in the Q-band of the TmTPZnPz (**27b**) complex and an increase in absorption between 450 and 550 nm, Figure 5.2(b). This type of behaviour is typical of ring reduction in porphyrazine [255] and phthalocyanine [213] complexes and suggests formation of monoanion species. The Q band originates from the highest occupied molecular orbital (HOMO) to the lowest unoccupied molecular orbital (LUMO). Thus addition of QDs to TmTPZnPz(-2) (**27b**) resulted in the reduction of the latter complex to TmTPZnPz(-3)

(**27b**), suggesting electron transfer from the valence band of the QDs to the LUMO of the TmTPZnPz (**27b**) species, (Inset in Figure 5.2(b)).

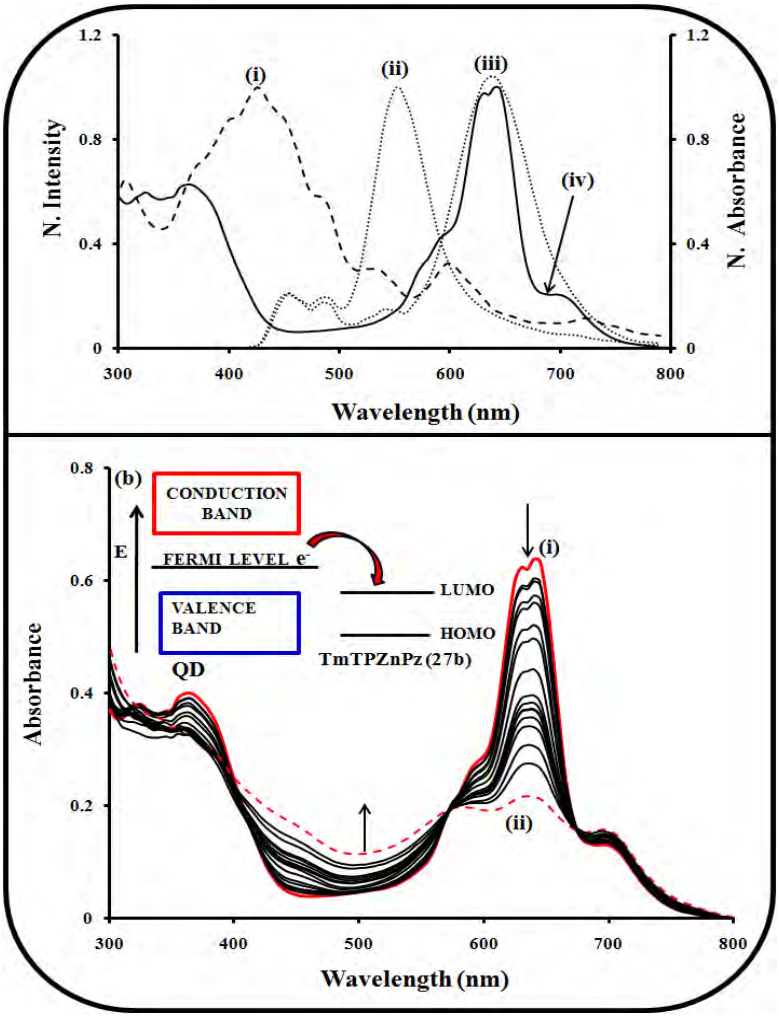

Figure 5.2: (a) Emission spectra of ME ZnS (i), ME CdTe (ii) and TGA CdTe (iii) QDs overlaid with absorption spectra of TmTPZnPz (27b) (iv), (b) typical absorption spectral changes observed on adding increments of TGA QDs to TmTPZnPz (27b) in pH 7.4 buffer solution. {TmTPZnPz (27b) alone (i) and TmTPZnPz (27b) with excess QDs (ii), [TmTPZnPz] = 6 × 10^{-6} M}

The reduction of complex **27b** by QDs, observed in Figure 5.2(b), was confirmed by addition of chemical oxidants ($FeCl_3$ or bromine), which resulted in the full regeneration of the Q band as shown in Figure 5.3(a,iii). In order to confirm the reduction of **27b** without a doubt, chemical reducing agents such as sodium borohydride ($NaBH_4$) were added to a solution of complex **27b** (shown in Figure

5.3(b)) and resulted in similar behaviour to that observed with QD addition to complex **27b** in solution. A considerable regeneration of the Q-band of the porphyrazine on addition of ferric chloride was also observed for **27b** reduced with $NaBH_4$ Figure 5.3(b,iii)).

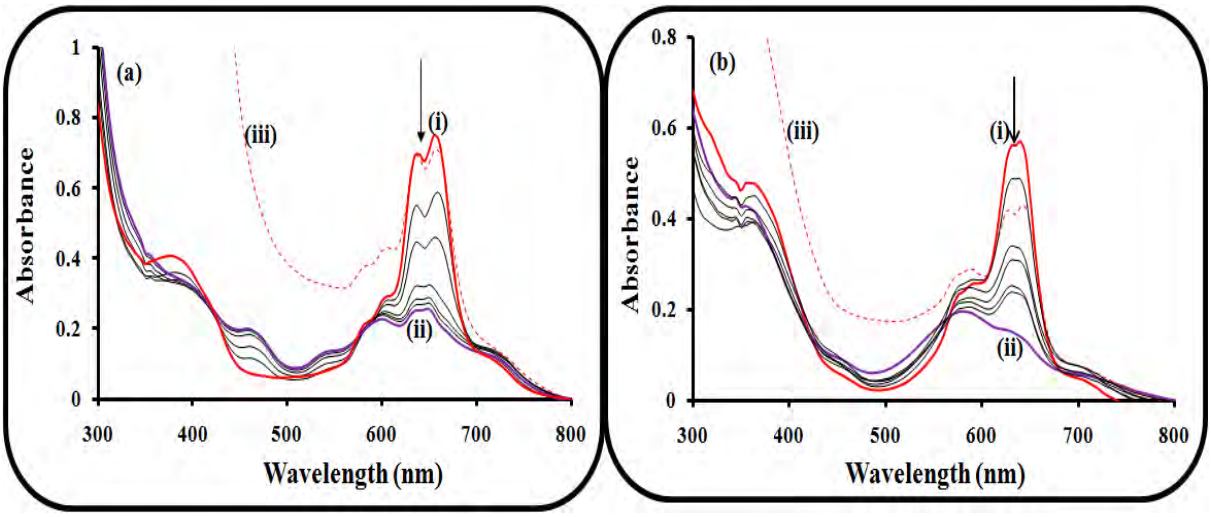

Figure 5.3: (a) Absorption spectra for TmTPZnPz (27b) alone (i), TmTPZnPz (27b) with excess QDs (ii) and TmTPZnPz (27b) with excess QDs and ferric chloride (iii), (b) absorption spectra of TmTPZnPz (27b) alone (i), TmTPZnPz (27b) with excess $NaBH_4$ (ii) and TmTPZnPz (27b) with excess $NaBH_4$ and ferric chloride (iii). {(a) [TmTPZnPz] = 6 x 10^{-6} M, (b) [TmTPZnPz] = 5 × 10^{-6} M}

Quaternized MPc complexes (32b, 34 and 35)

Complexes **32b**, **34** and **35** all have a quaternized pyridine ring as a substituent on the periphery of the Pc ring as opposed to complex **27b** where the benzene ring of the Pc has been replaced by a pyridine ring which is as well quaternized. As with **27b**, the complexes **32b**, **34** and **35** underwent absorption spectral changes without photolysis in the presence of QDs. In addition to the fact that complexes **32b**, **34** and **35** are all positively charged, they all commonly have thio bridges. The addition of QDs to complexes **32b**, **34** and **35** resulted in quenching of the absorbance of the respective complexes in the presence of either TGA or MPA CdTe QDs in aqueous media. However the results obtained were slightly different from those obtained for

27b in that they do not show clear ring reduction as was observed with the quaternized porphyrazine, Figure 5.4(a-c).

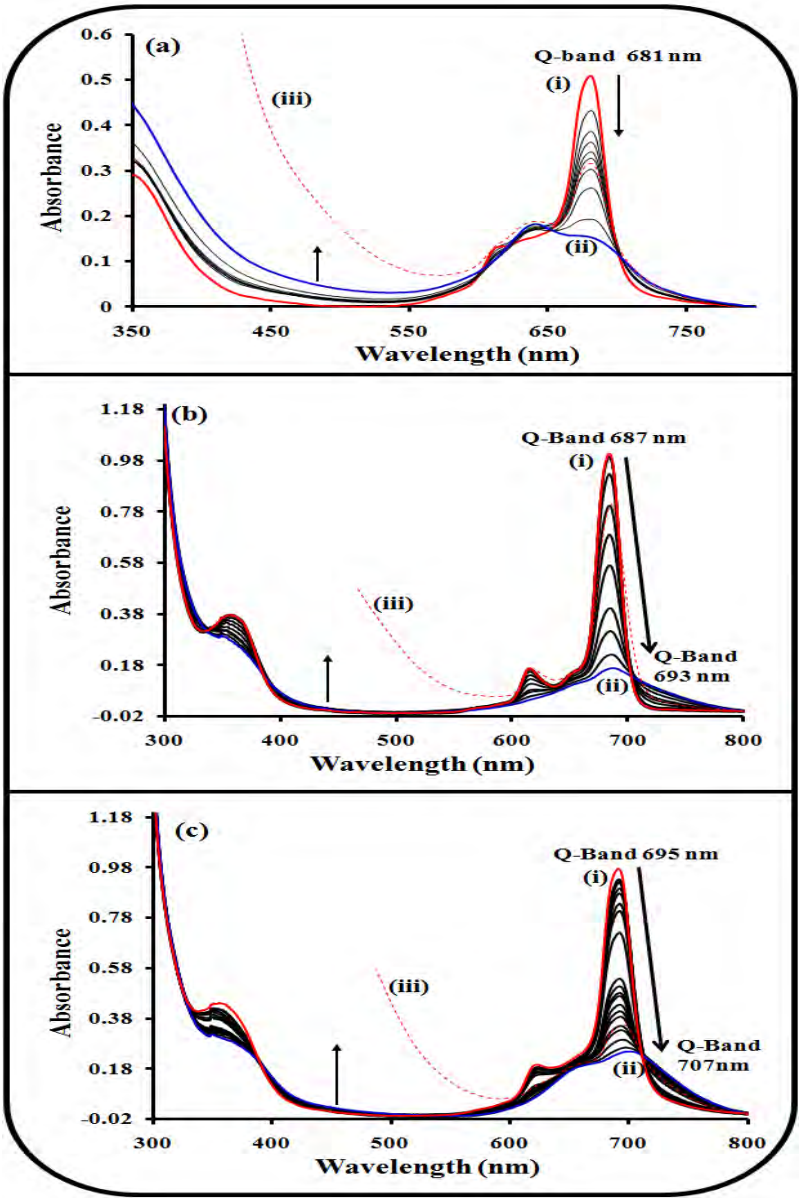

Figure 5.4: Absorption spectral changes for (a) TmTMPyZnPc (32b) in (1:1) pyridine:water, (b) (Cl)GaTmTMPyPc (34) and (c) (Cl)InTmTMPyPc (35) in (1:1) ethanol:water. [(i) MPc alone, (ii) MPc with excess MPA CdTe QDs and (iii) addition of ferric chloride to a mixture of MPc with excess MPA CdTe QDs in aqueous media]. {(a) [32b] = 5 × 10^{-6} M, (b) [34] = 7 × 10^{-6} M, (c) [35] = 7 × 10^{-6} M}

The addition of the MPA QDs to complexes **32b** (in a (1:1) pyridine:water solvent mixture), **34** or **35** (both in a (1:1) ethanol:water solvent mixture), resulted in the

absorption and emission spectral changes shown in Figure 5.4(a-c). These observed changes occurred without photolysis of the MPc complexes in solution. The gradual decrease in the Q-band of the complexes **32b**, **34** and **35** was not accompanied by a clear increase in absorption between 450 and 600 nm (Figure 5.4(a-c)) which would strongly suggest ring reduction of the MPc species as observed in Figure 5.2(b). An incomplete regeneration of the MPcs Q-band spectrum was observed on addition of oxidizing agents (ferric chloride and bromine) suggesting that the process under observation was not a pure ring reduction process. In addition, a shift in the Q-band positions for complexes **34** and **35** was realized, also indicative that the encountered behaviour was not a result of plain ring reduction. The shape of the spectra for the complexes **32b**, **34** and **35** after addition of excess QDs, Figure 5.4(a-c, ii) suggests the possibility of aggregation. This is probable because of the possibility of formation of electrostatic clusters (stable ion pair complexes) between the negatively charged QDs and the positively charged MPc complexes **32b**, **34** and **35**.

An investigation was carried out to determine the effect of the capping agent used to stabilize the CdTe QDs employed in the titration of the MPc complexes. The addition of the capping agent alone (mercaptopropionic acid, MPA) resulted in the spectral changes similar to those observed on addition of QDs to solutions of **34** and **35** in that a broad red-shifted absorption band was observed at the same position as observed on addition of QDs, Figure 5.5(b and c, ii). This shift to the red on addition of QDs or capping agent to the complexes **34** and **35** in solution was observed in both aqueous and organic media. A red-shifting of the Q-band peak was also observed for **32b** with addition of MPA (Figure 5.5(a)) which was not observed with the addition of MPA CdTe QDs, Figure 5.4(a). These red-shifts in the Q-band spectra could be associated with the rarely observed J aggregates which are rare in non-aqueous media [257]. The reduction of complexes **32b**, **34** and **35** by MPA is possible because MPA is also known to be a mild reducing agent [258]. The spectral changes resulting from the addition of the QD stabilizing group (MPA) could also be partially reversed (for **34** and **35**) by the addition of an oxidizing agent (ferric chloride) to complexes

32b, **34** and **35**, Figure 5.5(a-c, iii). There was however, no regeneration of the Q-band observed for complex **32b** upon addition of ferric chloride.

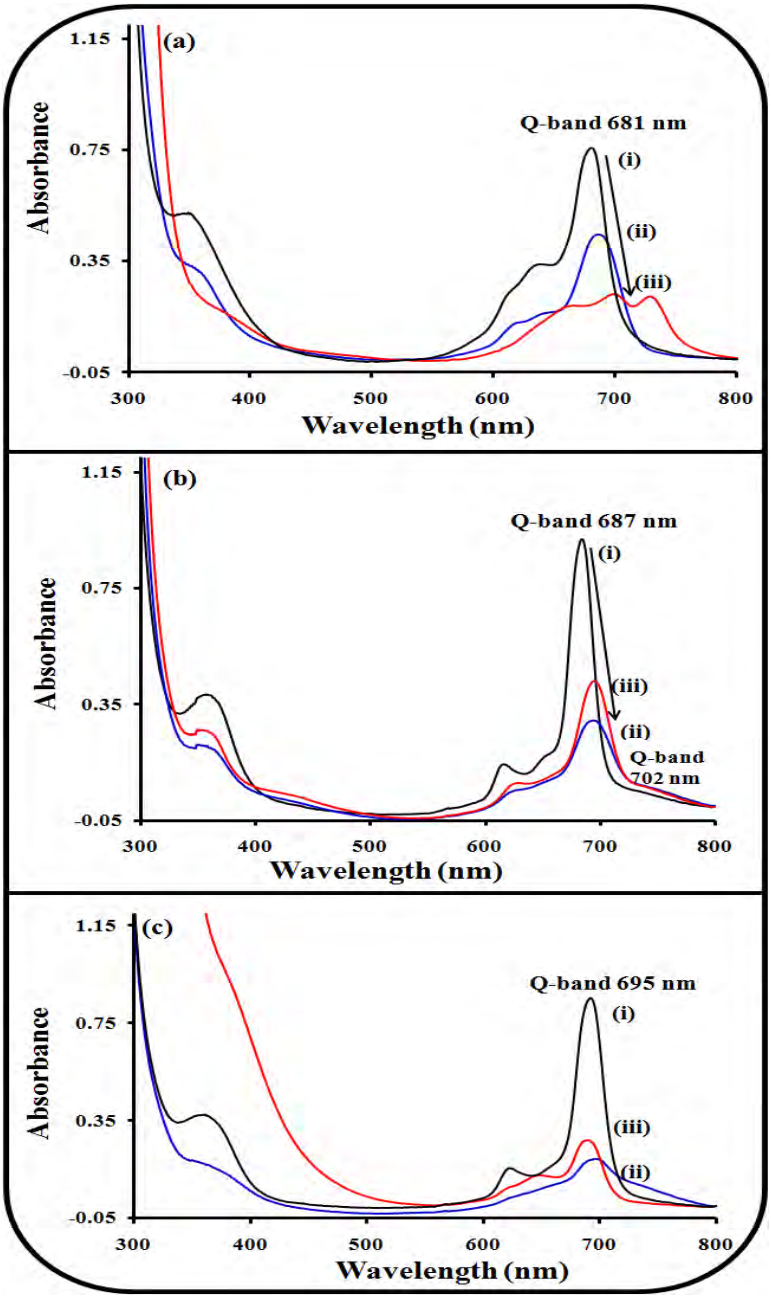

Figure 5.5: Absorption spectral changes for (a) TmTMPyZnPc (32b) in (1:1) pyridine: water, (b) (Cl)GaTmTMPyPc (34) and (c) (Cl)InTmTMPyPc (35) in (1:1) ethanol:water. [(i) MPc alone, (ii) MPc with excess MPA and (iii) addition of ferric chloride to a mixture of MPc with excess MPA]. {(a) [32b] = 6 × 10^{-6} M, (b) [34] = 7 × 10^{-6} M, (c) [35] = 7 × 10^{-6} M}

The spectral changes obtained and presented in this work show that it is not the QDs, but the capping agent which is involved in the transformation of the MPc complexes **32b**, **34** and **35**. It is possible from the spectral changes observed that, either MPA or the MPA QDs reduce the quaternized (hence positively charged) nitrogens on the pyridine substituents on the Pc ring during formation of stable electrostatic clusters, since typical spectra due to pure ring reduction were not observed.

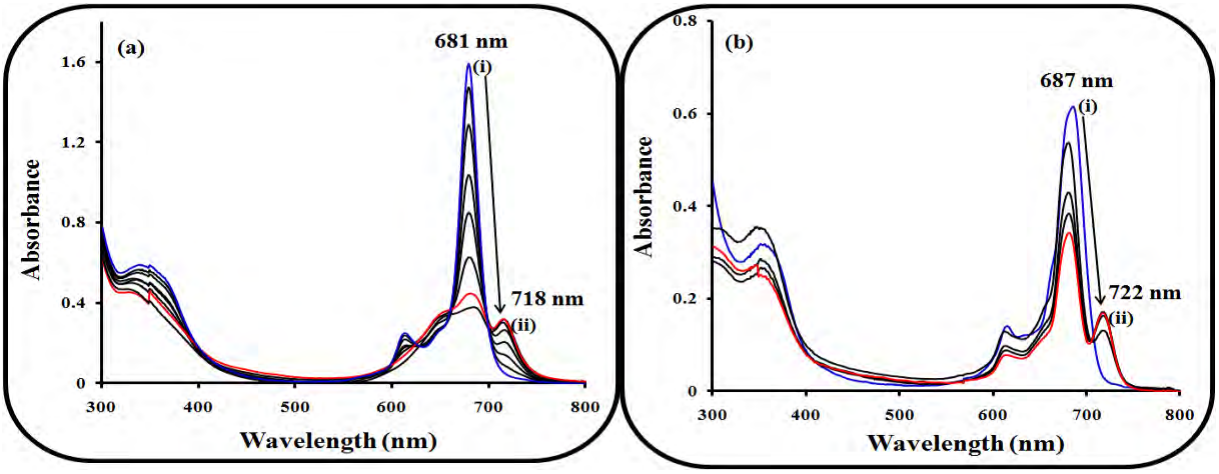

Figure 5.6: Absorption spectra for the protonation of (a) TmTMPyZnPc (32b) and (b) (Cl)GaTmTMPyPc (34) with TFA. {(i) MPc alone and (ii) MPc and final TFA addition, (a) [32b] = 3 × 10^{-5} M and (b) [34] = 6 × 10^{-6} M} (Protonation carried out in (1:1) ethanol:water solvent mixture for both complexes)

A comparison of protonated spectra for the positively charged MPcs using TmTMPyZnPc (**32b**) and (Cl)GaTmTMPyPc (**34**) as examples (Figure 5.6((a) and (b)) with the corresponding spectra for the MPcs upon addition of excess MPA capping agent (Figure 5.5((a) and (b), ii)) shows that they are quite different from each other. The protonation of aza nitrogens of Pcs is expected in acidic media or in the presence of a protonating agent such as trifluoroacetic acid (TFA) and results in the loss of symmetry of the protonated MPc as shown in Figure 5.6((a) and (b) [175,259].

Quaternized complex 31b and neutral quaternizable complexes 40 and 41

The other positively charged MPc studied in this work is TmTPyZnPc (**31b**). This MPc complex however did not show the same spectral changes as the rest of the quaternized MPcs **27b**, **32b**, **34** and **35** in the presence of QDs (**31b** does not undergo major spectral changes without photolysis as is the case with neutral complexes **40** and **41**). Complex **31b** showed similar behaviour to the neutral quaternizable complexes TtfmPyZnPc (**40**) and TtfmMPyZnPc (**41**). Figure 5.7(a-c) shows the spectra of the respective phthalocyanine complexes, TmTPyZnPc (**31b**), TtfmPyZnPc (**40**) and TtfmMPyZnPc (**41**) alone (i), MPA CdTe QDs alone (ii) and respective MPc in the presence of QDs (iii). In Figure 5.7(b) and (c) the ground state absorption spectra show evidence for the formation of a ground state complex between the QDs and the neutral quaternizable ZnPc complexes **40** and **41**. This ground state complex which is possibly formed by adsorption is evidenced by a 2 nm shift of the Q-band positions of the complexes **40** and **41** upon addition of the QDs to the solutions of the respective MPcs. This shift in the Q-band was however not observed for the quaternized complex **31b** when QDs were added, Figure 5.7(a)**.**

Spectral changes observed in Figure 5.4(a) for TmTMPyZnPc (**32b**, containing thio bridges) were not observed for TmTPyZnPc (**31b**, containing oxo bridges in Figure 5.7(a)) in aqueous media. However the quaternizable complexes TtfmMPyZnPc (**41**, containing thio bridges) and TtfmPyZnPc (**40**, containing oxo bridges) both showed the same behaviour in organic solvents DMSO and pyridine (Figure 5.7(b) and (c), in pyridine). These results suggest that the thio and oxo bridges play a big role in the spectral changes of the MPc complexes observed in the presence of QDs. Furthermore, the quaternization of complexes also has a bearing on the behaviour of MPc complexes in the presence of QDs as observed for the positively charged complexes TmTPyZnPc (**31b**) and TmTMPyZnPc (**32b**) compared to the neutral quaternizable complexes TtfmPyZnPc (**40**) and TtfmMPyZnPc (**41**). However, the solvents employed for the studies also influence the MPc behaviour in a mixture with QDs as judged from Figure 5.7(b) and (c).

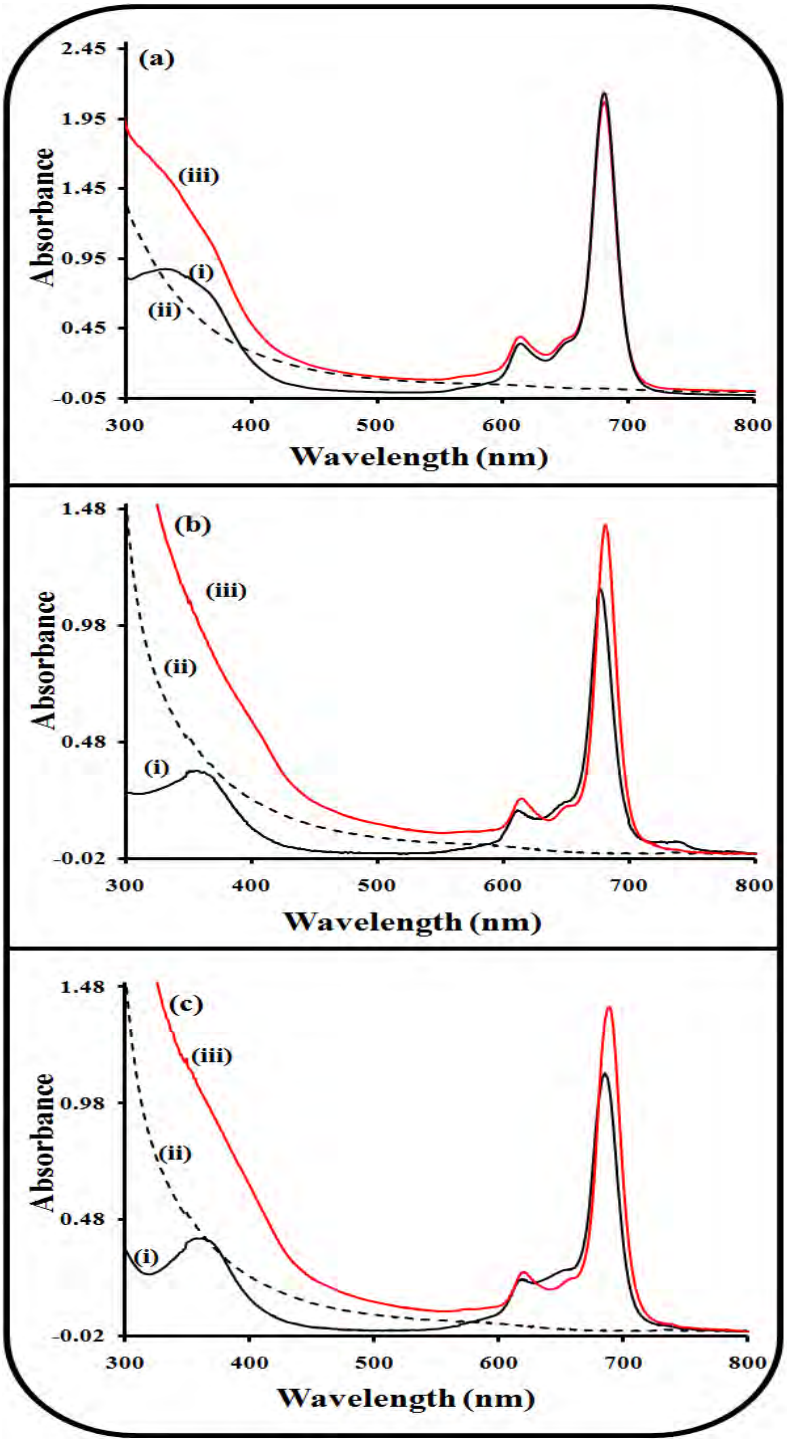

Figure 5.7: Absorption spectra for MPc alone (i), MPA CdTe QDs alone (ii) and a mixture of MPc and MPA CdTe QDs (iii) for TmTPyZnPc (31b) in (a), TtfmTPyZnPc (40) in (b) and TtfmTMPyZnPc (41) in (c). (Studies carried out in (1:1) pyridine:water solvent mixture for complex 31b and in pyridine for 40 and 41). {(a) [31b] = 8 × 10^{-6} M, (b) [40] = 7 × 10^{-6} M, (c) [41] = 7 × 10^{-6} M, [QDs] = 1mg/1mL}

5.1.1.2 Fluorescence quenching studies of quaternized porphyrazine complex by QDs

The fluorescence emission spectra of complex **27b** was in the same manner to the absorbance, quenched with incremental additions of QDs to the porphyrazine as shown in Figure 5.8. However there was no emission peak corresponding to the weak absorption due to the anion radical between 500 and 600 nm. The reason for a lack of an emission peak corresponding to the TmTPZnPz(-3) (**27b**) species could be due to the fact there is a very weak absorption of the anion radical. In addition to this, the presence of paramagnetic species would encourage intersystem crossing to the triplet state and hence result in very weak or no fluorescence for this anionic species.

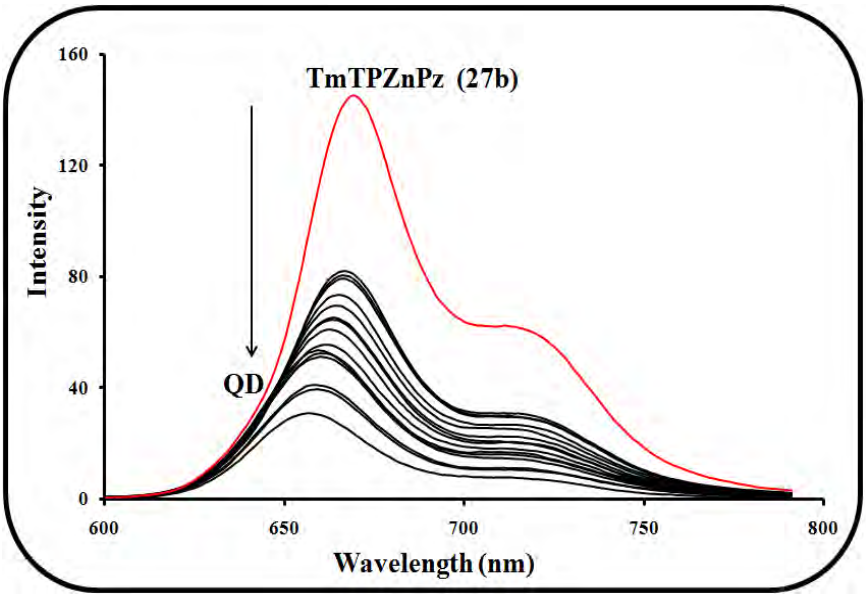

Figure 5.8: Emission spectral changes of TmTPZnPz (27b) (1.65 × 10^{-5} M) with addition of QDs (1μg μL^{-1} aliquots).

A study of the fluorescence emission of QDs on addition of increments of **27b** also showed continual quenching of the QDs emission, Figure 5.9(a). Stern–Volmer studies were carried out to determine the quenching constant K_{SV} using equation 5.1 (same as equation 1.5).

$$\frac{F_0}{F} = 1 + K_{SV}[Q] \qquad (5.1)$$

The number of macrocyclic units (n) that bind to each QD and the binding constant k_b were determined through the use of equation 5.2 (same as equation 1.7).

$$\log\left[\frac{(F_0 - F)}{F - F_\infty}\right] = \log k_b + n\log[Q] \qquad (5.2)$$

All the data obtained from the quenching studies of QDs by complex **27b** are shown in Table 5.1. Figure 5.9(a) shows the emission spectral changes of TGA CdTe QDs as they are gradually titrated with TmTPZnPz (**27b**) of varying concentrations (0 to 1.71 × 10^{-6} M) accompanied by an inset of a plot of F_0/F versus [**27b**]. The Figure 5.9(b) shows a plot of log $(F_0\text{-}F)/(F\text{-}F_\infty)$ versus log [**27b**].

The considerably large k_b values obtained for the titration of the QDs with varying concentrations of complex **27b** indicate that there is a strong binding between the QDs and TmTPZnPz (**27b**). The k_b values generally decreased with increase in the size of the TGA CdTe QDs with the exception of the 3.45 nm QDs, Table 5.1, suggesting that smaller QDs bind to TmTPZnPz (**27b**) more strongly. In addition to information obtained about the binding constants, the value of n (number of binding sites on QDs) was determined to be two for all the sizes of the QDs employed. This suggests that two molecules of complex **27b** attach themselves to one QD.

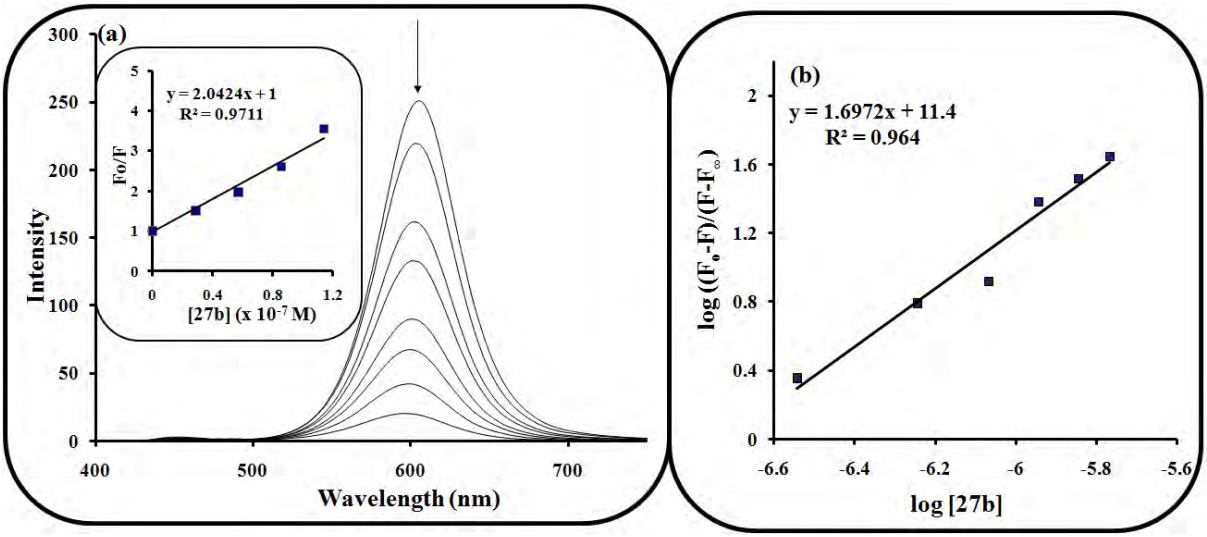

Figure 5.9: Emission spectral changes of (a) TGA CdTe QDs (1 mg mL^{-1}) titrated with TmTPZnPz (27b) (0 to 1.71 × 10^{-6} M) with an inset of a Plot of F_0/F versus [27b] and (b) plot of log $(F_0\text{-}F)/(F\text{-}F_\infty)$ versus log [27b]).

Table 5.1: Variation of binding and quenching constants of TmTPZnPz (27b) with different QD sizes.

[a]QD	Emission wavelength λ (nm)	Size/nm (D)	k_b /10^{-10} M^{-1}	K_{SV}/10^{-5} M^{-1}	n
TGA CdTe	528	2.95	2500	8.3	2.24
	546	3.20	25	10	1.89
	573	3.45	720	20	2.07
	608	3.73	41	9.7	1.91
	626	3.94	25	100	1.70
	636	4.09	2.7	100	1.60
ME CdTe	572	3.29	0.52	0.50	1.80
ME ZnS	422	2.9	11.6	0.62	2.22

[a]**A pH 7.4 buffer solution was used for all quenching studies.**

The linear plot in the inset shown in Figure 5.9(a) confirms that the quenching equation (equation 5.1) is obeyed. The K_{SV} values generally (with the exception of QDs of size 3.73 nm) exhibited an increase with an increase in the size of the TGA QDs as shown in Table 5.1. As a result the fluorescence emission of larger QDs is quenched more efficiently. The k_b and K_{SV} values for the 3.29 nm ME CdTe QDs were smaller than those obtained for CdTe-TGA QDs. The K_{SV} values for both ME CdTe and ME ZnS QDs were both rather low. However, the k_b values for ZnS QDs were in the same range as those for TGA CdTe QDs, Table 5.1.

A linear dependence for the reduction of TmTPZnPz (**27b**) by different sizes of QDs is observed in Figure 5.10 (data derived from figure 5.2(b)). The slope of the reduction process increases with an increase in the size of the QDs in Figure 5.10(a) (for ME CdTe QDs), suggesting that larger QDs reduce **27b** more readily than the smaller ones. For TGA CdTe QDs (Figure 5.10(b)), the largest slope was also observed for the largest QD size, however the trend was not clear for the smaller

QDs. According to literature, smaller quantum dots are more difficult to oxidize compared to the larger ones [65]. The oxidation potential values for the TGA CdTe QDs in Table 3.2 showed a shift to less positive values with increase in QD size, showing an ease of oxidation as described in literature [65,67]. Consequently the smaller QDs reduce the TmTPZnPc (**27b**) complex with more difficulty compared to larger quantum dots, hence the latter QDs have a steeper (largest) slopes, in Figure 5.10(a) and (b).

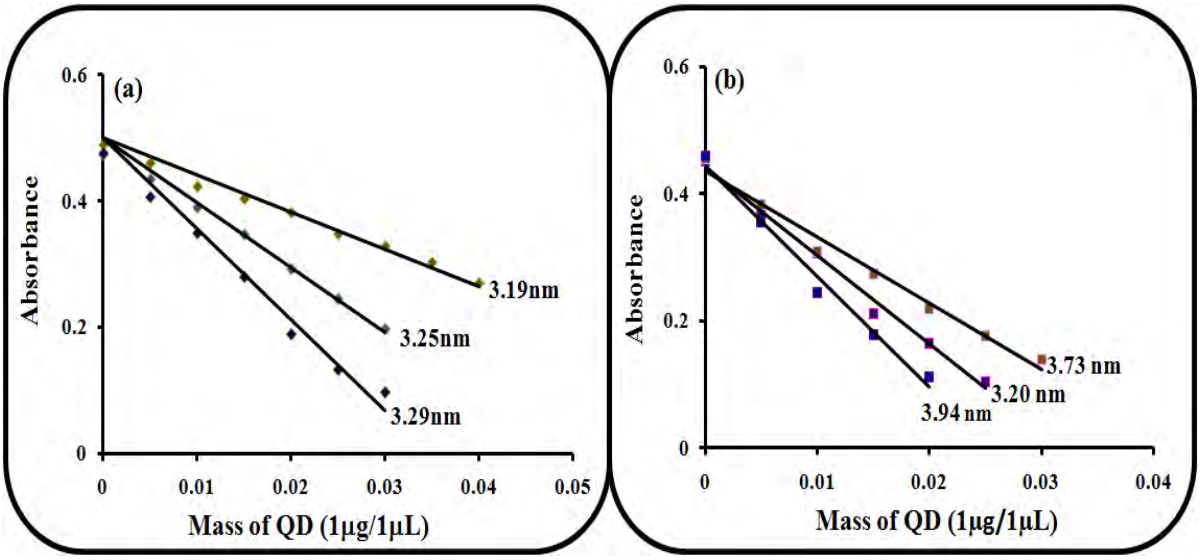

Figure 5.10: Plot of absorbance of TmTPZnPz (27b) versus the concentration of QDs for the titration of 27b with different sizes of QDs of (a) ME CdTe and (b) TGA CdTe QDs.

The studies carried out on complex **27b** in the presence of QDs clearly show that the QDs used (ME ZnS, ME CdTe and TGA CdTe QDs) all caused ring reduction of the quaternized complex **27b** resulting in the quenching of the absorbance and emission of this complex in the presence of QDs.

5.1.1.3 Fluorescence quenching studies of neutral quaternizable complexes by QDs

The bimolecular quenching constant (k_q) was determined for the quenching of MPA CdTe QDs by neutral complexes **40** and **41**. The values of k_q were determined through the use of equation 5.3 (same as equation 1.6). The fluorescence lifetime of the QDs ($\tau_{F(QD)}$) in the absence of the quencher (complexes **40** and **41**) was determined through time correlated single photon counting measurements.

$$K_{SV} = k_q \tau_{F(QD)} \qquad (5.3)$$

The k_q values determined for the quenching of QDs by the complexes TtfmPyZnPc (**40**) and TtfmMPyZnPc (**41**) are of the order of 10^{13} dm^3 mol^{-1} s^{-1}, Table 5.2. These k_q values which are higher than the proposed values for dynamic quenching of the order of 10^{10} dm^3 mol^{-1} s^{-1} suggest that the mode of quenching is static [260]. The k_b values were of the order of 10^5 suggesting strong interaction of the complexes **40** and **41** and the MPA QDs (Table 5.2), but they were less than values obtained for the interaction of QDs and complex **27b**.

Table 5.2: Binding and quenching constants of TtfmPyZnPc (40) and TtfmMPyZnPc (41) with MPA CdTe QDs. (in Pyridine and DMSO, with 1% water)

[a]MPc	Solvent	$k_q/10^{-13}M^{-1}$	$k_b/10^{-5}M^{-1}$	$K_{SV}/10^{-5}$ M^{-1}	n
TtfmPyZnPc (40)	DMSO	1.75	1.68	5.99	1.06
	Pyridine	3.01	0.22	6.01	0.91
TtfmMPyZnPc (41)	DMSO	4.56	2.86	15.53	1.03
	Pyridine	8.15	0.53	14.95	0.90

[a]MPA CdTe QDs of 4.54 nm size were employed in quenching studies.

The value of n was found to be near unity, indicating that one ZnPc molecule interacts with a single QD. The K_{SV} values obtained for the titration of the MPA CdTe QDs with complexes **40** and **41** were also large and of the order of 10^5 M^{-1} and

are comparable to those obtained for complex **27b** which are of the same order of magnitude. The differences observed with the binding constants and the number of binding sites from the quenching studies with complexes **40** and **41** compared to those obtained from studies with **27b** could result from a number of factors. These differences may be attributed to the solvent used, since it influences the degree of ionization of both QDs and Pc complexes in solution. The process resulting from the interaction of the complexes and the QDs at the Pc derivative and QD interface e.g. reduction of the porphyrazine ring for **27b** and energy transfer for complexes **40** and **41** may also lead to the observed differences in the k_b constants and n values.

5.1.2 Negatively charged MPcs in the presence of QDs

The behaviour of negatively charged MPcs **28**, **29**, **30**, **36**, **37** and **39d** in the presence of negatively charged CdTe QDs (with ME, TGA or MPA stabilizer groups) was investigated. QDs with ME and TGA capping agents were used for complexes **28**, **29** and **30** while MPA capped QDs were employed for **36**, **37** and **39d**. Aqueous solvent media that rendered the MPc complexes monomeric was used in these studies e.g. (1:1) ethanol:water or (1:1) ethanol:NaOH 0.01 M solvent mixtures. The absorption spectra of the MPc **30**, **36** and **39d** are shown as representatives in the absence (i) and presence (iii) of the respective QDs is shown in Figure 5.11(a-c). The spectra of QDs alone Figure 5.11(a-c, (ii)) is also included for comparison. There was no shift in the Q-band absorption maxima of the negatively charged MPcs upon addition of QDs as shown in Figure 5.11(a-c). This shift in absorbance maxima is usually observed as an indication of the formation of a ground state complex [261]. The rest of the negatively charged MPc complexes (**28**, **29** and **37**) demonstrated similar spectral behaviour to that observed in Figure 5.11(a-c) in aqueous media.

The CdTe QDs and MPcs are negatively charged by virtue of the terminal carboxyl moieties of the TGA and MPA cappings for the QDs, and of the carboxy substituents for the complexes **29**, **30**, **36**, **37** and **39d.** On the other hand ZnTSPc (**28**) has sulfonate

substituents which render the complex negatively charged in water. As a result the type of interactions envisaged between the QDs and the MPcs are adsorptive in nature.

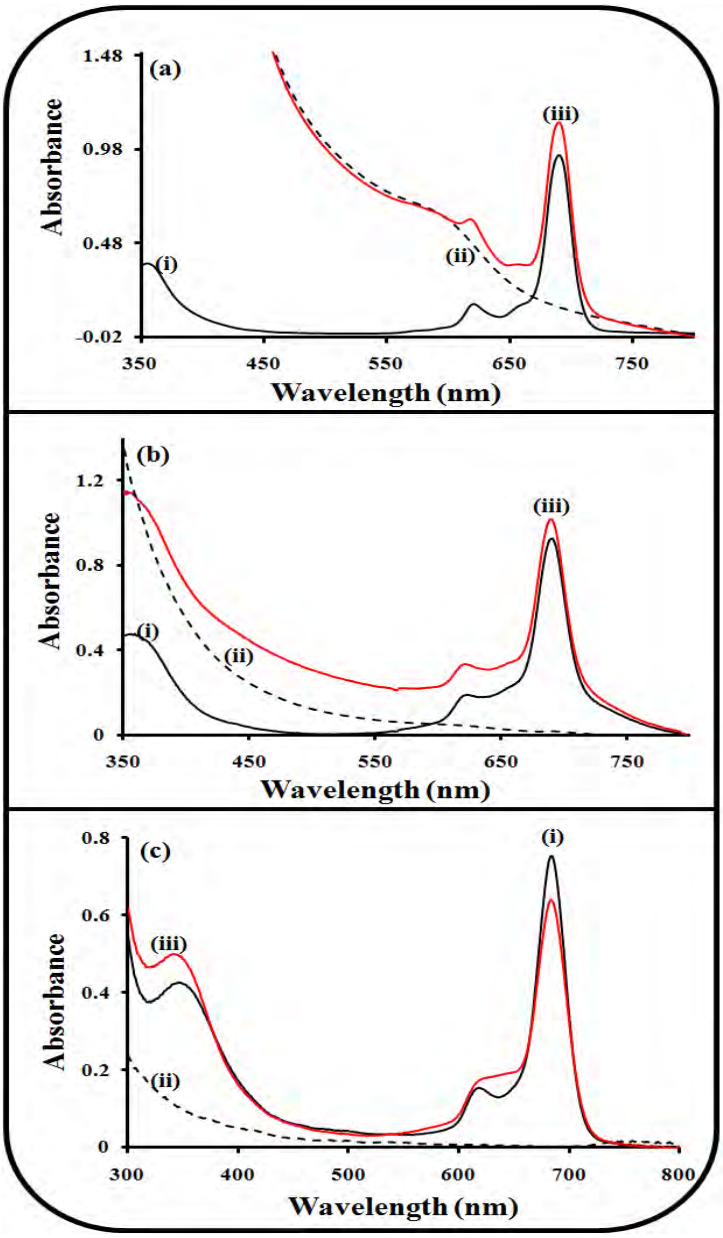

Figure 5.11: Absorption spectra for MPc alone (i), MPA CdTe QDs alone (ii) and a mixture of MPc and CdTe QDs (iii) for (a) ZnOCPc (30), (b) TMmTAAZnPc (36) and (c) TMPAZnPc (39d). (Studies carried out in (1:1) ethanol:NaOH 0.01 M for (a) and (c) and a (1:1) pyridine:water solvent mixture for (b), TGA CdTe QDs used in (a) and MPA CdTe QDs used in (b) and (c)).{[MPc] = ~8 × 10^{-6} M, [QD] = 1mg/1mL}

5.1.3 Förster Resonance Energy Transfer between QDs and MPcs

Förster resonance energy transfer (FRET) is a non-radiative transfer of energy from a donor chromophore to an acceptor chromophore (or flourophores if they are fluorescent in nature). The probability of FRET taking place depends upon the amount of spectral overlap between the emission spectrum of the donor (QDs) and the absorption spectrum of the acceptor (MPcs) as shown for representative complexes **30**, **36** and **39d** and CdTe QDs in Figure 5.12(a-c). The absorption spectra of the MPc complexes **30**, **36** and **39d** is overlaid with the emission spectra of TGA (for **30**) and MPA (for **36** and **39d**) CdTe QDs for an estimation of the amount of spectral overlap (J). The J term value can be calculated from equation 5.4 (same as equation 1.11).

$$J = \int f_D(\lambda)\, \varepsilon_A(\lambda)\, \lambda^4\, \partial\lambda \qquad (5.4)$$

A large J value indicates good spectral overlap between the emission spectrum of the donor and the absorption spectrum of the acceptor, thus giving an estimation of a good donor–acceptor oscillator match and hence a greater probability for the occurrence of FRET. Typical J values are of the order 10^{-14} cm^6 for porphyrin based molecules [193]. Figure 5.12(a-c) shows that the negatively charged MPc complexes **30**, **36** and **39d** had a good overlap factor with the QDs used. The same was observed for negatively charged complexes **28**, **29** and **37** as well as for the positively charged complex **31b** and the neutral complexes **40** and **41** in all the solvent media used for FRET studies. The other positively charged complexes **27b**, **34** and **35** did not show FRET but exhibited ring reduction (**27b**) or aggregation from the electrostatic assembly of ion-pairs (**34** and **35**). Complexes **31b** and **40** both have oxo bridges while **41** has a thio bridge, but both **40** and **41** show FRET in DMSO and pyridine.

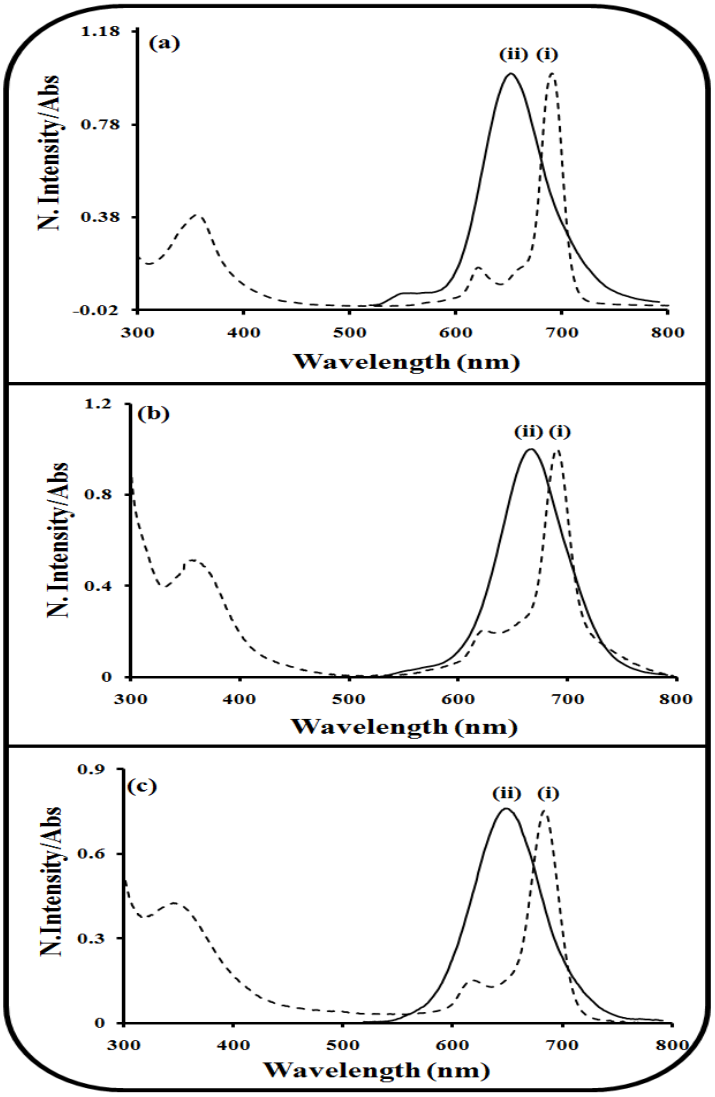

Figure 5.12: Absorption spectra of MPc (i) and emission of CdTe QDs (ii) for (a) ZnOCPc (30), (b) TMmTAAZnPc (36) and (c) TMPAZnPc (39d). (TGA CdTe QDs used in (a), MPA CdTe QDs used in (b) and (c) and also a (1:1) ethanol:water solvent mixture used in (a) and (c) while a (1:1) pyridine:water solvent mixture used in (b)). {[MPc] = 8 × 10^{-6} M, [QD] = 1mg/1mL}

It appears that complexes with oxo bridges undergo FRET more readily than thio bridge counterparts especially in aqueous media. However when organic solvents like DMSO or pyridine are used the MPc complexes with thio bridges may also undergo FRET as has been shown to be the case for complexes **40** and **41** Figure 5.13((c) and (d)).

The excitation of the CdTe QDs (with ME, TGA or MPA capping) at 500 nm (where the MPc does not absorb) in the presence of the respective MPc in solution resulted in a significant fluorescence of the MPc complex (shown in Figure 5.13(a-d, curves (iii)). Thus Figure 5.13(a-d) shows a clear transfer of energy (FRET) from the QDs to the MPc complexes as suggested by the increase in the emission spectra of MPc complex in the presence of QDs. An insignificant emission by the MPc complexes (in the absence of QDs) is observed on excitation at 500 nm, Figure 5.13(a-d, curves ii). The fluorescence spectra showing the FRET photoprocess for the representative phthalocyanine complexes **30**, **39d**, **40** and **41** shown in Figure 5.13(a-d) are analogous to those of the rest of the MPcs which undergo FRET. The spectra generally show significant quenching of the QD emission as a result of FRET, Figure 5.13(b-d, curves (i) and (iii)).

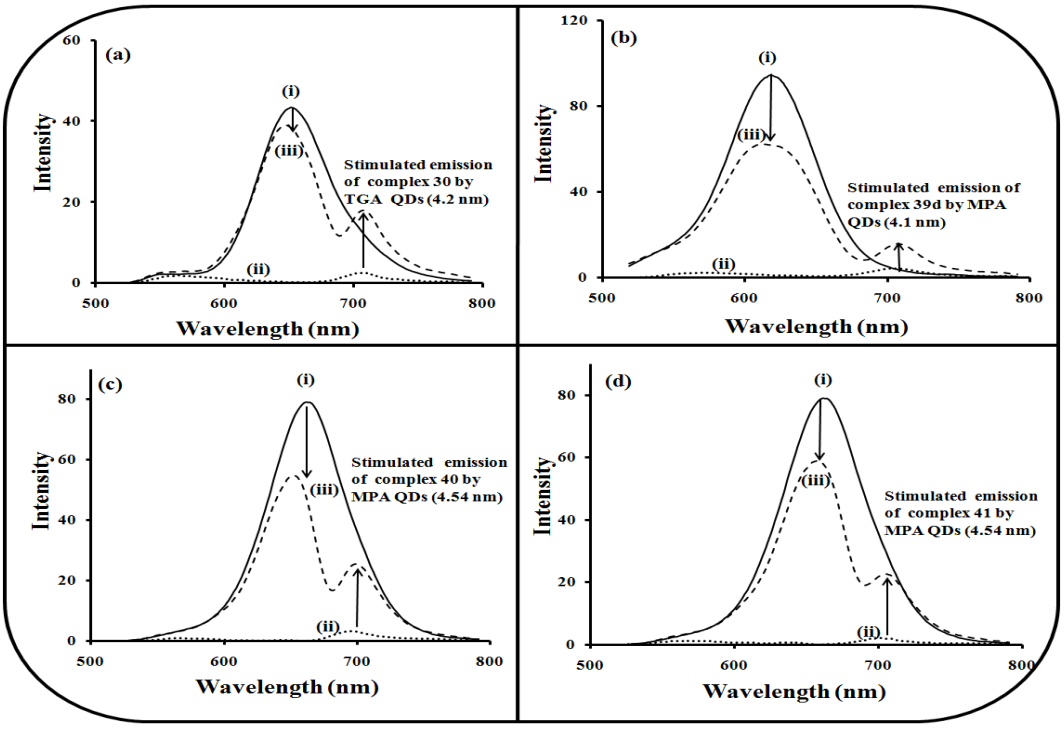

Figure 5.13: Emission spectra for CdTe QDs alone (i), MPc complex alone (ii) and CdTe QDs in the presence of MPc complex (iii) for (a) ZnOCPc (30), (b) TMPAZnPc (39d), (c) TtfmPyZnPc (40) and (d) TtfmMPyZnPc (41). ((1:1) ethanol:NaOH 0.01 M solvent mixture used in (a) and (b) while pyridine with 1% water was used in (c) and (d)). {[QD] = 1mg 1mL^{-1}, [MPc] = 8 × 10^{-6} M}

The efficiency of FRET was determined with the use of equation 5.5 (same as equation 1.8). This equation employs the fluorescence quantum yield of the donor in the presence ($\Phi_{F(DA)}$) and absence ($\Phi_{F(D)}$) of the acceptor. The $\Phi_{F(D)}$ and $\Phi_{F(DA)}$ values for the QDs used in this thesis are presented in Table 5.3. The fluorescence quantum yields of the donor (QDs) generally decreased in the presence of the acceptor (MPcs) as shown in Table 5.3.

$$Eff = 1 - \frac{\Phi_{F(DA)}}{\Phi_{F(D)}} \qquad (5.5)$$

The FRET efficiency (*Eff*) is also related to the centre to centre distance between the donor and acceptor chromophores (r) and the Förster distance, R_0 (Å) which is the critical distance at which 50% FRET efficiency is expected by equation 5.6 (same as 1.9)

$$Eff = \frac{R_0^{\,6}}{R_0^{\,6} + r^6} \qquad (5.6)$$

The Förster distance values (R_0) for all complexes undergoing FRET were determined through the use of the PhotochemCAD programme and are listed in Table 5.4. The centre to centre distances (r) were calculated from equation 5.6 and are also shown in Table 5.4. Smaller r values are expected to result in higher FRET efficiencies as these would allow for increased long range dipole-dipole coupling between the donor and acceptor resulting in efficient energy transfer [191]. According to the results in Table 5.4 the positively charged MPc complex TmTPyZnPc (**31b**) and the quaternizable complexes TtfmPyZnPc (**40**) and TtfmMPyZnPc (**41**) generally showed much lower J term values. The negatively charged MPc complexes ZnTSPc (**28**), ZnTCPc (**29**), ZnOCPc (**30**), TMmTAAZnPc (**36**) and OMmTAAZnPc (**37**) displayed larger J values with the exception of TMPAZnPc (**39d**), which had low J values in all the solvents employed.

Table 5.3: Fluorescence quantum yields of CdTe QDs with different cappings in the absence and presence of MPc complexes.

[a]QD capping	Solvent	MPc	$\Phi_{F(QD)}$	$\Phi^{Mix}_{F(QD)}$	QD Size (nm)
ME	[b] (1:1) EtOH:NaOH	28	0.037	0.011	3.29
		29		0.017	
		30		0.012	
TGA	[b] (1:1) EtOH:NaOH	28	0.11	0.014	4.19
		29		0.060	
		30		0.018	
TGA	[c] (1:1) pyr:H_2O	31b	0.12	0.095	4.09
MPA	[c] (1:1) pyr:H_2O	31b	0.21	0.17	4.19
MPA	[c] (1:1) pyr:H_2O	36	0.21	0.12	4.54
		37		0.15	
MPA	DMSO (1% H_2O)	40	0.22	0.12	4.54
		41		0.15	
	Pyridine (1% H_2O)	40	0.11	0.10	
		41		0.10	
MPA	DMSO	39d	0.32	0.19	4.1
	DMF	39d	0.21	0.10	
	[b] (1:1) EtOH:NaOH	39d	0.22	0.15	

[a]($\lambda_{excitation}$ = 500 nm), [b]Represents a (1:1) ethanol:NaOH 0.01 M solvent mixture and [c]Represents a (1:1) pyridine:water solvent mixture.

The FRET efficiencies for the complexes in the presence of CdTe QDs were either very low or mediocre except for TMPAZnPc (**39d**) in DMF which showed the highest efficiency of 58%. Complex **39d** in DMF showed the lowest value of r compared to all

Table 5.4: Energy transfer parameters for MPc-CdTe QD interactions in various solvents.

MPc and CdTe QDs	Solvent	J/10^{13}cm^6	R_0(Å)	r(Å)	*Eff*
ZnTSPc (28) + (TGA) QDs	[a](1:1)EtOH:NaOH	18	57	67	[c]0.30
ZnTCPc (29) + (TGA) QDs	[a](1:1)EtOH:NaOH	7.2	49	63	[c]0.20
ZnOCPc (30) + (TGA) QDs	[a](1:1)EtOH:NaOH	7.9	50	60	[c]0.20
TmTPyZnPc(31b)+ MPA QDs	[b](1:1) Pyr:H_2O	1.36	40	50	0.21
TmTPyZnPc(31b)+ TGA QDs	[b](1:1) Pyr:H_2O	1.17	35	44	0.21
TtfmPyZnPc(40)+ MPA QDs	DMSO	0.12	52	54	0.45
TtfmPyZnPc(40)+ MPA QDs	Pyridine	0.10	58	66	[c]0.32
TtfmMPyZnPc(41)+MPA QDs	DMSO	0.11	52	59	0.31
TtfmMPyZnPc(41)+MPA QDs	Pyridine	0.12	59	72	[c]0.24
TMmTAAZnPc(36)+MPA QDs	[b](1:1) Pyr:H_2O	3.15	46	48	0.43
OMmTAAZnPc(37)+MPA QDs	[b](1:1) Pyr:H_2O	2.64	45	51	0.30
TMPAZnPc(39d) + MPA QDs	DMSO	0.71	38	40	0.42
TMPAZnPc(39d) + MPA QDs	DMF	0.70	36	34	0.52
TMPAZnPc(39d) + MPA QDs	[a](1:1)EtOH:NaOH	0.34	33	37	0.32

[a]Represents a (1:1) ethanol:NaOH 0.01M solvent mixture and [b]Represents a (1:1) pyridine:water solvent mixture ($\lambda_{excitation}$=500nm), [c]See supplementary material.

the values obtained with the MPc complexes and in addition to this, it also showed a small R_0 value quite close to the r value and an acceptable J term value (~7 x 10^{-14} cm^6) which could have all contributed to the moderate (58%) FRET efficiency obtained for this complex.

Table 5.4 shows the general trend observed with centre to centre distance (r) values that were greater than the Förster distance values (R_0). This combination of r values that were greater than the R_0 values resulted in especially low FRET efficiencies mostly varying between 20 and 33% {observed for complexes **28**, **29**, **30**, **31b**, **37**, **40 (**in pyridine) and **41**}. However, it was also observed that when the r and R_0 values **{**for complexes **36**, **40** (in DMSO) and **39d}** were close to each other, this resulted in enhanced FRET efficiencies ranging between 40 and 58%. In general complex **39d** showed the smallest value of both the r and R_0 values in DMSO, DMF and the (1:1) ethanol:NaOH 0.01M solvent mixture employed for FRET studies. Although studies with TmTPyZnPc (**31b**) showed fairly small r values with r and R_0 values which were close to each other (in the (1:1) pyridine:water solvent mixture) for FRET studies with the MPA CdTe QDs, the FRET efficiency was rather low (21 %). The lower FRET efficiency observed for the MPc complex **31b** even with favourable r and R_0 values may possibly be due to the tetra positive charge on the Pc ring of this complex.

The type of MPcs (neutral, negatively or positively charged) and solvent employed in FRET studies affect the FRET efficiency. This is because both the solvent and the MPc have a direct effect on the monodispersity of CdTe QDs in solution. As a result the monodispersity of CdTe QDs in different solvents and in the presence of MPc complexes was estimated through the use of atomic force microscopy. Complexes **36** and **37** were the only MPcs selected to determine the effect of MPc complexes on the monodispersity of QDs. Figure 5.14 shows the AFM data obtained and this data provides information about surface morphology of CdTe QDs on a cross section of the glass surface coating from a 0.01 M NaOH solution (A), (1:1) pyridine:NaOH 0.01 M solvent mixture (B) and in the presence of the complexes TMmTAAZnPc (**36)** (C) and OMmTAAZnPc (**37)** (D) **{**(C) and (D) are both in the (1:1) pyridine:NaOH solvent mixture}. In the 0.01 M NaOH solution, the CdTe QDs show a size distribution from 4 nm to 24 nm (histogram, E) however populations with size distributions from 12 nm and below in the section analysed occurred more frequently suggesting that CdTe QDs are not totally monodisperse even in basic media. However, in the solvent mixture containing pyridine, the QDs show a size

distribution of up to 30 nm (histogram, F) which is a wider distribution, suggesting that aggregation tendencies are worsened in this solvent system. The QDs also showed a size distribution of up to 30 nm (histogram, G) in the presence of complex **36**. However, in the presence of complex **37** the size distribution of the QDs went up to 40 nm (histogram, H). This behaviour shows that the monodispersity of QDs is solvent dependent and that the addition of MPc complexes to a QD solution affects the monodispersity of these nanoparticles [251]. The general trend displayed by the AFM images was (in Figure 5.14) that clusters of a size distribution of 15 nm and less were still more predominant for all of the samples indicating that the more aggregated clusters occur less frequently. Since aggregation of the QDs was minimal with complex **36**, the FRET efficiency was only slightly affected for complex **36**, but it was significantly lowered for complex **37** which caused greater aggregation of QDs in solution, Table 5.4.

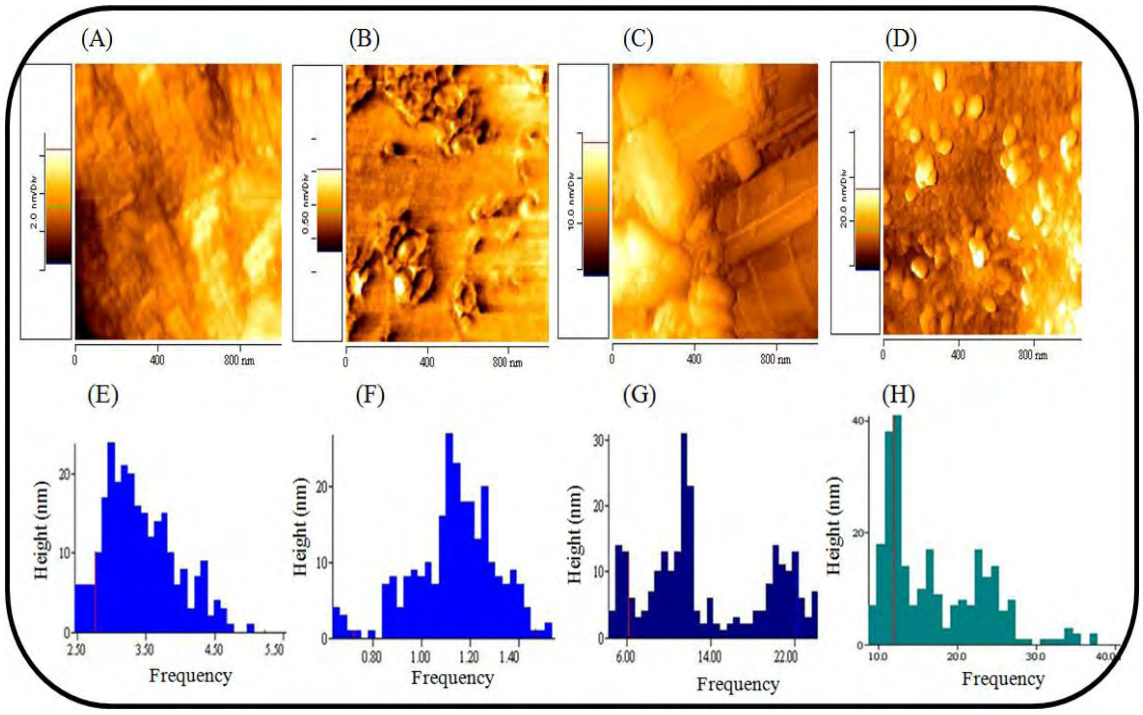

Figure 5.14: AFM images of MPA CdTe QDs deposited on a glass surface from 0.1 M NaOH (A), 0.1 M NaOH:Pyridine (B), QDs and TmMTAAZnPc (36) (C), QDs and OmMTAAZnPc (37) (D) and corresponding histograms (E-H). {(C) and (D) are in the (1:1) pyridine:NaOH 0.01 M solvent mixture}

5.2 Interaction of 1,6-hexanedithiol substituted ZnPc with AuNPs

Complex THdTZnPc (**42**) was chosen specifically for the study with tetraoctylammonium bromide (TOAB) stabilized AuNPs because the substituents of this phthalocyanine each terminate with a thiol moiety. The thiol groups allow for attachment of complex **42** onto the AuNPs since they are known to have a high affinity for gold surfaces. An indication of the formation of the MPc-AuNP conjugate is shown in Figure 5.15 and the accompanying inset. The absorption spectra of complex **42** alone (i), the mixture of complex **42** and TOAB AuNPs (ii) and the **42**-AuNP conjugate (iii) at the Q-band position are shown as normalized spectra in Figure 5.15 in $CHCl_3$. The normalized superimposed spectra show that there is a slight shift of the Q-band position from 705 nm for complex **42** alone to 702 nm for MPc in the mixture with TOAB AuNPs and a shift to 697 nm for complex **42** in the **42**-AuNP conjugate. All the spectral shifts of the Q-band position of the Pc are towards the blue. The relatively large blue shift of the MPc in the **42**-AuNP conjugate shows that the terminal sulfur groups are engaged in linking complex **42** to the TOAB AuNPs.

The inset shown in Figure 5.15 shows the Uv-Vis spectra of the TOAB AuNPs alone (a), complex **42** alone (b), a mixture of complex **42** and the TOAB AuNPs (c) and the **42**-AuNP conjugate (d). A shift in the surface plasmon band of the AuNPs upon conjugation to THdTZnPc (**42**) (all spectra obtained in $CHCl_3$) is observed as discussed in chapter 3. The surface plasmon band for the TOAB stabilized AuNPs is at ~ 389 nm in $CHCl_3$, Figure 5.15 (inset, curve (a)). However, this plasmon band merges with the B-band of complex **42** showing wavelength maxima at 426 nm for the **42**-AuNP conjugate in $CHCl_3$, Figure 5.15 (inset, curve (d)). The change in the surface plasmon absorption band is indicative of modification of the AuNPs. The observed spectral changes for the gold nanoparticle surface plasmon band in the **42**-AuNP conjugate (Figure 5.15) indicate that the attachment of complex **42** to the AuNPs was successful. Also shown in the inset of Figure 5.15 is the absorbance of the mixture of AuNPs with complex **42** (Figure 5.15 (inset, curve (c)). This spectrum

shows the resulting merger of the B-band of the complex **42** with the surface plasmon band of the AuNPs with the amalgamated peak appearing at 384 nm in $CHCl_3$.

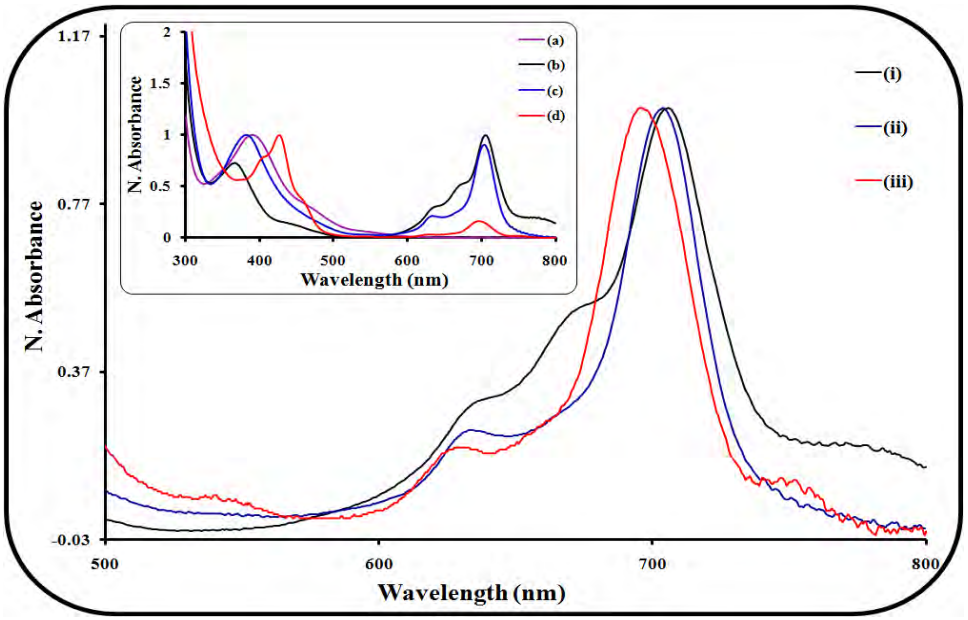

Figure 5.15: Normalized visible absorption spectra of THdTZnPc (42) alone (i), mixture of 42 and AuNPs (ii) and 42-AuNP conjugate (iii) at Q-band region in $CHCl_3$. (Inset: UV-Vis absorption spectra of TOAB AuNPs (2) (a) complex 42 alone (b), mixture of complex 42 and AuNPs (2) (c) and 42-AuNP conjugate (44) (d) in $CHCl_3$). {[42] = 4 × 10^{-6} M, [2] = 1mg/1mL, [44] = 2mg/1mL}

The absorption of the **42**-AuNP conjugate (curve (iii)) is narrower compared to the absorption of **42** alone (curve (i)), (Figure 5.15). This observed broadness of the Q-band absorption (for complex **42**) is possibly the result of aggregation. The addition of AuNPs to the MPc solution was observed to break the aggregation of complex **42**, as judged by the narrowing of the Q-band in the mixture (Figure 5.15 (curve (ii)). This effect of monomerization of the MPc Q-band is also observed in the conjugate where there is no sign of aggregation for complex **42** in the **42**-AuNP conjugate, Figure 5.15. Complex **42** is suggested to attach to the AuNPs via a coordinate covalent bond.

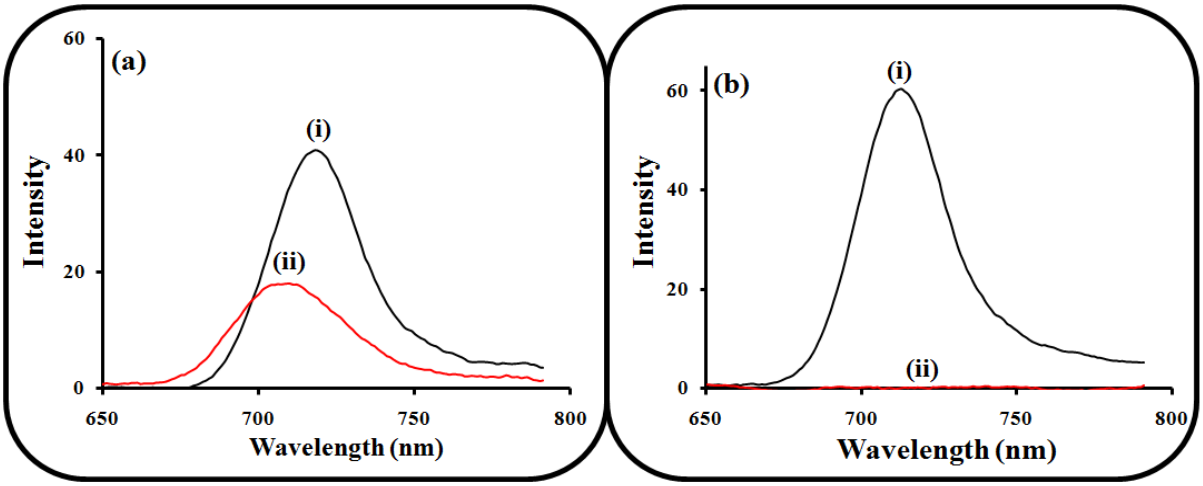

Figure 5.16: Emission spectra of (i) THdTZnPc (42) and (ii) 42-AuNP conjugate (44) in DMSO (a) and in DMF (b). {[42] = 4 × 10^{-6} M, [44] = 2mg/1mL}

The fluorescence of complex **42** attached to the AuNPs was quenched significantly in DMSO and DMF, (Figure 5.16) and this is possibly due to the to TOAB stabilized AuNPs which are non fluorescent. This behavior is expected since the MPc molecules in the **42**-AuNP conjugate are anticipated to either have interactions with the AuNPs that quench the emission of the Pc or to form H-aggregates (depending on their arrangement on the AuNP) which are known to be non-fluorescent [170]. However, aggregation does not play a role in this work as shown in Figure 5.15.

5.3 Triplet state data of all MPcs studied in the presence of nanoparticles

The photophysical properties of MPc complexes in the absence and presence of different nanoparticles (ME, TGA and MPA stabilized CdTe QDs and AuNPs) are investigated in this work. The transient spectra of one of the MPc complexes TMmTAAZnPc (**36**) in the absence (curve i) and presence (curve ii) of MPA CdTe QDs is shown in Figure 5.17 (similar behavior is displayed by the rest of the MPcs). As shown in Figure 5.17 complex **36** maintained its monomeric nature in the excited state in both the absence and presence of the QDs with both spectra at the same wavelength maxima.

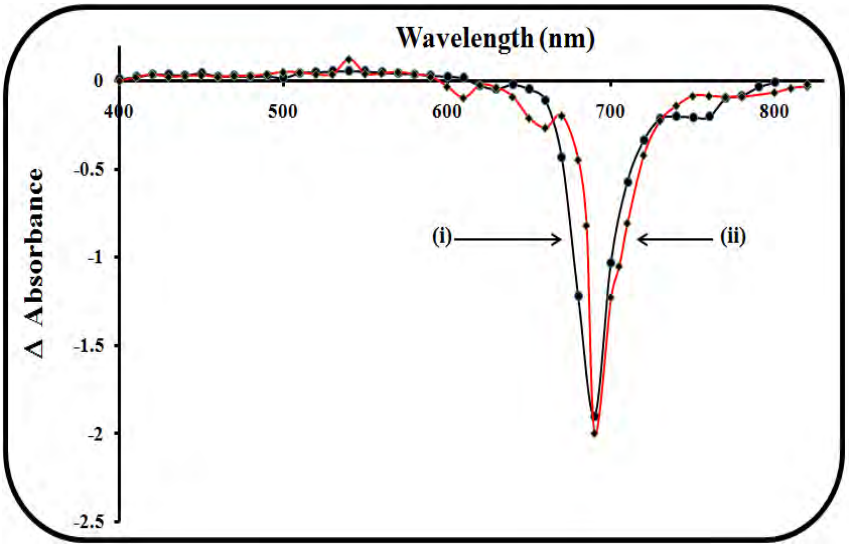

Figure 5.17: Transient differential spectrum for TMmTAAZnPc (36) alone (i) and TMmTAAZnPc (36) mixed with MPA CdTe QDs (ii) ($\lambda_{excitation}$ = 687 nm in (1:1) pyridine:NaOH 0.01 M solvent mixture). {[36] = 3 × 10^{-5} M}

The photophysical parameters (Φ_T and τ_T values) obtained are listed in Table 5.5. The tabulated results (Table 5.5) show that Φ_T values of ZnOCPc (**30**) both in the presence and absence of QDs were much larger than those of complexes ZnTSPc (**28**) and ZnTCPc (**29**). The Φ_T values were expected to increase in the presence of the CdTe QDs due to the heavy atom effect (from the constituent Cd and Te atoms) which encourages intersystem crossing (ISC) but the Φ_T values of the MPcs **28**, **29** and **30** decreased [53,131]. A decrease in Φ_T values was generally observed with the exception of ZnTCPc (**29**) in the presence of TGA CdTe QDs in (1:1) ethanol:NaOH 0.01 M where the Φ_T value slightly increased. The triplet lifetimes of the complexes (**28**, **29** and **30)** were generally higher in the presence of QDs (except for **28** and **30** in the presence of ME CdTe QDs).

A slight increase was observed for the Φ_T value of TmTPyZnPc (**31b**) in the presence of TGA CdTe QDs. The τ_T value for **31b** in the presence of QDs on the other hand was significantly enhanced (Table 5.5). The enhancement of τ_T values in the presence of QDs has been reported [201].

Table 5.5: Photophysical data of all MPcs studied in the presence of nanoparticles.

Abbreviation MPc	Solvent	NPs	Φ_T	$\Phi^{Mix}_{T(ZnPc)}$	τ_T (μs)	$\tau^{Mix}_{T(ZnPc)}$ (μs)
ZnTSPc (28)	[a]EtOH+NaOH	TGA CdTe	0.56	0.25	170	230
	[a]EtOH+NaOH	ME CdTe	0.56	0.44	170	160
ZnTCPc (29)	[a]EtOH+NaOH	TGA CdTe	0.50	0.53	600	1300
	[a]EtOH+NaOH	ME CdTe	0.50	0.34	600	730
ZnOCPc (30)	[a]EtOH+NaOH	TGA CdTe	0.75	0.63	140	190
	[a]EtOH+NaOH	ME CdTe	0.75	0.72	140	130
TmTPyZnPc (31b)	[b]Pyr + H_2O	TGA CdTe	0.78	0.80	30	360
TMmTAAZnPc (36)	[a]EtOH+NaOH	MPA CdTe	0.54	0.71	160	260
OMmTAAZnPc (37)	[a]EtOH+NaOH	MPA CdTe	0.67	0.84	50	120
TMPAZnPc (39d)	[c]DMSO	MPA CdTe	0.88	0.94	230	210
	[c]DMF	MPA CdTe	0.61	0.67	320	180
	[a]EtOH+NaOH	MPA CdTe	0.63	0.80	13	188
TtfmPyZnPc (40)	[d]DMSO	MPA CdTe	0.74	0.88	210	262
	[d]Pyridine	MPA CdTe	0.76	0.88	11	184
TtfmMPyZnPc (41)	[d]DMSO	MPA CdTe	0.86	0.88	140	263
	[d]Pyridine	MPA CdTe	0.83	0.90	5	119
THdTZnPc (42)	DMSO	AuNPs	0.67	0.80[e]	76	84[e]
	DMF	AuNPs	0.63	0.75[e]	210	304[e]

[a]Represents a (1:1) ethanol:NaOH (0.01 M) solvent mixture and [b]Represents a (1:1) pyridine:water solvent mixture, [c]Represents the solvents DMSO and DMF with ~ 10 % water, [c]Represents the solvents DMSO and pyridine with ~ 1 % water, [e]The values are for the 42-AuNP conjugate.

A considerable increase of the Φ_T and τ_T values in the presence of the MPA CdTe QDs was also observed for both TMmTAAZnPc (**36**) and OMmTAAZnPc (**37**). It was observed that TMPAZnPc (**39d**) showed an increase in the Φ_T values in DMSO, DMF and the aqueous solvent mixture employed in the presence of MPA CdTe QDs. The τ_T values for complex **39d** in the mixture with QDs decreased slightly in DMSO and DMF but they showed a significant increase (in the 1:1 ethanol:NaOH 0.01M solvent mixture). Complexes **40** (TtfmPyZnPc) and **41** (TtfmMPyZnPc) both exhibited enhanced Φ_T and τ_T values in both DMSO and pyridine. The increase of τ_T values was more significant in pyridine than in DMSO as observed in Table 5.5. In addition to the results obtained for the different MPcs in the presence of CdTe QDs, studies were also carried out on complex THdTZnPc (**42**) and the conjugate of complex **42** and AuNPs (**42**-AuNP) (Table 5.5). As observed from Table 5.5 complex **42** in the **42**-AuNP conjugate displayed fairly enhanced Φ_T values and slightly increased τ_T values in DMSO and fairly increased τ_T values in DMF.

The lack of increase of Φ_T values in some complexes (**28**, **29** and **30**) despite the heavy atom effect is surprising but has been encountered in literature for some MPc complexes [131,202]. The mechanism behind the increase observed for τ_T values is not known. It is possible that the complex formed (either by adsorptive forces or electrostatic forces) from the binding of MPcs on to QDs could help stabilize the triplet state of the MPcs in the complex thereby allowing the MPcs to stay longer in the triplet state. These enhanced triplet lifetime values of MPcs in the presence of QDs are desirable as they would allow the excited MPc molecules to stay longer in the triplet state thereby allowing for increased collisional and diffusional interactions between the MPc molecules and ground state molecular oxygen ($^3O_2$) molecules. These interactions would in turn result in a greater production of singlet oxygen ($^1O_2$) which is necessary for photosensitized reactions. The data listed in Table 5.5 suggests that the use of MPc complexes in combination with nanoparticles would enhance the photosensitizer properties of MPcs significantly. These strengthened

photosensitizing properties would thus make for remarkable photosensitizer candidates in PDT.

5.4 Fluorescence Lifetimes of CdTe QDs in the presence of MPcs

Time resolved luminescence measurements of CdTe QDs in the absence and presence of MPc complexes may result in either biexponetial or triexponential decay kinetics [62-64]. The fluorescence lifetime measurements were carried out for the QDs in the presence of neutral, positively charged or negatively charged MPc complexes in different solvents. It has been generally suggested that the longer fluorescence lifetimes of QDs result from electron-hole recombination from the surface defects (states) while the shorter lifetimes are attributed to recombination in the core states of the QDs [62,63]. In general a higher amplitude gave an indication of a greater population of the particular recombinant species in solution. Generally biexponential decay kinetics for the QDs were observed in the presence of positively charged MPcs **34** and **35**, and also for the quaternizable complexes **40** and **41** in all the solvents employed for the studies. Table 5.6 shows the data obtained for the interactions between the QDs and quaternized MPc complexes (Cl)GaTmTMPyPc (**34**) and (Cl)InTmTMPyPc (**35**) in DMSO and in the (1:1) ethanol:water solvent mixture.

The data in Table 5.6 shows lowering of the longer lifetime (τ_{F1}) of the QDs in both aqueous media (from 25.4 ns to 15.3 ns and 6.4 ns) and DMSO (from 32.0 ns to 30.6 ns and 17.7 ns) upon addition of complexes **34** and **35** respectively indicating that the surface states are involved in the quenching process, with complex **35** resulting in greater quenching effects in both solvents. The QDs alone in solution showed a greater abundance for the τ_{F1} species, but the addition of MPc complexes **34** and **35** to the QDs resulted in τ_{F2} species becoming the one with greater abundance in aqueous solution. In DMSO the τ_{F1} species of QDs has a greater abundance in both the absence and presence of QDs. There was slight reduction of the shorter lifetimes (τ_{F2}) for the mixture of MPcs and QDs in DMSO (no change was observed in aqueous media)

suggesting the interaction between the complexes **34** and **35** only mildly affects recombination from the core states.

Table 5.6: Fluorescence lifetime measurements from interactions between CdTe-MPA QDs and complexes (Cl)GaTmMPyPc (34) and (Cl)InTmMPyPc (35) (in DMSO and aqueous solution {(1:1) ethanol:water }, LED excitation source).

Sample	Solvent	[a] τ_{F1} (ns)	[a] τ_{F2} (ns)	[b] α_1	[b] α_2
[d]MPA QDs	EtOH:H_2O	25.4 ± 0.2	1.4± 0.2	0.86	0.14
(Cl)GaTmTMPyPc (34) + MPA QDs	EtOH:H_2O	15.3 ± 0.2	1.4± 0.05	0.30	0.70
(Cl)InTmTMPyPc (35) + MPA QDs	EtOH:H_2O	6.4± 0.2	1.4± 0.05	0.15	0.85
[d]MPA QDs	[c]DMSO	32.0 ± 0.2	4.6 ± 0.3	0.78	0.22
(Cl)GaTmTMPyPc (34) + MPA QDs	[c]DMSO	30.6 ± 0.2	3.9 ± 0.2	0.78	0.22
(Cl)InTmTMPyPc (35) + MPA QDs	[c]DMSO	17.7 ± 0.3	3.4± 0.1	0.56	0.44

[a] fluorescence lifetimes at MPA-QD emission, [b]α denotes the amplitude fraction, [c]Represents DMSO with ~ 10 % water, [d]The MPA QDs size = 4.54 nm.

Table 5.7 shows the data obtained for fluorescence lifetime measurements of QDs in the mixture with complexes neutral complexes **40** and **41**. The measurements taken in pyridine show reduction of the longer lifetime τ_{F1} of the QDs (from 18.4 ns to 13.3 ns and 14.2 ns respectively) upon addition of complexes TtfmPyZnPc (**40**) and TtfmMPyZnPc (**41**) indicating that the surface states are involved in the quenching process. In pyridine, the QD lifetimes in the absence and the presence of complexes **40** and **41** had a larger population of the τ_{F2} species of the QDs (shorter fluorescence lifetimes). The shorter lifetimes in pyridine were also slightly reduced in the presence of the MPcs as shown in Table 5.7. However, in DMSO there was no apparent quenching of the QDs fluorescence lifetime in the presence of the MPc complexes **40** and **41**. The τ_{F1} species of QDs (longer

fluorescence lifetimes) were more predominant for studies in DMSO. There was an apparent lack of change for the lifetime values in DMSO in the presence of complexes **40** and **41**. This observation may be attributed to the very weak signal of the quenched QDs.

Table 5.7: Fluorescence lifetime measurements from interactions between TtfmPyZnPc (40), TtfmMPyZnPc (41) complexes and CdTe-MPA QDs (in pyridine and DMSO with 1% water, LED excitation source).

Sample	Solvent	[a] τ_{F1} (ns)	[a] τ_{F2} (ns)	[b] α_1	[b] α_2
[c]MPA QDs	Pyridine	18.4 ±0.2	4.0 ±0.2	0.47	0.53
TtfmPyZnPc (40) + MPA QDs	Pyridine	13.3 ±0.3	3.1 ±0.1	0.37	0.63
TtfmMPyZnPc (41) + MPA QDs	Pyridine	14.2± 0.5	3.3 ± 0.2	0.34	0.66
[c]MPA QDs	DMSO	34.0 ±1.2	3.7 ±0.7	0.75	0.25
TtfmPyZnPc (40) + MPA QDs	DMSO	33.3 ±0.8	4.0 ±0.5	0.60	0.40
TtfmMPyZnPc (41) +MPA QDs	DMSO	34.1 ±1.5	3.8 ±0.4	0.65	0.35

[a] fluorescence lifetimes at MPA-QD emission, [b] α denotes the fraction of the amplitude, [c]The MPA QDs size = 4.54 nm.

Studies carried out with negatively charged MPc complexes TMmTAAZnPc (**36**), OMmTAAZnPc (**37**) and TMPAZnPc (**39d**) showed similar quenching behaviour to that of the positively charged and neutral MPcs (**34**, **35**, **40** and **41**) upon addition of these complexes to the QDs solution. Table 5.8 shows the data obtained for complexes **36** and **37** in the (1:1) pyridine:NaOH 0.01M solvent mixture. The MPA QDs showed biexponential decay kinetics for the study with these complexes. A reduction in the longer lifetime (τ_{F1}) was observed for **36** and **37** (from 30.3 ns to 19.0 ns and 21.4 ns respectively) in the aqueous solvent mixture employed, Table 5.8. The shorter lifetime (τ_{F2}) was also reduced (from 8.4 ns to 4.7 ns and 2.0 ns) in the

presence of **36** and **37** respectively. The fact that both the long and short lifetimes of QDs are reduced in the presence of complexes **36** and **37** indicates that the quenching process affects the recombination within both the core and surface states. A greater abundance for the τ_{F1} species of the QDs was observed for the QDs alone but the addition of MPc complexes **36** and **37** to the QDs resulted in τ_{F2} species becoming the one with greater abundance in the aqueous solvent mixture.

Table 5.8: Fluorescence lifetime measurements from interactions between TmMTAAZnPc (36), OmMTAAZnPc (37) complexes and CdTe-MPA QDs (in a (1:1) Pyridine:NaOH 0.01M solvent mixture, LED excitation source).

Sample	Solvent	[a]τ_{F1} (ns)	[a]τ_{F2} (ns)	[b]α_1	[b]α_2
[c]MPA QDs	Pyr:NaOH	30.3±0.5	8.4±0.6	0.64	0.36
TMmTAAZnPc (36) + MPA QDs	Pyr:NaOH	19.0±0.9	4.7±0.3	0.47	0.53
OMmTAAZnPc (37) + MPA QDs	Pyr:NaOH	21.4±1.9	2.0±0.3	0.30	0.70

[a] fluorescence lifetimes at MPA-QD emission, [b] α denotes the fraction of the amplitude, [c]The MPA QDs size = 4.54 nm.

Triexponential decay kinetics were observed for QDs (alone and in the presence of TMPAZnPc (**39d**)) in Table 5.9, possibly because a different excitation source (laser) was used thus resulting in greater resolution and higher accuracy. As stated before, the shorter lifetimes (τ_{F3}) are attributed to the carrier recombination within the core states while the much longer lifetimes (τ_{F1}) are assigned for the carrier recombination processes in the surface defects sites [64]. The intermediate fluorescence lifetime component (τ_{F2}) is assigned to the radiative electron-hole recombination processes at the surface states [64]. The average amplitude weighted lifetimes (τ_{av}) were calculated and are shown in Table 5.9. The τ_{av} values (of QDs alone or in the presence of complex **39d**) in DMSO were observed to be the lowest compared to those in the other solvents used. There was a decrease in the lifetimes τ_{F1}, τ_{F2} and τ_{F3} of QDs in the

presence of complex **39d** in all solvents used. The τ_{F1} species of the QDs was in greater abundance for QDs alone than in the presence of **39d** for all solvents. In the ethanol:NaOH 0.01M solvent mixture, the τ_{F1} species of the QDs (for quantum dots alone) was more abundant than the τ_{F2} and τ_{F3} species of the QDs before addition of **39d**. When **39d** was added to the QDs, the τ_{F2} and τ_{F3} species of the QDs become more abundant in the aqueous solvent mixture.

Table 5.9: Fluorescence lifetime measurements from interactions between MPA CdTe QDs and TMPAZnPc (39d) (in DMSO and DMF with 10% water and {(1:1) ethanol: 0.01M NaOH}, laser excitation source).

Sample	[a]τ_{F1} (ns)	[b]α_1	[a]τ_{F2} (ns)	[b]α_2	[a]τ_{F3} (ns)	[b]α_3	τ_{av} (ns)
[c]MPA QDs (DMSO)	30.9± 0.9	0.07	11.5 ±0.1	0.43	2.1± 0.04	0.51	8.1
TMPAZnPc (39d) +MPA QDs (DMSO)	14.1± 0.1	0.03	2.4± 0.05	0.03	0.02±0.001	0.95	0.5
[c]MPA QDs (DMF)	32.6± 0.3	0.33	7.2 ± 0.1	0.46	1.7 ± 0.1	0.21	14.4
TMPAZnPc (39d) +MPA QDs (DMF)	9.0 ± 0.1	0.04	2.2± 0.03	0.17	0.4± 0.03	0.79	1.1
[c]MPA QDs ((1:1) EtOH:NaOH)	24.3± 0.2	0.63	17.6 ±0.9	0.11	1.6 ± 0.1	0.26	17.7
TMPAZnPc(39d)+MPA QDs (EtOH:NaOH)	12.8±0.07	0.27	2.6± 0.05	0.27	0.3± 0.02	0.46	4.3

[a] fluorescence lifetimes at MPA-QD emission, [b]α denotes the amplitude fraction, [c]The MPA QDs size = 4.1 nm.

The data shown in Tables 5.6 to 5.9 shows differences in the lifetimes of the MPA CdTe QDs in various solvents. It was also noted that the QDs lifetimes seemed to vary even in more or less the same solvent system e.g. lifetimes in DMSO in tables 5.6, 5.7 and 5.9. The slight differences observed may however be acceptable for two reasons. QD lifetimes are highly dependent on factors such as the size of the

nanoparticle, capping agent, and the solvent employed. The capping agent employed was the same for all the lifetime measurements taken and was thus not an influential factor for the differences observed. On the other hand, the size of the QDs used was the same for Tables 5.6, 5.7 and 5.8 (4.54 nm) but different for Table 5.9 (4.1 nm). As a result, the difference in QD lifetimes in DMSO for Table 5.9 (30.9 ns) compared to those in Table 5.6 (32.0 ns) and Table 5.7 (34.0 ns) could possibly be due to the difference in size of the QDs employed. The second reason for the differences in lifetimes observed in Tables 5.6, 5.7 and 5.9 stems from the fact that even though the main composition of the solvent used was DMSO, it had varying water content (for dissolution of QDs) in each of the Tables. In Table 5.6, DMSO contained ~ 10% water, while in Table 5.7, DMSO had a 1 % water content, and in Table 5.9 the water content was also ~ 10% but the size of the QDs used was different from that employed in the rest of the lifetime studies. The lifetimes were also different in the aqueous solvent mixtures but the content of the aqueous solvent mixtures was also different for Table 5.8 ((1:1) pyridine:water) compared to that in Table 5.6 and 5.9 (both (1:1) ethanol:NaOH). The QD lifetimes in Table 5.6 (25.4 ns) and Table 5.9 (24.3 ns) were very close to each other but siginificantly different from that in Table 5.8 (30.3 ns). The difference in lifetime values from Table 5.6 (biexponential kinetics) and 5.9 (triexponential kinetics) is due to the use of the LED excitation source (less resolution) in Table 5.6 compared to the laser excitation source (higher resolution) used in Table 5.9 allowing for the observation of the short lifetime τ_{F3}.

5.5 Conclusions

This work shows results of the interaction between CdTe QDs and water soluble MPcs. The results herein indicate that the photophysicochemical properties of both the negatively charged and the positively charged MPcs are enhanced in the mixture with CdTe QDs. As a result the combined use of QDs and MPcs is shown to lead to improved photosensitizers with potential applications in photodynamic therapy of cancer. Interactions between positively charged MPcs and QDs lead to clear ring

reduction in the case of TmTPZnPz (**27b**) and formation of ion-pair complexes with TmTMPyZnPc (**32b**), (Cl)GaTmTMPyPc (**34**) and (Cl)InTmTMPyPc (**35**) suggestive of possible reduction of the quaternized mercaptopyridine substituent. The formation of these ion-pair clusters between the negatively charged QDs and the quaternized complexes **32b**, **34** and **35** also resulted in aggregation most likely fostered by the electrostatic forces between the MPcs and QDs. FRET was observed for all the negatively charged MPcs (**28**, **29**, **30**, **36**, **37** and **39d**) showing monomeric behaviour in solution but it was also observed for the positively charged complex **31b** and the neutral quaternizable complexes **40** and **41** in organic solvents (DMSO and pyridine). The FRET photoprocess resulted in quenched QD fluorescence lifetimes. The complex **42** was successfully linked to the AuNPs leading to the formation of the **42**-AuNP conjugate which showed improved photophysicochemical properties.

General Conclusions and Future Prospects

6

This chapter reviews results for all the syntheses, and the studies carried out for the purpose of this thesis. It also includes plans for future work.

6.1 General Conclusions

The negatively charged phthalocyanines synthesized in this work have the following substituents on the peripheral (β) position of the respective MPc ring (with MPc central metal ions in brackets): sulfonate (Zn^{2+}), carboxy (Zn^{2+}), 2-mercapto-5-methylthiazole aceticacid (Zn^{2+}), mercaptoacetic acid (Ga^{3+}, In^{3+}, Si^{4+} and Zn^{2+}) and 3-mercaptopropionic acid (Ga^{3+}, In^{3+}, Si^{4+} and Zn^{2+}). Positively charged complexes on the other hand were obtained by quaternization of the following substituent groups: 2-hydroxypyridine (Zn^{2+}), 2-mercaptoyridine (Ga^{3+}, In^{3+}, Si^{4+}, Sn^{4+} and Zn^{2+}) and a pyridinium ring replacing a benzene ring for the porphyrazine complex (Zn^{2+}). The water-soluble MPcs were found to be highly aggregated in water or basic aqueous media (except for ZnOCPc, **30**), but this aggregation was counteracted by the use of organic solvents like ethanol, methanol and pyridine. The use of surfactants such as Triton-X 100 was also observed to break the aggregation of these MPc complexes. Novel MPcs synthesized with the 2-mercaptopyridine substituent and Ga^{3+}, In^{3+}, Si^{4+} and Sn^{2+} as the central metal ions are organic media soluble.

All the MPcs synthesized displayed intense absorption in the visible/near IR region. The photophysicochemical properties of the synthesized MPc complexes in organic and aqueous media were investigated and are reported in this work. Results obtained for the photophysicochemical properties indicate that these properties are highly reliant on the central metal of the MPc, but they also (to some degree) depend on the substituent and the solvent used for the studies. The photophysical properties of the metallophthalocyanines were also shown to show significant improvement in the presence of nanoparticles (CdTe QDs and AuNPs). Furthermore the triplet lifetime of the MPcs in the presence of nanoparticles was also considerably enhanced in some cases. MPcs containing large central metal ions such as Sn^{2+} and In^{3+} (for complexes **33b** and **33d**) were found to show loss of symmetry on excitation in the solvents DMF and DMSO.

Förster resonance energy transfer was observed for all the negatively charged MPcs showing monomericity in solution as suggested by the stimulated emission of the

respective MPc in solution with QDs. However FRET was also observed for the positively charged complex **31b** and the neutral complexes **40** and **41** in organic media such as DMSO, DMF and pyridine. The MPc-QD complexes that showed similar r and R_0 values generally exhibited the highest FRET efficiencies. Quenching of the QD emission was observed to be brought about by either adsorptive or electrostatic interactive forces between QDs and MPcs. In addition to these forces, the QD emission was also shown to be quenched by the occurrence of FRET. The time correlated single photon counting fluorescence lifetime measurements gave the indication that surface states were deeply involved in the interaction with MPcs, and also in the quenching of the QD lifetimes (either due to FRET or pure quenching processes).

6.2 Future Prospects

A lot of debate has gone into the use of nanoparticles in biomedical applications, with the toxicity of these materials as the issue of prime concern. The development of 'less toxic' or biocompatible nanoparticles could solve this current problem. It is also of great importance that such biocompatible nanoparticles be designed and synthesized so that they afford magnetic, photophysicochemical and imaging properties that may be exploited in treatments such as hyperthermia therapy, photothermal therapy or PDT. Since it is imperative that MPcs that serve as outstanding photosensitizers be able to reach the target site (in appreciable quantities) in any form of treatment, the conjugation of such MPcs to antibodies or amino acids specific to the respective site needs to be closely studied so as to foster the efficiency of treatments. In addition, MPc complexes can be designed and synthesized that will show high photoluminescence, monomeric behaviour in aqueous media and appreciable photoactivity.

References

[1] D. Gerion, F. Pinaud, S. C.Williams, W. J. Parak, D. Zanchet, S. Weiss, P.Alivisatos. *J. Phys. Chem.B.,* **105** (2001) 8861.

[2] O. I. Micic, J. Nozik, T. Rajh. *J. Phys. Chem.,* **97** (1993) 1199.

[3] S. Nie, A. M, Smith. *Analyst.,* **129** (2004) 672.

[4] N. Gaponik, V. D. Talapin, K. Hoppe, E.V. Shevchenko, A. Kornowski, A. Eychmuller, H. Weller. *J. Phys. Chem. B.,* **106** (2002) 7177.

[5] R. E. Bailey, A. M. Smith, S. Nie. *Physica E.,* **25** (2004) 1.

[6] Z. Lin, S. Cui, H. Zhang, Q. Chen, B. Yang, X. Su, J. Zhang, Q. Jin. *Anal. Biochem.,* **319** (2003) 239.

[7] N. Kaji, M. Tokeshi, Y. Baba. *Anal. Scie.,* **23** (2007) 21.

[8] W. C.W. Chan, D. J. Maxwell, X. H. Gao, R. E. Bailey, M. Y. Han, S. M. Nie, *Curr. Opin. Biotechnol.,* **13** (2002) 40.

[9] Y. Bae, N. Myung, A. J. Bard, *Nano Lett.,* **4** (2004) 1153.

[10] P. Nasser, S. W. Koch, A. Mysrowicz, *in Introduction to Semiconductor Optics*. Englewood Cliffs, Prentice Hall, (1993).

[11] W. Schroter, in *Handbook of semiconductor technology, electronic structure and properties of semiconductors*, Wiley VCH, Weinheim, (2000).

[12] V. I. Klimov, *Los Alamos Science.,* **28** (2003) 214.

[13] J. A. Hollingsworth, V. I. Klimov, *in Semiconductor and Metal Nanocrystals: Synthesis and Electronic and Optical Properties*, V. I. Klimov (Ed.), Marcel Dekker, New York. (2004) p1-64.

[14] A. P. Alivisatos, *J. Phys. Chem.,* **100** (1996) 13226.

[15] B. Rogers, S. Pennathur, J. Adams, *in Nanotechnology: Understanding small systems*, CRC Press, Taylor and Francis Group, Boca Raton, (2008).

[16] A. Eychmuller, A. L. Rogach, *Pure Appl. Chem.,* **72** (2000) 179.

[17] L. Qu, X. Peng, *J. Am. Chem. Soc.,* **124** (2002) 2049.

[18] H. Zhang, L. Wang, H. Xiong, L. Hu, B. Yang, W. Li, *Adv. Mater.*, **15** (2003) 1712.

[19] A. Shavel, N. Gaponik, A. Eychmuller, *J. Phys. Chem. B.*, **110** (2006) 19280.

[20] U. R. Genger, M. Grabolle, S. C. Jaricot, R. Nitschke, T. Nann, *Nature Methods.*, **5** (2008) 763.

[21] A. L. Rogach, *Mat. Scie. Eng. B.*, **435** (2000) 69.

[22] X. Gao, W. C. W. Chan, S. Nie, *J. Biomed. Optics.*, **7** (2002) 532.

[23] E. R. Goldman, I. L. Medintz, H. Mattoussi, *Anal. Bioanal. Chem.*, **384** (2006) 560.

[24] R. Bakalova, H. Ohba, Z. Zhelev, M. Ishikawa, Y. Baba, *Nature Biotech.*, **22** (2004) 1360.

[25] A. C. S. Samia, X. Chen, C. Burda, *J. Am. Chem. Soc.*, **125** (2003) 15736.

[26] R. Bonnet, *Chem. Soc. Rev.*, (1995) 19.

[27] L. Goldstein, F. Glas, J. Y. Marzin, M. N. Charasse, G. L. Roux, *Appl. Phys. Lett.*, **47** (1985) 1099.

[28] C. Grigoriu, Y. Kuroki, I. Nicolae, X. Zhu, M. Hirai, H. Suematsu. M. Takata. K. Yatsui. *J. Opt. Adv. Mater.*, **7** (2005) 2979.

[29] C. B. Murray, C. R. Kagan, M. G. Bawendi, *Ann. Rev. Mater. Sci.*, **30** (2000) 545.

[30] I. L. Medintz, H.T. Uyeda, E. R. Goldman, H. Mattoussi, *Nat. Mat.*, **4** (2005) 435.

[31] A. L. Rogach, D. S. Kotysh, M. Harrison, N. A. Kotov, *Chem. Mater.*, **12** (2000) 1526.

[32] A. L. Rogach, A. Kornowski, M. Gao, A. Eychmuller, H. Weller. *J. Phys. Chem. B.*, **103** (1999) 3065.

[33] Y. Chen, Z. Rosenzweig, *Anal. Chem.*, **74** (2002) 5132.

[34] N. Kumbhojkar, V. V. Nikesh. A. Kshirsagar, S. Mahamuni. *J. Appl. Phys.*, **88** (2000) 6260.

[35] E. M. Wong, J. E. Bonevich, P. C. Searson, *J. Phys,Chem. B.*, **102** (1998) 7770.

[36] S. Santra, K. M. Wang, R. Tapee, W. H. Tan, *J. Biomed. Opt.*, **6** (2001) 160.

[37] J. M. Tsay, M. Pflughoefft, L. A. Bentolila, S. Weiss, *J. Am. Chem. Soc.*, **126** (2004) 1926.

[38] F. Boulmedais, P. Bauchat, M. J. Brienne, I. Amal, F. Artzner, T. Gacoin, M. Dahan, V. M. Artzner, *Langmuir.,* **22** (2006) 9797.

[39] A. M. Iga, J. H. P. Robertson, M. C. Winslet, A. M. Seifalian, *J. Biomed. Biotech.,* (2007), doi:10.1155/2007/76087.

[40] M. Brust, M. Walker, D. Bethell, D. J. Schffrin, R. Whyman, *J. Chem. Soc. Chem. Commun.,* (1994) 801.

[41] W. Li, Q. X. Jia, H. L. Wang, *Polymer.,* **47** (2006) 23.

[42] Y. Tan, X. Dai, Y. Li, D. Zhu, *J. Mater. Chem.,* **13** (2003) 1069.

[43] K. S. Kim, D. Demerelnyamba, H. Lee, *Langmuir.,* **20** (2004) 556.

[44] M. De Graef, in Introduction to Conventional Transmission Electron Microscopy, Cambridge University Press, (2003).

[45] C. T. K. -H. Stadtländer, in Modern Research and Educational Topics in Microscopy., A. Mèndez and J. Diaz (Eds), (2007) p122.

[46] L. Cheng, X. Liu, J. Lei, H. Ju, *Anal. Chem.,* **82** (2010) 3359.

[47] X. Wang, J. Zhuang, Q. Peng, Y. Li, *Nature.,* **437** (2005) 121.

[48] M. J. Murcia, D. L. Shaw, H. Woodruff, C. A. Naumann, B. A. Young, E. C. Long, *Chem. Mater.,* **18** (2006) 2219.

[49] Q. Zhang, T. Atay, J. R. Tischler, M. S. Bradley, V. Bulović, A. V. Nurmikko, *Nature nanotech.,* **2**, (2007), 555.

[50] W. W. Yu, L. Qu, W. Guo, X. Peng. *Chem. Mat.,* **15** (2003) 2854.

[51] S. Sapra, and D. D. Sarma, *Pramana.,* **65 (**2005) 565.

[52] A. L. Patterson, *Phys. Rev.,* **56** (1939) 978.

[53] W. Chidawanyika, C. Litwinski, E. Antunes, T. Nyokong, *J. Photochem. Photobiol A. Chem.,* **212** (2010) 27.

[54] Y. Wang, N. Herron, *J. Phys. Chem.,* **95** (1991) 525.

[55] M. Kuno, J. K. Lee, B. O. Dabbousi, F. V. Mikulec, M. G. Bawendi, *J. Chem. Phys.,* **106** (1997) 9869.

[56] L.S. Li, J. Hu, W. Yang, A. P. Alivisatos, *Nano Lett.,* **1** (2001) 349.

[57] C. B. Murray, D. J. Norris, M. G. Bawendi, *J. Am. Chem. Soc.,* **115** (1993) 8706.

[58] A. L. Rogach, L. Katsikas, A. Kornowski, D. Su, A. Eychmuller, H. Weller. *Ber. Bunsenges. Phys. Chem.,* **100** (1996) 1772.

[59] J. Guo, W. Yang, C. Wang, *J. Phys. Chem.,* **109** (2005) 17467.

[60] S. Dayal, C. Burda, *J. Am.Chem. Soc.,* **129** (2007) 7977.

[61] S. F. Wuister, I. Swart, F. van Driel, S. G. Hickey, C. M. Donega, *Nano Lett.,* **3** (2003) 503.

[62] M. G. Bawendi, P. J. Carroll, W. L. Wilson, L. E. Brus, *J. Chem. Phys.,* **96** (1992) 946.

[63] S. J.Byrne, B. le Bon, S. A. Corr, M. Stefanko, C. O'Connor, Y. K. Gun'ko, Y. P. Rakovich, J. F. Donegan, Y. Williams, Y. Volkov, P. Evans, *ChemMedChem.*, **2** (2007) 183.

[64] S. Mikel, A. Miguel, D. Correa, M. L. Luis, D. Abderrazzak, *J. Photochem. Photobiol. A:Chem.*, **196** (2008) 51.

[65] S. K. Poznyak, N. P. Osipovich, A. Shavel, D. V. Talapin, M. Gao, A. Eychmüller,

N. Gaponik. *J. Phys. Chem. B.*, **109** (2005) 1094.

[66] H. Peng, L. Zhang, C. Soeller, J. T. Sejdic, *J. Lumin.*, **127** (2007) 721.

[67] C. Querner, P. Reiss, S. Sadki, M. Zagorska, *A. Pron. Phys. Chem. Chem. Phys.,* **7** (2005) 3204.

[68] A. von Braun, J. Tscherniac, *Ber. Deut. Chem. Ges.,* **40** (1907) 2709.

[69] H. De Diesbach, E. von der Weid, *Helv. Chim. Acta.,* **10** (1927) 886.

[70] L. R. Milgrom, In *The colours of life: An introduction to the chemistry of porphyrins and related compounds*, Oxford University Press, (1997).

[71] R. P. Linstead, *J. Chem. Soc.,* (1934) 1016.

[72] R. P. Linstead, A. R. Lowe, *J. Chem. Soc.,* (1934) 1022.

[73] C. E. Dent, R. P. Linstead, *J. Chem. Soc.,* (1934) 1033.

[74] N. B. McKeown, *Chem. Ind.,* (1999) 92.

[75] J. M. Robertson, *J. Chem. Soc.,* (1936) 1195.

[76] J. D. Spikes, *J. Photochem. Photobiol. B.,* **6** (1990) 259.

[77] J. Zagal, F. Bedioui: N4-macrocyclic metal complexes, J. P. Dodelet (Eds)

Springer, New York (2006).

[78] K. I. Ozoemena, T. Nyokong, *In: Encyclopedia of Sensors,* C.A. Grimes, E.C. Dickey, M.V. Pishko (Eds.), American Scientific Publishers, California, Vol. **3**, (2006), p. 157 (Chapter E, and references therein).

[79] S. Griveau, J. Pavez, J.H. Zagal, *J. Electroanal. Chem.,* **497** (2001) 75.

[80] P. Tau, T. Nyokong, *J. Mol. Catal. A. Chem.,* **273** (2007) 149.

[81] D. Worhle, O. Suvorova, R. Gerdes, O. Bartels, L. Lapok, N. Baziakina, S. Makarov, A. Slodek. *J. Porphyrins Phthalocyanines.,* **8** (2004) 1020.

[82] M. F. Joseph, J.K. Thomas, V.E. Sven, *J. Am. Chem. Soc.*, **121** (1999) 3453.

[83] W. S. Struve, *J. Phys. Chem. B.*, **103** (1999) 6835.

[84] G. De la torre, C.G. Claessens, T. Torres, *Chem. Commun.,* (2007) 2000.

[85] M. Durmuş, S. Yeşilot, V. Ahsen, *New J. Chem.,* **30** (2006) 675.

[86] M. Bouvet, in: K. Kadish, K. M. Smith, R. Guilard (Eds.), The Porphyrin Handbook, Academic Press, Boston, Vol. **19**, (2003) pp. 37-104.

[87] M. S. Wesley, E. V. Johan, M. A. Cynthia, *Adv. Drug Deliv. Rev.,* **56** (2004) 53.

[88] M. W. Cecilia, H. S. Taroh, X. Liang-yan, H. G. Nahida, L. O. Nancy, *Cancer Lett.,* **179** (2002) 43.

[89] J. Levy, *Photochem. Photobiol.*, **64** (1996) 737.

[90] D.G. Hilmey, M. Abe, M. I. Nelen, C. E.Stilts, G. A.Baker, S. N. Baker, F. V. Bright, S. R. Davies, S.O. Gollnick, A. R. Oseroff, S. L. Gibson, R. Hilf, M. R.J. Detty, *Med. Chem.,* **45** (2002) 449.

[91] R. Bonnet, In *Chemical Aspects of Photodynamic Therapy*, Gordon and Breach Science Publishers, Amsterdam, (2000).

[92] R. R. Allison, G. H. Downie, R. Cuenca, X. H. Hu, C. J. H. Childs, C. H. Sibata, *Photodiagnosis and Photodynamic Therapy.,* **1** (2004) 27.

[93] T. Torres, *J. Porphyrins Phthalocyanines.,* **4** (2000) 325.

[94] M. J. Stilman, T. Nyokong, In Phthalocyanines*: Properties and Applications,* C. C. Leznoff, A. B. P. Lever (Eds), VCH Publishers, New York, Vol.**1** (1989).

[95] E. Ben-Hur, W.S. Chan, *In Porphyrin Handbook: phthalocyanine properties and materials*, Kadish KM, Smith KM, Guilard R (eds), Academic Press, New York,Vol. **19** (2003) Chp.117.

[96] T. Fukuda, K. Ono, S. Homma, *N. Kobayashi, Chem. Lett.,* **32** (2003) 736.

[97] M. L. Friedel, B. F. Hoskins, R. L. Martin, S. A. Mason, *J. Chem. Soc., Chem. Commun.* (1970) 400.

[98] G. P. Moss, Eur. *J. Biochem.,* **178** (1988) 277.

[99] G. P. Moss, *Pure Appl. Chem.,* **59** (1987) 779.

[100] K. Kasuga, M. Tsutsui, *Coord. Chem. Rev.,* **32** (1980) 67.

[101] D. Wöhrle, G. Schnurpfeil, G. Knothe., *Dyes and Pigments.,* **18** (1992) 91.

[102] H. Shirai, A. Maruyama, K. Kobayashi, N. Hojo, *Makromol. Chem.,* **181** (1980) 575.

[103] F. Yilmaz, D. Atilla, V. Ahsen, *Polyhedron.,* **23** (2004) 1931.

[104] M. Brewis, M. Helliwell, N. B. McKeown, S. Reynolds, A. Shawcross, *Tetrahedron Lett.,* **42** (2001) 813.

[105] M. Hanack, M. Lang, *Adv. Mater.,* **6** (1994) 819

[106] N. B. McKeown, I. Chambrier, M. J. Cook, *J. Chem. Soc. Perkin Trans. I.,* (1990) 1169.

[107] H. Vollman In: *Chemistry of Synthetic Dyes,* K. Venkataraman (ed.), Academic Press, New York, (1971) 283.

[108] S. Foley, G. Jones, R. Luizzi, D. J. McGarvey, M. H. Perry, T. G. Truscott, *J. Chem. Soc., Perkin Trans. 2.,* (1997) 1725.

[109] M. Hanack, H. Heckmann, R. Polley, in *Houben-Weyl: Methods of Organic Synthesis,* M. Hanack (Ed.), Thieme, Stuttgart, Supplementary Vol. E9d (1997) p 717.

[110] C. C. Leznoff, S. M. Marcuccio, S. Greenberg, A.B.P. Lever, K. B. Tomer, *Can. J. Chem.,* **63** (1985) 623.

[111] F. Henari, A. Davey, W. Blau, P. Haisch, M. Hanack, *J.Porphyrins Phthalocyanines.,* **3** (1999) 331.

[112] W. J. Schutte, M. Sluyters-Rehbach, J. H. Sluyters, *J. Phys. Chem.,* **97** (1993) 6069.

[113] E. Palomares, M. V. Martinez-Diaz, S. A. Haque, T. Torres, J. R. Durrant, *Chem. Commun.,* (2004) 2112.

[114] M. Sommerauer, C. Rager, M. Hanack. *J. Am. Chem. Soc.,* **118** (1996) 10085.

[115] M. Gouterman, *J. Mol. Spectrosc.* **6** (1961) 138.

[116] A. G. Dandridge, H. A. E. Drescher, J. Thamas, *Scottish Dyes Ltd.,* (1929) GB322169.

[117] J. H. Weber, D. H. Busch, *Inorg Chem.,* **4** (1965) 469.

[118] K. Sakamoto, E. Ohno, *Prog. Org. Coating.,* **31** (1997) 139.

[119] R. W. Boyle, J. E. van Lier, *Synlett.,* (1993) 351.

[120] M. O. Liu, C. H.Tai, M. Z.Sain, A. T. Hu, F. J. Chou, *J. Photochem. Photobiol. A. Chem.,* **164** (2004) 131.

[121] M. Ambroz, A. Beeby, A. J. MacRobert, M. S. C. Simpson, R. K.Svensen, D. Phillips, *J. Photochem. Photobiol. B: Biol.,* **9** (1991) 87.

[122] S. V. Kudrevich, M. G. Galpern, J. E. van Lier, *Synthesis.,* (1994) 779.

[123] N. A. Wiedekehr, *J. Braz. Chem. Soc.,* **7** (1996)7.

[124] R. P. Linstead, E. G. Noble, J. M. Wright, *J. Chem. Soc.,* (1937) 911.

[125] K. Sakamoto, F. Shibamiya, *J. Jpn. Soc. Colour Mater.,* **59** (1986) 517.

[126] T. D. Smith, H. Livorness, H. Taylor, J. R. Pilbrow, G. R. Sinclair, *J. Chem. Soc. Dalton Trans.,* (1983) 139.

[127] J. G. Avila-Zàrraga, R. Martínez, *Syn. Commun.,* **31** (2001) 2177.

[128] M. P. De Filipis, D. Dei, L. Fantetti, G. Roncucci, *Tetrahedron Letters.,* **41** (2000) 9143.

[129] W. Chidawanyika, A. Ogunsipe, T. Nyokong, *New. J. Chem.,* **31** (2007) 377.

[130] N. Saydan, M. Durmuş, M. G. Dizge, H. Yaman, A. G. Gürek, E. Antunes, T. Nyokong, V. Ahsen, *J. Porphyrins Phthalocyanines.,* **13** (2009) 1.

[131] M. Idowu, J. –Y. Chen, T. Nyokong, *New J. Chem.,* **32** (2008) 290.

[132] J. Britton, E. Antunes, T. Nyokong, *Inorg. Chem. Commun.,* **12** (2009) 828.

[133] P. Margaron, R. Langlois, J. E. van Lier, S. Gaspard, *J. Photochem. Photobiol. B:Biol.,* **14** (1992) 187.

[134] S. Dayal, C. Burda, *J. Am. Chem. Soc.,* **130** (2008) 2890.

[135] M. Durmuş, T. Nyokong, *Polyhedron.,* **26** (2007) 2767.

[136] A.C. Tedesco, J.C.G. Rotta, C. N. Lunardi, *Curr. Org. Chem.,* **7** (2003) 187.

[137] K. Ishii, N. Kobayashi in: The Porphyrin Handbook. K.M. Kadish, K.M. Smith, R. Guilard, Eds. Elsevier, Vol **16** (2003) Chp. 1.

[138] D. C. Hone, P. I. Walker, R. E. Gowing, S. Fitzgerald, A. Beeby, I. Chambrier, M. J. Cook, D. A. Russell, *Langmuir.,* **18** (2002) 2985.

[139] A. Kotiaho, R. Lahtinen, A. Efimov, H. K. Metsberg, E. Sariola, H. Lehtivuori, N. V. Tkachenko, H. Lemmetyinen, *J. Phys. Chem.C.,* **114** (2010) 162.

[140] A. B. P. Lever, *Adv. Inorg. Radiochem.,* **7** (1965) 27.

[141] M. J. Stillman, A. J. Thomsom, *J. Chem.Soc. Faraday Trans,* II., **70** (1974) 790.

[142] J. Mack, M. J. Stillman, *J. Am. Chem. Soc.,* **116** (1994) 1292.

[143] J. R. Darwent, P. Douglas, A. Harriman, G. Porter, M. C. Richoux, *Chem. Rev.,* **44** (1982) 83.

[144] T. Nyokong, Z. Gasyna, M. J. Stillman, *Inorg. Chem.,* **26** (1987) 1087.

[145] A. B. P. Lever, S. R. Pickens, P. C. Minor, S. Licoccia, B. S. Ramaswamy, K. Magnell, *J. Am. Chem. Soc.,* **103** (1981) 6800.

[146] A. M. Schaffer, M. Gouterman, E. R. Davidson. *Theoret. Chim. Acta,* **30** (1973) 9.

[147] Gouterman, G. H. Wagniere, L. C.Snyder, *J. Mol. Spectrosc.,* **11** (1963) 108.

[148] T. Fukuda, S. Homma, N. Kobayashi, *Chem. Eur. J.,* **11** (2005) 5205.

[149] N. Kobayashi, N. Sasaki, Y. Higashi, T. Osa, *J. Inorg. Chem.,* **34** (1995) 1636.

[150] N. Kobayashi, H. Ogata, N. Nonaka, E. A. Luk'yanets, *Chem. Eur. J.,* **9** (2003) 5123.

[151] N. Kobayashi, N. Konami, *In Phthalocyanines: Properties and Applications,* C. C. Leznoff, A. B. P. Lever, VCH Publishers, New York, Vol. **4** (1999) 343.

[152] A. Ogunsipe, D. Maree, T. Nyokong, *J. Mol. Struct.,* **650** (2003) 131.

[153] A. R Monahan, J. A. Brado, F.A. DeLuca, *J. Phys. Chem.,* **76** (1972) 446.

[154] Z. A. Schelly, R. D. Farina, E. M. Eyring, *J. Phys. Chem.,* **74** (1970) 617.

[155] S. Dhami, D. Phillips, *J. Photochem. Photobiol. A. Chem.,* **100** (1996) 77.

[156] Z. A. Schelly, D. J. Howard, P. Hemmes, E. M. Eyring, *J. Phys. Chem.,* **74** (1974) 3040.

[157] R. B. Ostler, A. D. Scully, A. G. Taylor, I. R. Gould, T. A. Smith, A. Waite, D. Phillips, *Photochem. Photobiol.,* **71** (2000) 397.

[158] H. Abramczyk, I. Szymczyk, G. Waliszewska, A, Lebioda, *J. Phys. Chem.,* **108** (2004) 264.

[159] E. Coates, *J. Soc. Dyers. Col.,* **85** (1969) 355.

[160] K. Bernauer, S. Fallab, Fasciculus VII XLV (1962) 2487.

[161] A. Skorobogaty, T. D. Smith, G. Dougherty, J. R. Pilbrow, *J. Chem. Soc.,* (1985) 651.

[162] W.A. Nevin, W. Liu, S. Greenberg, M. R. Hempstead, S. M. Maruccio, M. M. Melnik. C. C. Leznoff, A. B. P. Lever, *Inorg. Chem.,* **26** (1987) 291.

[163] E. Schnabel, H. Nöther, H. Kuhn, *In Chemistry of Natural and Synthetic Colouring Matters,* T. S. Gore, B. S. Joshi, S. V. Sunthankar, B. D. Tilak (Eds.)Academic Press, New York, (1962) p561-572.

[164] H. Engelkamp, R. J. M. Nolte, *J. Porphyrins and Phthalocyanines.,* **4** (2000) 454.

[165] Z. Gasyna, N. Kobayashi, M. J. Stillman, *J. Chem. Soc. Dalton trans.,* (1989) 2397

[166] M. Kasha, *Radiat. Res.,* **20** (1963) 55.

[167] M. Kasha, H. R. Rawls, M. Ashraf El-Bayoumi, *Pure. Appl. Chem.,* **11** (1965) 371.

[168] H. Ogata, R. Higashi, N. Kobayashi, *J. Porphyrins Phthalocyanines.,* **7** (2003) 551.

[169] R. D. George, A. W. Snow, J. S. Shirk, W. R. Barger, *J. Porphyrins Phthalocyanines.,* **2** (1998) 1.

[170] A. W. Snow, *In The Porphyrin Handbook,* K. M. Kadish, K. M. Smith, R. Guillard, (Eds.) Elsevier Science, New York, Vol. **17** (2003) Ch. 109.

[171] N. B. McKeown, *J. Mater. Chem.,* **10** (2000) 1979.

[172] A. P. De Silva, H. Q. N. Gunaratne, T. Gunnlaugsson, A. J. M. Huxley, C. P. McCoy, J. T. Rademacher, T. E. Rice, *Chem. Rev.,* **97** (1997) 1515.

[173] A. Ogunsipe, T. Nyokong, *J. Photochem. Photobiol. A: Chem.,* **173** (2005) 211.

[174] N. Kobayashi, K. Nakai, Chem. Commun., (2007) 4077.

[175] A. Ogunsipe, T. Nyokong, *J. Mol. Struct.,* **689** (2004) 89.

[176] T. H. Tran Thi, C. Desforge, C. Thiec, S. Gaspard, *J. Phys. Chem.,* **93** (1989) 1226.

[177] S. Fery-Forgues, D. Lavabre, *J. Chem. Educ.,* **76** (1999) 1260.

[178] J. Fu, X.Y. Li, D. K. P.Ng, C. Wu, *Langmuir.,* **18** (2002) 3843.

[179]. A. Ogunsipe, J.-Y. Chen, T. Nyokong, *New J. Chem.,* **28** (2004) 822.

[180] R.F. Kubin, A.N. Fletcher, *J. Lumin.,* **27** (1982) 455.

[181] J. R. Lakowiecz, *Principles of Fluorescence Spectroscopy 2nd edn.*; Kluwer Academic/Plenum Publishers, New York, (1999).

[182] S. Dhami, A. J. Mello, G. Rumbles, S. M. Bishop, D. Phillips, A. Beeby, *Photochem. Photobiol.,* **61** (1995) 341.

[183] T. W. J. Gadella Jr, R. M. Clegg, T. M. Jovin, *Bioimaging.,* **2** (1994) 139.

[184] H. C. Gerritsen, R. Sanders, A. Draaijer, *Proc. SPIE.,* **2329** (1994) 260.

[185] X. F. Wang, T. Uchida, M . Maeshima, S. Minami, *Appl. Spectrosc.,* **45** (1991) 560.

[186] J. C. Swarts, M. D. Maree, *J. Porphyrins Phthalocyanines.,* **11** (2007) 613.

[187] H. Du, R. A. Fuh, J. Li, L. A. Cockan, J. S. Lindsey, *Photochem. Photobiol.,* **68** (1998) 141.

[188] S. J. Strickler, R. A. Berg, *J. Phys. Chem.,* **37** (1962) 814.

[189] J. R. Lakowiecz, Principles of Fluorescence Spectroscopy, 3rd edn. Springer, New York, 2006.

[190] J. Turro, *In Modern Molecular Photochemistry,* The Benjamin/ Cunnings Publishing Co. Inc., New York (1978).

[191] T. H. Förster, *Disc. Far. Soc.,* **27** (1959) 7.

[192] A. Periasamy, *In Molecular Imaging: FRET Microscopy and Spectroscopy,* ed. N. R. Day, Oxford University Press, New York, (2005).

[193] J. S. Hsiao, B. P. Krueger, R.W. Wagner, T. E. Johnson, J. K. Delaney, D. C. Mauzerall, G. R. Fleming, J. S. Lindsey, D. F. Bocian, R. J. Donohoe, *J. Am. Chem. Soc.,* **118** (1996) 11181.

[194] L. Stryer, *Annu. Rev. Biochem.,* **47** (1978) 819.

[195] P. Jacques, A. M. Braun, *Helv. Chim. Acta.,* **64** (1981) 1800.

[196] J. M. Dixon, M. Taniguchi, J. S. Lindsey, *Photochem. Photobiol.,* **81** (2005) 212.

[197] S. Dayal, R. Krolicki, Y. Lou, X. Qiu, J. C. Berlin, M. E.Kenney, C.Burda, *Appl. Phys. B.,* **84** (2006) 309.

[198] S. Dayal, J. Li, Y. –S. Li, H. Wu, A. C. S. Samia, M. E. Kenney, C. Burda, *Photochem. Photobiol.,* **84** (2007) 243.

[199] S. Dayal, Y. Lou, A. C. S. Samia, J. C. Berlin, M. E. Kenney, C. Burda, *J. Am. Chem. Soc.,* **128** (2006) 13974.

[200] S. Dayal, C. Burda, *Photochem. Photobiol. Sci.,* **7** (2008) 605.

[201] J. Ma, J.-Y. Chen, M. Idowu, T. Nyokong, *J. Phy. Chem. B.,* **112** (2008) 4465.

[202] M. Idowu, T. Nyokong, *J. Luminescence.,* **129** (2009) 356.

[203] J. Britton, E. Antunes, T. Nyokong, *J. Photochem. Photobiol. A. Chem.,* **210** (2010) 1.

[204] J. H. Brannon, D. Magde, *J. Am. Chem. Soc.,* **102** (1980) 62.

[205] P. Kubat, J. Mosinger, *J. Photochem. Photobiol. A. Chem.,* **96** (1993) 93.

[206] J. Kossanyi, D. Chahraoui, *Int. J. Photoenergy.,* **2** (2000) 9.

[207] T. Shen, Z. –L. Yuan, H. –J. Xu, *Dyes and Pigments.,* **11** (1989) 77.

[208] P. S. Vincett, E. M. Voigt, K. E. Rieckhoff, *J. Chem. Phys.,* **55** (1971) 4131.

[209] D. S. Lawrence, D. G. Whitten, *Photochem. Photobiol.,* **64** (1996) 923.

[210] X. -F. Zhang, H. –J. Xu, *J. Chem. Soc. Fraday Trans.,* **89** (1993) 3347.

[211] M. G. Lagori, L. E. Dicello, E. S. Román, *J. Photochem. Photobiol. A. Chem*., **72** (1993) 153.

[212] M. D. Maree, N. Kuznetsova, T. Nyokong, *J. Photochem. Photobiol. A. Chem*., **140** (2001) 117.

[213] M. Durmuş, T. Nyokong, *Tetrahedron.,* **63** (2007) 1385.

[214] S. M. Bishop, A. Beeby, H. Meunier, A. W. Parker, M. S. C. Foley, D. Phillips, *J. Chem. Soc. Faraday Trans.*, **92** (1996) 2689.

[215] N. Kuznetsova, N. Gretsova, E. Kalmykova, E. Makarova, S. Dashkevich, V. Negrimovskii, O. Kaliya, E. Lukyanets, *Russ. J. Gen. Chem.,* **70** (2000) 133.

[216] W. Spiller, H. Kliesch, D. Wohrle, S. Hackbarth, B. Roder, G. Schnurpfeil, *J. Porphyrins Phthalocyanines.,* **2** (1998) 145.

[217] L. Shi. B. Hernandez, M. Selke, *J. Am. Chem.Soc.,* **128** (2006) 627.

[218] A. A. Frimer, *The Spectrum.,* **13** (2000) 9.

[219] S. Maree, T. Nyokong, *J. Porphyrins and Phthalocyanines.*, **5** (2002) 782.

[220] M. Idowu, T. Nyokong, *J. Photochem. Photobiol A: Chem.*, **188** (2007) 200.

[221] N. A. Kuznetsova, N. Gretsova, O. Yuzhakova, V. Negrimovsky, O. Kaliya, E. Luk'yanets, *Russ. J. Gen. Chem.,* **71 (**2001) 36.

[222] H. Li, T. F. Guarr, *J. Chem. Soc. Chem.Commun.,* (1989) 833.

[223] V. Nardello, J-M. Aubry, *Tetrahedron Lett.*, **38** (1997) 7361.

[224] N. Niedre, M. S. Patterson, B. C. Wilson, *Photochem. Photobiol.*, **75** (2003) 382.

[225] M. S. Patterson, S. J. Madsen, R. Wilson, *J. Photochem. Photobiol. B: Biol.*, **5** (1990) 69.

[226] D. D. Perrin, W. L. F. Armarego, *In Purification of Laboratory Chemicals*, 2nd Ed., Pergamon Press, Oxford, (1989).

[227] A. Harriman, M.C. Richoux, *J. Chem. Soc. Faraday Trans II.*, **76** (1980) 1618.

[228] F. Wilkinson, W. P. Helman, and A. B. Ross, *J. Phys. Chem. Ref. Data.*, **22** (1993) 113.

[229] D. Wohrle, J. Gritzel, I. Okura and S. Aono. *J. Chem. Soc. Perkin Trans II.*, (1985) 1171.

[230] K. Kasuga, M. Morisada, K. Sogabe and M. Handa. (1990). *Inorg. Chim. Acta.*, 174:161.

[231] S. Gaspard, *J. Chem. Soc. Perkin Trans.*, **2** (1989) 383.

[232] V. N. Nemykin, V. M. Mytsyk, S. V. Volkov, N. Kobayashi, *J. Porphyrins Phthalocyanines.*, **4** (2000) 551.

[233] N. Sehlotho, M. Durmus, V. Ahsen, T. Nyokong, *Inorg. Chem. Com.*, **11** (2008) 279.

[234] D. Denzler. M. Oschewski, K. Sattler. *J. Appl. Phys.*, **84** (1998) 2841.

[235] J. F. Suyver, S. F. Wuister, J. J. Kelly, A. Meijerink. *Nanolett.*, **1** (2001) 429.

[236] S. Mahamuni, A. A. Khosravi, M. Kundu, M. Kshirsagar, A. Bedekar, D. B. Avasare, P. Singh, S. K. Kulkarni, *J. Appl. Phys.*, **73** (1993) 5237.

[237] K.L. Kelly, E. Coronado, L. L. Zhao, G. C. Schatz, *J. Phys. Chem. B.*, **107** (2003) 668.

[238] C. Walkey, E. A. Sykes, W. C. W.Chan, *Hematology.*, (2009) 701.

[239] S. Eustis, M. A. El-Sayed, *Chem. Soc. Rev.*, **35** (2006) 209.

[240] T.G, Schaaff, M. N. Shafigullin, J. T. Khoury, I. Vezmar, R. L. Whetten, W. G. Cullen, P. N. First, C. Gutiérrez-Wing, J. Ascensio, M. J. Jose-Yacamán, *J. Phys. Chem. B.*, **101** (1997) 7885.

[241] D. V. Leff, L. Brandt, J. R. Heath, *Langmuir.*, **12** (1996) 4723.

[242] E. Jiménez, K. Abderrafi, J. Martínez-Pastor, R. Abargues, J. L. Valdés, R. Ibáñeze, *Superlattices and Microstructures.,* **43** (2008) 487.

[243] Y. Liu, Y-Li. Zhao, Y. Chen, M. Wang, *Macromol. Rapid Commun.,* **26** (2005) 401.

[244] M. Thamae, T. Nyokong, *J. Electroanal. Chem.,* **470** (1999) 126.

[245] K. Ozoemena, N. Kuznetsova, T. Nyokong, *J. Photochem. Photobiol. A. Chem.,* **139** (2001) 217.

[246] A. Suchan, J. Hurek, W. Waclawek, J. Nackiewicz, K. Ejsmont, *Polish J. Chem.,* **73** (1999) 2013.

[247] N. B. McKeown, *in The Porphyrin Handbook*, K. M. Kadish, K. M. Smith, R. Guilard (Eds.), Academic Press, New York, Vol. **15** (2003) Chapter 98.

[248] W. J. Kroenke, M. E. Kenney, *Inorg.Chem.,* **3** (1964) 251.

[249] C. W. Dirk, T. Inabe, K. F. Schoch, T. J. Marks, *J. Am. Chem. Soc.,* **105** (1983) 1539.

[250] T. Nyokong, H. Isago, *J. Porphyrins Phthalocyanines.,* **8** (2004) 1083.

[251] A. Mandal, N. Tamai, *J. Phys. Chem. C.,* **112** (2008) 8244.

[252] T. Nyokong, *Coord. Chem. Rev.,* **251** (2007) 1707.

[253] M. Idowu, A. Ogunsipe, T. Nyokong, *Spectrochimica Acta. A.,* **68** (2007) 995.

[254] M. G. Debacker, O. Deleplanque, B. Van Vlieberge, F. X. Sauvage, *Laser Chem.*, **8** (1988) 1.

[255] I. M. Seotsanyana, N. Kuznetsova, T. Nyokong, *J. Photochem. Photobiol. A. Chem.,* **140** (2001) 215.

[256] A. Ogunsipe, M. Durmuş, D. Atilla, A. G. Gürek, V. Ahsen, T. Nyokong, *Synthetic Metals.,* **158** (2008) 839.

[257] H. Isago, *Chem. Commun.,* (2003) 1864.

[258] B. Karimi, D. Zareyee, *Synthesis.,* (2003) 1875.

[259] M. Durmuş, T. Nyokong, *Spectrochim. Acta: A.,* **69** (2008) 1170.

[260] S. L. Murov, I. Carmichael, G. L. Hug, Handbook of Photochemistry, eds. Marcel Dekker, Inc, New York, (1993).

[261] L. Shi, B. Hernandez, M. Selke, *J. Am. Chem. Soc.,* **128** (2006) 627.

Information involving: Table 5.4 on energy transfer parameters for MPc-CdTe QD interactions in various solvents (ᶜFrom page 172).

This supplementary material involves the following complexes: ZnTSPc (**28**), ZnTCPc (**29**), ZnOCPc (**30**), TtfmPyZnPc (**40**) and TtfmMPyZnPc (**41**) and the related calculations for the FRET efficiencies (*Eff*) and subsequent r value determination.

The decrease in QD emission that was observed on addition of the above mentioned MPcs to the QD solution did not indicate high FRET efficiencies while the *Eff* values obtained from calculations using equation 7.1 (same as equation 5.5) which involves the use of fluorescence quantum yields of QDs were quite high. On the other hand, equation 7.2 resulted in FRET efficiencies that corresponded well with the QD emission reduction in the presence of MPcs and was thus employed in the determination of the *Eff* and r values only for the complexes listed above (the results are shown in Table 5.4).

$$Eff = 1 - \frac{\Phi_{F(DA)}}{\Phi_{F(D)}} \tag{7.1}$$

$$Eff = 1 - \frac{F_{(DA)}}{F_{(D)}} \tag{7.2}$$

Theoretically the use of equation 7.2 is also acceptable [189].